Deep Eutectic Mixtures with Graphene and MWCNT Functionalized Nanofluids for Indirect Solar Desalination using Multistage Flash Approach

A Thesis

Submitted in Partial Fulfilment of the Requirement for the Degree *of*

DOCTOR OF PHILOSOPHY

in

Chemical Engineering

By

Nipu Kumar Das

Department of Chemical Engineering

Indian Institute of Technology Guwahati

Guwahati-781039, Assam, India

December, 2024

Dedicated to My Parents & Teachers

Indian Institute of Technology Guwahati

Department of Chemical Engineering

Statement

I, hereby declare that the content embodied in this thesis entitled **"Deep Eutectic Mixtures with Graphene and MWCNT Functionalized Nanofluids for Indirect Solar Desalination using Multistage Flash Approach"** is the result of investigations carried out by me at the Department of Chemical Engineering, Indian Institute of Technology Guwahati, Guwahati, India, under the supervision of **Prof. Tamal Banerjee.**

In keeping with the general practice of reporting scientific observations, due acknowledgements have been made wherever the work described is based on the findings of other investigators.

Guwahati,
December, 2024
Nipu Kumar Das

Indian Institute of Technology Guwahati

Department of Chemical Engineering

Certificate

It is certified that the work described in this thesis entitled **"Deep Eutectic Mixtures with Graphene and MWCNT Functionalized Nanofluids for Indirect Solar Desalination using Multistage Flash Approach"** by Mr. Nipu Kumar Das for the award of degree of Doctor of Philosophy is an authentic record of the results obtained from the research work carried out under our supervision at the Department of Chemical Engineering, Indian Institute of Technology Guwahati, Guwahati, India, and this work has not been submitted elsewhere for a degree.

Dr. Tamal Banerjee
Professor
Department of Chemical Engineering
IIT Guwahati, Guwahati – 781039
Assam, India

ACKNOWLEDGEMENTS

My doctoral dissertation would not have come to a successful completion without the help of several people. I would like to take this opportunity to express my sincere gratitude to all of them.

I extend my sincere gratitude and respect to my thesis adviser, **Prof. Tamal Banerjee**, Department of Chemical Engineering, for his exceptional and steadfast assistance. This thesis would not have been feasible without his wise supervision, unyielding support and encouragement at every stage of my work. I could consistently contact him to clarify my uncertainties, and he was invariably nice and accommodating in addressing my enquiries, despite his busy schedule. His punctuality, discipline, and unwavering dedication consistently astonished me. I feel profoundly fortunate to have received the opportunity to work under his esteemed leadership. I will always be profoundly appreciative of his affection and support for me. To be completely honest, all the knowledge I acquired during my research period was solely attributable to them. It was a distinct honour to collaborate with them. Many thanks sir, for your amazing assistance and support.

I would like to thank my doctoral committee members Prof. G. Pugazhenthi, Prof. Chandan Das, and Prof. Dipankar Narayan Basu, for their valuable suggestions and comments during all assessments of the Ph. D. program. I would like to also thank my comprehensive committee members **Prof. Kaustubha Mohanty** and **Prof. Gooh Pattader Partho Sarathi**

I would like to acknowledge to our academic collaborator **Prof. Suryasarathi Bose (**Professor, Materials Engineering, Indian Institute of Science Bangalore) **and Prof. Bhabani S Malik** (Professor, Department of Chemistry, Indian Institute of Technology Hyderabad) for providing me the opportunity to work under their valuable guidance. Their valuable knowledge

and insights were incredibly useful in carrying out the experiments. I would also like to thank to our foreign collaborator **prof. Andrey Shisov** (Department of Chemistry, Saint Petersburg State University) for providing me the opportunity to work on computational part.

I am thankfull to **Prof. Kaustubha Mohanty**, Head, Department of Chemical Engineering, for his administrative support. Furthermore, I would like to thank other faculty members, research scholars, supporting staff of the Department of Chemical Engineering, IIT Guwahati for their kind cooperation in all aspects.

I acknowledge Ministry of Human Resource Development (MHRD) and our institute for providing fellowship throughout the Ph. D. program. I would also like to acknowledge the Science and Engineering Research Board of the Government of India for sponsoring this work through the CRG/2018/000522 project for sanctioning the financial grant in the project titled "Deep Eutectic Mixtures with Graphene and MWCNT Functionalized Nanofluids for Indirect Solar Desalination using Multistage Flash Approach".

I would also like to thank Central Instruments Facility (CIF), IIT Guwahati and analytical laboratory of Chemical Engineering, IIT Guwahati for providing the characterizations analysis. PARAM-ISHAN supercomputer (162 nodes and 3024 cores in each node) is duly acknowledged for providing the enormous computational requirement to carry out the simulation and computational works.

Special thanks to academic people, Library facilities, chemical engineering department staff, security staff and Core I-IV people for their necessary support in every aspect. I would like to acknowledge Disang hostel, IIT Guwahati for becoming almost my second home during my doctoral journey.

I extend my sincere thanks to my lab seniors **Dr. Papu Kumar Naik**, **Dr. Pyarimohan Dehury**, **Dr. Upasana Mahanta**, **Dr.Venkateshwara Rao**, **Dr. Dhirendra K. Mishra**, **Dr.**

Nikhil Kumar, **Dr. Nabendu Paul** and **Dr. Arindam Dutta** for helping me to learn experiments, DFT and molecular dynamics simulation.

I sincerely acknowledge my research group members **Dr. Anoop Kishore Vatti**, **Dr Ramesh N Goswami, Dr. Sebina Yasmin, Raghibul Hussain, Rajib Nandi, Mangal, Mohamnad Kalim, Antaripa, Pratyashee Barukial, Hrishkesh Sharm, Risikesh Sharma** and **my past lab colleague Swetha, Diksha, G. Harish, Somtirtha, Uday** and **Anushka** for providing a co-operative research environment.

I would like to especially thanks to my seniors and mentors **Dr. Dhirendra Kumar Mishra, Dr. Hirakh Jyoti Das** and **Dr. Thockchom Birjit Sinha and Dr. Gunjurani Dutta** for their valuable advices guidance and unwavering support throughout my PhD journey.

I am especially thankful to my friends during my doctoral journey **Dr. SVG Kumari**, **Abhisek Bansal, Anil Kumar, Chandra Bhan, Plaban Jyoti Buraghoain, Nikhil Dhongde, Sayani Adhikari**, **Nagendra Prasad, Imran Hussain, Bijendra Sharma** for being a part of a wonderful journey throughout the time. I would also like to thank my friends **Saddam Hussain, Tafiq Hussain, Kamal Kalita, Pompy Bodo, Dhruba Jyoti Haloi, Puja Kalita, Sonali Bodo, Sintu Hazarika, Raj Deka, Siben Kalita, Debajit Barman, Nipom Das, Gautam Kalita, Dipankar Das** for being a part of a wonderful journey throughout the time.

I extend my sincere love and affection towards my cousins, **Pallab Tamuli, Geetanjali Talukdar, Dikon, Champak, Jintu** and many more.

Last but not least, I want to convey my sincere gratitude and unfathomable sense of indebtedness to my mother **Mrs. Tulashi Das** and my father **Mr. Nikunja Kumar Das**, for all their eternal love, invaluable support and sacrifices throughout my life. Special thanks to my elder sister **Kashmiri Pathak**, her husband **Chandan Pathak; Karabi Das and her husband Hirakh Joyti Das** and my brother **Nitu Kumar Das** who always strengthened my morale by supporting me and standing by me in all situations. I will be thankful to them and I promise I

shall never forget their uncountable help and encouragement. Whatever I have achieved till date and whatever I will achieve in future, everything is and will be possible because of the love and support of my parents and I feel truly indebted to them and they are always in my heart. I wish to thank many other people whose names are not mentioned here but this does not mean that I have forgotten their help. Above all, I am thankful to GOD for giving me a wonderful and healthy life.

"Do everything you have to do, but not with greed, not with ego, not with lust, not with envy but with love, compassion, humility and devotion".

- Lord Krishna to Arjun (Bhagavad Gita)

Nipu Kumar Das

Indian Institute of Technology, Guwahati
Department of Chemical Engineering
Guwahati, 781039, Assam, India

भारतीय प्रौद्योगिकी संस्थान, गुवाहाटी
केमिकल इंजीनियरिंग विभाग
गुवाहाटी, 781039, असम, भारत

Thesis title	Deep Eutectic Mixtures with Graphene and MWCNT Functionalized Nanofluids for Indirect Solar Desalination using Multistage Flash Approach
Roll NO	196107106
Name of the candidate	Nipu Kumar Das
Month/Year of submission	October, 2024

Ph.D Synopsis

The water crisis is an expanding global issue expected to increase in the next few years due to population expansion and restricted freshwater resources. Presently, 20% of the global population experiences water scarcity, with estimates indicating an increase to 40% during the next 15 years. Although the majority of the Earth's surface is covered with water, merely 0.5% is available for human utilisation. Desalination, the process of extracting salt from seawater and brackish water, has emerged as an essential solution to tackle water scarcity. Solar desalination, an energy-efficient and cost-effective technique, shows significant potential, but it presently absorbs merely 13% of solar energy. Desalination methods can be primarily classified into thermal and membrane-based procedures. Thermal desalination, illustrated by multi-effect distillation (MED) and multi stage flash (MSF) are used to evaporate and subsequently condense the water, yielding potable water. Desalination, however, requires substantial energy (75.2 TWh per year) and contributes to carbon emissions, which are projected to increase by 2040.

Developing an economical resolution to the water shortage presents a significant challenge, and numerous strategies have been created to tackle it. Conventional heat transfer fluids, including water, engine oil, and ethylene glycol, are widely utilised in industries such as desalination, cooling, and power generation; nevertheless, their suboptimal thermal qualities constrain efficiency. Researchers are currently concentrating on identifying novel, eco-friendly fluids with enhanced thermal conductivity. Nanomaterials, recognised for their remarkable thermal, mechanical, and electrical characteristics, have facilitated the production of nanofluids. These fluids, comprising nanoparticles less than 100 nm in size, enhance thermophysical parameters such as thermal conductivity and viscosity, thereby significantly enhancing heat transfer efficiency in industrial systems. Following sections summarizes the thesis.

The initial part of the thesis mainly focuses on the studies of nanofluid and its thermal behaviour through experimental and theoretical methods. Density functional theory (DFT) has been performed to investigate the stability of a bio based nanofluid. Dihydrolevoglucosenone, commercially known as Cyrene, is a biodegradable solvent with a multitude of potential applications in chemical reaction and heat transfer media. We report a nanofluid comprising Cyrene as a potential bio-organic thermal base media dispersed with multi-walled carbon nanotube (MWCNT) and carboxylic functionalized multi-walled carbon nanotube (MWCNT-COOH) nanoparticles. Two volume fractions (0.0016 and 0.0032) for MWCNT and 0.03 Vol% for MWCNT-COOH nanoparticles were added to enhance the heat transfer capacity of the resulting nanofluids. Thereafter, thermophysical properties were investigated in the temperature range of 30-85°C for both base fluid and nanofluids. The measured values were then compared with few commercial heat transfer fluids, such as, Paratherm GLT and Therminol VP, within the temperature range of 30-85°C. Further, the stability of the nanofluid was investigated by a combination of microscopic analysis, and zeta potential measurements.

Thereafter, forced convection experiments were performed in a circular tube section under both laminar and turbulent conditions to measure the local heat transfer coefficient alongside temperature profiles. Results showed that the nanofluid possessing 0.0032 volume fraction of MWCNT-Cyrene nanofluid at N_{Re} =1881 gave the highest heat transfer coefficient. The heat transfer coefficient of the nanofluid exhibited an upward trend with the increase of the Reynolds number. DFT was used to investigate the microstructure formed by Cyrene on the surface of single-walled carbon nanotube (SWCNT). The orbital energy and influence of interaction energy on the van der Waals (vdW) interactions of Cyrene and ethylene glycol with SWCNT and SWCNT-COOH were examined and correlated with the dispersive forces within the fluid. The orbital energy revealed the fact that the HOMO-LUMO energy gap of the Cyrene/SWCNT and Cyrene/SWCNT-COOH systems were reduced due to the mobility of Cyrene towards SWCNT surface, making it a stable nanofluid system. Reduced density gradient (RDG) analysis further demonstrated that weak vdW interactions were the primary driving force between solvent-SWCNT systems, primarily through X···π interactions. The thermal conductivity at various weight percentages of nanoparticles was determined using the reverse non-equilibrium molecular dynamics (NEMD) simulations and validated with experimental values. The microstructure of Cyrene on the surface of a single-walled carbon nanotube (SWCNT) and SWCNT-COOH was examined using DFT calculations. Our study shows that the composition of CNTs and the nanofluid temperature significantly impact the thermal conductivity of pure Cyrene.

The thesis also reports hydrophilic heat transfer fluid (HTF) containing deep eutectic solvent (DES) and MWCNT nanoparticles. The DES had a combination of methyltriphenylphosphonium bromide (MTPB) as hydrogen bond acceptor (HBA) and ethylene glycol (EG) as hydrogen bond donor (HBD) at a molar ratio of 1:4. Thereafter, the corresponding nanofluid was prepared by dispersing 0.02wt% MWCNT having a diameter 10-

30 nm in the base fluid. Prior to dispersion, the shape and morphology of the MWCNT were ascertained using both Field Emission Scanning Electron Microscope (FESEM) and Field Emission Transmission Electron Microscope (FETEM). The crystallinity and functional groups were investigated by X-ray Powder Diffraction meter (XRD) and Fourier Transform Infrared Spectroscopy (FTIR). The stability of the prepared nanofluid was initially performed using visual observation followed by zeta potential measurements. Thermo-gravimetric analysis (TGA) was performed to check the stability of nanofluid at a temperature close to 500°C at a heating rate of 10°C /min under nitrogen environment. Thermophysical properties such as density, viscosity, thermal conductivity, and specific heat of nanofluid were measured in the temperature range 25-85°C. It is evident from the experimental data that viscosity and density decrease with an increase in temperature. On the contrary, the specific heat and thermal conductivity of the nanofluid were found to increase with temperature. This is due to the induced Brownian motion of the nanoparticle, which results in higher kinetic energy at high temperature. In the penultimate section, Molecular Dynamic (MD) simulations were performed to compare and validate the results of thermal conductivity of nanofluid.

Further the thesis focuses on the application of the DES in the synthesis and characterization of amine functionalized graphene oxide (GO-NH_2) nanoparticles and its use as a heat transfer media in desalination application. It also reports the thermal properties and stability analysis of DES and GO-NH_2 based nanofluid. DES is here composed of Diphenyl ether as HBA and DL-Menthol as a HBD in the molar ratio 1:1. Nanofluid was prepared by a two-step method where two different concentrations of functionalized graphene nanofluids, namely 0.0033 volume fraction (NF1) and 0.0101 volume fraction (NF2) were reported. XRD and FTIR analyses were used to validate the nanoparticle's identity. Additionally, the morphology and composition of GO-NH_2 nanoparticles were investigated using FESEM, FETEM, and EDS analysis. Therafter, the stability of nanofluids was assessed using zeta

potential measurements. The zeta potential measurements revealed increased stability, indicating that no agglomeration occurred in the DES-based nanofluid. Excellent thermal conductivity enhancement was observed at a higher temperature for the GO-NH_2 nanofluid. The density and viscosity of the base fluid and nanofluid decreased with an increase in temperature from 25-85°C. Further, the specific heat capacity of nanofluids also increased with the increase in temperature and volume fractions of nanofluid. Thermo-gravimetric analysis (TGA) was also performed to evaluate the thermal degradation of the nanofluid under nitrogen atmosphere. The nanofuid was used in a brine recirculation multistage flash desalination where the gained output ratio (GOR) of less than 10 was obtained using ASPEN simulations.

In the conclusion part of the solvent, a natural deep eutectic solvent (NADES) was considered as a new class of bio-based heat transfer fluid. NADES are environmentally friendly solvents derived from natural, biodegradable substances such as sugars, amino acids, and organic acids. NADES serve as sustainable substitutes for conventional solvents, encouraging the use of ecologically conscious methods. Here the NADES comprises of lauric acid and DL menthol as HBD and HBA at specific molar ratio. Two nanoparticles, MWCNT and MWCNT-COOH are dispersed to prepare different volume fractions of nanofluids. Different characterization methods, including XRD, FT-IR, Raman, EDS, FESEM, and FETEM were used to characterize the MWCNT and MWCNT-COOH nanoparticles. The measurement of viscosity, density, and specific heat was performed in the temperature range of 30-90°C. Thermal conductivity, one of the key factors in thermal energy storage, was measured and compared to the Hamilton-Crossover model. The maximum enhancement of thermal conductivity was found to be 40.93% and 108.05% at 50 °C for MWCNT and MWCNT-COOH nanoparticles respectively. Dispersion behaviour and stability analysis have been evaluated through zeta potential analysis. Heat transfer coefficients, Nusselt number, and fluid temperature of base fluid NADES and 0.125 vol% of MWCNT-COOH concentration

nanofluids were evaluated under constant heat flux through forced convection experiment. The experiment was carried out at three different Reynolds number in the laminar region. Higher heat transfer coefficient was observed for nanofluids compared to the NADES. The DFT calculation, including QTAIM and non-covalent interaction (NCI), demonstrated the interaction between nanoparticles and base fluid. The results showed that MWCNT-COOH based nanofluids could be prepared successfully on a large scale, and their exceptional performance highlights their potential utility in thermal energy systems. A graphical abstract and summary of the entire thesis is given below.

Keywords: Nanofluid, Deep Eutectic Solvent, Multi Walled Carbon Nanotube, Density Functional Theory, Molecular Dynamics Simulations

Graphical Abstract

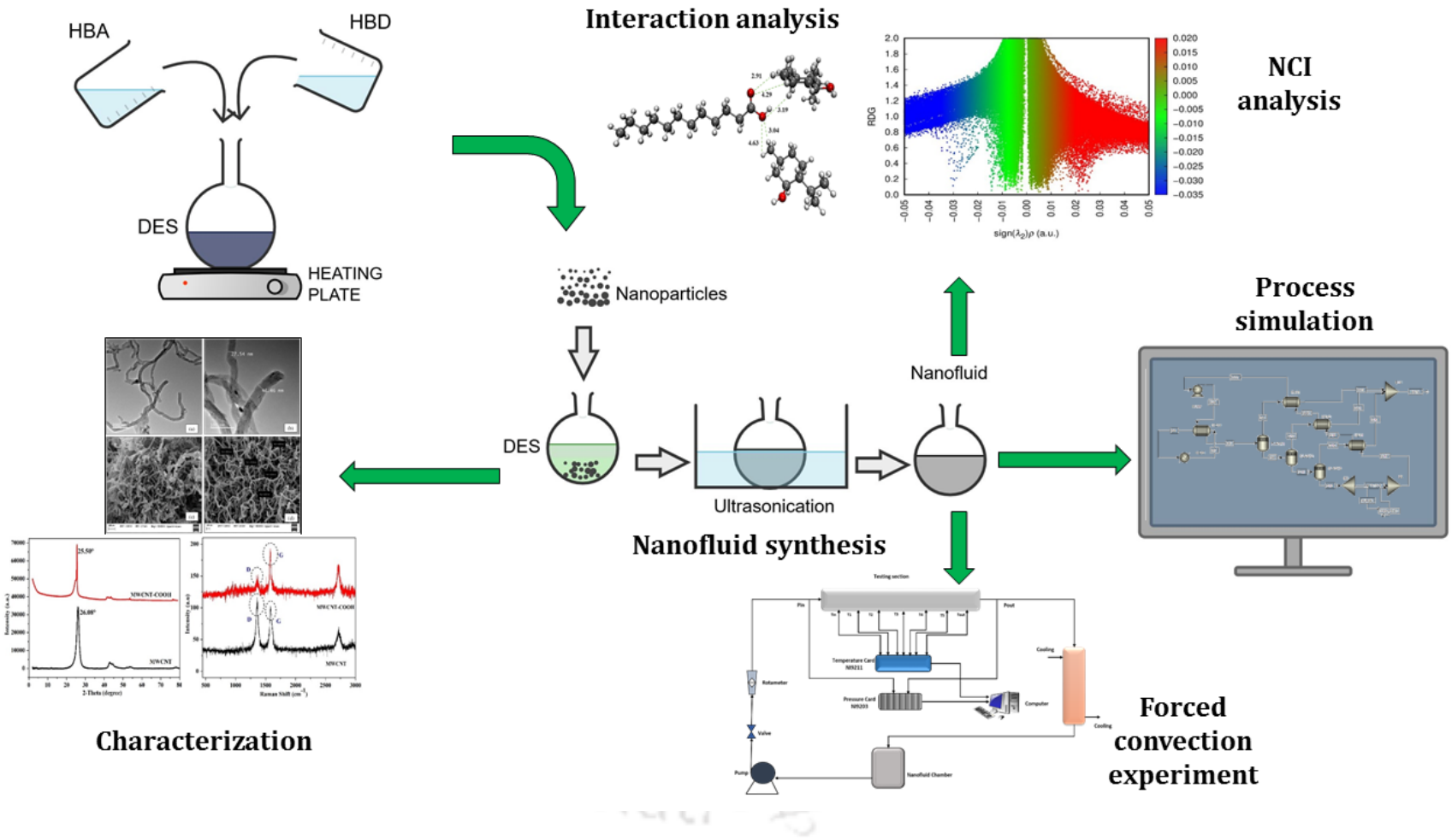

Table of Contents

List of Figures

List of Tables

List of Abbreviations and Symbols

Abbreviations

AIM	Atoms-in-molecules
AMBER	Assisted Model Building with Energy Refinement
BCP	Bond critical points
B3LYP	Becke three-parameter, Lee-Yang-Parr
BSSE	Basis Set Superposition Error
CHELPG	CHarges from Electrostatic Potentials using a Grid based method
CN	Coordination Number
CNT	Carbon Nanotube
COSMO-RS	COnductor like Screening MOdel for Real Solvents
CT	Charge Transfer
CP	Counter poise
D3BJ	Becke-Johnson damping (Three Parameter)
DES	Deep Eutectic Solvent
DFT	Density Functional Theory
DSC	Differential Scanning Calorimeter
EDS	Energy Disperse Spectroscopy
EDL	Electric Double Layer
FMO	Frontier Molecular Orbital
FETEM	Field Emission Transmission Electron Microscope
FESEM	Field Emission Scanning Electron Microscope
FTIR	Fourier Transform Infrared
GO	Graphene Oxide
HBA	Hydrogen Bond Acceptor
HBD	Hydrogen Bond Donor
HF	Hartree–Fock
HTF	Heat Transfer Fluid
HOMO	Highest Occupied Molecular Orbital
IE	Interaction Energy
IL	Ionic Liquid
LUMO	Lowest Unoccupied Molecular Orbitals
MD	Molecular Dynamics
MWCNT	Multi Walled Carbon Nanotube
MSD	Mean Squared Displacement
NEMD	Non Equilibrium Molecular Dynamic Simulation
NBO	Natural Bonding Orbitals
NCI	Non-covalent Interaction
NMR	Nuclear Magnetic Resonance
PCM	Polarizable Continuum Model
QC	Quantum Chemical
QTAIM	Quantum Theory of Atoms in Molecules

RDF	Radial Distribution Functions
RNEMD	Reverse Non Equilibrium Molecular Dynamics
RDG	Reduced Density Gradient
RESP	Restrained Electrostatic Potential
SLE	Solid-Liquid Equilibrium
SWCNT	Single Walled Carbon Nanotube
SMD	Solvation model based on density
THEDES	Therapeutic DESs
VMD	Visual Molecular Dynamics
vdW	van der Waals
XRD	X-ray Diffractometer

List of symbols

m	Mass
k	Thermal conductivity
Cp	Specific heat
N_{Re}	Reynolds number
Cy	Cyrene
q	Heat flux
Q	Heat transfer rate
T	Temperature
Nu	Nusselt number
h	Heat transfer coefficient
bf	Base fluid
nf	Nanofluid
ΔE_{AB}	Total energy of the solvent

Greeks Letters

Φ	Volume fraction
ρ	Density
μ	Viscosity

Nanofluid Abbreviations

SL NO.	Nanofluid Systems	Nanofluid Concentrations	Abbreviations
1	Cyrene+MWCNT	0.32 Vol%	NF1
2	Cyrene+MWCNT	0.16 Vol%	NF2
3	Cyrene+MWCNT-COOH	0.03 Vol%	NF3
4	(MTPB+EG)/MWCNT	0.02 wt%	NF4
5	(Diphenyl ether+DL menthol)/GO-NH_2	0.33 Vol%	NF5
6	(Diphenyl ether+DL menthol)/GO-NH_2	1.01 Vol%	NF6
7	(Lauric acid+DL menthol)/MWCNT	0.125 Vol%	NF7
8	(Lauric acid+DL menthol)/MWCNT	0.3 Vol%	NF8
9	(Lauric acid+DL menthol)/MWCNT	0.5 Vol%	NF9
10	(Lauric acid+DL menthol)/MWCNT-COOH	0.125 Vol%	f-NF7
11	(Lauric acid+DL menthol)/MWCNT-COOH	0.3 Vol%	f-NF8
12	(Lauric acid+DL menthol)/MWCNT-COOH	0.5 Vol%	f-NF9

Chapter-1

Introduction and Literature Review for Deep Eutectic Solvents (DES) base Nanofluid and its Applications

1. Introduction

1.1 Green energy

Global energy consumption is expected to double by 2050 and more than quadruple by the end of the century. Even incremental improvements to existing energy networks will not be adequate to address increasing demand sustainably. Securing an adequate supply of renewable energy for the future is an enormous task for humanity. The substantial gap between our present use of solar energy and the large untapped capacity of this energy source is a prominent concern in energy research. Abundant and clean solar electricity is the most optimal solution to fulfil our future energy requirements. The fact that it is easily available, free of international conflict, and does not pollute the environment or change the climate is a huge advantage [1]. With the recent demand for renewable energies, it is important to give attention to cost-effective techniques dealing with solar energy.

Solar energy is one of the major renewable sources for thermal applications, including desalination systems, due to the ease of availability and predictability[2]. Many solar based thermal systems are used for generating electricity, water desalination, buildings air-conditioning, and water heating. Among the renewable energy sources, solar energy have the potential to reduce the negative effects of climate change and encourage the development of renewable energy sources [3]. Hence, the advancement of solar energy will have a crucial impact on ensuring a sustainable future for Earth. But the efficiency of the thermal performance of solar energy-based desalination systems is the primary concern among the researchers. Modification of efficiency can be categorized based on improving solar radiation absorption, improving the efficiency of the applied media, and improving the heat transfer media [4].

Water crisis is one of the global challenging and it will be more scared in the forthcoming years. Due to the rapid growth in the population, there is a limited availability of fresh water sources, which has led to the development of advanced technologies for

desalination of brackish water and seawater. These technologies aim to fulfil the growing demand for safe drinking water, addressing both social and economic demands [5]. Globally 20% world population experiences water scarcity and it is believed that this value will increase approximately up-to 40% in next 15 years. Figure 1.1 reflect the reservoir of water storage in India. The remaining fresh source of water cannot fulfil the current global demand [6]. Although the earth's surface is mostly covered with water, only a small fraction of around 0.5% is accessible and appropriate for human use. Out of the total water, 99.5% is made up of freshwater, which may be further divided into a polar ice caps and glaciers (2.5%) and, sea- and brackish water sources (97%). Desalination is a potential method to tackle water scarcity by extracting salt from marine and brackish water sources.

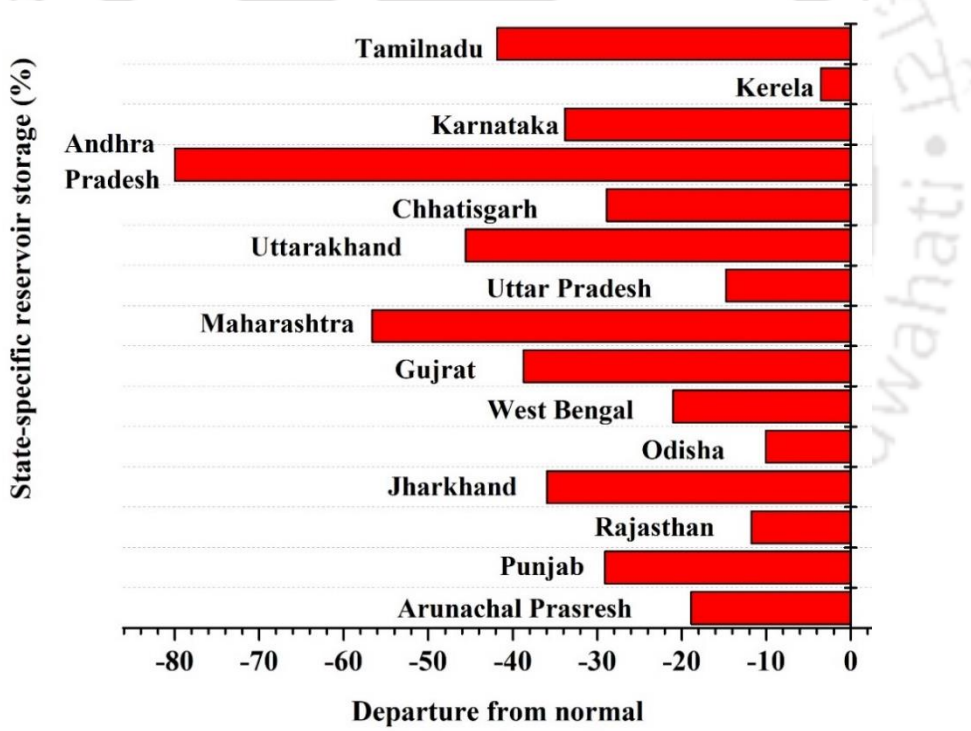

Figure 1.1 State specific reservoir storage in India (data obtained from Scopus)

Solar desalination technique is the existing technique that has huge potential to purify saline water with low energy and operating cost. Only 13% of solar energy can be harvested

directly by sea water from the solar energy. Numerous desalination techniques have been developed, and the annual energy consumption of these procedures worldwide amounts to around 75.2 Terawatt hours (TWh). However, desalination facilities emit around 76 million tonnes (Mt) of carbon dioxide (CO_2) annually; by 2040, this amount is predicted to rise to 218 Mt [7, 8].

In general, desalination techniques can be broadly divided into two distinct categories: thermal desalination techniques and membrane-based techniques. Both these processes separate salt water into low salt concentration water or potable water. The high salt concentration water is referred as brine water. Some of the important desalination process are shown in Figure 1.2

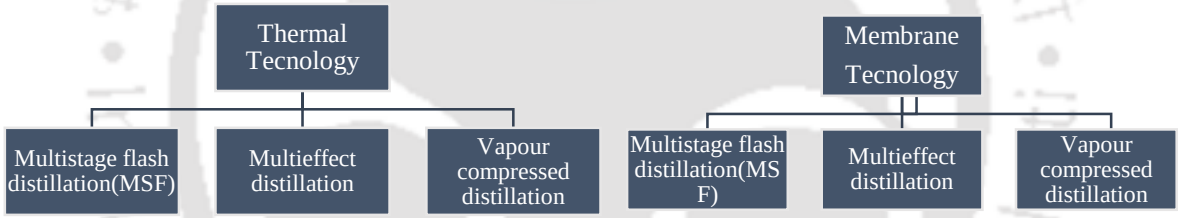

Figure 1.2. Classification of desalination process

In phase change or thermal desalination process, heating phenomena is involved where salt containing water is heated and evaporated. It is collected as condensed vapor with high pressure to produce distilled water [9]. Important commercial thermal desalination process involves Multi Stage Flash (MSF), Mechanical Vapor Compression (MVC) and Multi Effect Distillation (MED). The MED or the first desalination unit contain series of stages. Each stage has different ambient pressure. For the first stage, a heat source is employed to raise the input water's temperature to 110 °C. This heat can be produced by a boiler powered by a renewable

energy source, waste heat, or fossil fuel. In order to further boil saltwater, steam is created in a serial pattern and sent from the first stage through a tube to the succeeding stages[10, 11]. The feed water is initially heated to its boiling point and then distributed evenly across the several stages. Subsequently, the heated water is dispersed onto the surface of the tubes and the surface of the tubes are heated by the application of steam, causing the steam contained within the tubes to undergo condensation. As a result, water on the surface of the tubes are vaporized.

In many parts of the world, particularly the Arab Gulf states, the most popular method for desalinating water is the multi-stage flash (MSF) procedure. The MSF method currently accounts for more than 80% of saltwater desalination in Gulf countries[12].The MSF process possesses numerous attractive attributes that distinguish it from alternative desalination techniques. Since its establishment in the late 1950s, considerable field expertise has been acquired in domains such as process technology, design, construction, and operation. This has resulted in the establishment of clear and reliable operational protocols. Moreover, innovations have addressed and mitigated numerous operating issues, including scale accumulation, foaming, fouling, and corrosion [13-15]. Kabeel et al [16] used Al_2O_3 nanoparticles containing brine water in solar still. Productivity of corrugated wick solar still was further improved by 285 % and 255 % using Cu_2O and Al_2O_3 nanoparticles [17]. Nowadays, nanofluids have gained prominence in solar energy applications. Many researchers have investigated the thermal performance of direct adsorption solar collector using different nanofluids. Otanicar et al. [18] used different nanofluids (graphite, carbon and silver) and calculated the thermal performance of direct absorption parabolic trough collector (DAPTC) both experimentally and numerically. Results showed that thermal efficiency was enhanced with an increase in the volume fractions of nanofluid. Bortola et al. [19] calculated the thermal efficiency of SWCNT-water nanofluid in DAPTC experimentally. They got an 87% increment in thermal efficiency but found lack of stability of nanofluid. Multi Stage Flash (MSF) desalination system is the first choice of many

researchers and industries over RO and MED plants as MSF plants can be used to produce both electricity and water and the plant is not affected by high feed temperature and salinity. Overall it produces high quality of feed water. Considering the aforementioned factors, it is clear that the Multi-Stage Flash (MSF) system is likely to remain the predominant desalination method, especially in the Middle East. The configuration of the MSF unit has been displayed in Figure 1.3.

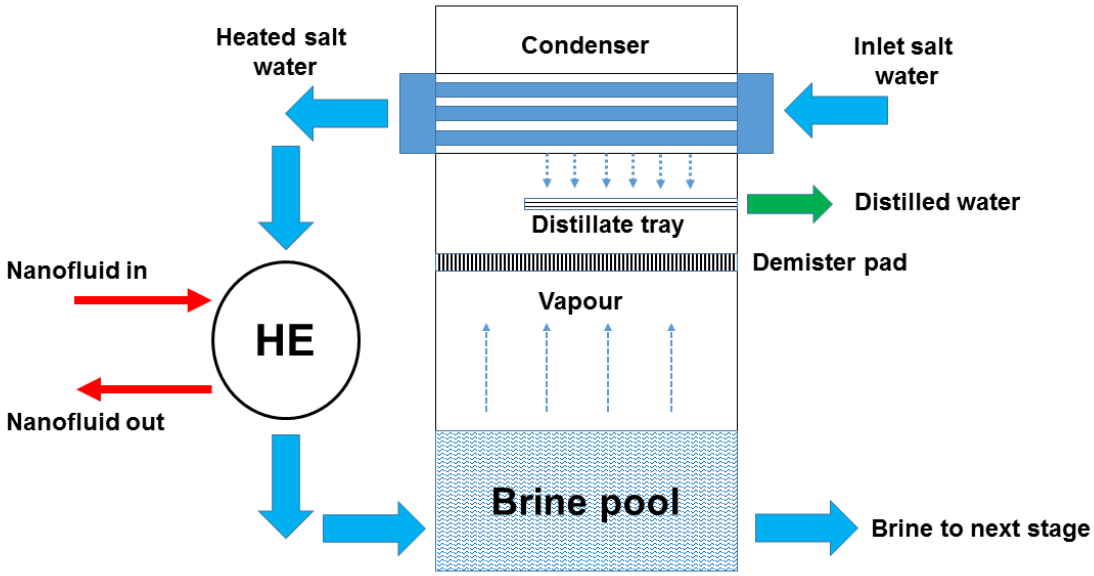

Figure 1.3: Schematic diagram of a MSF unit

Each MSF unit consist of different parts including brine pool, demister pad, distillate tray and feed pre heater [20]. The saline solution having a specific flow rate gets heated in the heat exchanger up to the top brine temperature. In an MSF process, the heating of the saline water enters chamber at decreasing pressures. Because of the reduced pressure, sudden flashing of the saline solution takes place, which results in the formation of vapors of fresh water formed. The vapors then pass through the demister pad. The demister pad is employed to

prevent flow of brine droplet with the fresh water vapors such that the distillate products free of salt. The vapours subsequently condense on the pre-heater's surface, transferring their latent heat of condensation to the recycled brine circulating through its tubes. The distillate is gathered in the distillate tray. The residual concentrated brine and distillate then enters the subsequent chamber, which operates at a lower pressure than the preceding one. The flashing of brine occurs once more, results in the formation of vapours. The latent heat of vapour condensation at each stage is employed to heat the recycled brine. The procedure is thus repeated through each flashing chamber, and distillates are collected at the last flashing stage [21]. The heat rejection stages and the heat recovery stages make up the two portions of the total number of stages in the BR-MSF system. The recovery heat section is utilised to extract the latent energy of vapors. The heat rejection portion is designed to dissipate excess heat through the heat exchanger system using cold ocean water.

1.2 Requirement of Nanofluids in Heat Transfer Application

Conventional fluid like water, engine oil, ethylene glycol plays an important role in many industrial applications including desalination system, refrigerating system, cooling tower, power sector, food processing industries and refineries. A challenging part of these industries is low thermal behaviour of heat transfer fluid. Due to poor heat transfer properties and because of environmental concern, researchers have explored heat transfer fluid which is basically low toxic, environment friendly and shows good heat transfer characteristic [22]. Nanomaterials have captured the attention of research groups across various fields, including material science, electronics, mechanics, and healthcare. Their exceptional optical, mechanical, electrical, and thermal properties make them highly sought after. The progress in nano materials has led to the development of a new class of fluids called nanofluids [23]. Small size nanoparticles, size < 100 nm when dispersed into the base fluid, enhances its thermophysical properties including

thermal conductivity, viscosity, specific heat and density. This improves the thermal performance of the heat transfer system [24].

Nanofluid was first designed by Stephen U.S. Choi in the year 1995 at Argonne National Laboratory, USA [24]. Thereafter, numerous articles are published on nanofluids from 2006 to 2023 (Figure 2.1). Nanofluid has wide applications in solar energy sector, industrial cooling applications, nuclear reactor and extraction of geothermal power [25]. Further nanofluid can also be found in the application of pharmaceutical industries [26, 27], reducing building pollutant [28, 29], biomedical applications [30] and sunscreen product [29]. Long term stability of nanoparticle dispersion is a key challenge. Nanofluids are primarily defined through the overwhelming influence of Brownian motion, which prevents any settling caused by gravity. Therefore, a nanofluid may be considered stable in theory, as long as the particles remain sufficiently small, typically about 100 nm. Literature reports the different stabilization method of nanofluid which includes (i) changing the pH value of suspension, (ii) using surface activator and (iii) using ultra-sonication. The use of these approaches is dependent upon the specific application of the nanofluid.

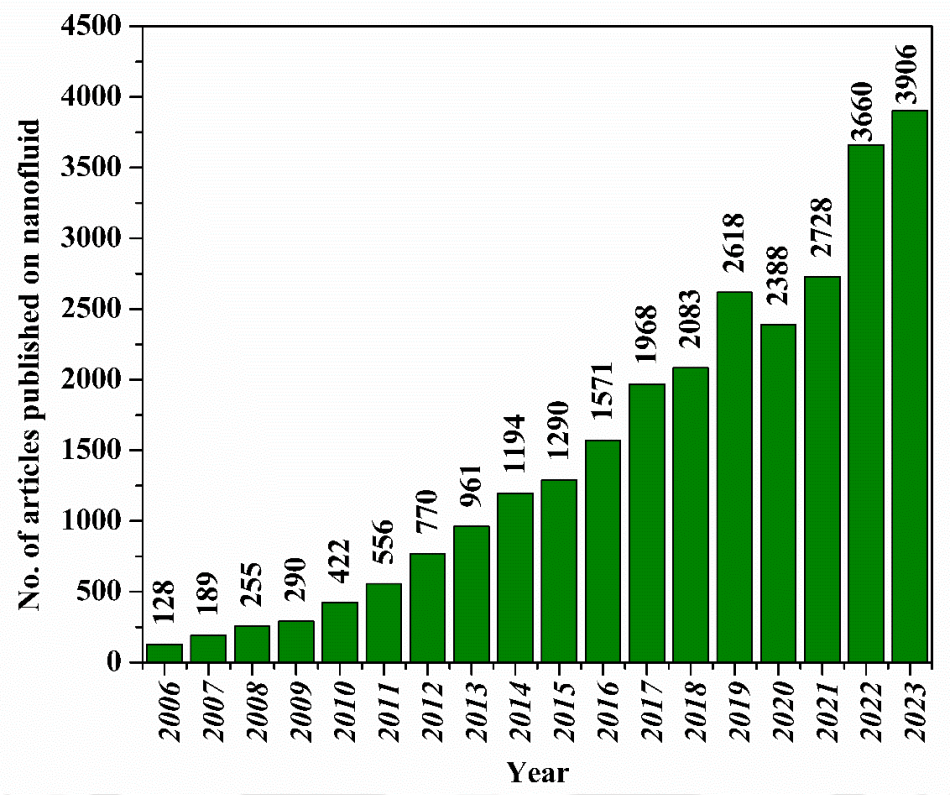

Figure 1.4. Number of articles published on nanofluids from 2006 to 2023, as per Scopus database

Garg et, al.[21] reported a desalination unit using multistage flash (MSF) system with brine recirculation (BR) configuration. Nanofluid was used to heat the BR-MSF which is coupled with direct absorption solar collector (DASC) with the help of counter current heat exchanger. Aim of the study was to measure the system performance in terms of gain output ratio (GOR) along with thermal performance of the DASC based brine recirculation multi stage flash desalination system.

Another desalination system based on parabolic trough collector (PTC) was performed and results were compared with the DASC based BR-MSF system. It has been found that the thermal performance of the DASC based system is 11% higher as compared to the PTC-based system. Nafey et. al [31] reported a small desalination unit using single stage flash evaporation process. A nanofluid was used to increase the heat transfer coefficient and thermal properties

of the nanofluid were improved by dispersing different concentration of the nanoparticles. Sabiha et. al [32] reported an enclosed type Evacuated U-Tube Solar Collector (ETSC) by using water based Singled Walled Carbon Nanotube (SWCNT). Different volume concentrations of SWCNT nanofluid namely 0.05, 0.1, 0.2 were carried out and thermal performance was measured. Both water and SWCNT nanofluid at different flow rates of 0.008, 0.017 and 0.025 kg/s were used and thermal performance of the collector was measured. It was found that the performance efficiency of the collector with SWCNT nanofluid was much higher than that of water as a working fluid. Efficiency was higher at 93.43 % for 0.2 vol% SWCNT nanofluid. Tong et. al [33] conducted an experiment on an enclosed type evacuated U-tube solar collector (EEUSC) by using Multi Water Carbon Nanotube (MWCNT)-water nanofluid. It had been shown that heat transfer coefficient of the MWCNT nanofluid was much higher than that of water. An analytical method (simulation) was developed to measure the performance of the U-tube solar collector efficiency and it was found that by increasing the solar radiation in low radiation condition, thermal efficiency of the collector increases.

Amrollahi et. al [34] measured the heat transfer coefficient of functionalized nanofluid under both laminar and turbulent boundary condition flowing through a horizontal tube. It has been reported that at lower temperature, heat transfer coefficient in turbulent region is much higher than the heat transfer coefficient in laminar region and heat transfer coefficient is 25% more than in the pure water. Arshad et. al [35] also studied graphene based nanofluids and their preparation, characterization, transport characteristics and industrial applications. Xuan and Li [36] measured heat transfer coefficient and friction factor of a working fluid in a tube. Here, Cu-water nanofluid was used as a working fluid. They investigated convective heat transfer features and flow performance of nanofluids in turbulent fluid. The nanoparticles enhanced the heat transfer coefficient of the nanofluid and friction factor when compared to the base fluid under same Reynolds number. Pak and Cho [37] investigated experimentally the

turbulent friction and heat transfer behaviour of dispersed fluids (i.e. ultrafine metallic oxide particles suspended in water) in a circular pipe. Two different metallic oxide particles, γ-alumina (Al_2O_3) and titanium dioxide (TiO_2) with mean diameters of 13 and 27 nm, were used as a suspended particle. They found that Nusselt number of the dispersed fluid increases with increasing volume concentration as well as Reynolds number. Frolov et. al [38] studied the effect of salt at different concentrations on carbon nanotube (CNT) which is dispersed in organic solvents like N-methyl-2-pyrrolidine (NMP). They used Sodium Iodide (NaI) salt to study the mechanism of interaction between salts and CNT surface. They observed that NMP-CNT dispersion becomes less thermodynamically stable when salt concentration increases. As the salt concentration increases the aggregation of the CNT occurred.

1.2.1 Nanofluid Preparation and Types of Nanofluid

Nanofluids are determined in the manner they are dispersed in a specific base fluid. Diverse nanoparticles, including metallic particles such as copper, silver, and gold; ceramics such as aluminium oxide, copper oxide, titanium oxide, and silicon oxide; carbon-based materials such as single and multi-walled carbon nanotubes and graphene; as well as hybrid and functionalised nanoparticles, are dispersed in various base fluids like water, oil, glycols, ethylene, and acetone to create nanofluids. The formulation and stability of nanofluids are essential prerequisites for their effective investigation and use in many applications.

Figure 1.5 illustrates the preparation techniques for nanofluid: (a) the one-step [39] and (b) two-step approaches[40], together with their respective advantages and disadvantages. The efficient and cost-effective approach for the large-scale production of nanoparticles is via the two-step process. In two step preparation method, nanofibers or any other nano-structured materials are initially synthesized as dry powders via physical or chemical methods. Thereafter the synthesized dry powders are dispersed in base fluids. Dispersion stability of nanoparticle is studied by TEM, centrifugal, dynamic light scattering and zeta potential. A schematic

diagram of two step preparation method is shown in Figure 1.6. Another approach, the single-step process entails the prompt production and distribution of nanoparticles within the base fluid. This technique prevents drying and storing, leading to reduced sedimentation, absence of oxidation, and very stable nanofluids. Nevertheless, the output of nanoparticles is exceedingly poor, rendering applicable for small-scale production. The two step method involves the use of ball mills, ultra-sonication and homogenisers depending on the specific requirements. This approach is significantly more successful in enhancing performance compared to the one-step method. Nevertheless, nanofluids synthesised with the two-step process exhibit significant agglomeration, resulting in reduced stability compared to those produced by the one-step method [41].

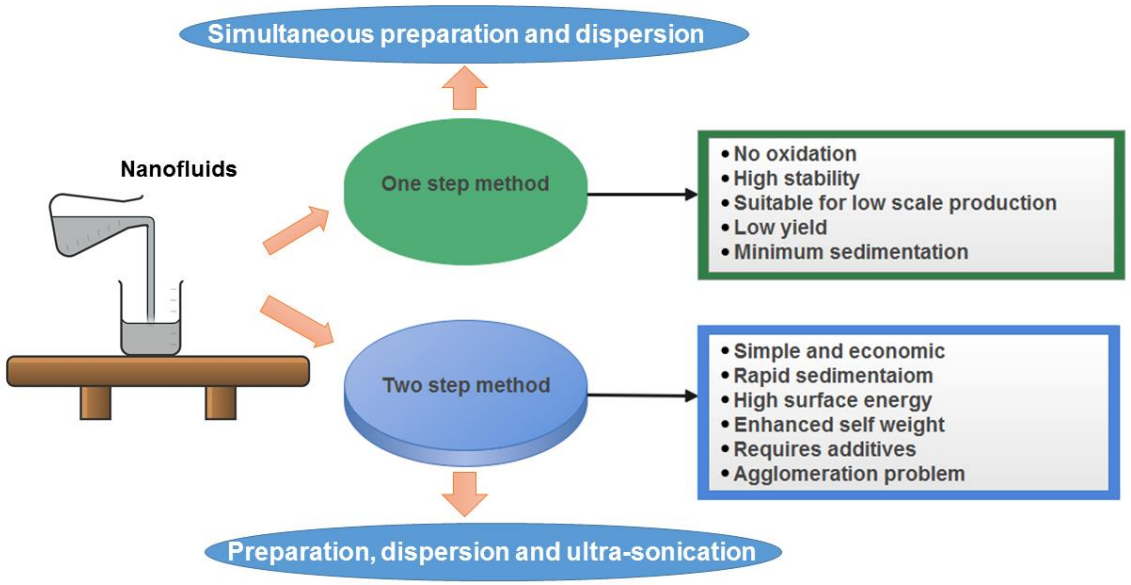

Figure 1.5. Preparation methods of nanofluid

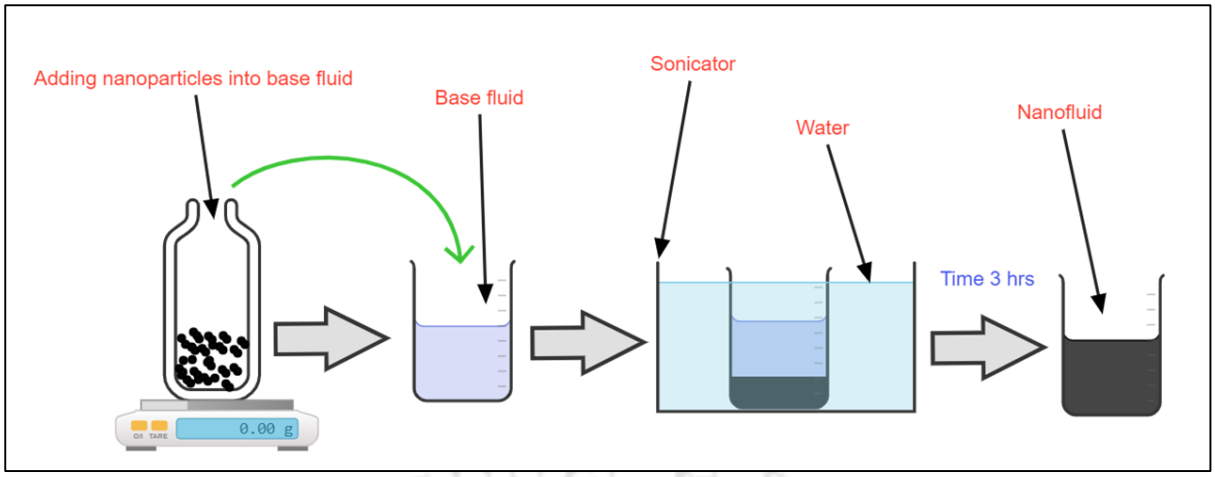

Figure 1.6. Schematic diagram of two step preparation method

The types of Nanofluids are listed below

(a) Single material nanofluid: Nanofluid that form from the mixture of base fluid and single element of nanoparticles like, MWCNT/Water, Al_2O_3/water, Cu/ethylene glycol**.**

(b) Hybrid nanofluid: This kind of nanofluid contains more than one nanoparticle dispersed in the base fluid. This novel technique aims to improve the thermal characteristics of nanofluid beyond the capabilities of individual nanoparticles. Here it involves a combination of metallic (e.g., copper, silver), metal oxide (e.g., aluminium oxide, titanium dioxide), carbon-based (e.g., graphene, carbon nanotubes), or other types of nanoparticles. Ensuring the long-term stability of hybrid nanofluids remains a challenge, as nanoparticles tend to settle or agglomerate over time [42].

1.2.2 Base Fluid Used in the Nanofluids

Nanofluids can be formulated with a variety of base fluids, each chosen based on the desired application and properties. Base fluid has the biggest impact on the thermophysical properties of the nanofluid, including thermal conductivity enhancement which largely depends on the

based fluid. Some of the basefluid includes water, ethylene glycol, engine oil and ionic liquids. Researchers and engineers modify nanofluids for various applications, such as industrial cooling and heating, complex energy systems, and biomedical applications, by the selection of an appropriate base fluid. Figure 1.7 display the number of publications on base fluids used in the synthesis of nanofluid.

1.2.2.1 Water and Ethylene Glycol Base Fluid

Water-based nanofluids represent a promising advancement in the field of heat transfer and thermal management. Their enhanced thermal properties make them suitable for a variety of applications, though challenges related to stability, cost, and environmental impact need to be addressed for widespread application. Fedele et al [43] used three nanoparticles namely titanium oxide (TiO_2), copper oxide (CuO) and single wall carbon nanohorn (SWCNH), dispersed in water by homogenization method. To eliminate agglomeration of nanoparticles, four dispersant compound (citric acid, hydrochloric acid, polyethylene glycol(PEG) and sodium *n*-dodecyl sulphate(SDS)) has been used.

Results found that PEG and SDS showed good dispersion for TiO_2 and SWCNHs. Water/SWCNHs at 0.01, 0.1 and 1 wt% proved to be very stable for at least 25 days. Murshed et al [44] dispersed spherical rod shaped TiO_2 nanoparticles in de-ionized water and prepared 0.5-5 vol% nanofluid. It was reported that the thermal conductivity for TiO_2/water nanofluid for 15mm TiO_2 nanoparticles showed 29.70% enhancement at 5% particle volume concentrations, whereas TiO_2 with 10 nm×40 mm rod shaped nanoparticle showed a 32% enhancement. Similar results have been reported by Masuda et al [45] where Al_2O_3 (13 mm) nanoparticle dispersed in water gave 32% enhancement when volume concentration increased from 1-4.3%. Rashmi et al [46] used both water and ethylene glycol and mixed them with

multi walled carbon nanotube at 0.1 and 0.02 wt% in order to study their corrosion rate and heat transfer efficiency. They reported that the corrosion rate for aluminium, stainless steel and copper) were found to be lower using CNT nanofluid. The rate of corrosion increased with the increasing temperature. Ray and Das [47] used water and ethylene glycol at 60:40 and prepared nanofluids with three nanoparticles Al_2O_3, CuO and SiO_2 at particle volume concentrations 1-6 vol%. It was observed that 1 vol% concentration of nanofluid showed better thermal property results compare to higher volume concentrations. Similar nanoparticles have been used by Sidik et al.[48] used where water and ethylene glycol at 50:50 molar ratios was used to prepare nanofluid.

Computational studies have been performed to investigate the heat transfer performance. The study determined that the thermal conductivity of nanoparticles has a direct and proportionate impact on the thermal conductivity of nanofluids. Paul et al. [49] utilised mechanical alloying to produce Al-5 wt% Zn nanoparticles, which were subsequently dispersed in ethylene glycol at a concentration of 0.01-0.10 vol%. The thermal conductivity of nanofluids is shown to be significantly influenced by factors such as the volume concentration, particle size, fluid temperature, and stability of the distributed nanoparticles in the base fluid. An increase in thermal conductivity of 16% was reported for $Al_{95}Zn_{05}$ nanofluids with a volume concentration of 0.10%.

1.2.2.2 Engine Oil Base Fluid

Kole and Dey [50] used engine oil nanofluid using CuO nanoparticles and studied the thermal conductivity of the nanofluid. Measurement of thermal conductivity was done at temperature range between 5-80ºC. their result showed 10.4% thermal conductivity enhancement at 0.025 volume fraction at room temperature. The enhancement gave a higher thermal conductivity up to 11.9% at 80°C. Saeedinia et al. [51] investigated the viscosity of stable CuO–base oil

nanofluids. This experiment was conducted with varying particle weight fractions of 0.2% to 2% at multiple temperatures. Experimental results clearly demonstrated that dynamic viscosity markedly increases with the elevation of nanoparticle concentration. A greater increase was noted at the lower temperatures of the nanofluids.

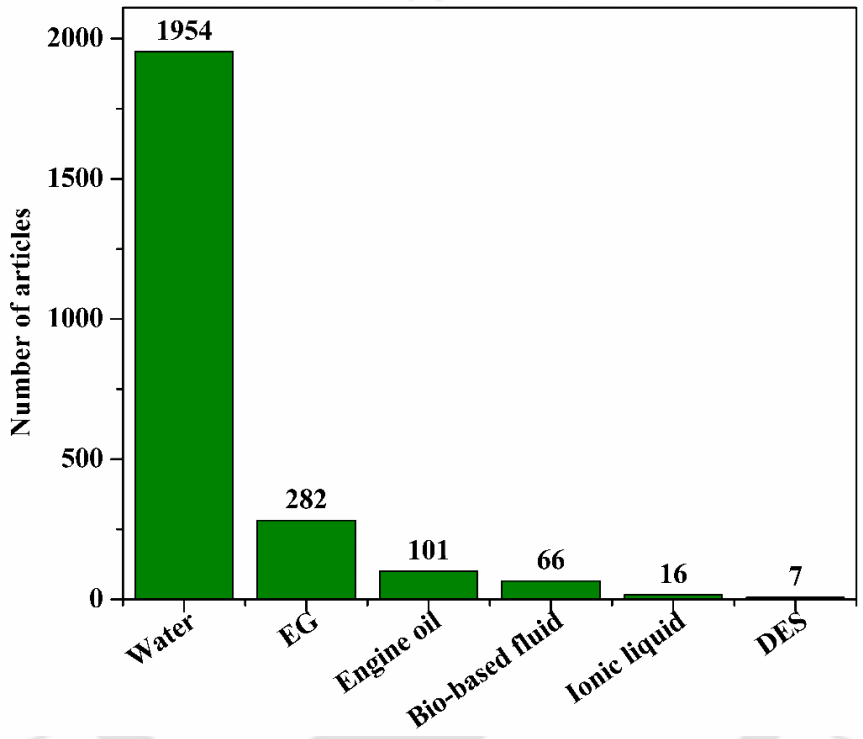

Figure 1.7 Number of publications on base fluids used in the synthesis of nanofluid

1.3 Nanofluid as Heat Transfer Fluid

The nanofluids have already been documented and are known to enhance the thermo-physical properties of the fluid [23, 52]. Overall they should have high thermal stability at high temperature, high thermal storage capacity, high heat capacity, thermal conductivity, heat transfer coefficient and constant heat flux. It is reported that the thermal conductivity and heat transfer coefficient increases with the concentration of nanoparticle [44, 53-58]. Further the specific heat and viscosity of the nanofluid is also a function of concentrations and

temperature[51, 59-65]. To maintain high thermal conductivity for a longer time span, the nanofluid needs to inhibit the aggregation behaviour. To overcome this, functionalized multi walled carbon nano tube (MWCNT) conjugated with either Hydrogen Bond Acceptor (HBA) or Hydrogen Bond Donor (HBD) molecules can be one of the desired improvement. The base fluid or the deep eutectic solvents (DES) and is the present interest of the thesis. Deep Eutectic Solvents are solvents which were first introduced by Abott et. al [66]. DES is a new class of ionic liquids (ILs) which have more advantages to use than ILs as a thermal fluid [67].

Garg et, al.[21] reported a desalination unit using multistage flash (MSF) system with brine recirculation (BR) configuration. A nanofluid was used to heat the BR-MSF which is coupled with direct absorption solar collector (DASC) with the help of counter current heat exchanger. Aim of this study was to measure the system performance in terms gain output ratio (GOR) along with thermal performance of the DASC based brine recirculation multi stage flash desalination system. Another desalination system based on parabolic trough collector (PTC) was performed and results were compared with the DASC based BR-MSF system. It has been found that the thermal performance of the DASC based system is 11% higher as compared to the PTC-based system. Nafey et. al [31] reported a small desalination unit using single stage flash evaporation process. A nanofluid was used to increase the heat transfer coefficient and thermal properties of the nanofluid was improved by a higher concentration of the nanoparticles.

Sabiha et. al [32] reported an enclosed type Evacuated U-Tube Solar Collector (ETSC) by using water based Singled Walled Carbon Nanotube (SWCNT). Different volume concentrations of SWCNT nanofluid namely 0.05, 0.1, 0.2 were carried out and thermal performance was measured. Both water and SWCNT nanofluid at different flow rates of 0.008, 0.017 and 0.025 kg/s were used and thermal performance of the collector was measured. It was found that the performance efficiency of the collector with SWCNT nanofluid was much higher

than that of water as a working fluid. Efficiency was higher at 93.43 % for 0.2 vol% SWCNT nanofluid. Tong et. al [33] conducted an experiment on an enclosed type evacuated U-tube solar collector (EEUSC) by using MWCNT-water nanofluid. It had been shown that heat transfer coefficient of the MWCNT nanofluid was much higher than that of water. An analytical method was developed to measure the performance of the U-tube solar collector efficiency and it was found that an increase in the solar radiation in low radiation condition increases the thermal efficiency of the collector.

Amrollahi et. al [34] measured the heat transfer coefficient of functionalized nanofluid under both laminar and turbulent boundary condition through a horizontal tube. It has been reported that in lower temperature heat transfer coefficient in turbulent region is much higher than the heat transfer coefficient in laminar region. The heat transfer coefficient was also found to be 25% more than in the pure water. Arshad et. al [35] studied graphene based nanofluids and their preparation, characterization, transport characteristics and industrial applications. Xuan and Li [36] measured heat transfer coefficient and friction factor of a working fluid in a tube. Here Cu-water nanofluid was used as a working fluid. They investigated convective heat transfer and flow performance of nanofluids in turbulent fluid.

Pak and Cho [37] investigated experimentally the turbulent friction and heat transfer behaviour of dispersed fluids (i.e. ultrafine metallic oxide particles suspended in water) in a circular pipe. Two different metallic oxide particles, γ-alumina (Al_2O_3) and titanium dioxide (TiO_2) with mean diameters of 13 and 27 nm, were used as suspended particles. They found that Nusselt number of the dispersed fluid increases with increasing volume concentration as well as Reynolds number. Frolov et. al [38] studied the effect of salt at different concentrations on carbon nanotube (CNT) which is dispersed in organic solvents such as N-methyl-2-pyrrolidine (NMP). They used Sodium Iodide (NaI) salt to study the mechanism of interaction between salts and CNT surface. They observed that NMP-CNT dispersion becomes less

thermodynamically stable when salt concentration increases. With high salt concentration aggregation of the CNT occurs. Kharisov et. al [68] studied the atomistic simulations of the solubilisation of the single walled Carbon nanotube (SWCNT) in toluene. They investigated the entropy of the toluene and solvation Gibbs free energy for nanotube in toluene. It was found that suspension of SWCNT in toluene is not stable. Walvekar et al. [69] studied thermal stability of CNT/DESs based nanofluid mainly, Methyl-triphenylphosphonium bromide (MTPB) as HBA and choline chloride (ChCl), and ethylene glycol (EG) and triethylene glycol (TEG) as HBD. The incorporation of CNT in DESs improved their thermal stabilities, activation energies, and kinetic characteristics. The observation implies that the thermal stability enhanced from 105 °C and 128 °C to 130 °C and 220 °C for EG and TEG respectively. Mohsenzadeh, et al.[70] also reported enhanced heavy oil recovery using deep eutectic solvents. They conducted core flooded experiment at reservoir condition. Arıkaya, et al. [71] reported DES used in esterification of lactic acid with ethanol.

Lee et. al. [72] reported thermal conductivity of fluids containing oxide nanofluids. They measured thermal conductivity by hot wire transient method. They found that nanofluids containing small amount of nanoparticles have high thermal conductivity than the same liquid without nanoparticles. Fang et. al[73] used phosphonium based Deep Eutectic solvents to study the conductivity and specific heat of the graphene based nanofluids. Different molar ratio of halide salts and HBD were used to synthesis DES. They found thermal conductivity enhancement upto 87% by stable graphene based nanofluids. Specific heat of the nanofluid were also found to increase with increase in temperature and concentration.

1.4 Stability and Thermophysical Properties of Nanofluid

The stability of nanofluids, crucial for better thermal performance, is frequently undermined by electrostatic and van der Waals interactions between nanoparticles and the surrounding liquid [74]**.** Aggregation of nanoparticles is due to the following reasons: (1) the van der Waals attractive forces on the particle surfaces induce attraction among the particles, leading to the formation of clusters of nanoparticles which settle down at the bottom of the vessel and ; (2) the steric and electrostatic repulsion mechanisms of the electrical double layer repulsive force, which tend to separate the particles from one another [75, 76]. Additional causes of instability include the shape and nature of the nanoparticles and the duration of the ultra-sonication process during formulation.

Some of the methods that can evaluate the stability of the nanofluid are sedimentation, spectral absorbency, zeta potential and microscopic observation. To verify stability, sedimentation in the generated nanofluid is monitored using photos taken over a predetermined time period. The primary disadvantage of this approach is a longer observational period. By detecting the absorption of nanofluids using UV–vis spectral analysis, the variation of nanofluid concentration with sedimentation time is reported.

Zeta potential analysis is another common method which uses electrophoretic behaviour [77]. The stabilisation theory [78] states that if zeta potential has a high absolute value, the electrostatic repulsions between the particles increase, which results in enhanced suspension stability. This is because the free charges in the base fluid get attracted to the opposite charges on the particle surface. It forms a layer also known as the stern layer, as shown in the Figure 1.8. The produced stern layer is surrounded by a second layer known as the diffuse layer, which is more diffusive and has its own unique charges. The potential difference between the base fluid and the stern layer in contact with the scattered particles, as depicted in Figure 1.8, is known as the zeta potential. When nanoparticles approach one another, the dominance

The presence of a high repulsive interaction potential is vital for maintaining stability. In cases where the nanofluid possesses a relatively lower magnitude, the van der Waals force gains strength, thereby contributing to the instability of the nanofluid. In order for nanofluids to remain stable, it is imperative for repulsive forces to prevail within the solution. According to Vandsburger [79], nanofluids reach a state of near-stability when their particles have a zeta potential value of about 30 mV. Optimal stability for nanofluids is achieved when the zeta potential value is in proximity to 45 mV. The exceptional stability of a nanofluid is realised when its zeta potential value exceeds ± 60 mV. The accepted zeta potential values are tabulated in table 1.1. By examining the size, shape, and distribution of the nanoparticles, which are often obtained using high magnification electron equipment like TEM and SEM, one can ascertain the accumulation of nanoparticles in the base fluid.

Table 1.1 Summary of zeta potential value

Zeta potential (mV)	Stability
0	Unstable
15	Unstable
30	Moderate stability
45	Good stability, possible settling
60	Very good stability, little settling

Nanofluids have superior thermophysical properties, including thermal conductivity, thermal diffusivity, viscosity, and convective heat transfer coefficients, in comparison to base fluids such as oil or water [80, 81]. Over the past decade, ongoing research has focused on enhancing the thermo-physical properties.

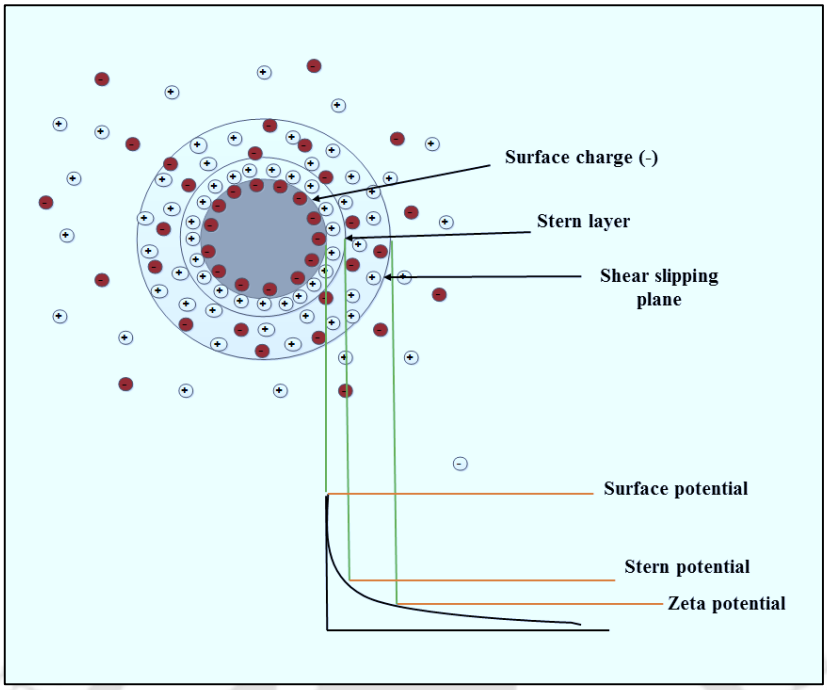

Figure 1.8 Schematic diagram of zeta potential of nanoparticles

1.4.1 Thermal Conductivity

Thermal conductivity is one of the governing parameter of the nanofluid applications. As discussed in the previous section thermal conductivity can be effected by various factors including Brownian motion, nanoparticle size and shape, nanoparticles clustering, type of base fluid, temperature and pH additives [82]. Teng et al. [83] discussed the nanoparticle size effect on thermal conductivity of Al_2O_3/water nanofluid. Experimental results demonstrate the increase in thermal conductivity with decrease in particle size. Alwi et al. [84] group investigated the influence of particle concentration and temperature on thermal conductivity of CuO/R134a nano-refrigerant. Their study reports the increase in thermal conductivity with both temperature and concentration of particles. Vadaz [85] reported thermal conductivity of nanofluid that enhances heat transfer efficiency.

It has been reported that large number of parameters, such as chemical composition of the solid particles, surfactant, particle properties, concentration of nanofluid and poly-

dispersity influences the thermal conductivity. Along with all of these, there are additional factors that can affect thermal conductivity of nanofluid, such as liquid nanolayer development around the nanoparticles, clustering of nanoparticles, and thermophoresis [86]. More significant are the van der Waal attraction forces, which attempt to attract and reduce the surface area of neighbouring carbon tubes, resulting in a reduction in heat conductivity. Munyalo and Zhang [87] reviewed the thermophysical properties of nanofluids based on nanoparticle size. It was found that a larger nanoparticle size decreases the thermal conductivity of the Nanofluid. Zhu et al. [88] reported the stability and improvements in thermal conductivity of Al_2O_3–H_2O nanofluid. It is reported that nanofluids exhibit a strong dependence on pH values. The thermal conductivity is found to enhance with the incorporation of an optimised SDBS dispersant. The outcome of thermal Conductivity exhibited a peak boost at 10.1% at 0.15 wt% suspension of nanoparticles.

Brownian motion is one of the important factor for enhancement of thermal conductivity of nanofluid. Furthermore, with temperature rise, kinetic energy of the nanoparticles increases which results in clustering of the nanoparticles due to the van der Waals attractive force. However, the stability of the nanofluid is affected by the formation of bigger clusters, which lowers its thermal conductivity. Evans et al. [89] conducted both experimental and molecular dynamics simulation of nanofluid and reported significant impact of Brownian motion on thermal conductivity. Thermophoresis is the movement of nanoparticles through the nanofluid under the influenced of thermal gradient [90]. This thermal gradient causes the particles to experience the net force in the direction of decreasing temperature. However, such Brownian motion-based movement results in convective currents that disturb the heat in the nanofluid system and thereby increase the thermal conductivity of nanofluid. Formation of nano layer of liquid around the nanoparticle plays an important role in thermal conductivity enhancement. The layer of liquid formed right next to the nanoparticles is expected to have

thermal conductivity that is comparable to the solid nanoparticle [91]. Along with Brownian motion, clustering and interfacial stacking also aid in heat transfer enhancement. In general, the MWCNT conducts heat energy via the vibrations of individual atoms or molecules. The atomic or molecular vibrational energy of the nanoparticles is referred to as phonons in this context. Thus, heat is transferred through nuclear vibrations via the transmission of phonons rather than electrons. Additionally, the rise in temperature allows for the expansion of the liquid. This thereby promotes the molecule's free mobility, boosting intermolecular collisions and heat transmission through conduction.

1.4.2 Viscosity

Viscosity is the another important property of nanofluid that influence the heat transfer applications as the pressure drop and cost of pumping power directly depends on it. There exists a limited number of papers addressing the rheological behaviour of nanofluids. Kang et al. [92] quantified the viscosities of ultra-dispersed diamond/ethylene glycol, silver/water, and silica/water nanofluids, observing viscosity increase of 50%, 30%, and 20% for UDD/EG, silver/water, and silica/water nanofluids at volume concentrations of 1%, 2%, and 3%, respectively. Prasher et al.[93] demonstrated the viscosity from shear rate in alumina/propylene glycol (PG) nanofluids. They reported the Newtonian characteristics of nanofluids and the increase in viscosity with higher nanoparticle volume concentration. A 30% increase in viscosity was seen at a 3% volume concentration, which was attributed to the aggregation of nanoparticles in the nanofluid, with the aggregates being approximately three times the size of the individual nanoparticles. Einstein was the first to compute the effective viscosity of suspended particles in the base fluid by utilising the phenomenological hydrodynamic equations. Einstein law of viscosity here is given by

$$\frac{\mu}{\mu_{bf}} = (1 + 2.5\varphi) \quad \textbf{(1)}$$

Where μ represents the viscosity of the nanofluid, μ_{bf} denotes the viscosity of the base fluid, and φ signifies the nanoparticle volume fraction. The effective viscosity of nanofluid is influenced by many parameters including, base fluid, nanoparticles concentration, shape and size of the particle, type of particles, temperature and pH. Nguyan et al. [94] examined the effect of temperature and particle volume concentrations on Al_2O_3/water nanofluid. They reported significant decline of viscosity with temperature and increase with particle volume concentrations. In their experiments, an additional factor emerged, known as the critical temperature. When this temperature is exceeded, the behaviour of the particle suspension seems to fluctuate, leading to a hysteresis effect. Kwak and Kim [95] shown that significant gains in heat conductivity are associated by significant increase in viscosity at low (<1%) nanoparticle volume fractions.

1.4.3 Density

Density is a crucial thermophysical characteristic, significantly influencing the evaluation of heat transfer performance in nanofluids. It directly influences the Reynolds number, friction factor, pumping power, pressure loss, and Nusselt number. The experimental investigations on the evaluation of the 'ρ' of nanofluids are insufficient. Consequently, the formulation of empirical correlations for the density (ρ) of nanofluids, considering nanoparticle morphology, base fluid, temperature, and concentration, is crucial for ascertaining precise density values. Pak and Cho used the equation (2) for micrometer size particles for nanometer size particles to calculate density.

$$\rho_{nf} = \varphi\rho_p + (1 - \varphi)\rho_f \quad \textbf{(2)}$$

Pastoriza-Gallego et al. [173] conducted an experimental investigation on three distinct nanofluids including varying concentrations (0.5% to 7% by weight) of Al_2O_3 nanoparticles suspended in water as base fluid. The density was determined at three temperatures mainly, 283.15 K, 298.15 K, and 313.15 K. The impact of smaller particles on volumetric behaviour was more pronounced. The density increases with the concentration of the nanoparticles. Vajjha et al [96] studied the density of alumina (Al_2O_3), antimony-tin-oxide (Sb_2O_5:SnO_2) and zinc oxide (ZnO) nanofluid. Their studies reported 8% variation with equation (2) for ZnO nanofluid, whereas excellent agreement was observed for Al_2O_3 and Sb_2O_5:SnO_2 nanofluid. Khanafer [97] provided a critical synthesis of the variations in the thermophysical characteristics of nanofluids. They established a correlation for the density of Al_2O_3/water nanofluid utilising the experimental data from Ho et al.[98]

1.4.4 Specific heat

Fluids with improved heat capacity are essential for economical and efficient heat transfer operations [74]. It directly correlates the thermal properties and performance of any material. For instance, materials with elevated specific heat capacity demonstrate their potential to store significant amounts of energy. Robertis et al.[59] employed the modulated temperature differential scanning calorimetry (MTDSC) method for the assessment of specific heat, indicating a strong correlation between the measured and tabulated values of the constituent components of nanofluids (ethylene glycol and copper). The findings indicated that, throughout the whole studied temperature range, the presence of copper nanoparticles in the base fluid modifies the properties of the melting and crystallisation processes and lowers the specific heat values of nanofluids. Tiznobaik and Shin [99] used four different sized silicon dioxide nanoparticles dispersed in a molten salt eutectic solvent. The findings indicated that the specific

heat capacity of nanomaterials uniformly increased by 25% as compared to the base fluid, irrespective of the size of the embedded nanoparticles.

1.5 Application of Nanofluid

Nanofluids exhibit superior heat transfer characteristics relative to conventional heat transfer fluids. The current research establishes that nanoparticles are employed to improve the thermal conductivity of base fluids. The increase in effective thermal conductivity is a crucial element for improving the heat transfer of traditional fluids. Nanofluid have shown great potential in many applications which includes, new generation cooling fluid in thermal management systems, in medical applications, antibacterial applications, medical applications, power generations, generation of new sensors, reactors, and transmission system. Figure 1.9 shown some applications of nanofluid.

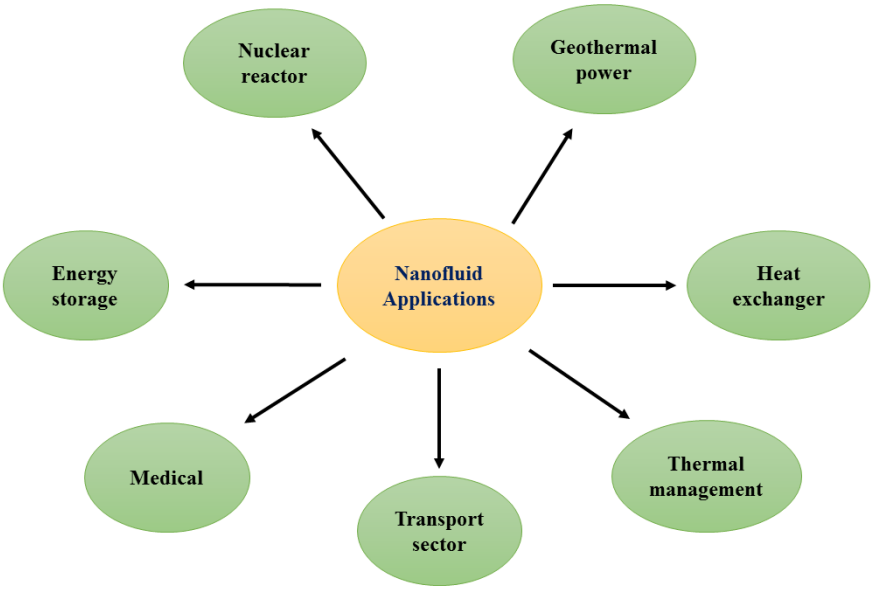

Figure 1.9 Applications of nanofluid [100]

1.6. Deep Eutectic Solvents (DES)

The innovative discovery of DESs, achieved by combining two or more distinct molecules in precise proportions, represents an important step in the field of alternative 'green' solvents [101]. Since its introduction by Abbott et al [101], in 2003 as choline chloride-urea deep eutectic solvent, other classes of deep eutectic solvents have also been discovered by various research groups.

A DES typically consists of two or three inexpensive and secure components that can interact via hydrogen bonds to generate a eutectic mixture. The resulting DES is characterised by melting values that are lower than those of each individual element. DESs typically exhibit considerable freezing point depression, remaining in a liquid condition at ambient temperatures up to 70°C. Figure 1.10 illustrates the binary phase diagram of a combination of A and B at different compositions. This helps us to examine the melting point of the mixture as a function of the mole fractions of the individual components. When mixed, the melting point of the combination progressively declines until it attains a minimum melting point composition known as the 'Deep eutectic point,' resulting in a mixture referred to as a 'deep' eutectic solvent (DES). The deep eutectic point is indicated in Figure 1.10 by the red arrow, where the emergence of a distinct liquid is observable. The most significant decrease in freezing point, ΔT_f, is linked to the eutectic point.

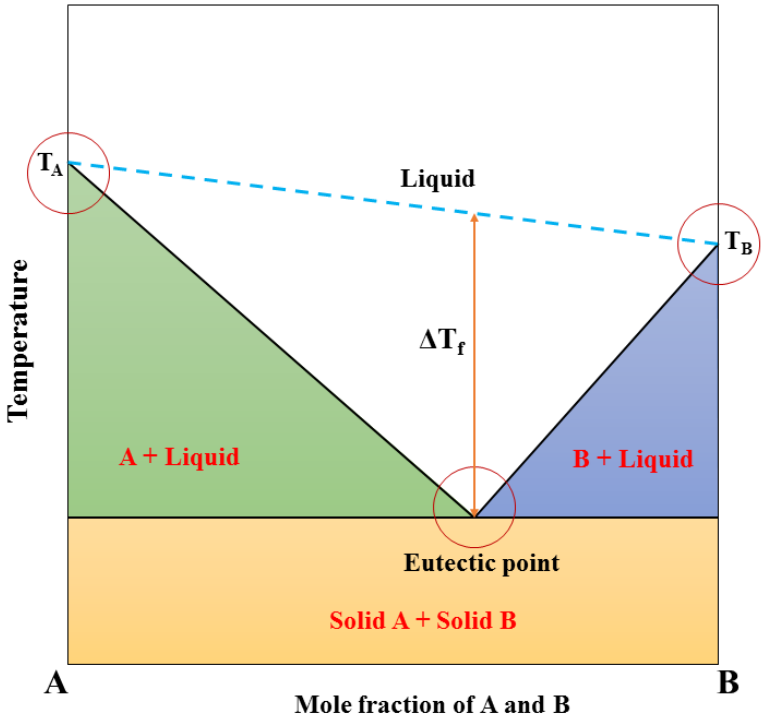

Figure 1.10 Solid-liquid schematic phase diagram of a binary mixture of two compounds A and B showing eutectic behaviour

The composition of the eutectic point is distinct to two compounds and cannot be changed, but one can operate above the eutectic point line depending on need and application and not always at the eutectic point. Based on the characteristics and groups of the precursor materials, four types of DESs (type I, type II, type III, and type IV) have been generally categorised since their creation. Recent research achievements have identified a novel category of deep eutectic solvents (DESs) consisting of non-ionic molecules as precursor components, designated as Type-V DES. This category of DESs predominantly comprises environmentally benign and innocuous substances that are readily available, hence presenting enhanced potential [102]. While it shows a reduction in melting points similar to DESs, it does not involve any ionic interactions. Instead, hydrogen bonding plays a particularly dominant role in this class of DESs[103]. Some of the common HBD and HBA are displayed in table 1.2.

Table 1.2. Classification of deep eutectic solvents

Types	*Formula*	*Terms*	*Example*
Type I	$Cat^+X^-+zMCl_x$	*M=Zn, In, Sn, AI, Fe*	$ChCl+ZnCl_2$
Type II	$Cat^+ X^-$ $+zMClx.yH20$	*M=Cr, Ni, Cu, Fe, Co*	$ChCl+CoCl_2.6H2O$
Type III	$Cat^+X^- +zRZ$	*M=Cr, Ni, Cu, Fe, Co*	*ChCl +U rea*
Type IV	$MCL_x +zRZ$	*M=Zn, AI, and Z=OH,* $CONH_2$	$ZnCl_2$ + *Urea*

Earlier studies predominantly used metal salts and their hydrates, as well as organic salts in conjunction with neutral substances, for the synthesis of deep eutectic solvents (DESs). These materials were favoured due to their cost-effectiveness and ease of manipulation, along with several other appealing characteristics, including low volatility, reduced toxicity, improved biocompatibility and biodegradability, and a non-corrosive nature, all of which were ideal for a solvent [104]. Consequently, the volume of publications has significantly risen in recent years regarding the utilisation of Deep Eutectic Solvents (DESs) across various applications, including metal ion extraction and removal, metal treatment, de-aromatization, desulfurization, denitrification of fuel, extraction of proteins, amino acids, and biomaterials, as well as electrochemistry and heat transfer fluid. Figure 1.11 illustrates the effective application of DESs across various scientific disciplines due to their numerous advantageous solvent properties.

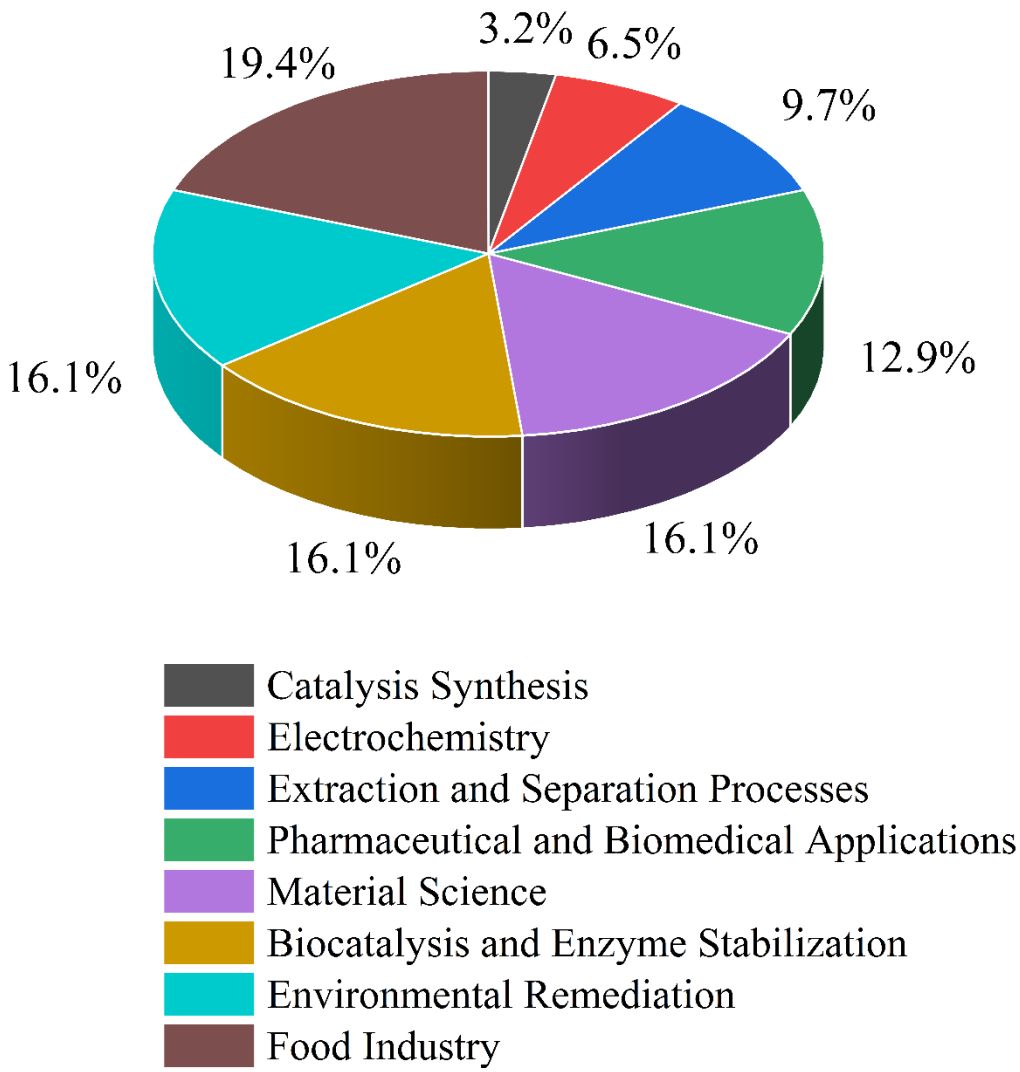

Figure 1.11 Potential applications of DES[105]

DES-based nanofluids exhibit significant potential for diverse applications, particularly in energy, heat transfer, and electrochemical domains, due to their adjustable features, environmental sustainability, and capacity to improve performance when integrated with nanoparticles. A typical preparation process for DES-based nanofluid was developed by Liu et al. [106] using silica nanoparticles and glycerol/ChCl. In this process, 100 ml of DES was mixed with a certain silica nanoparticle mass fraction, agitated for 2 hours at 353 K, then cooled to room temperature. After 2 hours of sonication, the suspension achieved homogeneity and

increased stability for the final nanofluid. Different DESs/carbon nanotube (CNT) nanofluids have been developed by Walvekar et al. [69] using ethylene glycol or triethylene glycol as hydrogen bond donors and methyl-triphenylphosphonium-bromide or choline chloride as hydrogen bond acceptors. It was possible to reduce the freezing points to about 117.9 ^{0}C and raise the thermal stability to 220 ^{0}C. Using molecular dynamics modelling, Jahanbakhsh-Bonab et al. [107] examined the structural and dynamical characteristics of DESs/boron nitride nanotube nanofluid. It was found that an increase in nanofluid viscosity is caused by a decrease in the diffusion coefficient of DESs species. The configuration and quantity of DESs species inside nanotubes are influenced by the diameter of the nanotube.

Dehury et al. [108] used Al_2O_3 nanoparticles dispersed in a DES which was generated by using triphenylphosphonium bromide and ethylene glycol based. They studied and examined the thermophysical properties of nanofluid at different temperature range. The outcome shows that the 1 wt% Al_2O_3 nanofluid's thermal conductivity is almost eight times greater than that of the base DESs. Using TEG and EG as HBDs and ChCl and MTPB as halide salts in varying molar ratios, Chen et al. [109] developed 33 distinct DESs. Stable nanofluids were produced by suspending carbon nanotubes (CNTs) in DESs at concentrations of 0.01–0.08 weight percent using sonication. To determine the stability of nanofluids, both visual observation and UV spectroscopy were utilised. Investigations showed that whereas CNT dispersed in DES consisting of EG and ammonium salt was stable for one day, the produced nanofluids with DES composed of EG and phosphonium salt that were stable for three days.

Another variety namely natural deep eutectic solvents (NADESs) were identified as the primary subclass of deep eutectic solvents (DES). The solubility of biomolecules (e.g., albumin, starch, and DNA) in NADESs surpasses that in water. Furthermore, they possess the capability to serve as extraction media for bioactive compounds. The HBDs and HBAs are

selected for the formulation of NADESs based on the following categories: organic acids, alcohols, sugars, ChCl, and amino acids [110]. Owing to its natural nature, it can be asserted that NADESs possess greater eco-labelling than other DESs.

Table 1.3. Some common examples of HBD and HBA

Hydrogen bond acceptor (HBA)	Hydrogen bond donor (HBD)
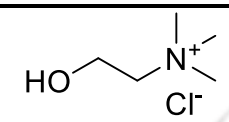 Choline chloride	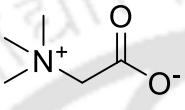 Betaine
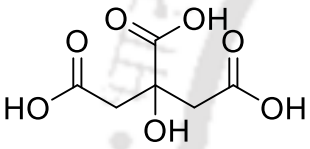 citric acid	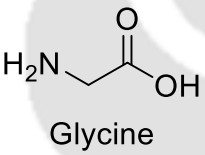 Glycine
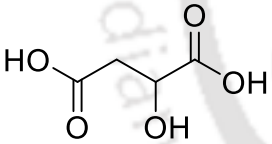 DL-Malic acid	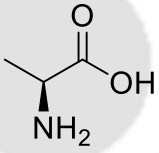 Alanine
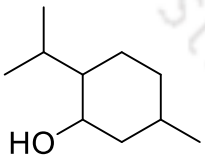 Menthol	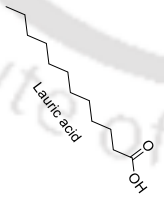
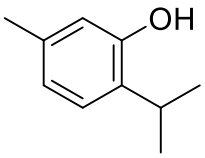 Thymol	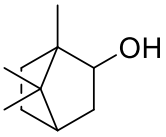 Borneol

Hydrogen bond donor (HBD)	
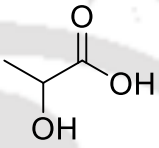 Lactic acid	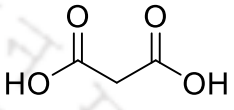 Malonic acid
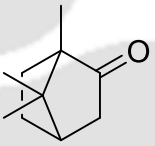 camphor	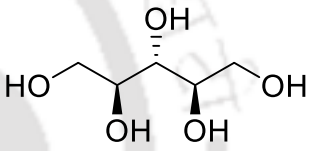 Adonitol
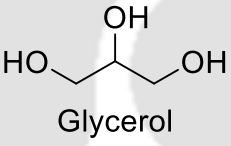 Glycerol	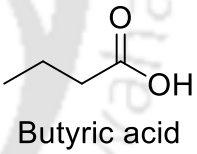 Butyric acid
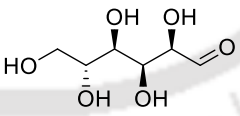 Glucose	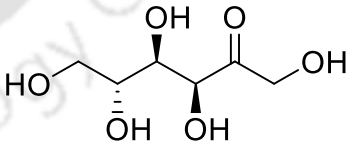 Fructose
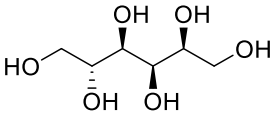 Sorbitol	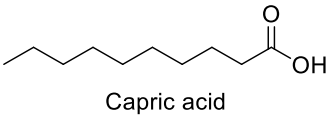 Capric acid

1.7 Physiochemical Properties of DES

Due to its environment friendly nature, some of the DES makes more suitable application in the field of green technology [111]. The physiochemical properties of DES depends on the nature of the HBD and HBA. Therefore, the physical properties of DES changes accordingly with the molar ratio of the HBA and HBD [112]. The physical properties of DES including density, viscosity, specific heat and thermal conductivity governs their applications [113]. According to Abott et al. [19], there is some lattice energy that controls the DES formation and it describes the interaction between HBD and HBA.

The effect of molar composition on the formation of DES has been studied by many researchers. Hayyan et al. [114] reported the effect of molar composition on the properties of ChCl and D-glucose. They have reported lower viscosity at ideal composition. Ibrahim et al. [115] varied the HBA salts paired with ethylene glycol, and compiled the physical property data at their respective eutectic values for different DES. Thus the eutectic point is the key parameter that characterize the DES and denotes the melting point of the system.

Viscosity is another important transport property of fluid, which describe the resistance of the fluid at a given share rate. This indicates that fluids with low viscosities flow effortlessly, whereas liquids with larger viscosities demonstrate sluggish, syrupy flow characteristics. Most of the DES have reported high viscosity at room temperature [112]. The presence of a comprehensive hydrogen bond network, along with van der Waals and electrostatic interactions between hydrogen bond donors and acceptors in DES, results in elevated viscosity and reduced ionic mobility within the limited void space of the liquid DES [116]. The viscosities of DESs have reported unmanageably high levels, complicating their practical utilisation in commercial applications and rendering them costlier than alternative solutions. Cui et al reported the viscosity measurement of ChCl based DES. They have fit their viscosity data with VFT (Vogel−Fulcher−Tammann equation) [117] and Arrhenius equation [118]. Mjalli et al. [119]

reported two empirical viscosity models derived from the VFT model of ChCl-based DES and compared the accuracy of the models to experimental values. Their findings indicate that the VFT-based empirical models are best suited for higher viscosity DES and closely match the experimental values. Abbott et al. [120] have indicated the fact that the viscosity of DESs composed of choline chloride and glycerol diminishes with the incorporation of organic salts. This is attributed to the significant decrease in glycerol viscosity resulting from the partial disruption of its hydrogen bond network.

The molecular packing and organisation of DESs, as well as the presence of holes and vacancies in the liquid DESs, influence their density. Because there is a big hole within the acetylcholine chloride, the density of the urea/choline chloride system is higher than that of urea/acetylcholine chloride [112]. The various molecule configurations in DES may be the cause of their density differences. The Hole theory can be used to understand the variation in DES density with regard to different parameters [121]. The density increases with a decrease in hole radius [116]. The density of DES can be altered by choosing the type and ratio of HBA and HBD.

One of the key physical properties of DESs is their specific heat capacity. The heat capacities of deep eutectic solvents (DESs) are significant, as most chemical engineering operations involve them, including the generation or transfer of heat, such as reactors or separation units [122]. The surface tension of DESs is another significant physical parameter that demonstrates the impact of molecular structure on the interaction strength between the HBA and HBD in DES mixtures. The surface tension of these solvents is significantly affected by the intermolecular interactions between HBAs and HBDs, which are essential for the formation of the DES mixture. The literature on surface tension of DES is quite limited as compared to the other thermophysical properties. The surface tension of DES shows high value for the viscous DES. The values of surface tension generally vary from 35 to 75 mN/m at room

temperature [123]. This physical property is crucial in various industries, including microfluidics, surface science, pharmaceuticals, and separation processes. The property is essential for defining and understanding fluid behaviour in applications that involve the mixing or pumping of multiple fluids [124].

1.8 Objective of the Thesis

The objective of the thesis is to examine the thermophysical characteristics, stability, and thermal performance of carbon-based nanoparticles in conjunction with Deep Eutectic Solvents (DES) and bio-based solvents for thermal management system applications. Computational studies are also essential to confirm experimental findings and enhance the understanding of the interaction mechanisms between fluids and nanoparticles. Consequently, this thesis examines both experimental and theoretical insights. In light of the current literature and identified research gap, the following objectives have been formulated for the thesis:

A) Formulation of bio-based solvent with pristine and functionalized multi-walled carbon nanotubes, and the determination of thermophysical properties of base fluid and nanofluid

B) Synthesis of Deep Eutectic Solvent (DES) and Natural Deep Eutectic Solvent(NADES)based on hybrid carbon based nanoparticles (Multi walled carbon nanotube and graphene oxide)

C) Preparation of different volume fractions of DES and NADES based nanofluid and measurement of their thermophysical properties at different temperature range

D) Evaluation of thermal parameters of nanofluids in forced convention regime at laminar and turbulent condition

E) Process Simulation of nanofluids as a thermic fluid in multistage flash desalination process

1.9 Outline of the Thesis

The current thesis is organised into following chapters

Chapter 2 investigate the potential applications of bio solvent based nanofluid as heat transfer media. Dihydrolevoglycosenone, commercially known as Cyrene, can be used as a thermal base media, dispersed with Multi-Walled Carbon Nanotube (MWCNT) and carboxyl functionalised MWCNT in order to synthesize bio-nanofluid. Thermophysical properties of bio-nanofluid including density, viscosity, specific heat and thermal conductivity has been measured at different temperature range. To better understand the DES-nanoparticle interactions, a molecular level investigation involving DFT (Density Functional Theory) and molecular dynamic (MD) simulation has been done and results were analyzed with experimental studies. This chapter has explored the possibilities of bio solvent-based nanofluids as heat transfer media for thermal energy storage. Due to the low stability behaviour of bio nanofluid, we have formulated the selection of different DESs and NADESs for heat transfer application in the subsequent chapter.

In **Chapter 3**, Methyl triphenyl phosphonium bromide (MTPB) and ethylene glycol (EG) are used as HBA and HBD to synthesis type III deep eutectic solvent (DES). Thereafter the thermophysical properties of prepared DES were measured. Nanofluid was synthesized by dispersing multi-walled carbon nanotube (MWCNT) using two step method. Furthermore, the thermophysical properties and the stability of nanofluid were determined at different temperatures. Thereafter MD simulation were used to predict the thermal conductivity of base fluid which was also validated by experimental data. To understanding the effect of nanoparticles on DES based application, Graphene oxide nanoparticles was thereafter selected to study the efficiency of nanofluid which is discussed in the next chapter.

Chapter 4 focuses on amine functionalised graphene oxide nanoparticles. Here, graphene oxide nanoparticles were functionalized by applying different chemical methods and dispersed in the specifically prepared DES comprising of diphenyl ether and DL menthol as hydrogen bond donor (HBD) and hydrogen bond acceptor (HBA) respectively. Thereafter, physical properties and stability analysis were adopted to further investigate the potential of the nanofluid. Furthermore, the nanofluid was used in a brine recirculation multistage flash desalination where the Gained Output ratio (GOR) was evaluated through process simulation.

Chapter 5 delves into alternative type of deep eutectic solvent, where the constituents occur naturally, thereby promoting its potential use as a heat transfer medium. D**L**-menthol and dodecanoic acid, commonly known as lauric acid, were used as the hydrogen bond acceptor (HBA) and hydrogen bond donor (HBD) to synthesize a natural deep eutectic solvent (NADES)-based nanofluid. Additionally, the chapter focuses on the thermal behaviour of the prepared nanofluid under both turbulent and laminar regimes. To understand the molecular mechanisms of NADES with nanoparticles, density functional theory (DFT) was employed. Computational analysis revealed the interaction energies within the fluid-particle system, which was demonstrated through stability analysis**. Chapter 6** concludes with a summary of the principal results of this thesis and a discussion of prospective directions for future research.

References

1. Lewis, N.S., et al., *Basic research needs for solar energy utilization. report of the basic energy sciences workshop on solar energy utilization, april 18-21, 2005*. 2005, DOESC (USDOE Office of Science (SC)).
2. Khanafer, K. and K. Vafai, *A review on the applications of nanofluids in solar energy field.* Renewable Energy, 2018. **123**: p. 398-406.
3. Rajgor, G., *Greater acceleration of renewables required to meet COP21 goal.* Renewable Energy Focus, 2016. **17**(5): p. 175-177.
4. Ghalandari, M., et al., *Applications of nanofluids containing carbon nanotubes in solar energy systems: A review.* Journal of Molecular Liquids, 2020. **313**: p. 113476.
5. Ali, M.T., H.E. Fath, and P.R. Armstrong, *A comprehensive techno-economical review of indirect solar desalination.* Renewable and Sustainable Energy Reviews, 2011. **15**(8): p. 4187-4199.
6. Hossain, M., et al., *A state-of-the-art review of hydropower in Malaysia as renewable energy: Current status and future prospects.* Energy strategy reviews, 2018. **22**: p. 426-437.
7. Lawal, D.U., M.A. Antar, and A.E. Khalifa, *Integration of a MSF desalination system with a HDH system for brine recovery.* Sustainability, 2021. **13**(6): p. 3506.
8. Shahzad, M.W., et al., *Energy-water-environment nexus underpinning future desalination sustainability.* Desalination, 2017. **413**: p. 52-64.
9. Gude, V.G. and V. Fthenakis, *Energy efficiency and renewable energy utilization in desalination systems.* Progress in Energy, 2020. **2**(2): p. 022003.
10. Rabiee, H., et al., *Energy-water nexus: renewable-integrated hybridized desalination systems.* Polygeneration with polystorage for chemical and energy hubs, 2019: p. 409-458.

11. Feria-Díaz, J.J., et al., *Commercial thermal technologies for desalination of water from renewable energies: a state of the art review.* Processes, 2021. **9**(2): p. 262.

12. Al-Wazzan, Y. and F. Al-Modaf, *Seawater desalination in Kuwait using multistage flash evaporation technology—historical overview.* Desalination, 2001. **134**(1-3): p. 257-267.

13. El-Dessouky, H.T., H.M. Ettouney, and Y. Al-Roumi, *Multi-stage flash desalination: present and future outlook.* Chemical Engineering Journal, 1999. **73**(2): p. 173-190.

14. Malik, A.U., T. Prakash, and I. Andijani, *Failure evaluation in desalination plants—some case studies.* Desalination, 1996. **105**(3): p. 283-295.

15. Al Sum, E., et al., *Vapour-side corrosion of copper base condenser tubes of the MSF desalination plants of Abu Dhabi.* Desalination, 1994. **97**(1-3): p. 109-119.

16. Kabeel, A., Z. Omara, and F. Essa, *Enhancement of modified solar still integrated with external condenser using nanofluids: An experimental approach.* Energy conversion and management, 2014. **78**: p. 493-498.

17. Omara, Z., A. Kabeel, and F. Essa, *Effect of using nanofluids and providing vacuum on the yield of corrugated wick solar still.* Energy conversion and management, 2015. **103**: p. 965-972.

18. Otanicar, T.P., et al., *Nanofluid-based direct absorption solar collector.* Journal of renewable and sustainable energy, 2010. **2**(3): p. 033102.

19. Bortolato, M., et al., *Investigation of a single wall carbon nanohorn-based nanofluid in a full-scale direct absorption parabolic trough solar collector.* Energy conversion and management, 2017. **150**: p. 693-703.

20. El-Dessouky, H., H.I. Shaban, and H. Al-Ramadan, *Steady-state analysis of multi-stage flash desalination process.* Desalination, 1995. **103**(3): p. 271-287.

21. Garg, K., et al., *Performance evaluation of a brine-recirculation multistage flash desalination system coupled with nanofluid-based direct absorption solar collector.* Renewable Energy, 2018. **122**: p. 140-151.

22. Duangthongsuk, W. and S. Wongwises, *An experimental study on the heat transfer performance and pressure drop of TiO2-water nanofluids flowing under a turbulent flow regime.* International journal of heat and mass transfer, 2010. **53**(1-3): p. 334-344.

23. Gupta, M., et al., *A review on thermophysical properties of nanofluids and heat transfer applications.* Renewable and Sustainable Energy Reviews, 2017. **74**: p. 638-670.

24. Devendiran, D.K. and V.A. Amirtham, *A review on preparation, characterization, properties and applications of nanofluids.* Renewable and Sustainable Energy Reviews, 2016. **60**: p. 21-40.

25. Wong, K.V. and O. De Leon, *Applications of nanofluids: current and future.* Advances in mechanical engineering, 2010. **2**: p. 519659.

26. Maier-Hauff, K., et al., *Intracranial thermotherapy using magnetic nanoparticles combined with external beam radiotherapy: results of a feasibility study on patients with glioblastoma multiforme.* Journal of neuro-oncology, 2007. **81**: p. 53-60.

27. Lapotko, D., *Plasmonic nanoparticle-generated photothermal bubbles and their biomedical applications.* Nanomedicine, 2009. **4**(7): p. 813-845.

28. Kulkarni, D.P., D.K. Das, and R.S. Vajjha, *Application of nanofluids in heating buildings and reducing pollution.* Applied Energy, 2009. **86**(12): p. 2566-2573.

29. Burnett, M.E. and S.Q. Wang, *Current sunscreen controversies: a critical review.* Photodermatology, photoimmunology & photomedicine, 2011. **27**(2): p. 58-67.

30. Vekas, L., D. Bica, and M.V. Avdeev, *Magnetic nanoparticles and concentrated magnetic nanofluids: Synthesis, properties and some applications.* China particuology, 2007. **5**(1-2): p. 43-49.

31. Nafey, A., et al., *Solar desalination using humidification dehumidification processes. Part I. A numerical investigation.* Energy conversion and management, 2004. **45**(7-8): p. 1243-1261.

32. Sabiha, M., et al., *Energy performance of an evacuated tube solar collector using single walled carbon nanotubes nanofluids.* Energy Conversion and Management, 2015. **105**: p. 1377-1388.

33. Tong, Y., J. Kim, and H. Cho, *Effects of thermal performance of enclosed-type evacuated U-tube solar collector with multi-walled carbon nanotube/water nanofluid.* Renewable energy, 2015. **83**: p. 463-473.

34. Amrollahi, A., et al., *Convection heat transfer of functionalized MWNT in aqueous fluids in laminar and turbulent flow at the entrance region.* International Communications in Heat and Mass Transfer, 2010. **37**(6): p. 717-723.

35. Arshad, A., et al., *A review on graphene based nanofluids: Preparation, characterization and applications.* Journal of Molecular Liquids, 2019. **279**: p. 444-484.

36. Li, Q. and Y. Xuan, *Convective heat transfer and flow characteristics of Cu-water nanofluid.* Science in China Series E: Technolgical Science, 2002. **45**(4): p. 408-416.

37. Pak, B.C. and Y.I. Cho, *Hydrodynamic and heat transfer study of dispersed fluids with submicron metallic oxide particles.* Experimental Heat Transfer an International Journal, 1998. **11**(2): p. 151-170.

38. Frolov, A.I., et al., *Molecular mechanisms of salt effects on carbon nanotube dispersions in an organic solvent (N-methyl-2-pyrrolidone).* Chemical science, 2012. **3**(2): p. 541-548.

39. Kong, L., J. Sun, and Y. Bao, *Preparation, characterization and tribological mechanism of nanofluids.* Rsc Advances, 2017. **7**(21): p. 12599-12609.

40. Suresh, S., et al., *Synthesis of Al2O3–Cu/water hybrid nanofluids using two step method and its thermo physical properties.* Colloids and Surfaces A: Physicochemical and Engineering Aspects, 2011. **388**(1-3): p. 41-48.

41. Salari, E., et al., *Thermal behaviour of aqueous iron oxide nano-fluid as a coolant on a flat disc heater under the pool boiling condition.* Heat and Mass Transfer, 2017. **53**: p. 265-275.

42. Chakraborty, S. and P. Kumar, *Nanofluids Long-term Stability Challenges and Guidelines.* 2022.

43. Fedele, L., et al., *Experimental stability analysis of different water-based nanofluids.* Nanoscale research letters, 2011. **6**: p. 1-8.

44. Murshed, S., K. Leong, and C. Yang, *Enhanced thermal conductivity of TiO2—water based nanofluids.* International Journal of thermal sciences, 2005. **44**(4): p. 367-373.

45. Masuda, H., et al., *Alteration of Thermal Conductivity and Viscosity of Liquid by Dispersing Ultra-Fine Particles. Dispersion of Al2O3, SiO2 and TiO2 Ultra-Fine Particles.* Netsu Bussei, 1993. **7**(4): p. 227-233.

46. Rashmi, W., et al., *Investigating corrosion effects and heat transfer enhancement in smaller size radiators using CNT-nanofluids.* Journal of materials science, 2014. **49**: p. 4544-4551.

47. Ray, D.R. and D.K. Das, *Superior performance of nanofluids in an automotive radiator.* Journal of Thermal Science and Engineering Applications, 2014. **6**(4): p. 041002.

48. Sidik, C., et al., *Computational analysis of nanofluids in vehicle radiator.* Applied Mechanics and Materials, 2015. **695**: p. 539-543.

49. Paul, G., et al., *Synthesis, characterization, and thermal property measurement of nano-Al95Zn05 dispersed nanofluid prepared by a two-step process.* International Journal of Heat and Mass Transfer, 2011. **54**(15-16): p. 3783-3788.

50. Kole, M. and T. Dey, *Effect of aggregation on the viscosity of copper oxide–gear oil nanofluids.* International Journal of Thermal Sciences, 2011. **50**(9): p. 1741-1747.

51. Saeedinia, M., M. Akhavan-Behabadi, and P. Razi, *Thermal and rheological characteristics of CuO–Base oil nanofluid flow inside a circular tube.* International Communications in Heat and Mass Transfer, 2012. **39**(1): p. 152-159.

52. Mahian, O., et al., *A review of the applications of nanofluids in solar energy.* International Journal of Heat and Mass Transfer, 2013. **57**(2): p. 582-594.

53. Asadi, A., et al., *An experimental investigation on the effects of ultrasonication time on stability and thermal conductivity of MWCNT-water nanofluid: Finding the optimum ultrasonication time.* Ultrasonics sonochemistry, 2019. **58**: p. 104639.

54. Haghighi, E., et al., *Shelf stability of nanofluids and its effect on thermal conductivity and viscosity.* Measurement Science and Technology, 2013. **24**(10): p. 105301.

55. Mahbubul, I., et al., *Stability, thermophysical properties and performance assessment of alumina–water nanofluid with emphasis on ultrasonication and storage period.* Powder Technology, 2019. **345**: p. 668-675.

56. Mahbubul, I., et al., *Optimization of ultrasonication period for better dispersion and stability of TiO2–water nanofluid.* Ultrasonics sonochemistry, 2017. **37**: p. 360-367.

57. Shahrul, I., et al., *A comparative review on the specific heat of nanofluids for energy perspective.* Renewable and sustainable energy reviews, 2014. **38**: p. 88-98.

58. Xie, H., et al., *Thermal conductivity enhancement of suspensions containing nanosized alumina particles.* Journal of applied physics, 2002. **91**(7): p. 4568-4572.

59. De Robertis, E., et al., *Application of the modulated temperature differential scanning calorimetry technique for the determination of the specific heat of copper nanofluids.* Applied Thermal Engineering, 2012. **41**: p. 10-17.

60. Saeedinia, M., M. Akhavan-Behabadi, and M. Nasr, *Experimental study on heat transfer and pressure drop of nanofluid flow in a horizontal coiled wire inserted tube under constant heat flux.* Experimental Thermal and Fluid Science, 2012. **36**: p. 158-168.

61. Sekhar, Y.R. and K. Sharma, *Study of viscosity and specific heat capacity characteristics of water-based Al2O3 nanofluids at low particle concentrations.* Journal of experimental Nanoscience, 2015. **10**(2): p. 86-102.

62. Shin, D. and D. Banerjee, *Enhancement of specific heat capacity of high-temperature silica-nanofluids synthesized in alkali chloride salt eutectics for solar thermal-energy storage applications.* International journal of heat and mass transfer, 2011. **54**(5-6): p. 1064-1070.

63. Vajjha, R.S. and D.K. Das, *Specific heat measurement of three nanofluids and development of new correlations.* Journal of heat transfer, 2009. **131**(7).

64. Xuan, Y. and W. Roetzel, *Conceptions for heat transfer correlation of nanofluids.* International Journal of heat and Mass transfer, 2000. **43**(19): p. 3701-3707.

65. Zhou, S.-Q. and R. Ni, *Measurement of the specific heat capacity of water-based Al 2 O 3 nanofluid.* Applied Physics Letters, 2008. **92**(9): p. 093123.

66. Abbott, A.P., et al., *Preparation of novel, moisture-stable, Lewis-acidic ionic liquids containing quaternary ammonium salts with functional side chainsElectronic supplementary information (ESI) available: plot of conductivity vs. temperature for the ionic liquid formed from zinc chloride and choline chloride (2∶1). See http://www. rsc. org/suppdata/cc/b1/b106357j.* Chemical Communications, 2001(19): p. 2010-2011.

67. Chen, Y. and T. Mu, *Application of deep eutectic solvents in biomass pretreatment and conversion.* Green Energy & Environment, 2019. **4**(2): p. 95-115.

68. Kharisov, B.I., O.V. Kharissova, and A.V. Dimas, *The dispersion, solubilization and stabilization in "solution" of single-walled carbon nanotubes.* RSC advances, 2016. **6**(73): p. 68760-68787.

69. Walvekar, R., et al., *Deep eutectic solvents-based CNT nanofluid–A potential alternative to conventional heat transfer fluids.* Journal of the Taiwan Institute of Chemical Engineers, 2021. **128**: p. 314-326.

70. Mohsenzadeh, A., et al., *The novel use of deep eutectic solvents for enhancing heavy oil recovery.* Journal of Petroleum Science and Engineering, 2015. **130**: p. 6-15.

71. Arıkaya, A., A.E. Ünlü, and S. Takaç, *Use of deep eutectic solvents in the enzyme catalysed production of ethyl lactate.* Process Biochemistry, 2019. **84**: p. 53-59.

72. Lee, S., et al., *Measuring thermal conductivity of fluids containing oxide nanoparticles.* 1999.

73. Fang, Y., et al., *Synthesis and thermo-physical properties of deep eutectic solvent-based graphene nanofluids.* Nanotechnology, 2016. **27**(7): p. 075702.

74. Dey, D., P. Kumar, and S. Samantaray, *A review of nanofluid preparation, stability, and thermo-physical properties.* Heat Transfer—Asian Research, 2017. **46**(8): p. 1413-1442.

75. Bushehri, M.K., A. Mohebbi, and H.H. Rafsanjani, *Prediction of thermal conductivity and viscosity of nanofluids by molecular dynamics simulation.* Journal of Engineering Thermophysics, 2016. **25**: p. 389-400.

76. Hong, J. and D. Kim, *Effects of aggregation on the thermal conductivity of alumina/water nanofluids.* Thermochimica acta, 2012. **542**: p. 28-32.

77. Lee, D., J.-W. Kim, and B.G. Kim, *A new parameter to control heat transport in nanofluids: surface charge state of the particle in suspension.* The Journal of Physical Chemistry B, 2006. **110**(9): p. 4323-4328.

78. Daungthongsuk, W. and S. Wongwises, *A critical review of convective heat transfer of nanofluids.* Renewable and sustainable energy reviews, 2007. **11**(5): p. 797-817.

79. Vandsburger, L., *Synthesis and covalent surface modification of carbon nanotubes for preparation of stabilized nanofluid suspensions.* 2009.

80. Das, S.K., S.U. Choi, and H.E. Patel, *Heat transfer in nanofluids—a review.* Heat transfer engineering, 2006. **27**(10): p. 3-19.

81. Wickramasinghe, K., et al., *Green Metalworking Fluids for sustainable machining applications: A review.* Journal of Cleaner Production, 2020. **257**: p. 120552.

82. Kumar, L.H., et al., *A review of recent advances in green nanofluids and their application in thermal systems.* Chemical Engineering Journal, 2022. **429**: p. 132321.

83. Teng, T.-P., et al., *The effect of alumina/water nanofluid particle size on thermal conductivity.* Applied Thermal Engineering, 2010. **30**(14-15): p. 2213-2218.

84. Alawi, O.A. and N.A.C. Sidik, *Influence of particle concentration and temperature on the thermophysical properties of CuO/R134a nanorefrigerant.* International Communications in Heat and Mass Transfer, 2014. **58**: p. 79-84.

85. Vadasz, P., *Heat conduction in nanofluid suspensions.* 2006.

86. Patel, J., et al., *A minireview on nanofluids for automotive applications: Current status and future perspectives.* Applied Thermal Engineering, 2022: p. 119428.

87. Munyalo, J.M. and X. Zhang, *Particle size effect on thermophysical properties of nanofluid and nanofluid based phase change materials: A review.* Journal of Molecular Liquids, 2018. **265**: p. 77-87.

88. Zhu, D., et al., *Dispersion behaviour and thermal conductivity characteristics of Al2O3–H2O nanofluids.* Current Applied Physics, 2009. **9**(1): p. 131-139.

89. Evans, W., J. Fish, and P. Keblinski, *Role of Brownian motion hydrodynamics on nanofluid thermal conductivity.* Applied physics letters, 2006. **88**(9).

90. Durgaprasad, P., et al., *Combined effects of Brownian motion and thermophoresis parameters on three-dimensional (3D) Casson nanofluid flow across the porous layers slendering sheet in a suspension of graphene nanoparticles.* Neural Computing and Applications, 2019. **31**(10): p. 6275-6286.

91. Jang, S.P. and S.U. Choi, *Role of Brownian motion in the enhanced thermal conductivity of nanofluids.* Applied physics letters, 2004. **84**(21): p. 4316-4318.

92. Kang, H.U., S.H. Kim, and J.M. Oh, *Estimation of thermal conductivity of nanofluid using experimental effective particle volume.* Experimental Heat Transfer, 2006. **19**(3): p. 181-191.

93. Prasher, R., et al., *Measurements of nanofluid viscosity and its implications for thermal applications.* Applied physics letters, 2006. **89**(13).

94. Nguyen, C., et al., *Viscosity data for Al2O3–water nanofluid—hysteresis: is heat transfer enhancement using nanofluids reliable?* International journal of thermal sciences, 2008. **47**(2): p. 103-111.

95. Kwak, K.-Y. and C.-Y. Kim, *Viscosity and thermal conductivity of copper oxide nanofluid dispersed in ethylene glycol.* Korea-Australia Rheology Journal, 2005. **17**(2): p. 35-40.

96. Vajjha, R., D. Das, and B. Mahagaonkar, *Density measurement of different nanofluids and their comparison with theory.* Petroleum Science and Technology, 2009. **27**(6): p. 612-624.

97. Khanafer, K. and K. Vafai, *A critical synthesis of thermophysical characteristics of nanofluids,* in *Nanotechnology and energy*. 2017, Jenny Stanford Publishing. p. 279-332.

98. Ho, C., et al., *Natural convection heat transfer of alumina-water nanofluid in vertical square enclosures: An experimental study.* International Journal of Thermal Sciences, 2010. **49**(8): p. 1345-1353.

99. Tiznobaik, H. and D. Shin, *Enhanced specific heat capacity of high-temperature molten salt-based nanofluids.* International Journal of Heat and Mass Transfer, 2013. **57**(2): p. 542-548.

100. Younes, H., et al., *Nanofluids: Key parameters to enhance thermal conductivity and its applications.* Applied Thermal Engineering, 2022. **207**: p. 118202.

101. Abbott, A.P., et al., *Novel solvent properties of choline chloride/urea mixtures.* Chemical communications, 2003(1): p. 70-71.

102. Naik, P.K., et al., *Deep Eutectic Solvents in Liquid-liquid Extraction: Correlation and Molecular Dynamics Simulation*. 2022: CRC Press.

103. Abranches, D.O., et al., *Phenolic hydrogen bond donors in the formation of non-ionic deep eutectic solvents: the quest for type V DES.* Chemical Communications, 2019. **55**(69): p. 10253-10256.

104. Abbott, A.P., et al., *Ionic liquid analogues formed from hydrated metal salts.* Chemistry–A European Journal, 2004. **10**(15): p. 3769-3774.

105. Smith, E.L., A.P. Abbott, and K.S. Ryder, *Deep eutectic solvents (DESs) and their applications.* Chemical reviews, 2014. **114**(21): p. 11060-11082.

106. Liu, C., et al., *Novel silica filled deep eutectic solvent based nanofluids for energy transportation.* ACS Sustainable Chemistry & Engineering, 2019. **7**(24): p. 20159-20169.

107. Jahanbakhsh-Bonab, P., et al., *Exploring the structural and transport properties of glyceline DES-Based boron nitride nanotube Nanofluid: The effects of nanotube diameter.* Journal of Molecular Liquids, 2021. **341**: p. 117277.

108. Dehury, P., A.K. Upadhyay, and T. Banerjee, *Evaluation and conceptual design of triphenylphosphonium bromide-based deep eutectic solvent as novel thermal nanofluid for concentrated solar power.* Bulletin of Materials Science, 2019. **42**(6): p. 262.

109. Chen, Y.Y., et al., *Stability and thermophysical studies on deep eutectic solvent based carbon nanotube nanofluid.* Materials Research Express, 2017. **4**(7): p. 075028.

110. Savi, L.K., et al., *Influence of temperature, water content and type of organic acid on the formation, stability and properties of functional natural deep eutectic solvents.* Fluid Phase Equilibria, 2019. **488**: p. 40-47.

111. Liu, Y., et al., *Natural deep eutectic solvents: properties, applications, and perspectives.* Journal of natural products, 2018. **81**(3): p. 679-690.

112. Omar, K.A. and R. Sadeghi, *Physicochemical properties of deep eutectic solvents: A review.* Journal of Molecular Liquids, 2022. **360**: p. 119524.

113. Qin, H., et al., *Overview of acidic deep eutectic solvents on synthesis, properties and applications.* Green Energy & Environment, 2020. **5**(1): p. 8-21.

114. Hayyan, A., et al., *Glucose-based deep eutectic solvents: Physical properties.* Journal of Molecular Liquids, 2013. **178**: p. 137-141.

115. Ibrahim, R.K., et al., *Physical properties of ethylene glycol-based deep eutectic solvents.* Journal of Molecular Liquids, 2019. **276**: p. 794-800.

116. Zhang, Q., et al., *Deep eutectic solvents: syntheses, properties and applications.* Chemical Society Reviews, 2012. **41**(21): p. 7108-7146.

117. Fulcher, G.S., *Analysis of recent measurements of the viscosity of glasses.* Journal of the American Ceramic Society, 1925. **8**(6): p. 339-355.

118. Yadav, A., et al., *Densities and dynamic viscosities of (choline chloride+ glycerol) deep eutectic solvent and its aqueous mixtures in the temperature range (283.15–363.15) K.* Fluid Phase Equilibria, 2014. **367**: p. 135-142.

119. Mjalli, F.S. and J. Naser, *Viscosity model for choline chloride-based deep eutectic solvents.* Asia-Pacific Journal of Chemical Engineering, 2015. **10**(2): p. 273-281.

120. Abbott, A.P., et al., *Glycerol eutectics as sustainable solvent systems.* Green Chemistry, 2011. **13**(1): p. 82-90.

121. Abbott, A.P., *Application of hole theory to the viscosity of ionic and molecular liquids.* ChemPhysChem, 2004. **5**(8): p. 1242-1246.

122. Taherzadeh, M., et al., *Estimation of the heat capacities of deep eutectic solvents.* Journal of Molecular Liquids, 2020. **307**: p. 112940.

123. García, G., et al., *Deep eutectic solvents: physicochemical properties and gas separation applications.* Energy & Fuels, 2015. **29**(4): p. 2616-2644.

124. Omar, K.A. and R. Sadeghi, *Database of deep eutectic solvents and their physical properties: A review.* Journal of Molecular Liquids, 2023. **384**: p. 121899.

Chapter-2

Dihydrolevoglycosenone as a Novel Bio-based Nanofluid for Thermal Energy Storage: Physiochemical and Quantum Chemical Insights

Dihydrolevoglycosenone as a Novel Bio-based Nanofluid for Thermal Energy Storage: Physiochemical and Quantum Chemical Insights

The chapter mainly focuses on the studies of green nanofluid and its thermal behaviour through experimentally and theoretically. Density functional theory (DFT) has been studied to investigate the stability of the green nanofluid. Bio-based Dihydrolevoglycosenone, commercially known as Cyrene, is a biodegradable solvent with a multitude of potential applications such as chemical reactions and heat transfer media. The current chapter reports a nanofluid comprising Cyrene as a potential bio-organic thermal base media dispersed with Multi-walled carbon nanotube (MWCNT) and carboxylic functionalized Multi-walled carbon nanotube (MWCNT-COO H) nanoparticles. Two volume fractions 0.0016 and 0.0032 for MWCNT and 0.03 Vol% for MWCNT-COOH nanoparticles were added to enhance the heat transfer capacity of the resulting nanofluids. Thereafter, thermophysical properties were reported in the temperature range of 30-85°C for both base fluid and nanofluids. The measured values were then compared with a commercial heat transfer fluid, Paramtherm GLT and Therminol VP, within the temperature range of 30-85°C. Further, the stability of the nanofluid was investigated by a combination ofvisual observation, microscopic analysis, and zeta potential measurements. Thereafter, forced convection experiments were performed in a circular tube section under both laminar and turbulent conditions to measure the local heat transfer coefficient alongside temperature profiles. Results showed that the nanofluid possessing 0.0032 volume fraction of MWCNT-Cyrene nanofluid at N_{Re} =1881 gave the highest heat transfer coefficient. The heat transfer coefficient of the nanofluid exhibited an upward trend with the increase of the Reynolds number. Density Functional Theory was also used to investigate the microstructure formed by Cyrene on the surface of Single-walled carbon

nanotube (SWCNT). The orbital energy and influence of interaction energy on the van der Waals(vdW) interactions of Cyrene and ethylene glycol with SWCNT and SWCNT-COOH were examined and correlated with the dispersive forces within the fluid. The orbital energy revealed the fact that the HOMO-LUMO energy gap of the Cyrene/SWCNT and Cyrene/SWCNT-COOH systems were reduced due to the approach of Cyrene towards SWCNT surface, making it a stable nanofluid system. Reduced density gradient (RDG) analysis further demonstrated that weak vdW interactions were the primary driving force between solvent-SWCNT systems, primarily through X···π interactions. The thermal conductivity at various weight percentages of nanoparticles was determined using the reverse non-equilibrium molecular dynamics (NEMD) simulations and validated with experimental values. The microstructure of Cyrene on the surface of a single-walled carbon nanotube (SWCNT) and SWCNT-COOH was examined using density functional theory (DFT) calculations. Our study shows that the composition of CNTs and the nanofluid temperature significantly impact the thermal conductivity of pure Cyrene

2.1. Introduction

With the recent demand for renewable energies, it is important to give attention to cost-effective techniques dealing with solar energy. Solar energy is one of the major renewable sources for thermal applications, including desalination systems, due to the ease of availability and predictability[1]. But the efficiency of the thermal performance of solar energy-based desalination systems is the primary concern among the researchers. Modification of efficiency can be categorized based on improving solar radiation absorption, improving the efficiency of the applied media, and improving the heat transfer media [2]. One of the major applications of nanofluid is used in solar desalination systems, where nanofluid is employed as heat transfer media. A lot of research have been carried out on the selection of nanofluids for heat transfer applications using nanoparticles [3-5].

Attractive physical properties such as high thermal stability at higher temperatures makes nanofluid a potential heat transfer fluid. Overall, they possess higher specific heat capacity and heat transfer coefficient. Researchers working on nanofluids have concluded that the base fluid thermal conductivity and heat transfer coefficient significantly increase with concentration[3, 4]. Colangelo et al. [5] used 3.0% volume concentration in a flat-type solar thermal collector and compared the thermophysical properties with water based nanofluid. They concluded that with increase in volume concentration, thermal conductivity and specific heat of nanofluid increases. Nanoparticles such as Multi-walled carbon nanotube (MWCNT), CuO and Au-based nanofluids have reported high thermal conductivity values[6]. Pakdaman et al.[7] investigated the overall performance of nanofluid containing heat transfer oil and MWCNT on a vertically helical coil tube whereby a maximum performance index of 5.1 was found. Mashhadian et al.[8] reported the thermophysical properties of a hybrid nanofluid (a mixture of MWCNT and Al_2O_3 nanoparticles dispersed in water) and investigated the thermal performance of direct adsorption parabolic trough solar plate collector (DASC). Three volume

concentrations of nanofluid, 0.01%, 0.02% and 0.04% were used as heat transfer fluids in the adsorption collector. Experimental data discloses the fact that the optical properties of nanofluids are better than base fluid. Experimental results show that CO_2 emissions and water consumption are reduced by up to 450.33 kg and 16.6 m^3 per collector when the hybrid nanofluid was used.

Munyalo and Zhang[9] reviewed the thermophysical properties of nanofluids based on nanoparticle size. It was found that a larger nanoparticle size decreases the thermal conductivity of the nanofluid. On the contrary, the surface tension increases with the size of the nanoparticle. Teemofeva et al.[10]conducted a similar work, examining the effect of particle shape on the thermophysical properties of an alumina-based nanofluid. The viscosity of nanofluid was discovered to be shape-dependent where higher viscosities were attained owing to the elongated nanoparticle size. The heat transfer coefficient, which is a function of pressure and temperature, is an essential characteristic of the nanofluid and may be used to compute heat flow and Nusselt number[11]. Naraki et al.[12] studied and analysed the heat transfer coefficient of Cu-water nanofluid at different volume concentrations. They compared the results with water-based nanofluid and found that the heat transfer coefficient decreases with increasing fluid temperature from 50-80°C. Further, the heat transfer coefficients were found to drastically increase with the volume concentrations of the nanofluid. Esfe et al.[13] used five different particle volume concentrations (less than 1%) of aluminium based nanofluid to investigate heat transfer coefficient in turbulent conditions. The results indicate that the pressure drop of the nanofluid is slightly higher than the base fluid.

According to literature available, thermal performance of the solar collector is greatly influenced by selection of base fluids and suspended solid particles[14]. Carbon nanotube has attractive and superior features including high aspect ratio, mechanical, thermal and optical

properties[15]. The thermal conductivity of carbon nanotubes is in the range of 2000-6000 W/m.K, which is significantly larger than that of silver and copper nanoparticles. Since the thermal conductivity of the solid particles determines the thermal conductivity of the nanofluid, the thermophysical characteristics of nanofluid containing carbon nanotubes makes it an ideal alternative for its use as heat transfer fluid. Numerous literature have reported remarkable advantages of Multi Walled Carbon Nanotube (MWCNT) [16, 17]when used in thermal fluid. Amrollahi et al.[18] used MWCNT in water to prepare nanofluid and later analysed heat transfer coefficient. They found 30-40% improvement on heat transfer coefficient under both laminar and turbulent flows at 0.25 wt% concentration. Other base fluids, such as water, ethylene glycol, and motor oil have also been reported with carbon tube nanoparticles so as to produce nanofluids as thermal storage media in solar thermal collectors[19, 20]. Thus the choice of base solvent is critical since it influences nanofluid properties including thermal conductivity, stability and its dispersion behaviour[21].

The present study aligns with our previous research [22], which aims to develop a functionalized CNT-based bio-solvent nanofluid with superior properties. The objective is to examine the bio-nanofluid's thermophysical characteristics and thermal efficiency and then explore its possible use in thermal management systems. In addition, reverse non-equilibrium molecular dynamics (RNEMD) simulations have been performed to compute the thermal conductivity of Cyrene and bio-nanofluid at predefined temperature. Cyrene, as developed by the Circa group [24], represents a promising development in the quest for eco-friendlier solvents. Its biodegradability, high boiling point (227°C), low toxicity, renewable sourcing, and alignment with green chemistry make it a valuable asset in efforts to reduce the environmental impact of industrial processes and chemical manufacturing [23]. The captivating characteristics of Cyrene as a high-value product are due to its molecular structure, which consists of fused multifunctional rings [24]. In the next sections, two volume fractions,

0.0016 and 0.0032 volume fraction MWCNT and 0.03 Vol% for carboxylic acid functionalized MWCNT dispersed in the base fluid Cyrene, which were synthesized using a two-step preparation process [25]. In this chapter, Cyrene and its respective MWCNT and MWCNT-COOH nanofluid are investigated as potential bio-organic heat transfer fluids (HTFs) and are then compared to the existing commercial HTF, Therminol 55 [26] and Paratherm GLT [27]. The comparison focuses on evaluating their thermal properties, stability, and overall performance to determine their viability as sustainable alternatives in thermal management applications. Further, DFT calculations are performed to probe the atomistic insights between Cyrene and CNTs. The heat transfer properties of both base fluid and nanofluids were investigated and analysed under laminar and turbulent flow regimes. Thereafter quantum chemical techniques are used to investigate the interactions between Cyrene and single-walled carbon nanotubes (SWCNT). A comparison was made between the nanofluid (Cyrene/SWCNT and Cyrene/SWCNT-COOH) and a conventionally used nanofluid in industry that is based on ethylene glycol (EG). Further the interactions between the solvents and SWCNT are investigated using non-bonded interaction energy, reduced density gradient (RDG), and HOMO-LUMO analyses so as to correlate the dispersion of the nanoparticles in the base fluid.

2.2. Experimental Details

2.2.1. Materials and Methods

Cyrene was obtained from Sigma Aldrich with >98.5% purity. TCI chemicals supplied Multi-walled carbon nanotubes (MWCNTs) with diameters of 15-40 nanometers and lengths of 5-15 micrometers. MWCNT-COOH used in this study was obtained from Ossila. These nanotubes had inner diameters ranging from 5-10 nm and outer diameters of 25 nm with lengths spanning 10-20 μm. To ascertain the composition of the Cyrene, ^{1}H NMR was performed (Figure A1 in appendix A). For NMR, solvent dimethyl sulfone oxide-d_6 (DMSO-d_6) was purchased from

Merck, Germany. The diameter and morphology of the carbon nanotube was analyzed by FETEM (JEOL-JEM2010) and FESEM (Sigma, Zeiss). X-ray diffractometer experiment (XRD, Bruke D8, advanced X-ray diffraction measurement system was performed at room temperature in the range of 2θ from 10 to 80° to analyze the crystallinity structure of the MWCNT. To further confirm the chemical structure and crystallinity of MWCNT, Raman spectroscopic analyses (Horiba Jobin Vyon, Model LabRam HR) was performed.

In this work, a two-step method [25] has been employed to prepare nanofluid by dispersing CNT into base solvent. The different volume fractions of nanofluids with their abbreviations are tabulated in the table 2.1. Nanofluids were prepared with the help of following empirical formula as obtained from the literature[28].

$$\varphi = \left(\frac{\left(\frac{m}{\rho}\right)_{mwcnt}}{\left(\frac{m}{\rho}\right)_{mwcnt} + \left(\frac{m}{\rho}\right)_{bf}} \right) \times 100 \qquad \textbf{(2.1)}$$

Here φ is the volume concentration (%), m is the mass (kg) and ρ is the density (kg/m^3).CNT was weighed on a digital weighing balance (Denver Instrument, Model SI-234) with an accuracy of ± 0.0001g. Thereafter the mixture was vigorously shaken on a vortex mixer (SPINX MC-01, Tarsons) at 800 rpm for efficient dispersion. The mixture was then placed in a sonication bath (GT-1990QTS) for 90 minutes to get a homogeneous and uniform suspension of nanoparticles that ensured the absence of aggregation of carbon nanotube (Figure 2.1). Employing an ultra-sonication method aided in the break-down of larger cluster of nanoparticles. It also helps the nanofluid to get stable for a longer time span [3]. Finally, the prepared nanofluid samples are kept at room temperature to observe any settlement of the nanoparticle in the base fluid for a certain number of days.

The stability of the nanofluids were observed by visual observation and zeta potential analysis. Prepared nanofluids were kept at room temperature for one week to observe the

settling effect of the nanofluids. The zeta potential of the nanofluids was performed with the help of the Delsa Nano instrument (Delsa Nano C, BECKMAN COULTER). Optical microscope images were captured using a high-resolution microscopic image (Axiostar plus, Carl Zeiss, Germany) to study the particle dispersion and cluster size in the nanofluid. Density was measured at different temperatures by using the Anton Paar DMA 4500 Densitometer.

Similarly, viscosity of base fluid and nanofluids were measured at temperature range of 30-85°C with an interfacial Rheometer (MCR 301, Anton Paar, Austria) having an accuracy of 0.001 mPa.s. The viscosity of the nanofluid was determined by the parallel plate method. Nearly 1 mL of sample was used for viscosity measurement. The parallel plate (PP-50) was used along with the inbuilt thermal jacket arrangement for maintaining a constant sample temperature within ±1 K. Thermal conductivity was determined by a KD2 Pro thermal property analyzer (Decagon device, USA). Before the measurements, standard glycerine and Millipore water were used as the calibrating agents. A heating plate with silicone oil bath was used to maintain a constant temperature. Further the free convection due to the high temperature measurements were avoided by decreasing the measuring cell diameter (7 mm). A 60mm (small) single needle (KS-1) sensor was used to measure the thermal conductivity with a temperature range of 223.15 K to 423.15 K having an accuracy of ±5%. The specific heat of base fluid and nanofluids at different temperatures were measured by Differential Scanning Calorimeter (DSC) (NETZSCH STA 449F3). The uncertainty calculations and values of all the properties are presented in table A1 in appendix A.

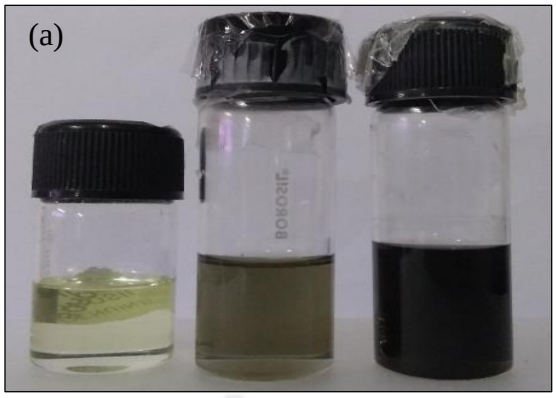

Figure 2.1. Photographs of base fluid and nanofluids after sonication

Table 2.1 Different volume fraction of nanofluids and their abbreviation

Abbreviation	Nanofluid	Volume fraction
NF1	Cyrene + MWCNT	0.0032
NF2	Cyrene + MWCNT	0.0016
NF3	Cyrene + MWCNT-COOH	0.0003

2.2.2 Experimental Setup and Forced Convection Studies

A convective heat transfer setup was built to measure heat transfer coefficient and Nusselt number of base fluid and nanofluid [29, 30]. The schematic diagram of the experimental setup is shown in Figure 2.2. The setup consists of a testing tube, a pump, a nanofluid chamber with flow control valves. Five thermocouples were arranged on the surface of the tube to measure the surface temperature. Further two thermocouples were placed in the inlet and outlet of the tube to measure the fluid temperature respectively. The details of experimental setup are given in appendix A.

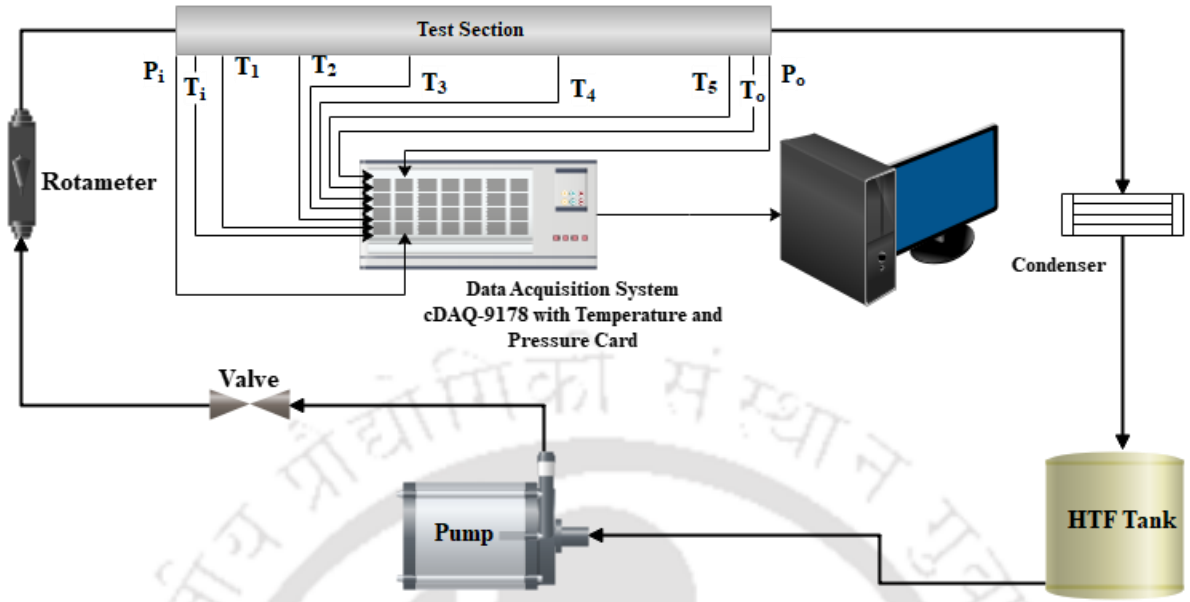

Figure 2.2. A schematic diagram of forced convection setup

2.3 Computational Details

2.3.1 Quantum Chemical Calculation

The optimization of solvent-nanotube structures was carried out by employing the density functional theory (DFT) based ωB97XD method in conjugation with the basis set 6-31G(d,p)[31-33]. The geometry optimization of various individual molecules and solvent-SWCNT systems was carried out without symmetry restriction. In addition, for the complexes of SWCNT, SWCNT-COOH, Cyrene, and ethylene glycol, numerous orientation originating from different relative positions and various conformations of the SWCNTs were explored, and in each case, the structure with the lowest energy value was selected. Gaussian 16.0 software [34] program was used to carry out all of the calculations pertaining to the electronic structure. The optimized structure of Cyrene, SWCNT and SWCNT-COOH were shown in Figure 2.3, were then utilized for single point energy calculations with a hybrid functional ωB97XD along with a more precise basis set 6-311++G(d,p) [35, 36] to enhance energy

accuracy. The ωB97XD functional utilizes long-range corrected hybrid density functional that includes dispersion correction based on Grimme's DFT-D3 method [37]. The accuracy and reproducibility have been proven by comparison to theoretical and experimental data [38].

The Geometry optimization and the subsequent computation of the interaction energy (IE) were both performed at the same theoretical level. The $IE_{(ads)}$ of the solvent and SWCNTs surface were calculated with the supramolecular technique and adjusted for basis set superposition error (BSSE) with the counterpoise (CP) method described by Boys and Bernardi, as shown in equation 2.2. To affirm that the stationary points represent real minimum points, the vibrational frequencies were calculated at the same level of theory. A constraint of the study is that it only examines the interaction of a solvent molecule with a single SWCNTs surface. This is an acceptable simplification, but far larger systems that are computationally tractable at this required level of theory will yield a higher degree of precision in the future.

$$\Delta E_{ads} = E_{CY/CNT} - E_{CNT} - E_{CY} \quad \textbf{(2.2)}$$

Here ΔE_{ads} is the adsorption energy of solvent and SWCNTs surface, while $E_{CY/CNT}$, $E_{CNT,}$ *and* E_{CY} are the total energy of Cyrene-SWCNT, SWCNT and Cyrene.

Furthermore, the non-covalent interaction (NCI)[39] or reduced density gradient (RDG) [40]analysis is carried out with the Multiwfn 3.7 [41] program in order to ascertain the contributions of the attractive and repulsive interactions. NCI analysis gives information on the distribution of electron density in molecular systems with low electron density and low gradient values. NCI analysis is the most common approach to examine the van der Waals (vdW) interaction, steric hindrance, and hydrogen bonds (HBs) in terms of pairwise interactions between atoms based on their vdW radii[42]. The chemical reactivity of the solvent-SWCNT system and its impact on the process have been predicted in terms of the HOMO-LUMO gap

[43]. This is an important study as it shall help us in comparing the dispersion effect of the nanoparticles within the bulk or the base fluid. It invariably shall allow us in predicting the extent of the heat transfer, as a good dispersion shall result in a high heat transfer coefficient due to the less resistance through the bulk media. In this manner one can compare the zeta potential values with the non-covalent interactions as obtained here.

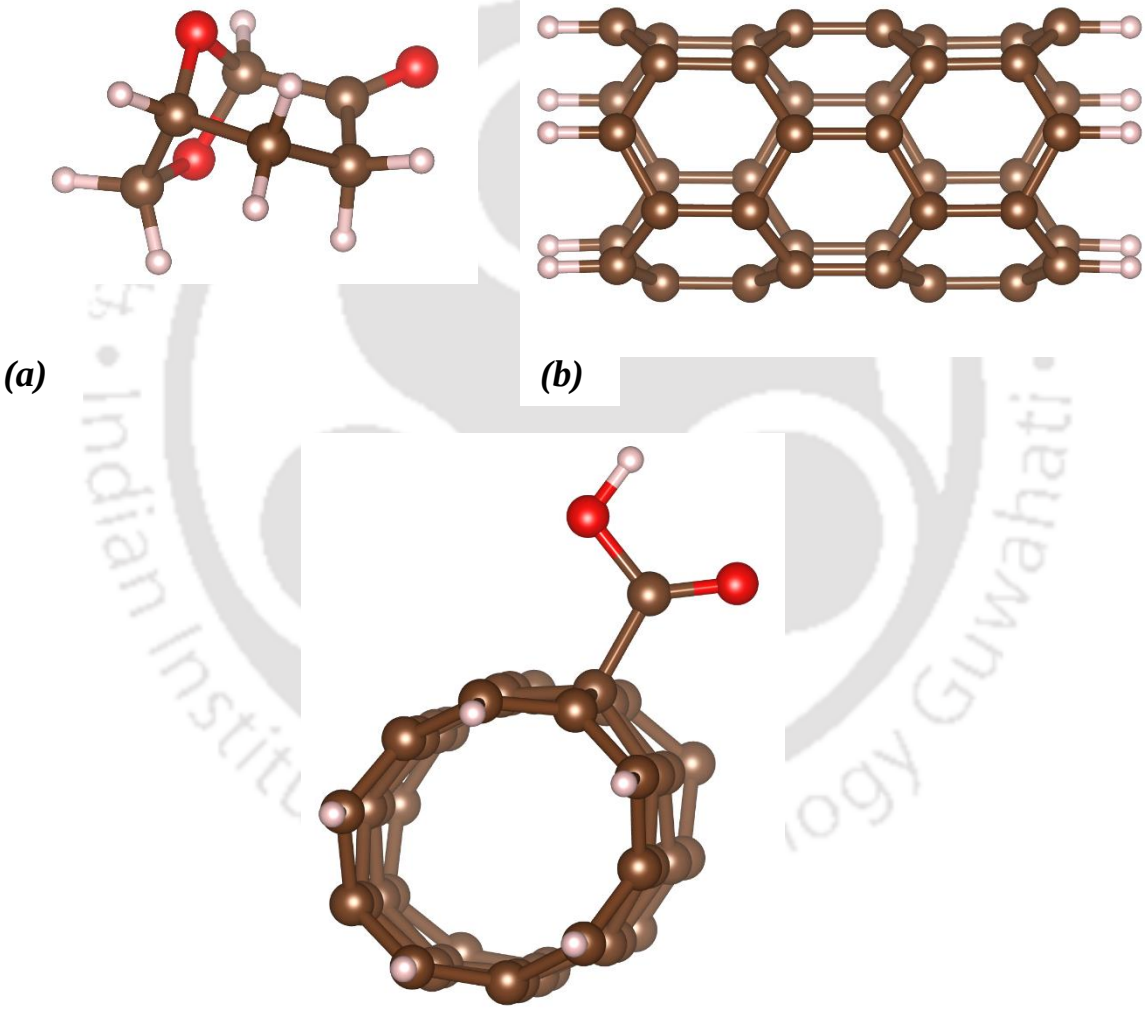

Figure 2.3 Optimized structures of (a) Cyrene, (b) Pristine SWCNT and (c) SWCNT-COOH at ωB97XD/6-31G(d,p) level of density functional theory

2.3.2 Reverse NEMD Computational Details

The explicit Cyrene molecules are considered to generate an amorphous cell, as shown in Figure 2.4. To perform thermal conductivity calculations, an orthorhombic box is considered based on the Müller-Plathe method [44], where box size is considered as $x \approx y \leq z/2$, as shown in Table 2.2. An armchair (6,6) SWCNT with a radius of 4.1 Å and length of 24.5 Å is considered, as shown in Figure 2.5 (a). The surface of SWCNT is functionalized with carboxyl groups, as shown in Figure 2.5 (b). In all our CNTs, ends are terminated with hydrogens. The DESMOND MD [45] tool is utilized for all MD simulations within the Schrödinger simulation software, Schrödinger release (2024-2). A time step of 1 femtosecond (fs) is employed for the integration of Newton's equations of motion in all our simulations. A cut-off distance of 14 Å was employed. We have used Optimized Potentials for Liquid Simulations (OPLS4) force fields [46] to accurately represent the bonded and Lennard-Jones interactions. The simulation scheme utilized in all systems is outlined in the subsequent steps: NPT molecular dynamics simulations for 5 ns are conducted to calculate the average volumes and densities. A temperature of 300 K and a pressure of 1 atm are utilized for the NPT simulation. The temperature and pressure were maintained at a constant level by employing the Nose-Hoover thermostat and Martyna-Tobias-Klein barostat, with coupling constants of 1 ps and 2 ps, respectively. Subsequently, reverse non-equilibrium molecular dynamics (NEMD) simulations were conducted with a production run of 80 nanoseconds in the NVE ensemble. To induce a heat flux and determine the temperature distribution, the simulation box is partitioned into 10 slabs perpendicular to the *z*-axis. The Müller-Plathe method is explained in the section. 2.4.6 in details.

Table 2.2 The number of Cyrene, CNTs and functionalized CNTs along with the simulation box sizes of nanofuids to calculate thermal conductivity are shown.

Fluid	Number of Cyrene Molecules	Number of CNTs	Simulation Box Size (Å^3)
Pure Cyrene	2000	0	54.1×54.9×112.9
Cyrene + (3) pristine CNT	2000	3	51.4×52.1×129.5
Cyrene + (10) pristine CNT	2000	10	51.0×50.4×143.2
Cyrene + (3) Carboxyl functionalized CNT	2000	3	51.8×51.7×130.1
Cyrene + (10) Carboxyl functionalized CNT	2000	10	51.3×50.6× 144.9

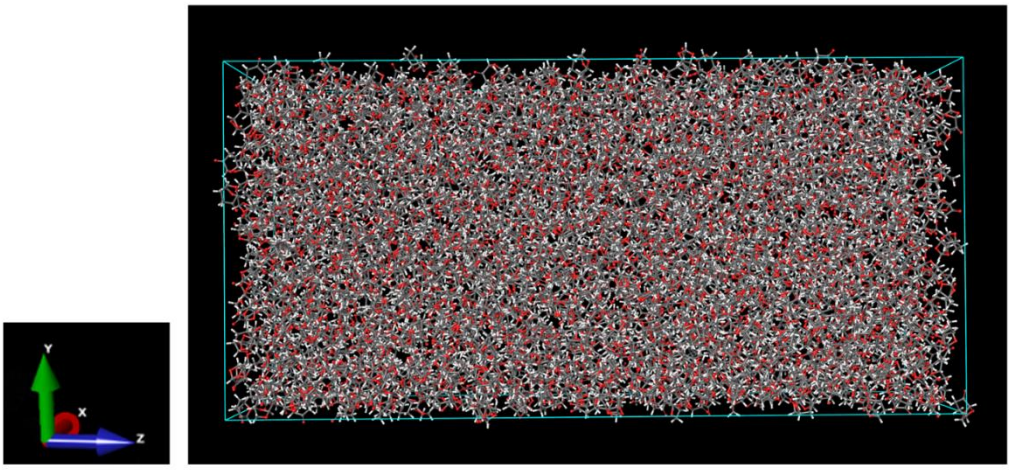

Figure 2.4 Snapshots of the NVE MD run showing Cyrene molecules in orthorhombic box. The color coding for atoms is as follows: carbon is grey, oxygen is red and hydrogen is white.

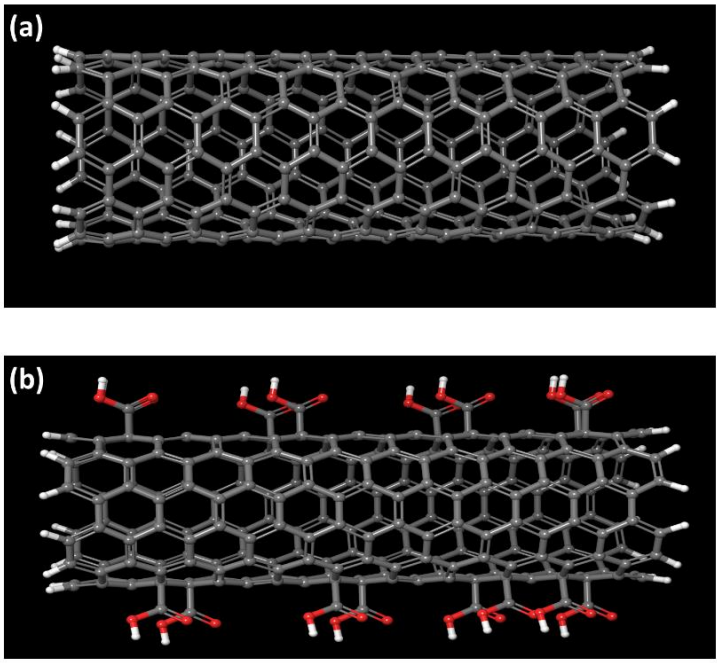

Figure 2.5 The atomistic structure of nanoparticles (a) pristine SWCNTs (b) SWCNTs functionalized with -COOH groups on surface. The colour coding for atoms is as follows: carbon is grey, oxygen is red and hydrogen is white.

2.4. Result and Discussion

2.4.1 Characterization of MWCNT and MWCNT-COOH Nanoparticles

The microstructure of CNTs was investigated through FETEM and FESEM images as shown in Figure 2.6(a, c) and (b, d). The FESEM images were captured at 100nm and 200 nm scale, where a randomly oriented fiber like CNT (order of micrometres) is readily visible. Several multi walled or layer structure of CNT were clearly seen in FETEM images (Figure 2.6(c) and 2.6(d)). It reveals the diameter of the CNTs which were in the range of ca. 20-40 nm. The structures claim that white spots on the CNT surface in Figure 2.6(b) indicate the presence of functional groups, which was not seen in Figure 2.6 (a), but there is limited elaboration on the nature or implications of these functional groups. The XRD pattern of MWCNT and MWCNT-COOH is displayed in Figure 2.7(a), which indicate the crystallinity structure of CNT. A sharp peak was observed at $2\theta=26.02°$ which indicated the crystallinity structure of the carbon

nanotube. The shift in the peak position from 26.02° to 25.50° and is attributed to the expansion of the interlayer d-spacing resulting from the presence of the COOH group. However, the (100), (004), and (110) atomic planes exhibit a low-intensity peak with 2θ values of 43.04°, 53.68°, 78.0° respectively showing that MWCNTs have crystalline structure. There were no additional peaks detected, indicating the nanotube's exceptional purity and lack of functionality. The findings from the Raman spectroscopy analysis (Figure 2.7(b)) are discussed, demonstrating the detection and characterization of different carbon allotropes as well as the presence of various functional groups. Although the D and G modes are acknowledged, the implications of the D/G ratio and sp3 group concentration in relation to the presence of functional groups are observed. Finally, the FT-IR spectra, as depicted in Figure 2.7(c), are presented, highlighting the characteristic O-H stretch and C=O bands commonly observed in carboxyl functional groups.

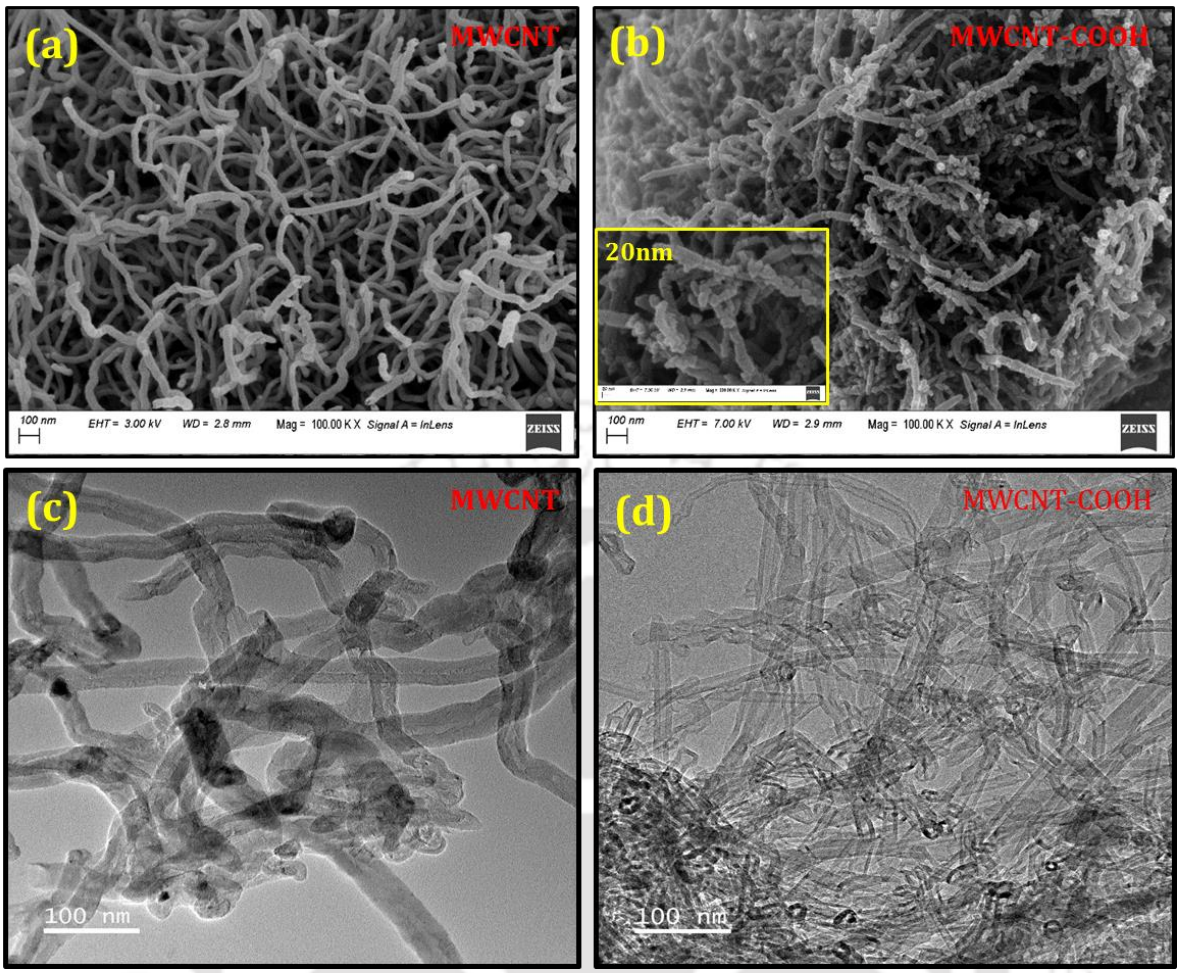

Figure 2.6. Characterization results of MWCNT and MWCNT-COOH nanoparticles (a) (b) FESEM, (c) and (d) FETEM

(a)

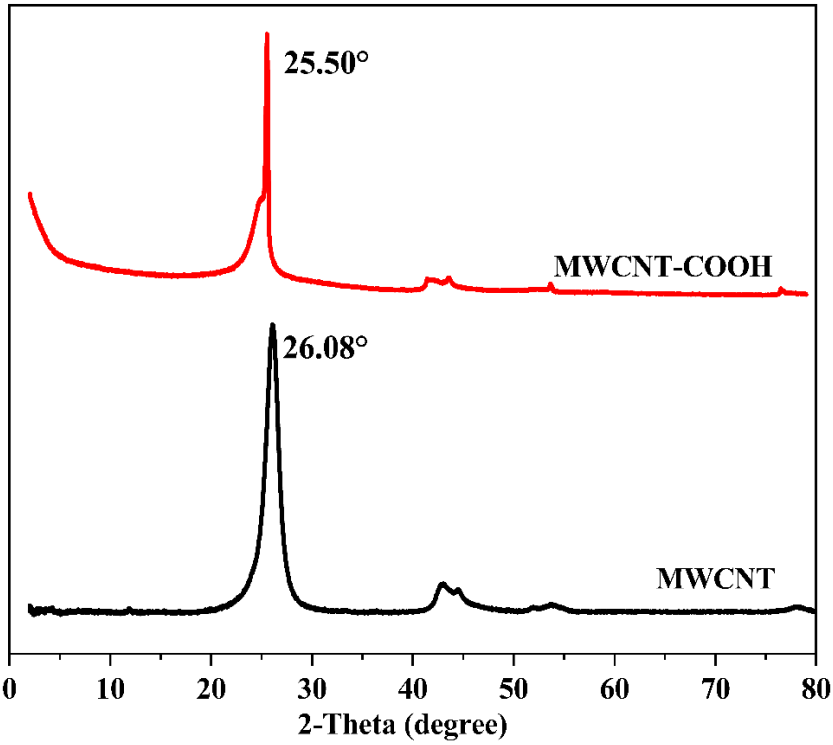

(b)

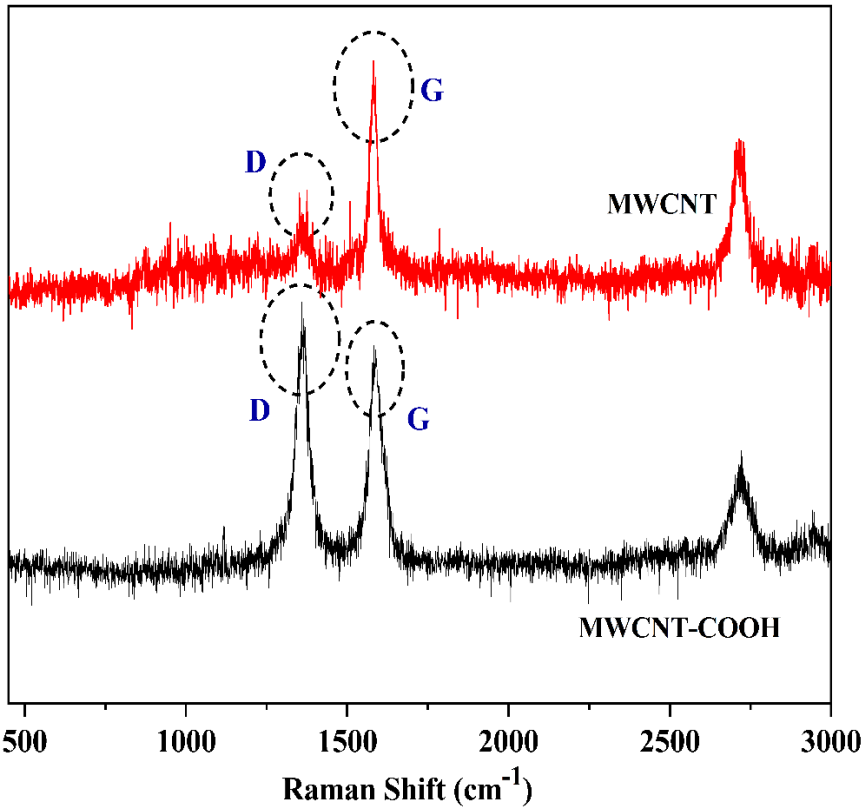

(c)

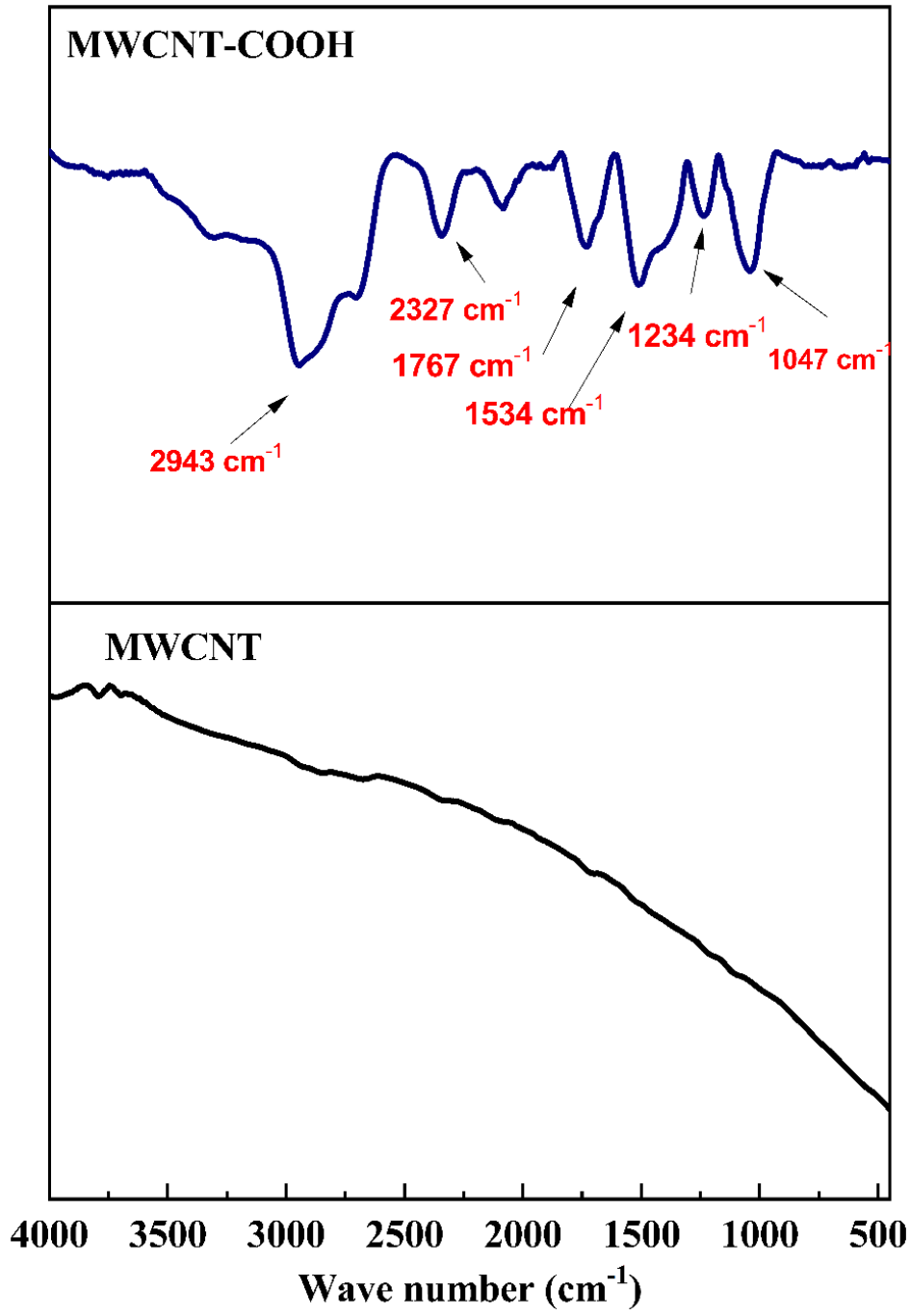

Figure 2.7. Characterization results of MWCNT and MWCNT-COOH nanoparticles (a) XRD, (b) Raman, and (c) FTIR spectroscopy

2.4.2 Thermophysical Properties

2.4.2.1 Thermal Conductivity

Thermal conductivity, specific heat, density, and dynamic viscosity are the critical parameters that define the thermal performance of the nanofluid. The thermophysical properties of nanofluid are mainly affected by the shape, size, particle aggregation, and volume fraction of the nanoparticles that are dispersed in the base fluid. The high volume to surface ratio of the nanotube causes high thermal conductivity of the nanofluid. This result is clearly observed from the experimental data as shown in Figure 2.8(a). The thermal conductivities of both base fluid and nanofluids were measured and plotted against different temperatures (25-85°C). The small particle size of nanofluids is responsible for the significant feature of micro-convections inside the fluid, which effectively promotes the dispersion of heat. The importance of this phenomenon becomes evident when examining the MWCNT-COOH base nanofluid. Due to the small size of the particles, micro-convection of the fluid takes place, which results in faster dispersion of heat in the fluid. It can be clearly seen from Figure 2.8, the thermal conductivity of both concentrations of nanofluids (NF1 and NF2) shows higher thermal conductivity than the base fluid and commercial heat transfer fluid Paratherm GLT [47]. The thermal conductivity of nanofluid increases with an increase in temperature as compared to that of the base fluid. This follows a general trend i.e. with increase in temperature, nanoparticles gain higher energy which results in a higher collision rate between the nanoparticles.

The thermal conductivity also depends on the nanofluid concentration. With the increase in the volume fraction, temperature effects increase the Brownian motion, affecting the thermal conductivity [48]. This is clearly seen in Figure 2.8(a), where NF1 possesses higher thermal conductivity than NF2 when the temperature rises. The greatest increase in thermal conductivity was 89.88% at 65°C for NF1.Table A2 in appendix A shows the thermal conductivity enhancement of the nanofluids at different temperatures. More significant are the

van der Waal attraction forces, which attempt to attract and reduce the surface area of neighbouring carbon tubes, resulting in a reduction in heat conductivity. Brownian motion is one of the important factor for enhancement of thermal conductivity of nanofluid. Thermal conductivity of the nanofluid largely depends on base fluid, shape and size of the nanoparticles, particle volume fraction respectively. Along with all of these, there are additional factors that can affect thermal conductivity of nanofluid, such as liquid nano-layer development around the nanoparticles, clustering of nanoparticles, and thermophoresis [49]. Furthermore, as the temperature rises, the kinetic energy of the nanoparticles increases which results clustering of the nanoparticles due to the van der Waals attractive force. However, the stability of the nanofluid is affected by the formation of bigger clusters, which lowers its thermal conductivity. Thermophoresis is the movement of nanoparticles through the nanofluid under the influenced of thermal gradient [50]. This thermal gradient causes the particles to experience the net force in the direction of decreasing temperature. However, such Brownian motion-based movement results in convective currents that disturb the heat in the nanofluid system and thereby increase the thermal conductivity of nanofluid. Formation of nano layer of liquid around the nanoparticles plays an important role in thermal conductivity enhancement. The layer of liquid formed right next to the nanoparticles is expected to have thermal conductivity that is comparable to the solid nanoparticle that helped the nanofluid conduct heat energy[51]. Along with Brownian motion, clustering and interfacial stacking also aid in heat transfer enhancement. In general, the MWCNT conducts heat energy via the vibrations of individual atoms or molecules. The atomic or molecular vibrational energy of the nanoparticles is referred to as phonons in this context. Thus, heat is transferred through nuclear vibrations via the transmission of phonons rather than electrons. Additionally, the rise in temperature allows for the expansion of the liquid. This thereby promotes the molecule's free mobility, boosting intermolecular collisions and heat transmission through conduction.

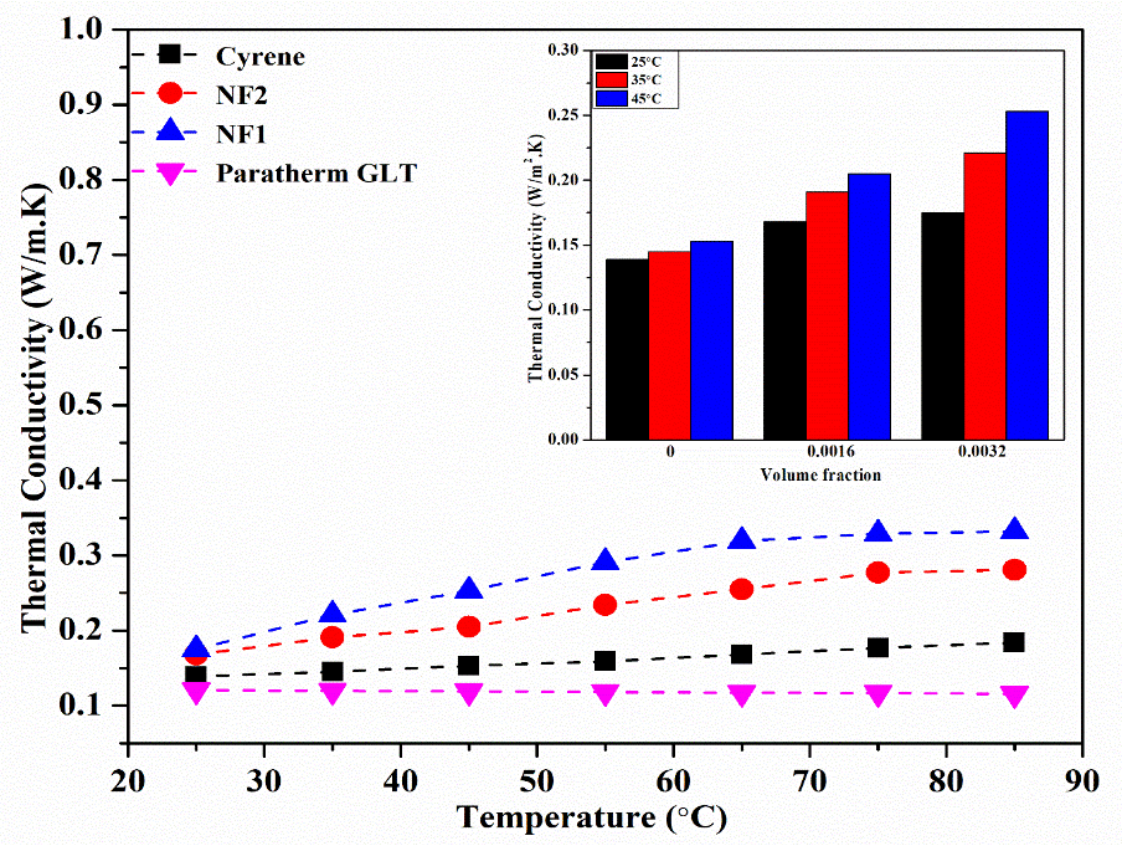

Figure 2.8 Thermal conductivity of MWCNT/Cyrene nanofluid at temperature range 25-85°C

The thermal conductivity of MWCNT-COOH/Cyrene base nanofluid (NF3) is shown in Figure 2.9(a), which shows that a nanofluid concentration of 0.03 vol% exhibits improved thermal conductivity compared to the base fluid and conventional HTFs like Therminol 55 and Paratherm GLT. Moreover, the thermal conductivity of the nanofluid has a continuous positive correlation with temperature, which is in line with the overall trend seen in which higher temperatures enhance the kinetic energy of nanoparticles, leading to increased collision rates between them. In the context of this investigation, a mathematical model was formulated to represent the thermal conductivity of the nanofluid as a function of temperature, exhibiting an

exponential relationship. The resulting regression value provides valuable insights into the thermal characteristics of the nanofluid across different thermal circumstances. A polynomial correlation of thermal conductivity as a function of temperature was developed for nanofluid with a regression value $R^2 = 0.91993$,as shown in Figure 2.9(a).

$$\kappa = -0.03878 + 0.00696T - 2.12392 \times 10^{-5}T^2 \quad \textbf{(2.3)}$$

Maxwell model [52] suggest an equation (Equation 2.4) for estimating thermal conductivity ratio and consider only the effect of volume fraction and the thermal conductivity of the component. It does not consider the effect of particle size, shape, temperature effect and viscosity of the base fluid.

$$\frac{k_{nf}}{k_{bf}} = \frac{k_p + 2k_{bf} + 2(k_p - k_{bf})\varphi}{k_p + 2k_{bf} + (k_p - k_{bf})\varphi} \quad \textbf{(2.4)}$$

The thermal conductivity of the base fluid, the nanoparticle, the nanofluid, and the volume fraction of the nanoparticles are represented by k_{bf}, k_p, and k_{nf}, respectively. Furthermore, Maxwell-Eucken [53] proposed one model to predict the k_{nf}which is given in Equation 2.5.

$$\frac{k_{nf}}{k_{bf}} = \frac{\left(1 + 2\varphi\left(1 - \left(\frac{k_{bf}}{k_p}\right)\right)\right) / \left(2\left(\frac{k_{bf}}{k_p}\right) + 1\right)}{\left(1 - \varphi\left(1 - \left(\frac{k_{bf}}{k_p}\right)\right)\right) / \left(\left(\frac{k_{bf}}{k_p}\right) + 1\right)} \quad \textbf{(2.5)}$$

The Hamilton Crosser model (H-C model) [54] modified the Maxwell model and considers the effect of particle shape is shown in Equation 2.6.

$$\frac{k_{nf}}{k_{bf}} = \frac{k_p + (n-1)k_{bf} - (n-1)(k_p - k_{bf})\varphi}{k_p + (n-1)k_{bf} + (k_p - k_{bf})\varphi} \quad \textbf{(2.6)}$$

Equation 2.7 yields the value of n, which is the coefficient of the nanoparticle shape.

$$n=\frac{3}{\psi} \quad \textbf{(2.7)}$$

ψ represents the ratio between the surface area of a sphere with the same volume as the nanoparticle and the surface area of the particle itself. The value of *n* is 3 for spherical particles and 6 for cylindrical nanoparticles. It can be seen from the Figure 2.9 (b) that H-C model and Maxwell-Eucke model are nearly close to the experimental results, whereas deviations are observed in Maxwell model.

(a)

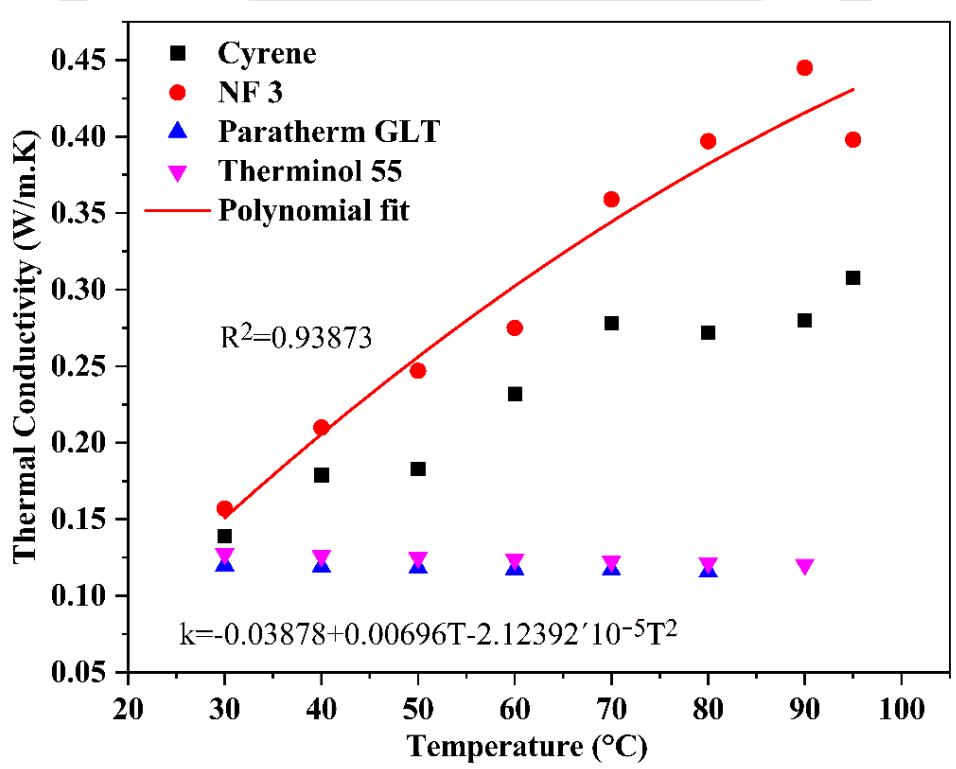

(b)

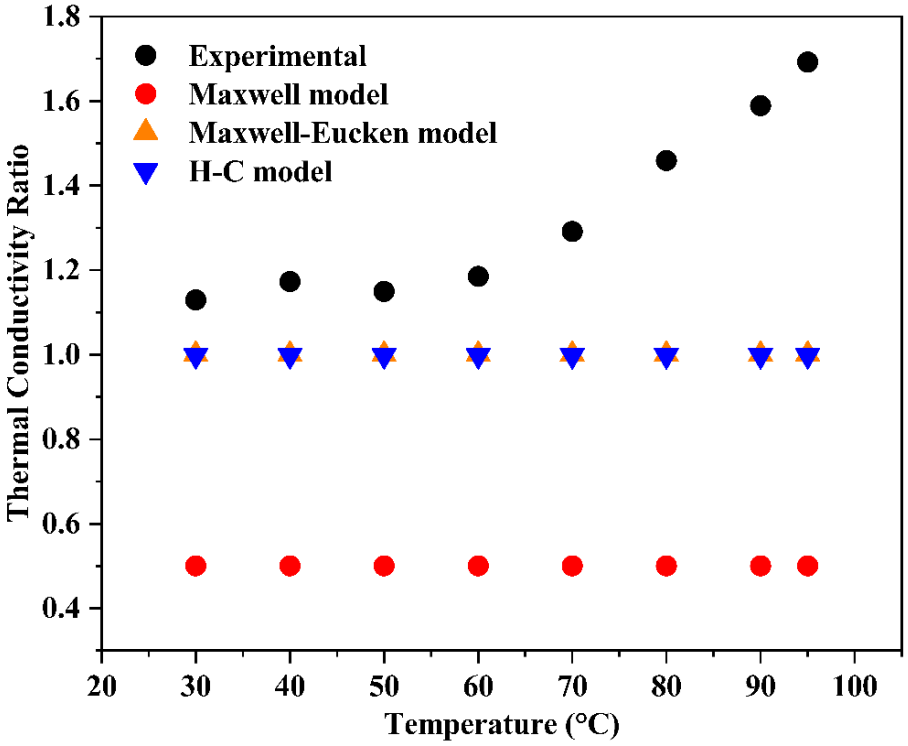

Figure 2.9. Thermal conductivity results of nanofluid (NF3) (a) variation with temperature (b) comparison of experimental results to the Maxwell model, Maxwell-Eucken model and H-C model

2.4.2.2 Density

Density plays an essential role in order to evaluate the thermophysical properties of nanofluid. The experimentally measured density are reported in Figure 2.10(a) and it is compared with a heat transfer fluid, Paratherm GLT. It was observed from the experimental data that the density of both base fluid, NF1 and NF2 decreases with an increase the temperature from 25-85°C. However, the addition of MWCNT nanoparticles leads to increase in the density of the nanofluid. It was observed that the nanofluids containing 0.0016 and 0.0032 volume fractions of MWCNT have a slightly higher density than the base fluid.

The measured density variation between the base fluid and the nanofluid is also significantly less. It should be noted that the size of the nanoparticle is responsible for thermal

expansion with an increase in temperature, which results in higher kinetic energy of the molecules. Experimentally determined values are compared to a standard model presented by Pak and Cho [55] as given in equation 2.8.

$$\rho_{nf}=\varphi_v\rho_{np}+(1-\varphi_v)\rho_{bf} \quad \textbf{(2.8)}$$

Where, ρ_{nf} is the nanofluid, ρ_{bf} is the base fluid, φ_v is the volume fraction and ρ_{np} is the density of nanoparticles.The comparison of experimental data with a conventional model is tabulated in table A3 given in appendix A. Similar phenomena as observed in the case of 0.03 vol% of MWCNT-COOH/Cyrene base nanofluid (NF3) is shown in Figure 2.10 (b). Nevertheless, the incorporation of MWCNT-COOH nanoparticles into the nanofluid leads to a marginal elevation in density. Furthermore, it is important to acknowledge that the disparity in density between the base fluid and the nanofluids is relatively moderate. Equation 2.9 establishes a linear association between density and temperature, with a regression value 'R^2' of 0.998 and a standard error value $\pm 4.542 \times 10^{-6}$.

$$\rho = 1.271049 - 9.9890 \times 10^{-4}T + 5.99401 \times 10^{-4}T^2 \quad \textbf{(2.9)}$$

Here ρ is the density (gm/cc) and T is the temperature (K) of the nanofluid

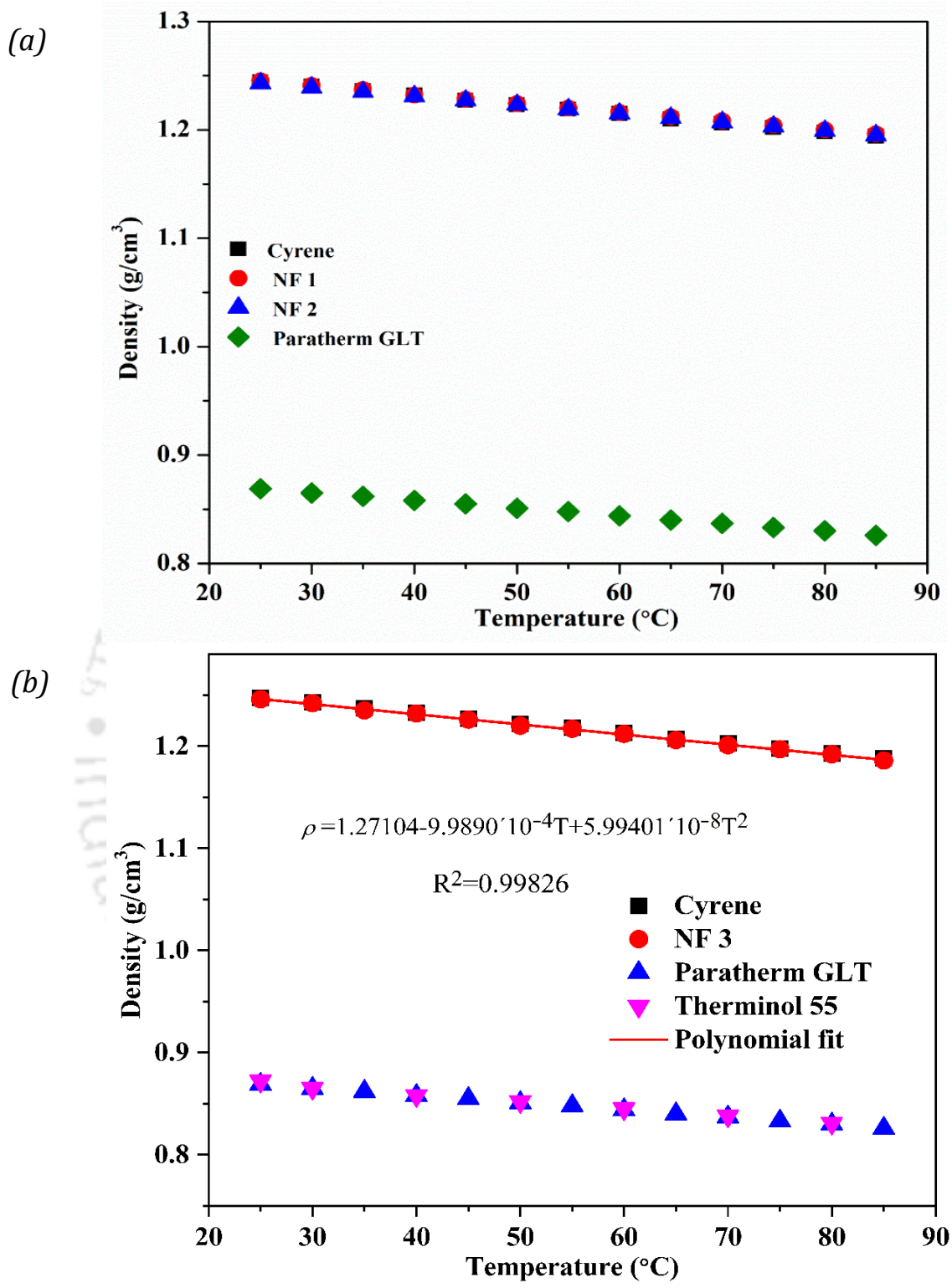

Figure 2.10. Experimental data of density (a) MWCNT/Cyrene (b) MWCNT-COOH/Cyrene nanofluid

2.4.2.3 Viscosity

Rheological behaviour of nanofluids (NF1 and NF2) and base fluid were investigated through rheometer at different temperatures and at a shear rate of 50 per second (s^{-1}). These were then compared with the result of commercial heat transfer fluid Paratherm GLT. Any rheological behaviour of fluid depends on increase in viscosity with nanoparticle concentrations and decrease in viscosity with rise in temperature[56]. These two aspects are clearly seen in our results. An exponential decreasing trend was observed in Figure2.11(a), where the viscosity of both the nanofluids, NF1 and NF2, and their corresponding base fluid decreases when the temperature rises from 25-85°C. Similarly, in the case of nanofluid NF3, similar trend was noted as shown in the Figure 2.11(b). Increasing the temperature weakens the intermolecular forces, resulting in a decrease in viscosity. In comparison to the commercial thermal fluid, base fluid and nanofluids has very less viscosity at room temperature. Further the addition of nanoparticle concentration in the base fluid increases the viscosity of the nanofluids, while such an effect is minimal at high temperature. The increase in the viscosity of the nanofluid is due to the decrease in the cohesive forces between the molecules at higher temperatures, which results in higher kinetic energy. As the kinetic energy increases, molecules are free to move, which leads to an increase in viscosity. It can be concluded that the viscosity of Nanofluid is affected by many factors such as volume concentration, shear rate, morphology of nanoparticles, and temperature. Lower the viscosity of the nanofluids, lower is the pressure drop, and hence, lower is the pumping power required. A conventional model as developed by Einstein [57](equation 2.10) was used to predict the viscosity of the nanofluid and a comparison with the experimental results were made.

$$\mu_{nf} = (1 + 2.5\varphi_v)\mu_{bf} \quad \textbf{(2.10)}$$

Here, μ_{nf} is the viscosity of the nanofluid, φ_v is the volume fraction and μ_{bf} is the viscosity of the base fluid.This is one of the many conventional models reported in the literature[58].The choice of the model is based on the value of the low concentration and does not consider the particle density effect, particle shape, size and agglomeration effect. The measured values are then compared to those obtained from the theoretical model as tabulated in A4 in appendix A. On closer inspection, it was found that the experimental results exceeded Einstein's theoretical predictions. This difference is due to the fact that it does not consider intramolecular attraction between the nanoparticles.

Moreover, the introduction of nanoparticle concentration into the base fluid results in an elevation of the viscosity of the nanofluids, although this effect is less pronounced at elevated temperatures [59]. A polynomial correlation was established using regression analysis, resulting in a R^2=0.995. This correlation can be used to estimate the viscosity of nanofluid at various volume concentrations, as described by Equation 2.11.

$$\mu = 0.02165 - 4.5136 \times 10^{-4}T + 2.7463 \times 10^{-6}T^2 \quad \textbf{(2.11)}$$

Here μ is the viscosity and T is the temperature of the nanofluid.

Finally, it can be inferred that the viscosity of nanofluids is influenced by several factors, including the nanoparticle concentration, shear rate, nanoparticle morphology, and temperature. The reduction in viscosity of nanofluids leads to a decrease in pressure drop, which in turn reduces the amount of pumping power required.

(a)

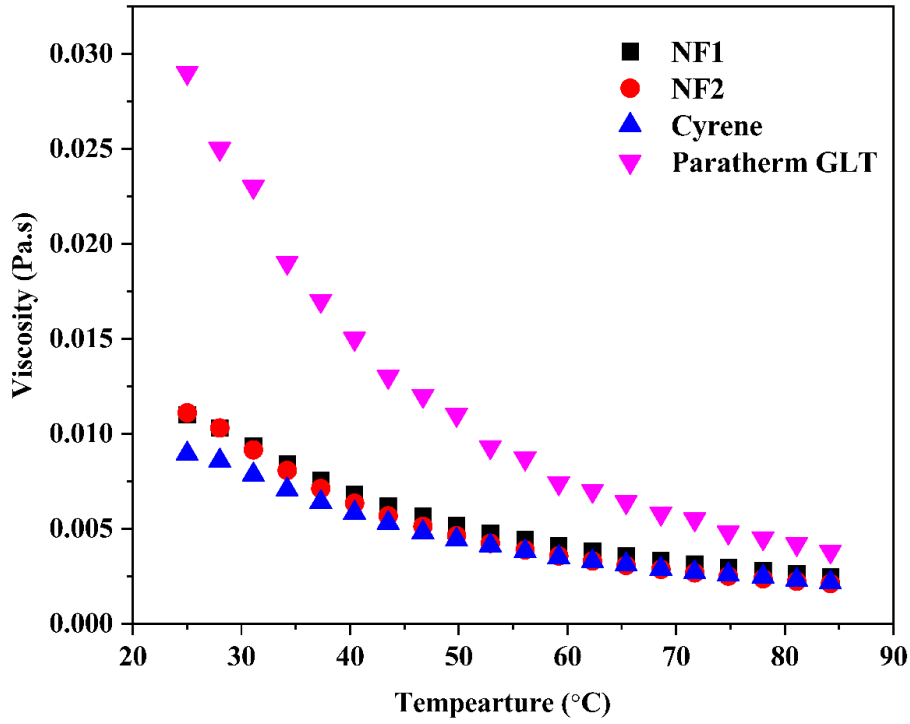

(b)

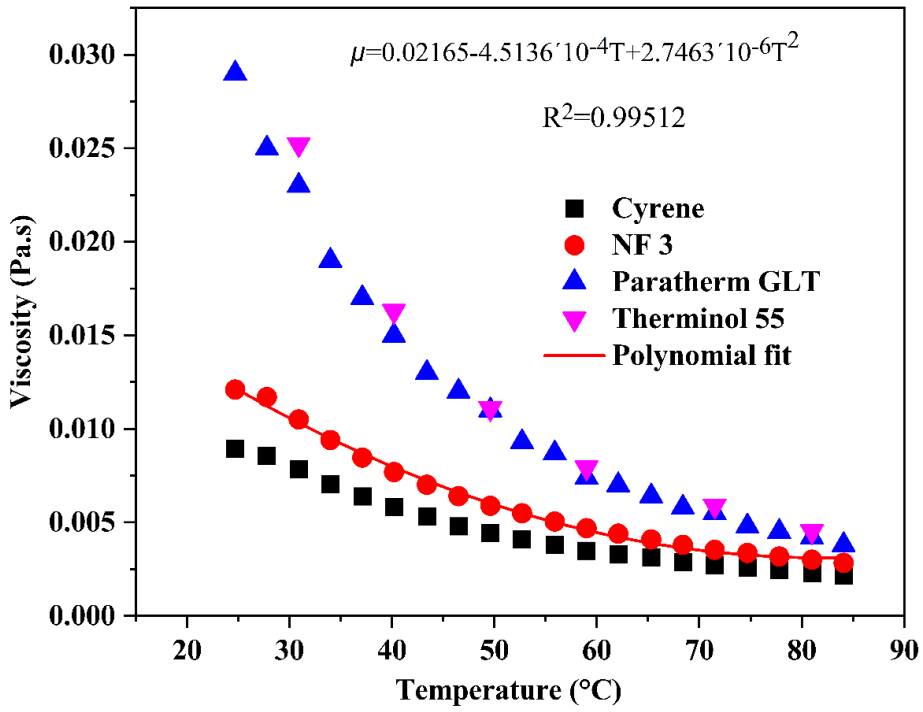

Figure 2.11. Viscosity values of base fluid and nanofluids (a) MWCNT/Cyrene (b) MWCNT-COOH/Cyrene

2.4.2.4 Specific Heat

The specific heat capacities of Cyrene, Cyrene/MWCNT and Cyrene/MWCNT-COOH nanofluids were measured at different temperatures by the sapphire method. Figure 2.12 (a) and 2.12(b) depicts the specific heat capacity at different temperatures. Measurement of specific heat capacity was done under nitrogen environment at heating rate of 20°C/min within temperature range of 35-90°C. It was clear from the experimental data that specific heat rises with rise in temperature. However, the addition of CNT nanoparticles enhanced the heat capacity of the nanofluids significantly. Since the specific heat of the carbon nanotube is greater than the base fluid, this causes a higher specific heat in the nanofluid. For Cyrene/MWCNT nanofluid system, an 11.25% enhancement was observed at 35°C when a small amount of nanotube concentration (NF2) was added to the base fluid. The enhancement was greatest at 65°C. However, by doubling the concentration of the nanofluid (NF1), enhancement increases to up to 62.95% at 35°C. The greatest enhancement was found at 75°C. It was seen that after 75°C, specific heat curves decrease with an increase in temperature. The results were compared with the commercially available thermal fluid Paratherm GLT, as shown in Figure 2.12(a). This can be explained as with an increase in temperature, the rise in the system's internal energy due to the fact that the vibrational and rotational energies of the molecules also increase., indicating adsorption of higher molar heat capacity by the molecules.

A notable enhancement of 29.3% has been observed at higher temperature for the case of NF3 nanofluid system. In order to provide context for these findings, a comparison is shown in Figure 2.12(b) with commercial HTG (Paratherm GLT and Therminol 55). Based on the experimental data with the function of temperature, a mathematical correlation was developed with regression value R^2=0.969 as shown in Figure 2.12(b) and given in Equation 2.12.

$$Cp = 1.17936 + 0.01509T - 3.87711 \times 10^{-5}T^2 \quad \textbf{(2.12)}$$

Here Cp is the specific heat capacity and T is the temperature of the nanofluid.

(a)

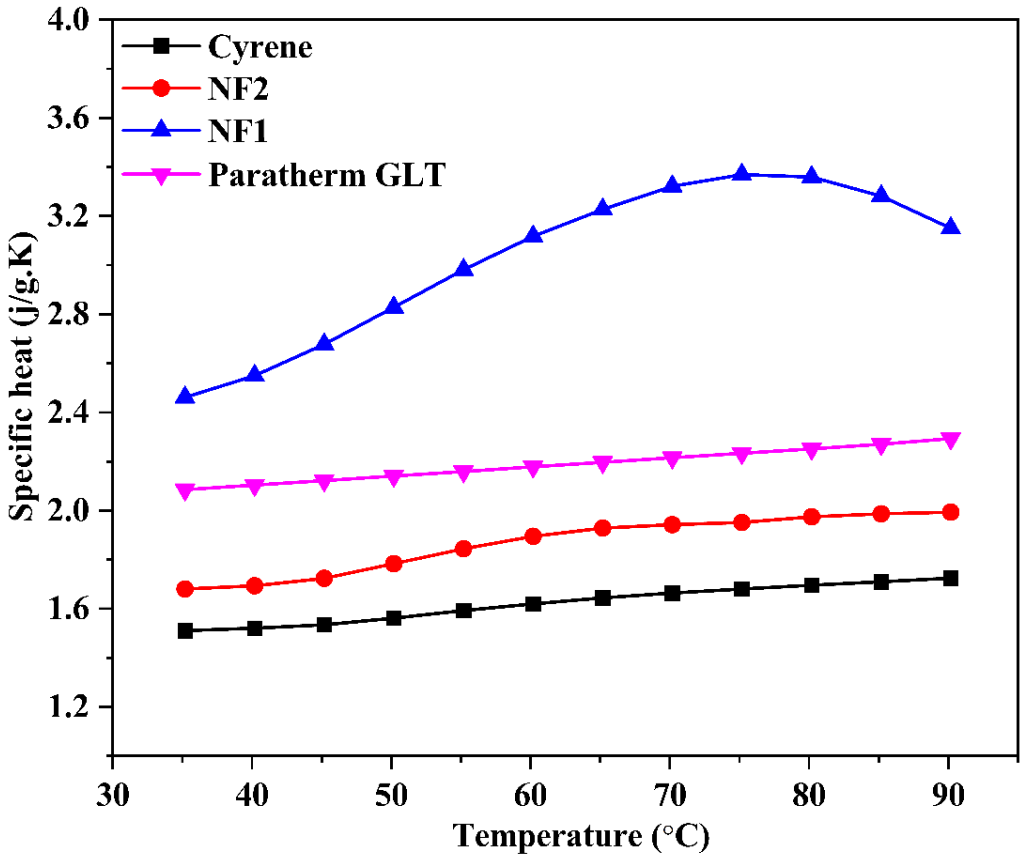

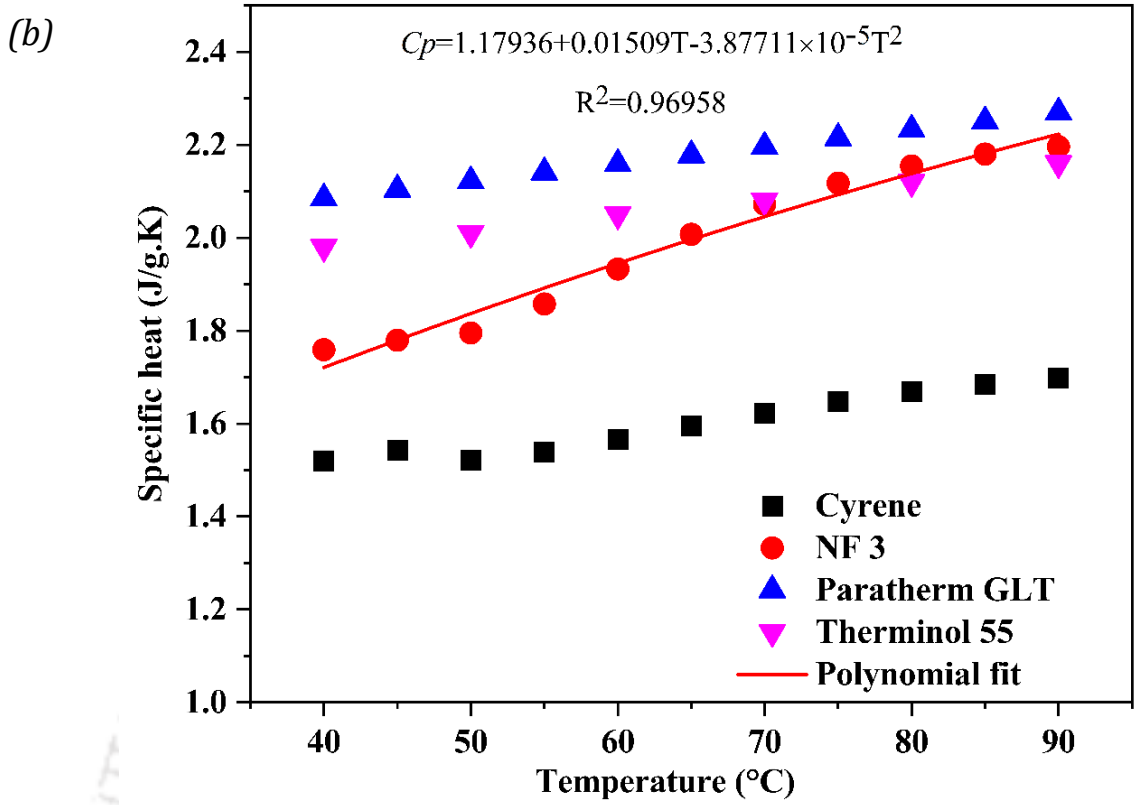

Figure 2.12. Specific heat of nanofluids at temeperature from 35-90°C (a) Cyrene/MWCNT (b) Cyrene/MWCNT-COOH nanofluid

The obtained results of thermophysical properties hence compared with literature Ilyas et al.[60], and the values between base fluid and nanofluids were found to be agreeing well. According to published data, the density difference between MWCNT-thermal oil nanofluid and base fluid was 0.76 kg/m^3 and 0.61 kg/m^3 at 30°C and 40°C, respectively. In present work the density changes between 30°C and 40°C were 0.001 and 0.002 kg/m^3, respectively at 0.0016 and 0.0032 volume fractions nanofluid. Similar results was reported in the literature Pyarimohan et al. [61], where minor difference of 0.55 kg/m^3 and 0.54 kg/m^3 was observed after addition of nanoparticles in the deep eutectic solvents. Similarly, the viscosity of the reported nanofluid and base fluid decreases with increased temperature, consistent with the literature [60, 61].

2.4.3. Stability of the Nanofluid

A primary technique to understand the dispersion behaviour of CNTs in base fluid and stability evaluation of nanofluid is its sedimentation[62]. This practice is based on the settlement of the nanoparticles at the bottom of the base fluid due to gravity. The higher sedimentation time indicates the higher stability of nanofluid. In our work, a 10 mL of a freshly prepared and sonicated sample was put inside a 10 mL vial was prepared and then kept at ambient conditions at a temperature of about 293 K over a period of 5 days. During this time, a daily visual inspection was performed for all concentrated nanofluids. It was observed that the nanoparticles are settled after five days, exhibiting poor dispersion behaviour. The images of nanofluids were captured after sonication after 24 hrs, 36 hrs and 48 hrs. The optical microscopic images of NF2 and NF1 after 48 hours are provided as Figure AS2 in appendix A. However, good dispersion behaviour of nanoparticles was observed for up-to 36 hours. Thereafter, a small agglomerate of the nanoparticles was observed after 36 hours in the base fluid due to van der Waal forces of attraction. The agglomeration of nanoparticles is caused by the adhesion of particles to each other, resulting in (sub)micron-sized entities. In contrast, nanoparticle agglomerates are the result of the formation of covalent or metallic interactions that are difficult to break. Viscosity and dipole moment of the base fluids appear to be two crucial parameters that affect the level of agglomeration. Fluids having a mid-level dipole moment are better candidates for formulating stable nanofluids. On the other hand, the fact that Cyrene has a higher dipole moment (3.4), enables the agglomeration between the nanoparticles. The overall observation of the nanofluid based on Cyrene-MWCNT can withstand stability of approximately three days during which they needs to be operated.

The stability and dispersion characteristics of nanofluids was further explored by the investigating the zeta potential value. The zeta potential was evaluated by measuring the electro kinetic potential in order to analyse the nanofluid's dispersion and stability [63, 64]. It was

observed that the zeta potential value of nanofluids NF1 and NF2 were -36.71mV and -91.00 mV whereas 191mV for nanofluid NF3, respectively as shown in Figure 2.13. The results showed that the nanoparticles were highly stable in base fluid. When nanoparticles are dispersed in the base fluid, there are two layers formed surrounding the particle. The closely attached layer with the particle is known as the stern layer. The diffuse layer is the next one up from the stern layer, and it is just tangentially bound to the nanoparticle. The two layers working together also known as electric double layer (EDL), is a neutral electrical configuration. Zeta potential is formed on the interface of EDL and is measured in millivolts at this point. A high zeta potential value implies higher repulsive forces, increasing the possibility of the agglomeration of particles. Due to the nanoparticle's large surface area and compact size, its surface area is reduced, resulting in strong van der Waal forces. These strong van der Waal forces attract the other particles and form an agglomerate. As per Vandsburger, Nanofluids are practically stable when the zeta potential of the particles is around $\pm$30 mV[65]. When the zeta potential is near to 45 mV, nanofluid stability is confirmed. If the value of the nanofluid is more than $\pm$60 mV, it has outstanding stability.

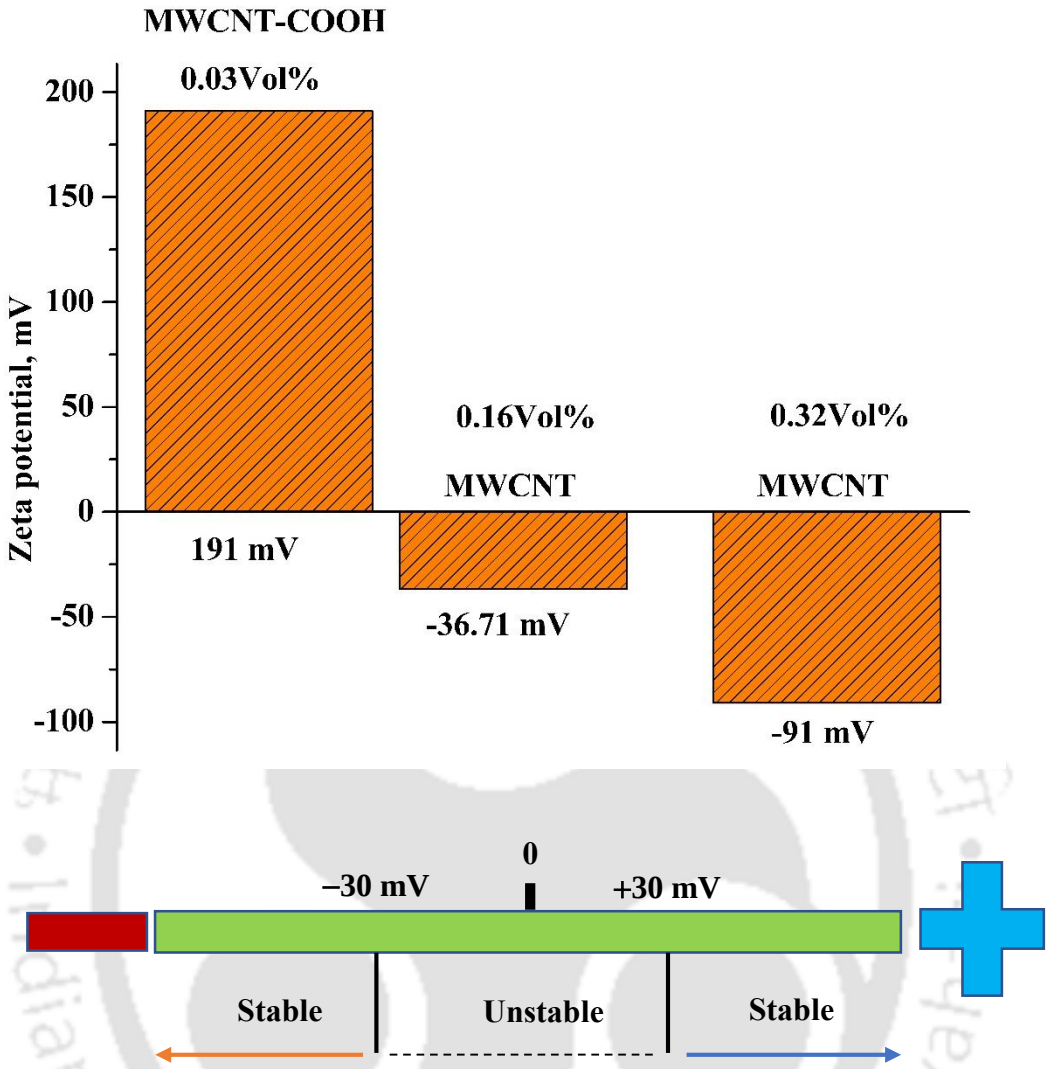

Figure 2.13. Zeta potential values for MWCNT-COOH and MWCNT base nanofluid

2.4.4. Forced Convection Studies

2.4.4.1 Forced Convection Studies: Cyrene/MWCNT Nanofluid

The forced convection experiments were carried out at three different Reynolds numbers with a constant heat flux of 13514.86 W/m^2. Heat transfer coefficients were calculated under the laminar condition at each testing section of the tube as per the experimental setup. The detailed calculation of heat transfer coefficients is given in the Appendix A. Figure 2.14(a) shows the axial variation of heat transfer coefficient at three different Reynolds numbers for base fluid. The convective heat transfer coefficient was found to increase with an increase in Reynolds number. The heat transfer coefficient is highest at N_{re}=1881 and decreases non-linearly with axial distance. This can be explained that with an increase in Reynolds number, the boundary layer thickness decreases, leading to a higher heat transfer rate. Local Nusselt number is calculated reported in Figure 2.14(b).

The significance of a higher Reynolds number implies higher heat transfer due to the fluid motion as compared to the heat transferred by the process of conduction. A remarkable enhancement in heat transfer coefficient was observed when 0.0016 and 0.0032 volume fraction of MWCNT were dispersed in base fluid. Figure 2.15(a) shows the effect of carbon nanotube concentrations on heat transfer coefficient along the axial distance of the tube at Reynolds numbers (N_{re}=1881, N_{re}=1129, and N_{re}=626). As expected, with increasing Reynolds number, the heat transfer coefficient of the nanofluid also increases. Possible reasons for this enhancement include nanoparticle size and the effect of the Brownian motion of particles, decreasing the particle's boundary layer thickness and mixing effect [66, 67]. Analogously, the local Nusselt number of the nanofluids and reported in Figure 2.15(b) along with base fluid data. Due to the high thermal conductivity and specific heat than base fluid, Nusselt number was found to increase at a higher rate than of the base fluid.

From Figure 2.16(a), it was observed that Nanofluid, NF1 possesses the highest heat transfer coefficient value at the N_{re}=1881, followed by nanofluid NF2, whereas a low heat transfer coefficient was observed at N_{re}=626 with volume fraction 0.0016 (NF2). Figure 2.16(b) represents the variation of heat transfer coefficient and Nusselt number of nanofluids NF1 and NF2. This was compared with base fluid at Reynolds number N_{re}=1881 along with the axial distance of the testing tube. It was noted that 19.06 % enhancement was observed when 0.0016 volume fraction nanofluid was used (NF2), whereas 46.58% enhancement was found for 0.0032 volume fraction of nanofluid. As discussed above, nanofluid with higher thermal conductivity increases the heat transfer coefficient of the fluid. Furthermore, when the Reynolds number increases, so does the Brownian motion of the nanoparticle, resulting in a high heat transfer coefficient. For base fluid and nanofluids, as the heat is transferred from the surface of the pipe to the fluid through conduction, the thickness of the boundary layer becomes very small. This is attributed to the increase in the heat transfer coefficient at the entrance region [68].

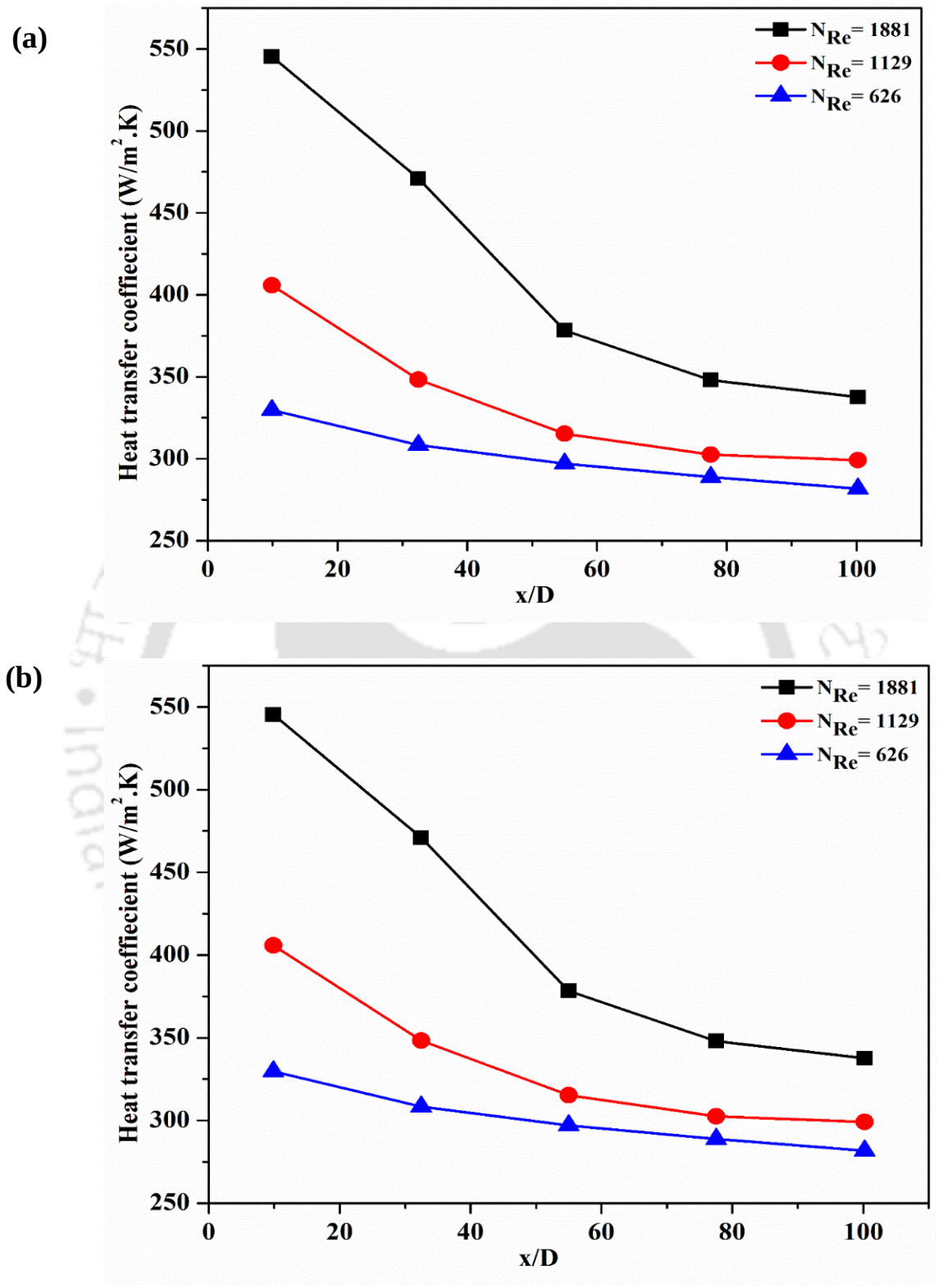

Figure 2.14. (a) Heat transfer coefficient and (b) Nusselt number of base fluid Cyrene at Reynolds number 1881, 1129 and 626

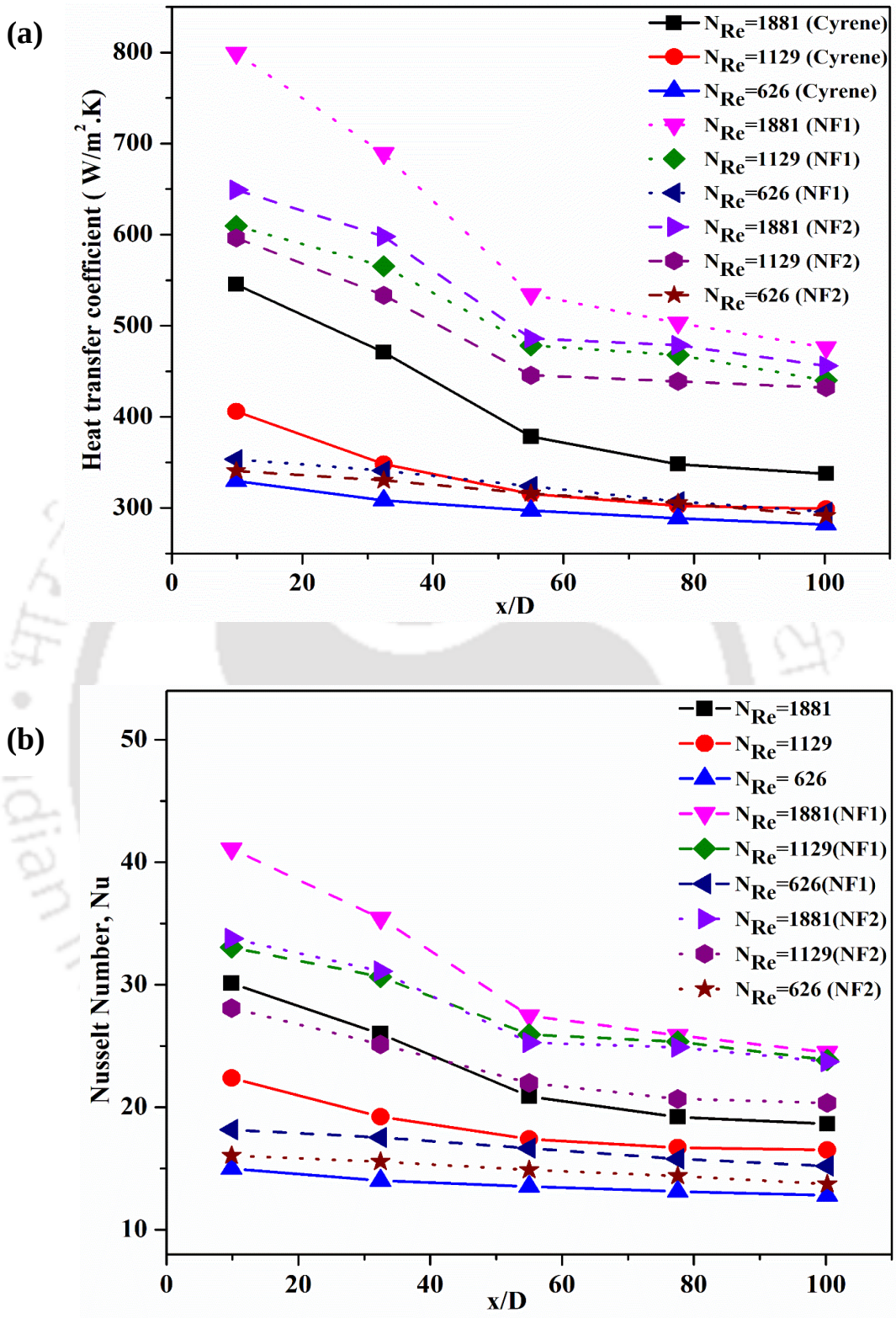

Figure 2.15. (a) Heat Transfer coefficient and (b) Nusselt number of base fluid and nanofluids (NF1 and NF2) at Reynolds number 1881, 1129 and 626

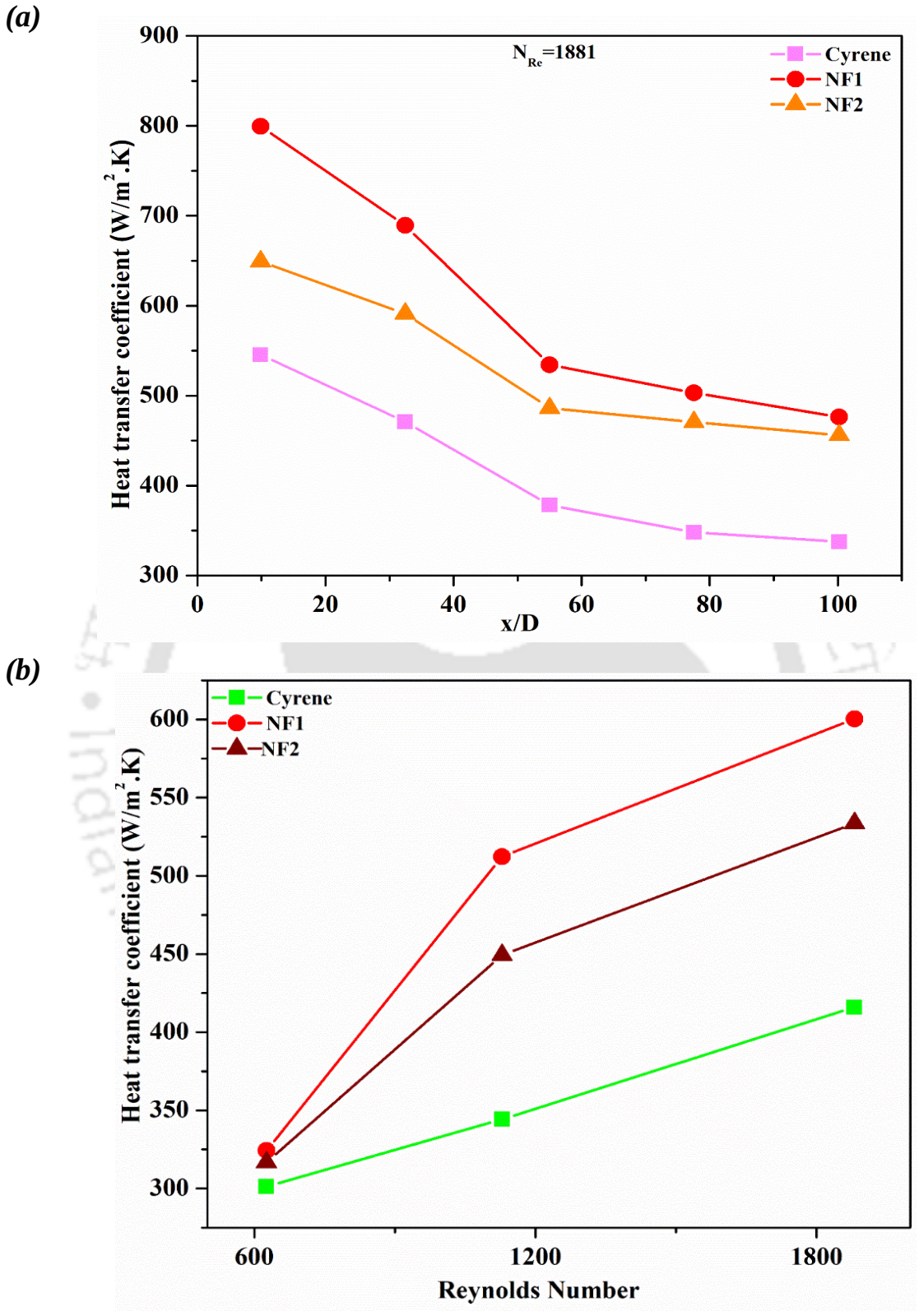

Figure 2.16. (a) Variation of Heat Transfer coefficient along with axial distance (b) Variation of Heat Transfer coefficient with Reynolds number of base fluid NF1 and NF2

As the fluid moves, the thickness of the boundary layer increases; as a result, the heat transfer coefficient decreases along with the length of the pipe. Also, nanoparticle concentration is highest at the entrance region resulting in non-uniform distribution of both thermal conductivity and viscosity, thereby reducing the thickness of the thermal boundary layer, which ultimately improves the heat transfer coefficient at the entrance region. According to previous work[67, 69, 70], other factors that is attributed to the increase in heat transfer coefficient includes the mixing effect of particles near the wall, high thermal conductivity, reduction of boundary layer thickness, and delay of boundary layer formation. Figure 2.17(a) and (b) represents the wall temperature and fluid temperature profile of base fluid and respective nanofluids. It was noted that inner wall temperature is higher in both nanofluids and base fluid at low Reynolds number. Compared to the base fluid, the wall temperatures of the nanofluid are less and decrease with increasing Reynolds number. This is because as the nanofluid flows through the tube, the nanoparticle strikes the tube wall and transfers thermal energy from the wall to the nanofluid. This lowers the wall temperature of the fluid. A similar result was reported by Fotukia [71], where tube wall temperature decreases by adding nanoparticles to the base fluid. When the fluid initially enters a pipe, it is not fully developed. Instead, before it fully develops, the fluid must travel a particular distance without being disturbed. This also holds true when a fluid travels a pipe system curve. This is due to the curve's disturbance of the fluid's velocity profile. It must therefore travel a given distance in a straight pipe to fully develop once again. Further the experimental obtained Nusselt number values of nanofluids were compared with Pyarimohan et al [61] where similar trend was observed. Overall, an improvement of convective heat transfer coefficient and Nusselt number in the laminar region were observed. The higher heat transfer coefficient was attributed to its thermal conductivity and the thickness of the hydrodynamic boundary layer and the shape of the nanoparticles.

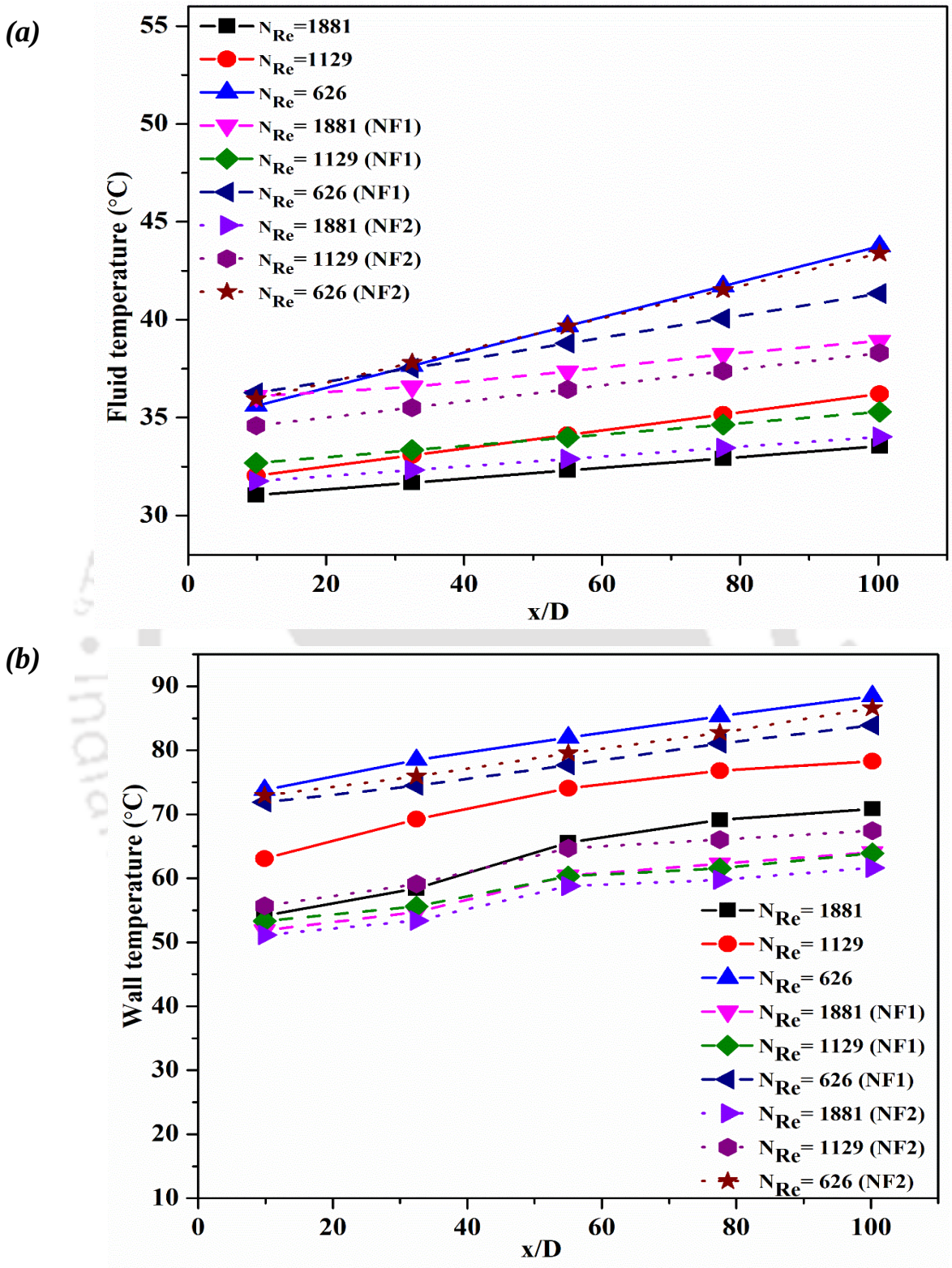

Figure 2.17. (a) Fluid temperature and (b) Wall temperature of base fluid and Cyrene/MWCNT nanofluids

2.4.4.2 Forced Convection Studies: Cyrene/MWCNT-COOH Nanofluid

With a constant heat flow of 12840.761 W/m^2, the forced convection experiments were conducted in a turbulent environment at various Reynolds numbers. Figure 2.18 (a) and (b) represents the fluid temperature and wall temperature of the Cyrene and Cyrene/MWCNT-COOH nanofluid. Both profiles show less linear increment along the length of the testing tube because of the longer residence time. Figure 2.19(a) depicts the axial distribution of the heat transfer coefficient for four discrete Reynolds numbers (11441, 14715, 19750, and 24159) for the base fluid Cyrene. In addition, the obtained results are compared to those of water at Reynolds numbers of 53033 and 64818. It is worth noting that the convective heat transfer coefficient exhibits an increase as the Reynolds numbers increases. The heat transfer coefficient reaches its maximum value at a Reynolds number of 19750 and exhibits a very stable trend along the axial direction. The observed behaviour can be attributed to the inverse relationship between the Reynolds number and the thickness of the boundary layer. As the Reynolds number increases, the boundary layer thickness decreases, resulting in an enhanced heat transfer rate.

The greater Reynolds number is associated with increased heat transfer resulting from fluid motion, in contrast to the heat transfer occurring through conduction. A significant increase in the heat transfer coefficient was found upon the addition of 0.03 vol% of MWCNT-COOH to the base fluid. The impact of varying CNTs concentrations on the heat transfer coefficient throughout the axial distance of the tube is illustrated in Figure 2.19(b). The Reynolds numbers considered in this study are 2709, 9738, 19420, and 16471. As predicted, the heat transfer coefficient of the nanofluid exhibited an upward trend with the increase of the Reynolds number. Potential reasons for this improvement include the size of the nanoparticles, their increased thermal conductivity, the impact of their Brownian motion, the reduction of the thickness of their boundary layer, and the mixing effect [54, 55].

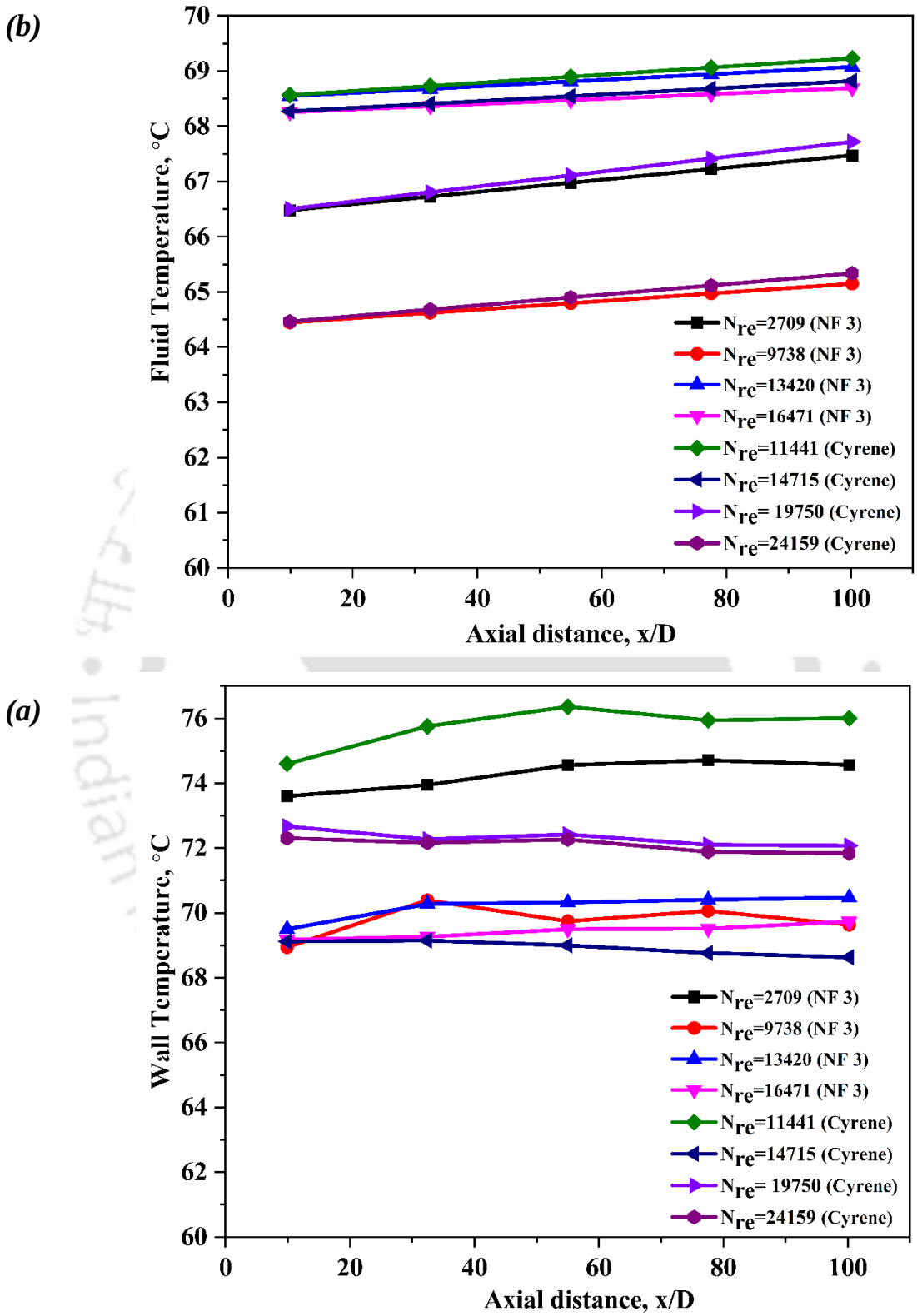

Figure 2.18. (a) Fluid temperature and (b) wall temperature profile for both Cyrene and Cyrene/MWCNT-COOH nanofluid (NF 3) along with testing section of the tube.

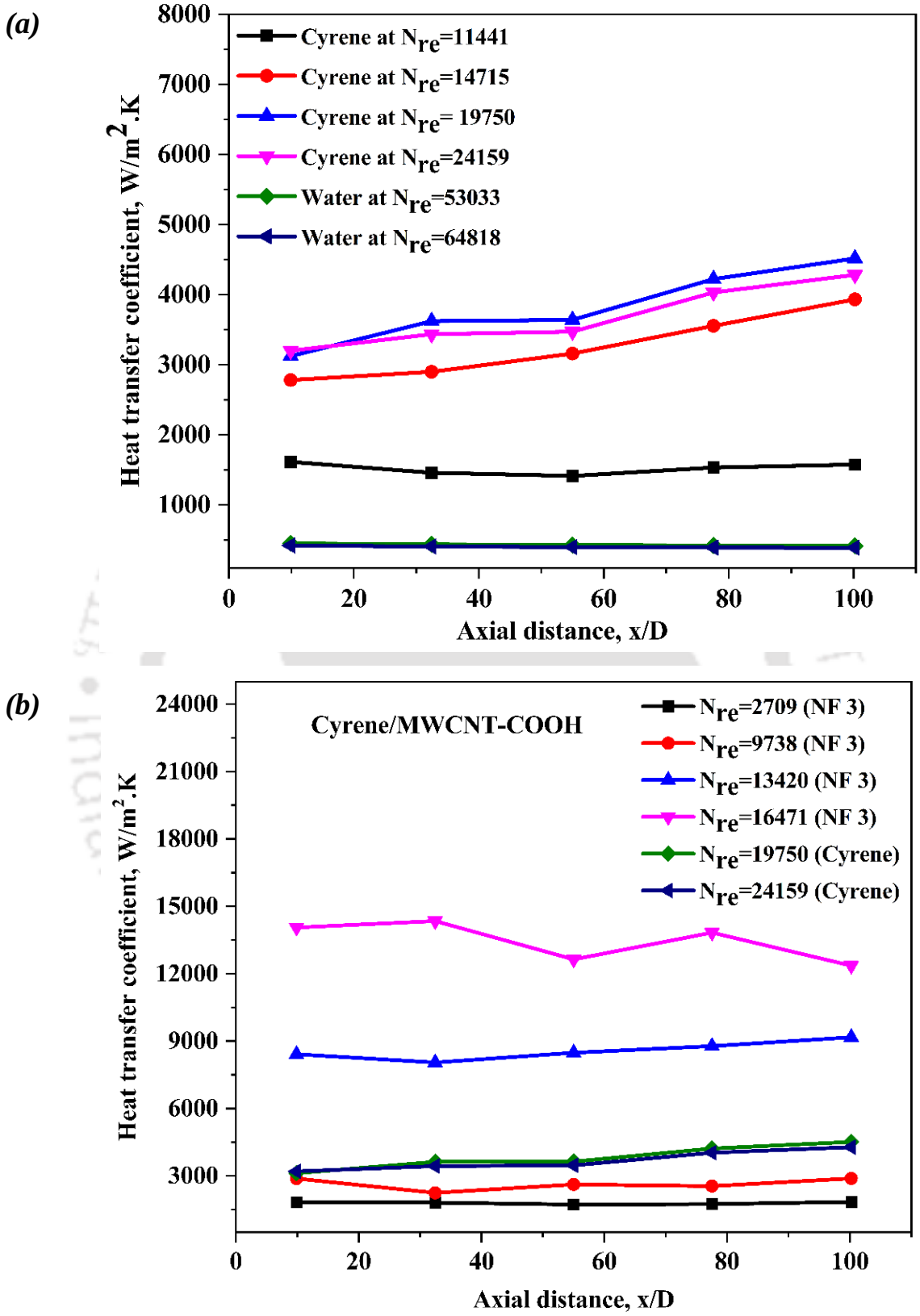

Figure 2.19. Heat transfer coefficient of (a) Cyrene and water, (b) Cyrene/MWCNT-COOH nanofluid at different Reynold numbers.

2.4.5 Quantum Chemical Calculation Results

2.4.5.1 Geometry Optimization

In this study, calculations were initiated by the geometry optimization of a simple (5,5) single-walled carbon nanotube whose ends were saturated with ten hydrogen atoms. This model has been utilized in prior studies for CNTs so as to ensure consistency and comparability of results. Furthermore, this model is prevalent in many other reports since the computational costs of the are minimized without the use of substantial approximation. The geometry optimization for Cyrene/SWCNT was compared with the optimized geometry of SWCNT coupled with the conventional thermal heat storage media, specifically ethylene glycol (EG). The initial optimized structures of individual molecules were used to generate the pair configuration of the EG/SWCNT and Cyrene/SWCNT system (Figure 2.20). It is clearly seen from the optimized geometry that the Cyrene molecules approach towards the carbon nanotube at different O (O_{56} and O_{57}) and H (H_{45}, H_{47}, and H_{54}) atoms and get induced towards carbon nanotube at positions C_7, C_8, C_{12}, C_{14}, and C_{16}. The corresponding C-H and O-C bond distances in Å are displayed in Figure 2.20. It is seen from the Cyrene/SWCNT pair system that when compared with EG/SWCNT pair system, bond distances between Cyrene/SWCNT atoms are a little higher.

In the case of the EG/SWCNT pair system, the shortest hydrogen bond interaction (C-H bond) was measured at 2.77 Å. For both the system, C-H bond distances are comparatively less than the C-O bonds, where predicted distances between O atoms and C atoms of EG (O_{49}-C_9 and O_{47}-C_{11}) and Cyrene (O_{56}-C_7 and O_{57}-C_{12}) molecules are 3.21, 3.57, 3.39 and 3.45 Å respectively. It was noted that with the introduction of Cyrene with SWCNT, the C-H and C-O bond distances provides a slight decrease in bond distances. However, the decrement in bond distances were very less in magnitude, indicating that the dominating interactions were weak van der Waal interactions. The interaction energies for EG/SWCNT and Cyrene/SWCNT

systems as calculated from equation 2.2 were -7.592 kcal/mol and -8.534 kcal/mol, respectively. The negative sign indicates the spontaneity of the interaction. The higher the negative value, higher is the interaction. The higher negative value for the interaction energy of the Cyrene/SWCNT complex system can be attributed to the higher charge transfer compared to the EG/SWCNT system, which exposes fewer active sites to SWCNT. The presence of a ketone group, which makes Cyrene a more polar molecule than EG, may further contribute to the magnitude of charge transfer within the Cyrene/SWCNT system.

The optimized results of both structures indicate a weak interaction between molecules of Cyrene and EG with SWCNT. Thus, one might deduce that the interaction between solvents and SWCNT is a physical process governed by van der Waals interactions. However, the significant interactions within Cyrene/SWCNT complex systems, in comparison to EG/SWCNT system, gives tenability with the experimental findings especially related to the zeta potential which indicates the dispersive nature and the subsequent stability. The weak van der Waal (vdW) interaction within the Cyrene/SWCNT complex system leads to the agglomeration of the CNT nanoparticles, which in turn results in a short term stability of the nanofluids. This is in line with the experimental evidence as reported in section 2.4.3 discussing the stability of nanofluids.

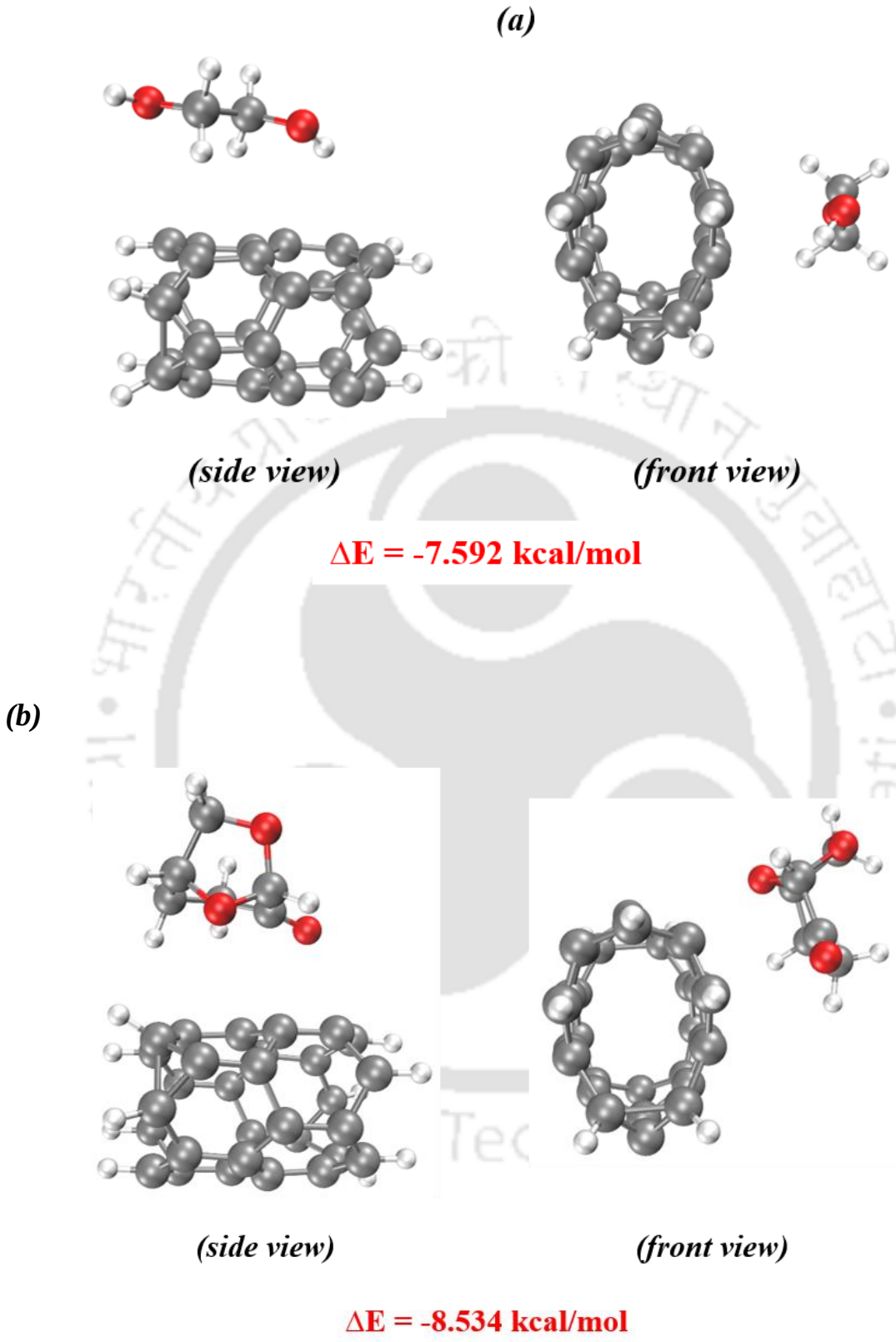

Figure 2.20. Optimized structures of (a) EG/SWCNT (b) Cyrene/SWCNT obtained using ωB97XD/6-31G(d,p) level of theory (side view and front view)

2.4.5.2 Non-Covalent Interactions Between SWCNT and Solvents

The reduced density gradient (RDG) analysis was executed in order to shed clarity on the role and relevance of non-covalent interactions in the interaction of base fluid with the surface of SWCNT. RDG establishes a connection between the real space function and the second intrinsic value of the electron density hessian matrix. The analysis (RDG) may serve as an indicator of the sort of weak interactions present in the system. On the basis of their intensities, types, and sites of action, RDG analysis can be used to depict intermolecular interactions.

The RDG scatterplots and surface distribution diagrams for the stable Cyrene/EG–SWCNT complex systems are depicted in Figure 2.21. Plots of the RDG against (sign λ_2)ρ, where (sign λ_2)ρ is the electron density multiplied by the sign of the second Hessian eigenvalue (sign λ_2)ρ , are used to create NCI plot to investigate the presence of weak interactions. The value of (sign λ_2) ρ is useful in predicting the nature of interaction. For a repulsive interaction we have (sign λ_2)ρ> 0 and for attractive interaction (sign λ_2)ρ < 0 [72]. A. Figure 2.21 displays strong attractions, strong repulsion, and vdW interactions in blue, red, and green color, respectively. As presented in Figure 2.21, when the thermal media (Cyrene and EG) were exposed on the surface of SWCNT, several spikes occurred in the low charge density region of the Cyrene/EG-SWCNT complexes, indicating that the Cyrene/EG-SWCNT complexes have weak interactions. The green region observed between Cyrene and SWCNT implies that weak van der Waals interactions play a significant role in Cyrene-SWCNT interactions (Figure 2.21 (a)).

The van der Waals interaction between the SWCNT surface and Cyrene occurs through X...π (X represents C, H, and O atoms of Cyrene). A similar pattern of results can be visualized in EG/SWCNT complex where the van der Waals interactions are the dominating intermolecular forces. Within the rings of the SWCNT and Cyrene structure, there is a clear indication of a spatial repulsive force, which is indicated by the red region. From NCI analysis,

it can be established that the large number of interactions between Cyrene/SWCNT complex systems enhances the interaction strength of Cyrene molecules on SWCNT surfaces and results in higher interaction energy values than other complexes. However, the large number of van der Waals interactions present within the Cyrene/SWCNT complex system provides a more stable nanofluid system in comparison to the conventional solvent system based on ethylene glycol.

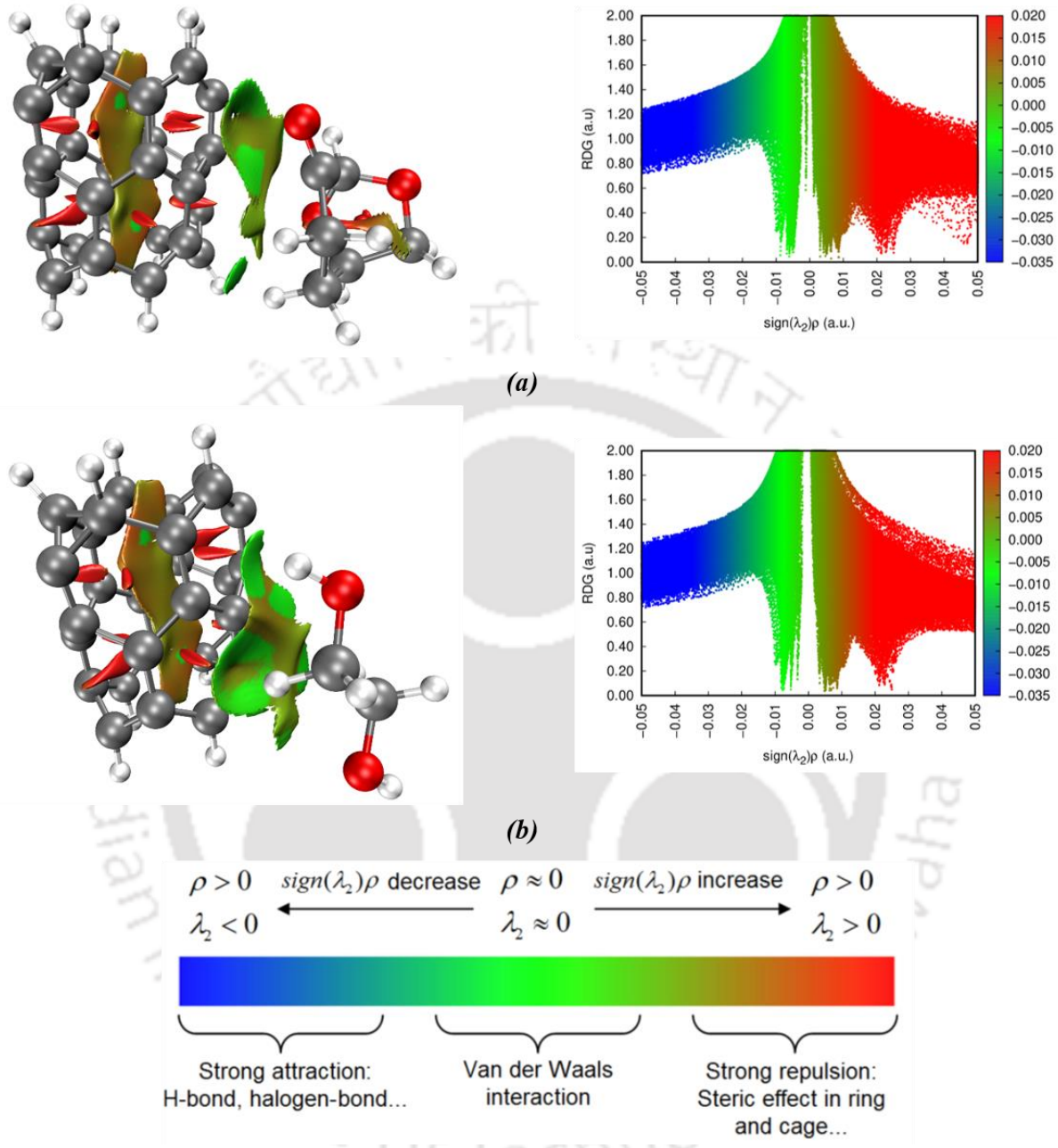

Figure 2.21. RDG isosurface and scatter graph of RDG for SWCNT-Cyrene and SWCNT-EG complex system

2.4.5.3 HOMO-LUMO Analysis

HOMO-LUMO energy gap is the key parameter to study the chemical stability of the system. This is the difference in energy between the highest occupied molecular orbital (HOMO) and the lowest unoccupied molecular orbital (LUMO. The relative energy of each orbital determines the magnitude of the HOMO-LUMO energy gap and helps us to determine the molecular electronic transport properties [73]. It is calculated by deducting the LUMO energy from the HOMO energy [74-76]. The large difference between the HOMO and LUMO energy suggests a greater degree of chemical kinetic stability and resistance to charge transfer. Similarly, a small energy gap indicates a high degree of polarization, as reaching the excited state needs just a minimal amount of energy. In contrast, a rise in HOMO energy combined with a drop in LUMO energy leads in a decrease in the HOMO–LUMO energy gap [77]. Small HOMO–LUMO gap indicate the presence of soft materials, whereas the hard materials represent the large energy gap of HOMO–LUMO. The kinetic stability and reactivity of the components were calculated through the value of the HOMO–LUMO energy band gap of the system.

The HOMO, LUMO and HOMO-LUMO energy gap of Cyrene, EG, and SWCNT configurations are shown in Figure 2.22. The HOMO–LUMO gap of complex systems (Cyrene/SWCNT and SWCNT/EG) indicate the presence of reactivity via electronic hopping energy. The HOMO–LUMO energy gaps of Cyrene/SWCNT and EG/SWCNT systems are displayed in Figure 2.23. From these Figures (2.22 and 2.23), it is clearly seen that the HOMO-LUMO energy gap of Cyrene/SWCNT reduces when Cyrene molecule is exposed to SWCNT. The respective values for Cyrene and Cyrene/SWCNT were 0.364 eV and 0.184 eV respectively. Similar results can be seen in the EG/SWCNT system also, where values are 0.501 eV for EG and 0.185 for EG/SWCNT respectively. These results reveal the fact that the presence of carbon nanotube (SWCNT) reduces the energy gap value and interact the

molecules more strongly with Cyrene. Larger value of energy gap for SWCNT/EG system indicate an unstable nanofluid system. It implies that the charge transfers and transfer of electrons is thermodynamically unfavourable in comparison to the Cyrene/SWCNT complex system. The lower interaction energy of EG/SWCNT complex system and higher HOMO-LUMO energy gap, presents a clear picture of the system, where it can be confirmed that the active sites of EG are less exposed to SWCNT thereby leading to an unstable nanofluid system. Therefore, Cyrene/SWCNT systems presents itself as a potential heat transfer media, with little corrections in its structure such as functionalization of the molecules with some electron withdrawing groups. The presence of electron withdrawing groups within Cyrene molecule can help in reducing the occurrence of agglomeration within nanoparticles due to the formation of covalent or metallic interactions.

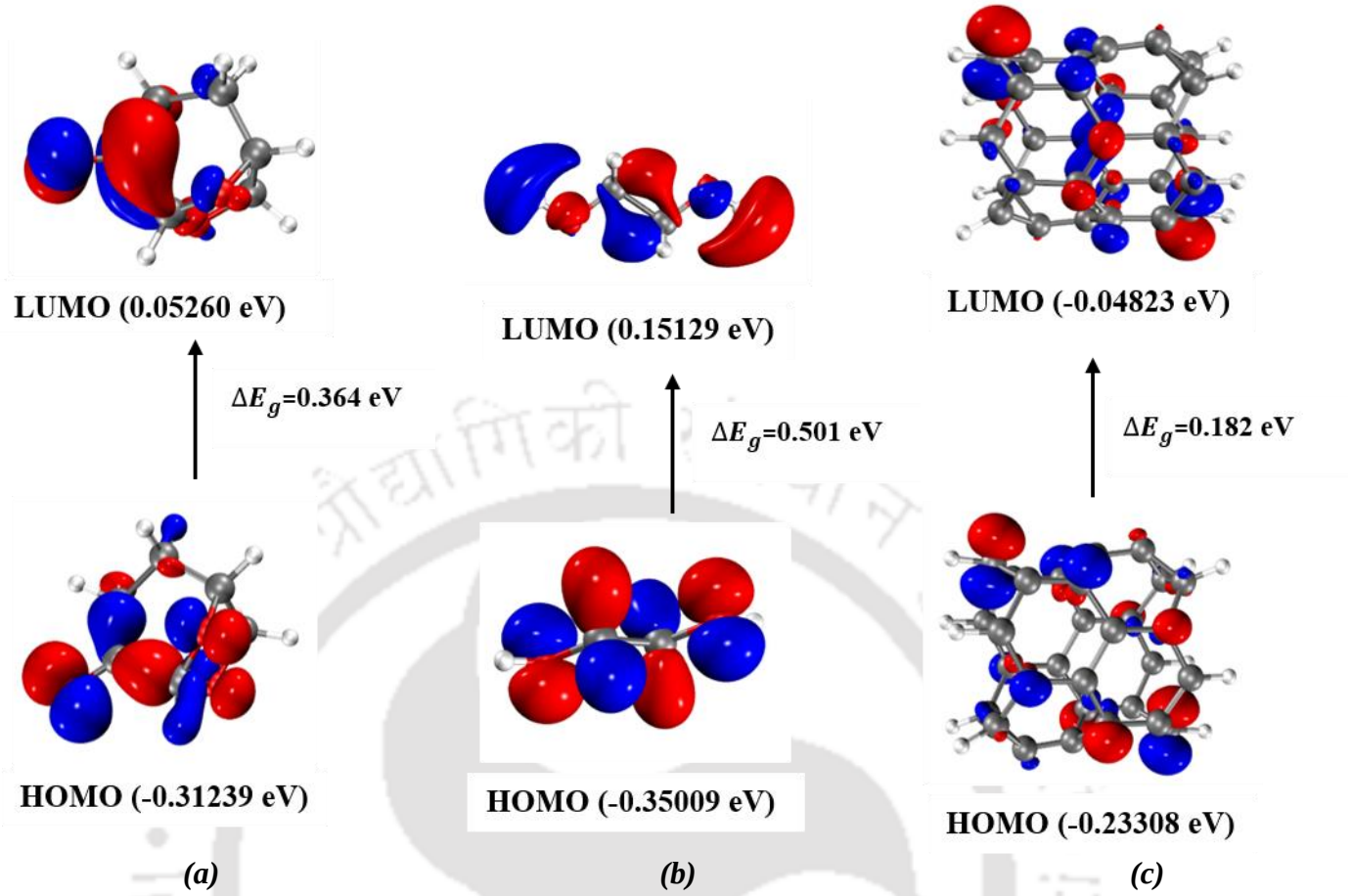

Figure 2.22. HOMO-LUMO energy gap of (a) Cyrene, (b) Ethylene Glycol (EG), and (c) SWCNT

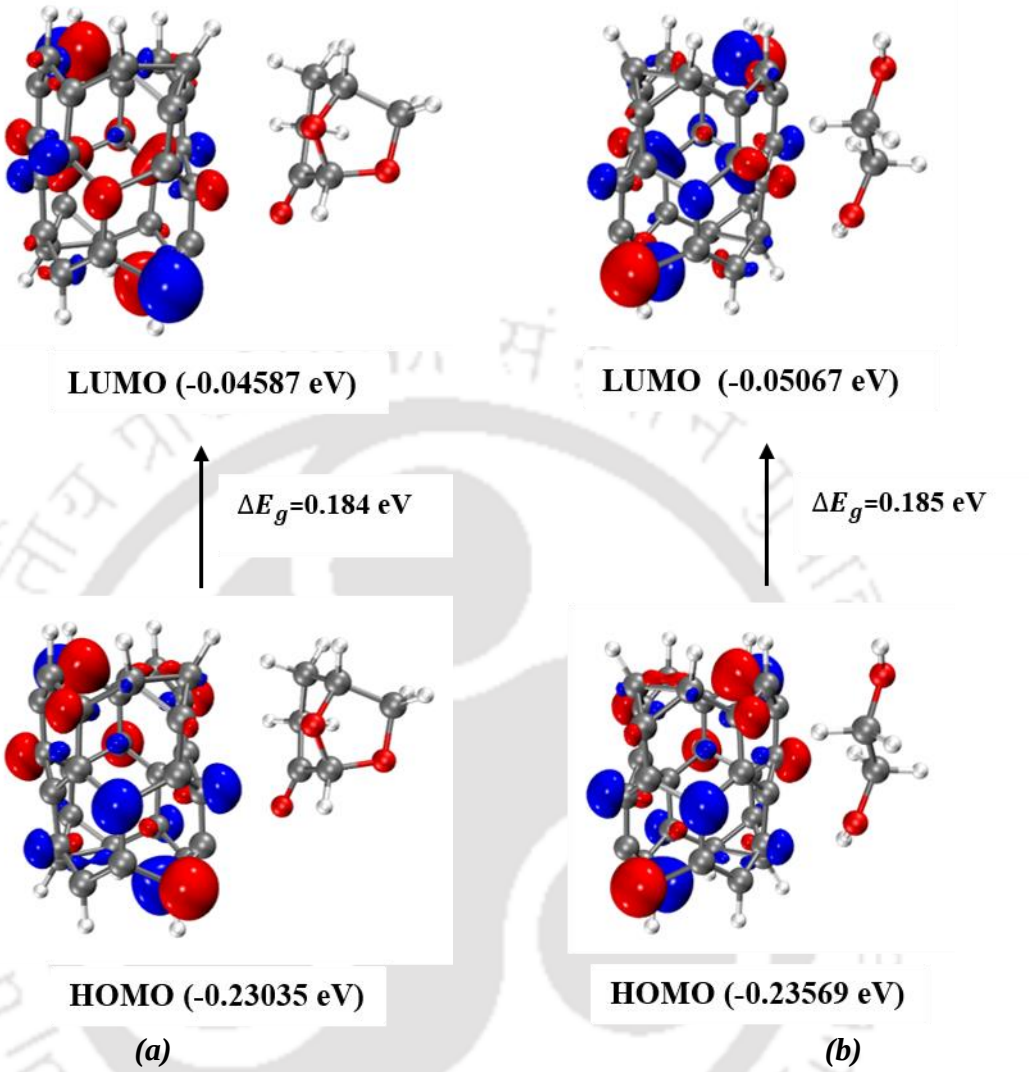

Figure 2.23. HOMO-LUMO energy gap of (a) Cyrene + SWCNT, and (b) EG + SWCNT

2.4.6 Reverse NEMD Simulation – Thermal Conductivity Results

The absence of a reliable and robust modelling approach has long hindered the determination of thermal conductivities using MD simulation. The requirement to define and compute a heat flux vector at the molecular scale has been the primary cause of this. The introduction of non-equilibrium methods, such as the heat-exchange method, reverse NEMD method, and dual-thermostat method, has estimated thermal conductivities more feasible. In this work, the reverse NEMD method is employed to calculate the thermal conductivity of nanofluids. This method involves partitioning the simulation box into small sections that extend in one direction. Heat flux is then induced by exchanging the velocities of the hottest atom in the cold section and the coldest atom in the hot section. The heat transfer between the hot and cold slabs is determined by:

$$q = \frac{\frac{1}{2}\sum(m_h v_h^2 - m_c\, v_c^2)}{2tL_xL_y} \tag{2.13}$$

The sum is taken across all exchange events that occur during the simulation time 't'. 'v_h'and 'v_c' represent the velocities of the hot and cold atoms, respectively, with masses 'm_h' and 'm_c'. The parameters in the denominator 'L_x' and 'L_y' represent the box dimension of the plane that is perpendicular to the flux in the z-direction. Thermal conductivity can be determined by measuring the temperature gradient in the z-direction and applying Fourier's equation of heat conduction.

$$k_{MD} = -\frac{q}{\langle\frac{\partial T}{\partial Z}\rangle} \tag{2.14}$$

Thermal conductivity simulations subject to inaccuracies due to finite size effects [56]. When calculating thermal conductivity, quantizing vibrational energy levels (phonons) introduces inaccuracies. Hence, corrections must be made to compensate for phonon scattering, which impacts the heat transfer. Further, the value of $C_v^q(T)$ can be determined from the vibrational density of states.

$$k_{corr}(T) = k_{MD}(T) \times \frac{C_v^q(T)}{3\ N\ k_B} \quad \textbf{(2.15)}$$

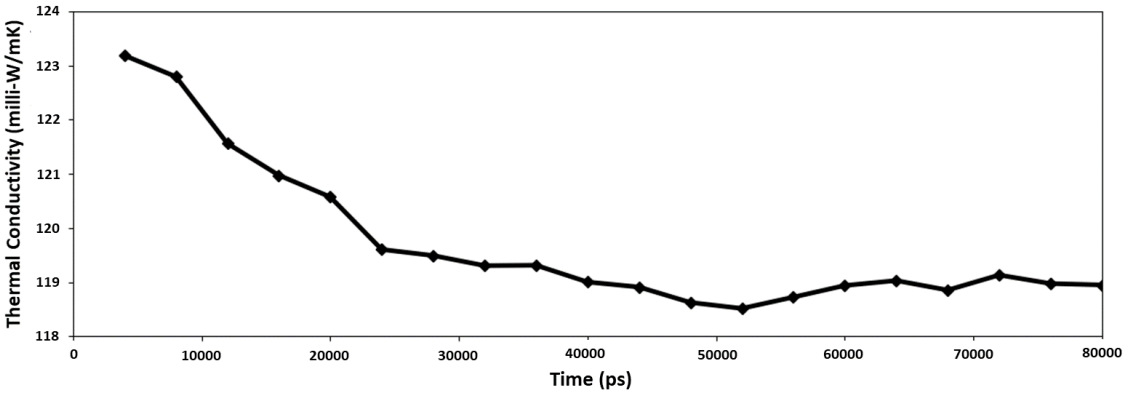

Figure 2.24 The thermal conductivity variation with respect to the simulation time for pure Cyrene.

The evaluated thermal conductivity of pure Cyrene variation with simulation time is shown in Figure 2.24. From Figure 2.24, it is evident that the thermal conductivity value of pure Cyrene is converged after 50 ns. The pure Cyrene thermal conductivity using reverse NEMD is found to be 118.95 milli-W/mK, whereas the experimental value is found to be 150 milli-W/mK[21]. The calculated thermal conductivity of the pure Cyrene, Cyrene+pristine SWCNTs, and Cyrene+carboxyl functionalized SWCNTs are summarized in Table 2.3. To probe the effects of temperature on thermal conductivity, we calculated thermal conductivity at 65 ^{0}C. We

observed a 9.9 % increase in thermal conductivity with reference to pure Cyrene at 26 ^{0}C. It is interesting to note that, on the addition of the 3 pristine CNTs (3 wt % nanoparticles), the thermal conductivity of the nanofluid increases to 123.38 milli-W/mK, whereas on the addition of the 10 pristine CNTs (~ 10 wt % nanoparticles) found to be 110.64 milli-W/mK at 26 ^{0}C. Therefore, a decrease in thermal conductivity by 6.9 % is observed with reference to pure Cyrene (118.95 milli-W/mK). This reduction in thermal conductivity is due to the fact that the pristine CNTs form aggregates, as shown in Figure 2.25 (a). Agglomeration reduces the nanofluid's thermal conductivity [21, 57, 58]. It is evident from the MD snapshots that in the case of the pristine CNTs, strong vdW interactions dominate leading to the formation of aggregates [59-61], which in turn reduces the surface area of the CNTs, whereas in the case of functionalized CNTs, the carboxyl group on the surface, hinder the vdW interactions among the CNTs. Therefore, the surface area of the nanoparticles is greater in the case of the functionalized nanoparticles than the pristine CNTs. It is interesting to note that the functionalization of the CNTs with a carboxyl group at higher concentrations (10 CNTs) increases the thermal conductivity by 8.6 %. It was observed from the study by Tian et al. [57] that lower concentrations of functionalized CNTs in the base fluid led to the improvement of the stability of the suspension but a slight decrease in the thermal conductivity. Overall, the higher thermal conductivity of the base fluids can be obtained by the functionalization of CNTs even at higher concentrations of functionalized nanoparticles; additionally, functionalization aids in the stabilization of the nanofluid.

Table 2.3 The calculated thermal conductivity of the pure Cyrene, Cyrene+pristine SWCNTs and Cyrene+carboxyl functionalized SWCNTs at 26 ^{o}C and 65 ^{o}C.

Fluid	Thermal Conductivity (milli-W/mK)	
	26 ^{o}C	**65 ^{o}C**
Pure Cyrene	118.95	130.81
Cyrene + (3) pristine CNT	123.38	133.99
Cyrene + (10) pristine CNT	110.64	123.51
Cyrene + (3) Carboxyl functionalized CNT	118.73	136.11
Cyrene + (10) Carboxyl functionalized CNT	120.23	138.82

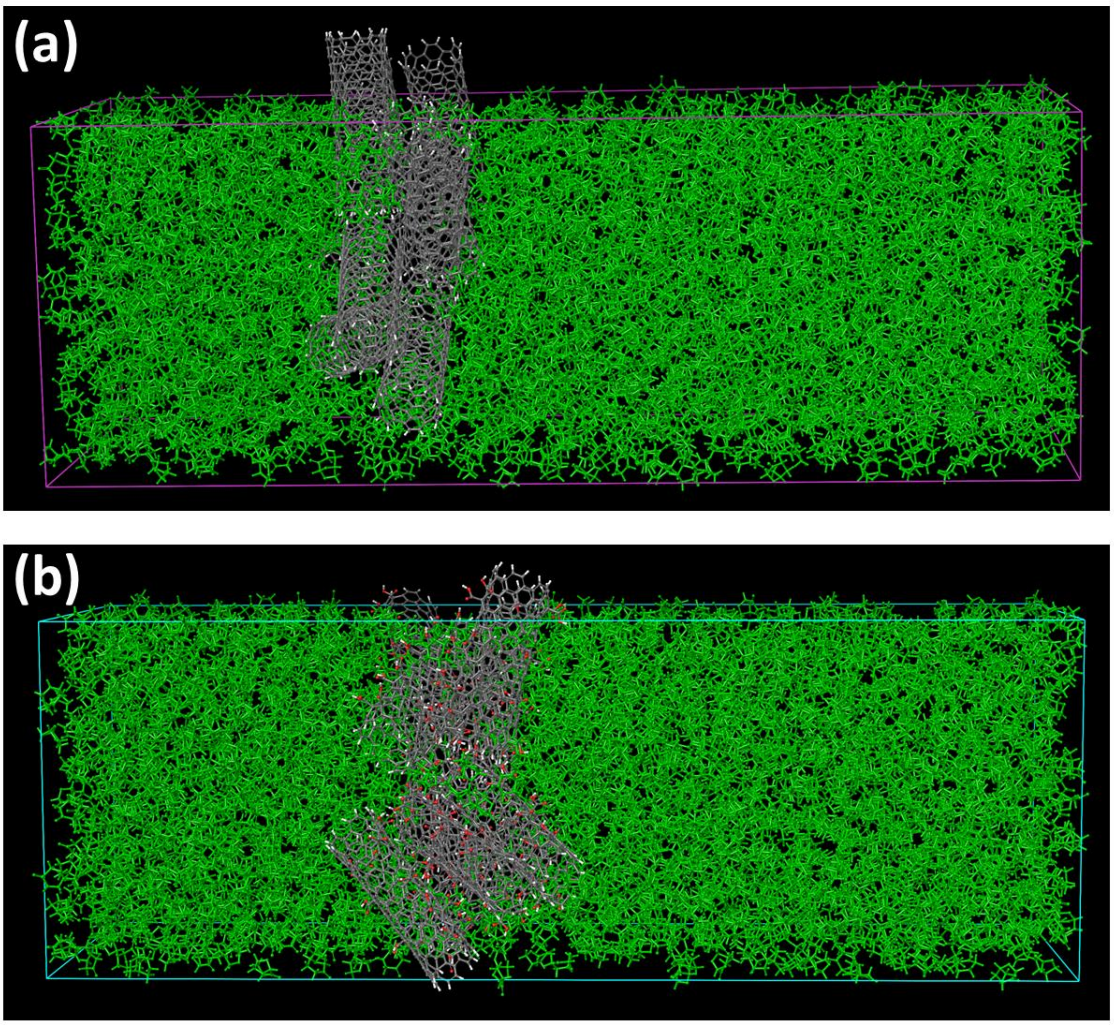

Figure 2.25: Snapshots of the NVE MD run showing Cyrene molecules along with (a) 10 pristine SWCNTs and (b) 10 carboxyl functionalized SWCNTs. The color coding for atoms is as follows: carbon is grey, oxygen is red, and hydrogen is white. Cyrene molecules are shown in green color for clear visibility of the CNTs.

2.5 Conclusion

The present chapter reports biomass-derived Cyrene can be used as a potential sustainable heat transfer media. The addition of a small amount of pristine carbon nanotube of volume fractions 0.0016 and 0.0032 and 0.0003 in functionalized carbon nanotube based nanofluids was seen to significantly enhance the thermophysical properties (density, viscosity, thermal conductivity, and specific heat capacity) as compared to base media namely Cyrene. Morphology and structure of MWCNT was confirmed by FESEM, FETEM, XRD and Raman spectroscopy analyses. The flow behaviour and thermal performance of Cyrene, Cyrene/MWCNT and Cyrene/MWCNT-COOH nanofluids were also investigated in the laminar region at different Reynolds numbers (1881, 1129, and 626 for Cyrene/MWCNT and2709, 9738, 13420, and 16471 for Cyrene/MWCNT-COOH). The enhancement of heat transfer was confirmed at a lower volume percent of nanoparticles. Here the nanoparticles lowered the thermal barrier layer and improved the heat transfer. The geometry optimization of individual molecules and Cyrene/SWCNT complexes in conjunction with the frontier molecular orbital analysis presents a detailed picture related to the stability of studied nanofluid systems. With a detailed RDG analysis it can be confirmed that weak vdW interactions between the base fluid (Cyrene) and SWCNT provide a platform for nanoparticles to interact with one another, which leads to agglomeration and decreased stability of the nanofluid. Our DFT calculations indicate that the interactions between Cyrene and CNT are controlled mainly by the weak vdW forces. Reverse NEMD simulations are used to validate the accuracy of the experimental thermal conductivity measurements. Further investigation and advancement in utilizing the capabilities of functionalized MWCNTs in thermal energy storage are anticipated to result in enhanced and environmentally friendly energy storage methods in the forthcoming years.

In summary, the present chapter gives information on bio-based nanofluid with two nanoparticles (MWCNT & MWCNT-COOH) and gives detailed insights into the properties of

the Cyrene and Cyrene based nanofluid. The deep eutectic solvent based nanofluid and their applications will be discussed in the subsequent chapter.

Reference

1. Khanafer, K. and K. Vafai, *A review on the applications of nanofluids in solar energy field.* Renewable Energy, 2018. **123**: p. 398-406.
2. Ghalandari, M., et al., *Applications of nanofluids containing carbon nanotubes in solar energy systems: A review*. Journal of Molecular Liquids, 2020. **313**: p. 113476.
3. Asadi, A., et al., *An experimental investigation on the effects of ultrasonication time on stability and thermal conductivity of MWCNT-water nanofluid: Finding the optimum ultrasonication time.* Ultrasonics sonochemistry, 2019. **58**: p. 104639.
4. Haghighi, E., et al., *Shelf stability of nanofluids and its effect on thermal conductivity and viscosity.* Measurement Science and Technology, 2013. **24**(10): p. 105301.
5. Colangelo, G., et al., *Experimental test of an innovative high concentration nanofluid solar collector.* Applied Energy, 2015. **154**: p. 874-881.
6. Kumar, S., et al., *Experimental investigation of a direct absorption solar collector using ultra stable gold plasmonic nanofluid under real outdoor conditions.* Renewable Energy, 2020. **162**: p. 1958-1969.
7. Pakdaman, M.F., M. Akhavan-Behabadi, and P. Razi, *An experimental investigation on thermo-physical properties and overall performance of MWCNT/heat transfer oil nanofluid flow inside vertical helically coiled tubes.* Experimental thermal and fluid science, 2012. **40**: p. 103-111.

8. Mashhadian, A., M.M. Heyhat, and O. Mahian, *Improving environmental performance of a direct absorption parabolic trough collector by using hybrid nanofluids.* Energy Conversion and Management, 2021. **244**: p. 114450.

9. Munyalo, J.M. and X. Zhang, *Particle size effect on thermophysical properties of nanofluid and nanofluid based phase change materials: A review*. Journal of Molecular Liquids, 2018. **265**: p. 77-87.

10. Timofeeva, E.V., J.L. Routbort, and D. Singh, *Particle shape effects on thermophysical properties of alumina nanofluids.* Journal of applied physics, 2009. **106**(1): p. 014304.

11. Malinowski, Z., J.G. Lenard, and M. Davies, *A study of the heat-transfer coefficient as a function of temperature and pressure.* Journal of materials processing technology, 1994. **41**(2): p. 125-142.

12. Naraki, M., et al., *Parametric study of overall heat transfer coefficient of CuO/water nanofluids in a car radiator*. International Journal of Thermal Sciences, 2013. **66**: p. 82-90.

13. Esfe, M.H., S. Saedodin, and M. Mahmoodi, *Experimental studies on the convective heat transfer performance and thermophysical properties of MgO–water nanofluid under turbulent flow*. Experimental thermal and fluid science, 2014. **52**: p. 68-78.

14. Tong, Y., et al., *Energy and exergy comparison of a flat-plate solar collector using water, Al2O3 nanofluid, and CuO nanofluid.* Applied Thermal Engineering, 2019. **159**: p. 113959.

15. Murshed, S.S. and C.N. De Castro, *Superior thermal features of carbon nanotubes-based nanofluids–A review*. Renewable and Sustainable Energy Reviews, 2014. **37**: p. 155-167.

16. Tong, Y., J. Kim, and H. Cho, *Effects of thermal performance of enclosed-type evacuated U-tube solar collector with multi-walled carbon nanotube/water nanofluid.* Renewable energy, 2015. **83**: p. 463-473.

17. Natarajan, E. and R. Sathish, *Role of nanofluids in solar water heater*. The International Journal of Advanced Manufacturing Technology, 2009: p. 1-5.

18. Amrollahi, A., et al., *Convection heat transfer of functionalized MWNT in aqueous fluids in laminar and turbulent flow at the entrance region.* International Communications in Heat and Mass Transfer, 2010. **37**(6): p. 717-723.

19. Jo, B. and D. Banerjee. *Study of high temperature nanofluids using carbon nanotubes (CNT) for solar thermal storage applications*. in *Energy Sustainability*. 2010.

20. Marcos, M.A., et al., *Influence of molecular mass of PEG on rheological behaviour of MWCNT-based nanofluids for thermal energy storage.* Journal of Molecular Liquids, 2020. **318**: p. 113965.

21. Kanti, P.K., et al., *Experimental and computational determination of heat transfer, entropy generation and pressure drop under turbulent flow in a tube with fly ash-Cu hybrid nanofluid.* International Journal of Thermal Sciences, 2021. **167**: p. 107016.

22. Das, N.K., et al., *Dihydrolevoglycosenone as a novel bio-based nanofluid for thermal energy storage: Physiochemical and quantum chemical insights.* Journal of Energy Storage, 2023. **59**: p. 106365.

23. Mouterde, L.M., F. Allais, and J.D. Stewart, *Enzymatic reduction of levoglucosenone by an alkene reductase (OYE 2.6): a sustainable metal-and dihydrogen-free access to the bio-based solvent Cyrene®.* Green Chemistry, 2018. **20**(24): p. 5528-5532.

24. Jessop, P.G., T. Ikariya, and R. Noyori, *Homogeneous catalysis in supercritical fluids.* Chemical Reviews, 1999. **99**(2): p. 475-494.

25. Sidik, N.A.C., et al., *A review on preparation methods and challenges of nanofluids.* International Communications in Heat and Mass Transfer, 2014. **54**: p. 115-125.

26. *Therminol 55, Therminol, Heat transfer fluids by Eastman*. 2023; Available from: https://www.therminol.com/heat-transfer-fluids.

27. fluid, P.H.t. *Paratherm GLT*. [cited 2022; Available from: https://www.paratherm.com/heat-transfer-fluids/paratherm-glt-htf/.

28. Asadi, A., *A guideline towards easing the decision-making process in selecting an effective nanofluid as a heat transfer fluid.* Energy Conversion and Management, 2018. **175**: p. 1-10.

29. Kanti, P.K., et al., *Experimental investigation on thermo-hydraulic performance of water-based fly ash–Cu hybrid nanofluid flow in a pipe at various inlet fluid temperatures.* International Communications in Heat and Mass Transfer, 2021. **124**: p. 105238.

30. Kanti, P., et al., *Entropy generation and friction factor analysis of fly ash nanofluids flowing in a horizontal tube: Experimental and numerical study.* International Journal of Thermal Sciences, 2021. **166**: p. 106972.

31. Schäfer, A., H. Horn, and R. Ahlrichs, *Fully optimized contracted Gaussian basis sets for atoms Li to Kr*. The Journal of Chemical Physics, 1992. **97**(4): p. 2571-2577.

32. Fu, Y. and D.J. Singh, *Applicability of the strongly constrained and appropriately normed density functional to transition-metal magnetism.* Physical Review Letters, 2018. **121**(20): p. 207201.

33. Becke, A.D., *Density-functional exchange-energy approximation with correct asymptotic behaviour*. Physical review A, 1988. **38**(6): p. 3098.

34. Frisch, M.J., et al., *Gaussian 16 Rev. C.01*. 2016: Wallingford, CT.

35. Tian, B., E.S. Eriksson, and L.A. Eriksson, *Can range-separated and hybrid DFT functionals predict low-lying excitations? A Tookad case study.* Journal of Chemical Theory and Computation, 2010. **6**(7): p. 2086-2094.

36. Fadili, D., S.M. Bouzzine, and M. Hamidi, *Study of the structural and optoelectronic properties of dye solar cells based on phosphonic acid anchoring by DFT functionals.* New Journal of Chemistry, 2021. **45**(5): p. 2723-2733.

37. Goerigk, L., H. Kruse, and S. Grimme, *Benchmarking density functional methods against the S66 and S66x8 datasets for non-covalent interactions.* ChemPhysChem, 2011. **12**(17): p. 3421-3433.

38. Do, K., et al., *Computational methodologies for developing structure–morphology–performance relationships in organic solar cells: A protocol review.* Chemistry of Materials, 2017. **29**(1): p. 346-354.

39. Johnson, E.R., et al., *Revealing Noncovalent Interactions.* Journal of the American Chemical Society, 2010. **132**(18): p. 6498-6506.

40. Boto, R.A., et al., *Interpretation of the reduced density gradient.* Molecular Physics, 2016. **114**(7-8): p. 1406-1414.

41. Lu, T., *Multiwfn.* Software manual. Version, 2014. **3**(6).

42. Contreras-García, J., et al., *NCIPLOT: a program for plotting noncovalent interaction regions.* Journal of chemical theory and computation, 2011. **7**(3): p. 625-632.

43. Chen, D. and H. Wang, *HOMO–LUMO gaps of homogeneous polycyclic aromatic hydrocarbon clusters.* The Journal of Physical Chemistry C, 2019. **123**(45): p. 27785-27793.

44. Müller-Plathe, F., *A simple nonequilibrium molecular dynamics method for calculating the thermal conductivity.* The Journal of chemical physics, 1997. **106**(14): p. 6082-6085.

45. Bowers, K.J., et al. *Scalable algorithms for molecular dynamics simulations on commodity clusters*. in *Proceedings of the 2006 ACM/IEEE Conference on Supercomputing*. 2006.

46. Lu, C., et al., *OPLS4: Improving force field accuracy on challenging regimes of chemical space.* Journal of chemical theory and computation, 2021. **17**(7): p. 4291-4300.

47. *PARATHERM™ GLT, Heat transfer fluid*. Available from: https://www.paratherm.co.uk/heat-transfer-fluids/paratherm-glt-htf/.

48. Kanti, P., et al., *Synthesis, characterization, stability, and thermal properties of graphene oxide based hybrid nanofluids for thermal applications: Experimental approach.* Diamond and Related Materials, 2022. **128**: p. 109265.

49. Patel, J., et al., *A minireview on nanofluids for automotive applications: Current status and future perspectives.* Applied Thermal Engineering, 2022: p. 119428.

50. Durgaprasad, P., et al., *Combined effects of Brownian motion and thermophoresis parameters on three-dimensional (3D) Casson nanofluid flow across the porous layers slendering sheet in a suspension of graphene nanoparticles.* Neural Computing and Applications, 2019. **31**(10): p. 6275-6286.

51. Jang, S.P. and S.U. Choi, *Role of Brownian motion in the enhanced thermal conductivity of nanofluids.* Applied physics letters, 2004. **84**(21): p. 4316-4318.

52. Leong, K., C. Yang, and S. Murshed, *A model for the thermal conductivity of nanofluids–the effect of interfacial layer*. Journal of nanoparticle research, 2006. **8**: p. 245-254.

53. Pal, R., *A novel method to determine the thermal conductivity of interfacial layers surrounding the nanoparticles of a nanofluid.* Nanomaterials, 2014. **4**(4): p. 844-855.

54. Yang, L. and X. Xu, *A renovated Hamilton–Crosser model for the effective thermal conductivity of CNTs nanofluids.* International Communications in Heat and Mass Transfer, 2017. **81**: p. 42-50.

55. Pak, B.C. and Y.I. Cho, *Hydrodynamic and heat transfer study of dispersed fluids with submicron metallic oxide particles.* Experimental Heat Transfer an International Journal, 1998. **11**(2): p. 151-170.

56. Aravind, S.J., et al., *Investigation of structural stability, dispersion, viscosity, and conductive heat transfer properties of functionalized carbon nanotube based nanofluids.* The Journal of Physical Chemistry C, 2011. **115**(34): p. 16737-16744.

57. Einstein, A., *A new determination of molecular dimensions.* Ann. Phys., 1906. **19**: p. 289-306.

58. Gupta, M., et al., *A review on thermophysical properties of nanofluids and heat transfer applications.* Renewable and Sustainable Energy Reviews, 2017. **74**: p. 638-670.

59. Das, N.K., et al., *Evaluation of Thermophysical Properties and Thermal Performance of Amine-Functionalized Graphene Oxide/Deep Eutectic Solvent Nanofluids as Heat-Transfer Media for Desalination Systems.* ACS Sustainable Chemistry & Engineering, 2023. **11**(14): p. 5376-5389.

60. Ilyas, S.U., R. Pendyala, and M. Narahari, *Stability and thermal analysis of MWCNT-thermal oil-based nanofluids.* Colloids and Surfaces A: Physicochemical and Engineering Aspects, 2017. **527**: p. 11-22.

61. Dehury, P., U. Mahanta, and T. Banerjee, *Comprehensive Assessment on the Use of Boron Nitride-Based Nanofluids Comprising Eutectic Mixtures of Diphenyl Ether and Menthol for Enhanced Thermal Media.* ACS Sustainable Chemistry & Engineering, 2020. **8**(38): p. 14595-14604.

62. Wei, X. and L. Wang, *Synthesis and thermal conductivity of microfluidic copper nanofluids.* Particuology, 2010. **8**(3): p. 262-271.

63. Vadasz, P., *Heat conduction in nanofluid suspensions.* 2006.

64. Lee, D., J.-W. Kim, and B.G. Kim, *A new parameter to control heat transport in nanofluids: surface charge state of the particle in suspension.* The Journal of Physical Chemistry B, 2006. **110**(9): p. 4323-4328.

65. Vandsburger, L., *Synthesis and covalent surface modification of carbon nanotubes for preparation of stabilized nanofluid suspensions.* 2009.

66. Chen, H., et al., *Heat transfer and flow behaviour of aqueous suspensions of titanate nanotubes (nanofluids).* Powder technology, 2008. **183**(1): p. 63-72.

67. Rashidi, F. and N.M. Nezamabad. *Experimental investigation of convective heat transfer coefficient of CNTs nanofluid under constant heat flux*. in *Proceedings of the world congress on engineering*. 2011. WCE London, UK.

68. Kanti, P., et al., *Thermal performance of fly ash nanofluids at various inlet fluid temperatures: An experimental study.* International Communications in Heat and Mass Transfer, 2020. **119**: p. 104926.

69. Ding, Y., et al., *Heat transfer of aqueous suspensions of carbon nanotubes (CNT nanofluids).* International Journal of Heat and Mass Transfer, 2006. **49**(1-2): p. 240-250.

70. Wen, D. and Y. Ding, *Experimental investigation into convective heat transfer of nanofluids at the entrance region under laminar flow conditions.* International journal of heat and mass transfer, 2004. **47**(24): p. 5181-5188.

71. Fotukian, S. and M.N. Esfahany, *Experimental study of turbulent convective heat transfer and pressure drop of dilute CuO/water nanofluid inside a circular tube.* International communications in heat and mass transfer, 2010. **37**(2): p. 214-219.

72. García, G., M. Atilhan, and S. Aparicio, *An approach for the rationalization of melting temperature for deep eutectic solvents from DFT.* Chemical Physics Letters, 2015. **634**: p. 151-155.

73. Mishra, D.K., et al., *Molecular and Spectroscopic Insights into a Metal Salt-Based Deep Eutectic Solvent: A Combined Quantum Theory of Atoms in Molecules, Noncovalent Interaction, and Density Functional Theory Study.* The Journal of Physical Chemistry A, 2021. **125**(44): p. 9680-9690.

74. Mosquera, M.A., *Support for the existence of invertible maps between electronic densities and non-analytic 1-body external potentials in non-relativistic time-dependent quantum mechanics.* The Journal of Chemical Physics, 2017. **147**(13): p. 134110.

75. Karabacak, M., M. Cinar, and M. Kurt, *Molecular structure and vibrational assignments of hippuric acid: A detailed density functional theoretical study.* Spectrochimica Acta Part A: Molecular and Biomolecular Spectroscopy, 2009. **74**(5): p. 1197-1203.

76. Bonness, S., et al., *Theoretical investigation on the second hyperpolarizabilities of open-shell singlet systems by spin-unrestricted density functional theory with long-range correction: Range separating parameter dependence.* Chemical Physics Letters, 2010. **493**(1-3): p. 195-199.

77. He, Y., et al., *Density functional theory study of adsorption of ionic liquids on graphene oxide surface.* Chemical Engineering Science, 2021. **245**: p. 116946

Chapter-3

Experimental and Molecular Dynamic Insights on the Thermophysical properties for MWCNT-Phosphonium based Eutectic Thermal Media

Experimental and Molecular Dynamic Insights on theThermophysical properties for MWCNT-Phosphoniumbased Eutectic Thermal Media

This current chapter report a novel green heat transfer fluid (HTF) containing Deep Eutectic Solvent (DES) and Multi-walled carbon nanotube (MWCNT) nanoparticle. DES is the combination of Methyltriphenylphosphonium bromide (MTPB) as HBA and Ethylene glycol (EG) as HBD at a molar ratio of 1:4. Thereafter, the corresponding nanofluid was prepared by dispersing 0.02wt% MWCNT having a diameter10-30 nm in the base fluid. Prior to dispersion, the shape and morphology of the MWCNT were ascertainedusing both Field Emission Scanning Electron Microscope (FESEM) and Field Emission Transmission Electron Microscope (FETEM). The crystallinity and functional groups were investigated by X-ray Powder Diffraction meter (XRD) and Fourier Transform Infrared Spectroscopy (FTIR). The stability of the prepared nanofluid was initially performed using visual observation followed by zeta potential measurements. Thermogravimetric analysis (TGA) was performed to check the stability of nanofluid at a temperature close to 500°C at a heating rate of 10°C /min under nitrogen environment. Thermophysical properties such as density, viscosity, thermal conductivity, and specific heat of nanofluid were measured in the temperature range 25-85°C. It is evident from the experimental data that viscosity and density decrease with an increase in temperature. On the contrary, the specific heat and thermal conductivity of the nanofluid were found to increase with temperature. This is due to the induced Brownian motion of the nanoparticle, which results in higher kinetic energy at high temperature. In the penultimate section, Molecular Dynamic (MD) simulations were performed to compare and validate the results of thermal conductivity of nanofluid.

3.1 Introduction

Environmental concerns have initiated researchers to create alternative, inexpensive, efficient, and sustainable energy sources due to the global warming induced by fossil fuel use. In terms of environmental concerns, the green solvent is one of the alternate methods for reducing the impact of pollution in applications such as extraction and thermal media. The use of green solvent or technology reduces wastewater pollutants, toxic chemical substances and also improves technology. Here 'green' refers to the preparation of chemicals such as solvents and fluids through non-fossil fuel sources. Pharmaceutical companies are now using greener synthesis routes for drug development so as to reduce pollution and manufacturing costs [1].

Researchers have developed a new type of environmentally friendly solvents called deep eutectic solvents (DES) as an alternative to conventional solvents. DES have several advantages over traditional solvents, including better biodegradability and biocompatibility, lower vapour pressure, reduced toxicity, lower cost, and easier preparation. These solvents address the limitations of conventional solvents [2-5]. They are analogous to Ionic Liquids (IL's), which are known for recent industrial applications [6]. Applications concerning IL's for extractions are also well documented [7-10]. For their interesting properties, IL's are alternative to conventional organic solvents [11-13]. But due to its high manufacturing and toxicity issues, primarily from their petroleum-based precursors, alternative solvents are still gaining importance. Further, most of the IL's are highly viscous and difficult to synthesize. With respect to thermal media, Wu et al. [14] synthesized IL's namely [C_4min] [PF_6], [C_8min] [PF_6], and [C_4 min] [Tf_2N] (Tf_2N: bistrifluoromethanesulflonimide) and used them as heat transfer fluid for solar thermal power plant.

Although, ionic liquids (ILs) can also be referred to as green solvents due to their excellent thermal and chemical stability and low volatility. But, they are less desirable in nanofluid applications due to their high toxicity and non-biodegradability as the most of them

has precursors based on petroleum. Further the complicated procedure of preparing ILs hinders it application as unlike DES, it requires a number of unit operations for its synthesis. Compared to IL, DES-based nanofluids are more environmentally benign and scale-up-friendly as some of them originate from natural precursors (betaine, urea) and are known as Natural Deep Eutectic Solvents (NADES) [15]. As the base fluid is formed by combining HBA and HBD, no waste product is generated throughout the preparation. This is why the current DES is adopted as base solvent in heat transfer applications due to their low viscosity and density. Industrially, DES-based nanofluids offer a more significant potential for usage as heat transfer fluids and energy harvesting applications than IL-based nanofluids [16].

Due to its attractive beneficial and enhanced properties, DES has promised several industrial applications in the food processing, power, extraction, and nanotechnology domains. Generically, DES are formed by mixing defined amount of Hydrogen Bond Donor (HBD) and Hydrogen Bond Acceptor (HBA). These are a certain class of liquids at ambient conditions (freezing points below 25°C), which are binary compositions of two components, a Hydrogen Bond Donor(HBD) and a Hydrogen Bond Acceptor(HBA), each of which has a melting point above that of the DES; hence they are eutectics. According to Abott et al. [4] the lattice energy decides the interaction between HBD and HBA and also point out the formation of an eutectic mixture. DES are subgroup of room-temperature ionic liquids (RTILs) but are binary mixtures contrary to ordinary IL's that are single substances. It has been said that DES are not novel compounds or a new type of compound but binary or ternary mixtures. Further, the presence of a eutectic point in a mixture cannot be used to define or characterize a DES since essentially all mixtures of compounds immiscible in the solid phase will present a eutectic point. Chen and Mu [17] used DES to treat and dissolve chemicals from biomass. Shisov et al. [18] reported various applications of DES in analytical chemistry. They also used DES to improve the nanoparticle extraction efficiency and used it in chromatography as a mobile phase additive.

Choi et al. [19] first introduced the term 'nanofluid', which defines as a liquid containing nanometre size particles. Nanofluid is employed as an excellent heat transfer medium in many practical applications due to its enhanced physical features[20-22], such as density, dynamic viscosity, specific heat, and thermal capacity. Several studies have been conducted using dispersed nanoparticles to assure the enhancement of the nanofluid's physical properties and thermal stability. Carbon nanotubes (CNTs) have sparked a lot of attention in recent years due to their exceptional electrical and mechanical capabilities[23]. Multi-walled carbon nanotube containing nanofluid leads to the enhancement of thermal conductivity. The increase of the ultra-sonication time is also known to increase the fluid's thermal conductivity up to a certain extent [24]. Similar work has been reported by Mahbubul et al. [25] where they studied the effect of ultra-sonication time on the stability and rheological properties of the nanofluid containing 0.5 vol% of spherical Al_2O_3 nanoparticles. They reported that increasing the ultra-sonication period leads to a decrease in the NF's dynamic viscosity. Y. Hwang et al. [26]used various nanoparticles such as MWCNT, fullerene, CuO, SiO_2 to prepare nanofluid in (a) water, (b) ethylene glycol, and (c) oil as a working fluid. The experimental results show that the thermal conductivity of the nanofluid rises as the volume fraction increases except for water-based fullerene nanoparticles.

Borode et al. [27] reported applications of carbon nanotube-based nanofluid in heat exchanger. The result shows that carbon-based nanofluid can improve the performance of the heat exchanger and reduce the heat exchange area. Ilyas et al. [28] synthesized Multi-walled carbon nanotube(MWCNT) and observed the stability of thermal oil-MWCNT based nanofluid at various concentrations 0-1 wt%. Similar work has been done by Salam and Burk [29], where they studied functionalized MWCNT with Polyethylene Glycol (PEG) and octadecylamine (ODA).Carbon-based nanoparticles can be used in industrial cooling operations [30], automotive cooling applications [31], electronic cooling (microchip cooling) [32, 33],

extraction of geothermal power and other energy sources [34], microscale fluidic applications [35] and solar desalination system [36]. All the application has been benefited from the use of using DES as a base fluid in the preparation of nanofluids. Nanofluids based on DES, may be also used in biomedical applications such as nanodrug delivery [37, 38], nano-cryosurgery [39] and cancer therapies [40] due to their low toxicity and environmental friendliness. Due to its high thermal conductivity, DES/MWCNT nanofluid is particularly well suited for heat transfer applications. The DES/MWCNT-based nanofluid has the potential to be used in multistage flash solar desalination systems.

In this chapter, MTPB as HBA and EG as HBD were mixed in the molar ratio 1:4 and used as base fluid. Thereafter, the nanofluid with MWCNT were prepared using a two-step method, by dispersing 0.02 wt% of MWCNT nanoparticles. Thermophysical properties of the MTPB-EG based DES and the thermal stability of the nanofluid were thereafter analyzed at high temperatures. Further, with the help of reverse non equilibrium molecular dynamic simulation, thermal conductivity of nanofluid has been studied and compared to the experimental values.

3.2 Experimental Details

3.2.1 Materials

Ethylene glycol(EG)($C_2H_6O_2$) with > 99% purity was obtained from Merck India. Methyltriphenylphosphonium bromide(MTPB)($C_{19}H_{18}BrP$) was purchased from SRL India Pvt. Ltd. with > 98% purity. Multi-Walled Carbon Nanotube (MWCNT) with 10-30 nm diameter and 5-15 micrometer length was obtained from TCI chemicals. The composition of DES was confirmed by Nuclear Magnetic Resonance Spectroscopy (^{1}H NMR). The chemical composition of MTPB, EG, and optimized structure of MWCNT are shown in table 3.1 and Figure 3.1

Table 3.1. Chemical compositions of DES

Name	CAS No.	Chemical Structure	Molecular formula	Number of moles
Methyltriphenyl phosphonium bromide [MTPB]	1779-49-3	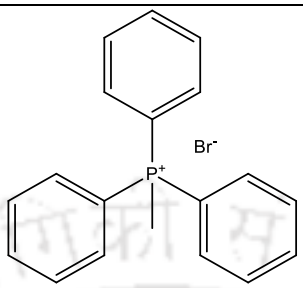	$C_{19}H_{18}BrP$	1
Ethylene glycol [EG]	107-21-1		$C_2H_6O_2$	4

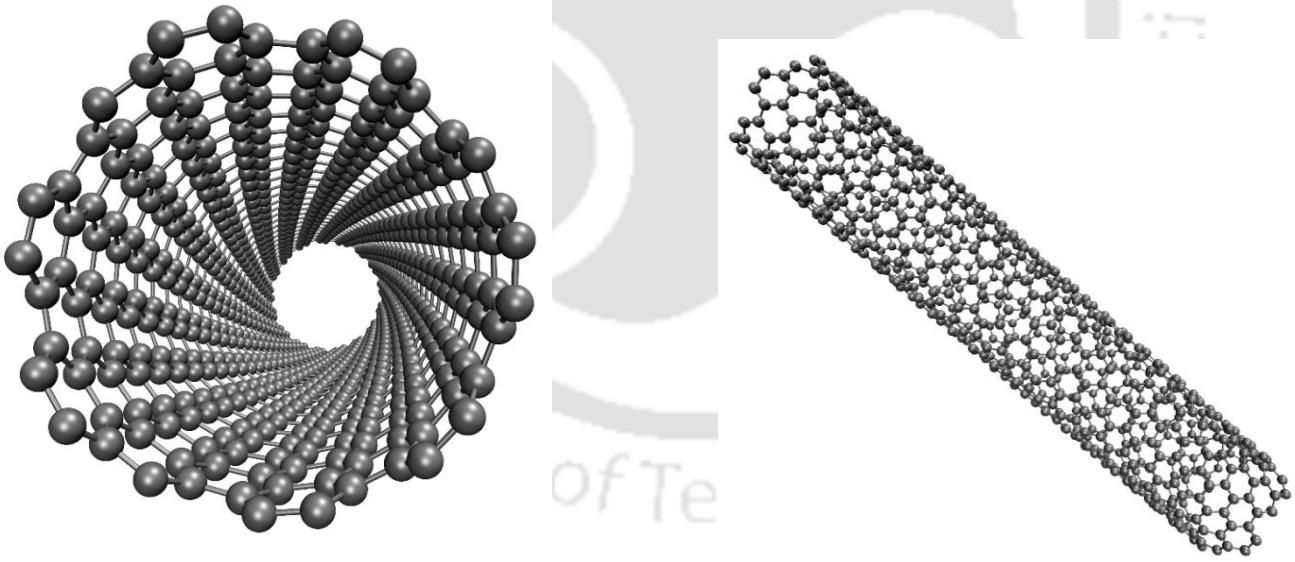

Figure 3.1 Front view and side view of single walled carbon nanotube (SWCNT)

3.2.2 Characterization of Multi-Walled Carbon Nanotube (MWCNT)

The morphology and shape of MWCNT nanoparticles were investigated by Field Emission Transmission Electron Microscope (FETEM, JEOL-JEM2010) and Field Emission Scanning Electron Microscope (FESEM Sigma 300, Zeiss). The crystallinity structure of MWCNT was analyzed by Powder X-ray Diffraction (XRD Bruke D8, advanced X-ray diffraction measurement system) at room temperature in the range of 2θ from 10 to 80º. Fourier Transform Infrared Spectra analyzer (FTIR, Perkin–Elmer, Norwalk, USA) was used to ascertain if any functional groups or chemicals were present in MWCNT and the nanofluid. The absorption spectra were recorded in the range between 500 to 4000 cm^{-1}.

3.2.3 Synthesis of MTPB-EG Based Deep Eutectic Solvent

DES was prepared by mixing 1 mole of MTPB and 4 mole of Ethylene Glycol in a round bottom flask. A reflux condenser was used to minimize the loss of vaporization. The mixer was stirred continuously on a magnetic stirrer hot plate (TARSONS SPINOT magnetic stirrer/hot plate-DIGITAL, MC 02, India) for 24 hours until a clear liquid was formed. The mixer was kept overnight at room temperature to observe solidification. When two components with higher melting points are mixed in a defined molar ratio, the resulting melting point is called eutectic point, which is less than the melting point of the individual component. DES are not novel compound or a new type of compound, but binary or ternary mixtures. It should be noted that the presence of a eutectic point in a mixture cannot be used to define or characterize a DES since essentially all mixtures of compounds immiscible in the solid phase will present a eutectic point Abott, et al. [4] attributed the first DES to a choline chloride and urea combination in 2003. Choline chloride has a melting point of 302°C, while urea has a melting point of 133°C. Their combined melting point is 120°C, which is lower than the melting points of urea and ChCl. The molar ratio can also be predicted by the COSMO-SAC model [17], where solid

Liquid Equilibria (SLE) prediction can be made prior to experimentation. In our work, we refer the DES or eutectic mixture to the pair HBD-HBA with a eutectic point dependent of the specific composition we are working with. From analysis of the ^{1}H NMR spectra of the prepared DES, we can confirm the (4:1) molar ratio of the DES.

3.2.4 Preparation of Nanofluids

The nanofluid formation is the vital step that shall help us enhance the thermal characteristics of heat transfer fluid. The agglomeration of the solid particle is critical and if it occurs, it shall lead to poor thermophysical properties of DES-based nanofluid. Agglomeration, cluster formation, and faster settlement in fluids are usually caused by high surface energies and subsequent interactions of nanoparticles. To maintain the improved thermal characteristics, a stable nanofluid must be synthesized. The maximum stability time can be defined as the amount of time that the nanofluids remains completely scattered [41].

Overall there are two primary methods for preparing nanofluid [42-45], namely: two-step method and one-step method. However, both methods have some advantages and disadvantages. Within the two-step preparation method, the first stage consists of the synthesis of nanotubes or nanofibres, in the form of dry powders via physical or chemical methods. Thereafter the synthesized dry powders are dispersed in base fluids. This process is recommended for the production of large-scale nanofluids[46, 47]. The size and shape of the nanoparticles are easily controlled in a two-step method. To alleviate the possible settling of the nanofluid, ultra-sonication and mechanical stirring are used to improve nanofluid dispersion. In the single-step process, the nanoparticle and base fluid are prepared and simultaneously dispersed to form nanofluid [42, 48]. Although the one-step method gives good stability and dispersion of the nanofluid, there is complexity involved in the preparation method

where the size, shape and concentration of the nanoparticles are difficult to control. Hence, we have adopted the two step process where the nanoparticle was directly purchased.

In this work, the dispersion stability of nanofluids are checked by performing Zeta potential measurement through Delsa Nano (Delsa Nano C, BECKMAN COULTER). A thermogravimetric analyzer (TGA) is used to determine the thermal stability of the nanofluid. The nanofluid is prepared by mixing 0.02 wt% of MWCNT in DES. The nanofluid was abbreviated as NF4 in this chapter. Initially, the mixture of solvents and MWCNT were mixed on a vortex mixer (SPINX MC-01, Tarsons). After mixing, the mixture was placed in an ultra-sonication chamber (GT-1990QTS) to get a homogeneous and uniform suspension of particles which prevented the agglomeration of carbon nanotube.

3.2.5 Thermophysical Properties

Measurement of thermophysical data of nanofluid gives information about the transport system of the fluid**.** The nanofluid was characterized by thermo-physical properties like density, viscosity, thermal conductivity, and specific heat capacity. All these properties were measured at different temperature ranges. The densities of DES and NF4 nanofluids were measured by using an Anton Paar Densitometer (DMA 4500 M) at various temperatures ranging from 25-85 ^{0}C. The accuracy of density measurement was estimated as 0.0001 g/cm^{3}. Density is the critical parameter for calculating the pressure loss and pumping power, and it works on the basis of the U-tube Oscillatory concept. It is made out of a single U-shaped glass tube that oscillates at a particular frequency. That frequency calculates the density of the sample.

Rheological properties of the nanofluid were measured using Anton Paar Interfacial Rheometer (Phsica MCR301). Viscosities were calculated within the temperature range 25-85 ^{0}C with an accuracy of $\pm$ 5%. The shear rate was measured in the range of 0-85 s^{-1}. The rheometer consists of a round parallel plate that is used to measure viscosity at various

temperature ranges. The thermal conductivity of DES and nanofluids was measured by KD2 pro thermal analyzer (Decagon Device, USA) at different temperatures with an accuracy of ±0.0096 W/m K. KD2 pro thermal analyzer worked on the principle-based on hot wire method. Specific heat capacity was measured by performing Temperature Module Differential Scanning Calorimeter (TMDSC: NETZSCH STA 449F3) at a temperature from 45-90°C. Sapphire is used as standard comparison material under nitrogen environment at a heating rate of 10°C/min. It was based on the principle of heat flow, which is a function of temperature that maintains sample and reference at the same temperature.

3.2.6 Stability Analysis

The particle-particle intermolecular force van der Waals attraction force dominates the other repulsive forces as it causes rapid settlement and agglomeration between the particles[46, 49]. As a result, it increases the size of the clusters, which may cause the reduction in thermal properties of the nanofluid. Therefore, the stability analysis of nanofluid is important before its use in application such as direct solar thermal absorption. We have adopted both visual observation and zeta potential analysis for the stability of the nanoparticles.

3.2.6.1 Visual Observation and Optical Microscopy

Here the nanofluid was prepared by a two-step method and sonicated for 8-10 minutes to make the suspension homogenous. The prepared nanofluid was kept at room temperature for four weeks undisturbed. Visual observation was formulated to view the settling of the nanofluid. Cluster size and nanotube dispersion in the nanofluid were observed by capturing theimages through an optical microscope (Axiostar plus, Carl Zeiss, Germany). The microscopic images were thereafter analyzed to study the particle dispersion in the working fluid.

3.2.6.2 Zeta Potential Measurement and Thermo Gravimetric Analysis (TGA)

Zeta potential measurement was measured by Delsa Nano (Delsa Nano C, BECKMAN COULTER) instrument to see the stability and particle size distributions of the particles in nanofluid. The electrical potential created at the solid-liquid interface as a result of the relative mobility of solid particles and liquid is referred to as the zeta potential [50]. According to Mehrali et al [51], the zeta potential value of − 30 mV to +30mV is considered stable. Whereas, Vandsburger [52] considered moderate stability when the zeta potential value is close to ± 30 mV. A value close to 45 mV ensures the complete stability of nanofluids. The high stability of the nanofluid system is demonstrated by a zeta potential value greater than ± 60 mV [53]. Thermo Gravimetric Analysis (TGA) (TG209 F1, Libra, NETZSCH, Germany) was also performed to determine the thermal stability of the nanofluid. The sample was studied under nitrogen atmosphere at a heating rate of 10 °C/min.

3.3 Computational Details

Classical molecular dynamics (MD) simulations were performed with the use of GROMACS 5.0.4[54, 55] and LAMMPS [56] software. The equilibration was carried out with GROMACS 5.0.4, and thermal conductivity calculations were performed with LAMMPS. OPLS-AA force fields were used to define the bonded and non-bonded terms[57]. The charge scaling of 0.8 was applied to the HBA and HBD similar to Ionic Liquids[58]. This is analogous in comparing the charge transfer effect in ILs. Earlier work has reported a scaling factor of 0.9 on the ions of [C_4mim][Cl] to give better results[59]. We have also showed that charge scaling factor gives appropriate structure and physical properties in one of our earlier studies [60].

`The initial structure of carbon nanotubes (CNT) was generated using the VMD software [61] .The *g_x2top* tool from the GROMACS 5.0.4 was used to generate the force field for the CNT. The HBA and HBD were optimized using Gaussian software [62] with B3LYP

[63-65] method and 6-311+G(2d,p) basis set. Partial charges were generated using the Antechamber package [66]. For the overall periodic box, 8 carbon nanotubes, 1600 ethylene glycol molecules as HBD, and 400 Methyltriphenylphosphonium bromide molecules as HBA were randomly packed into the cubic cell using Packmol software [67] (Figure 3.2).

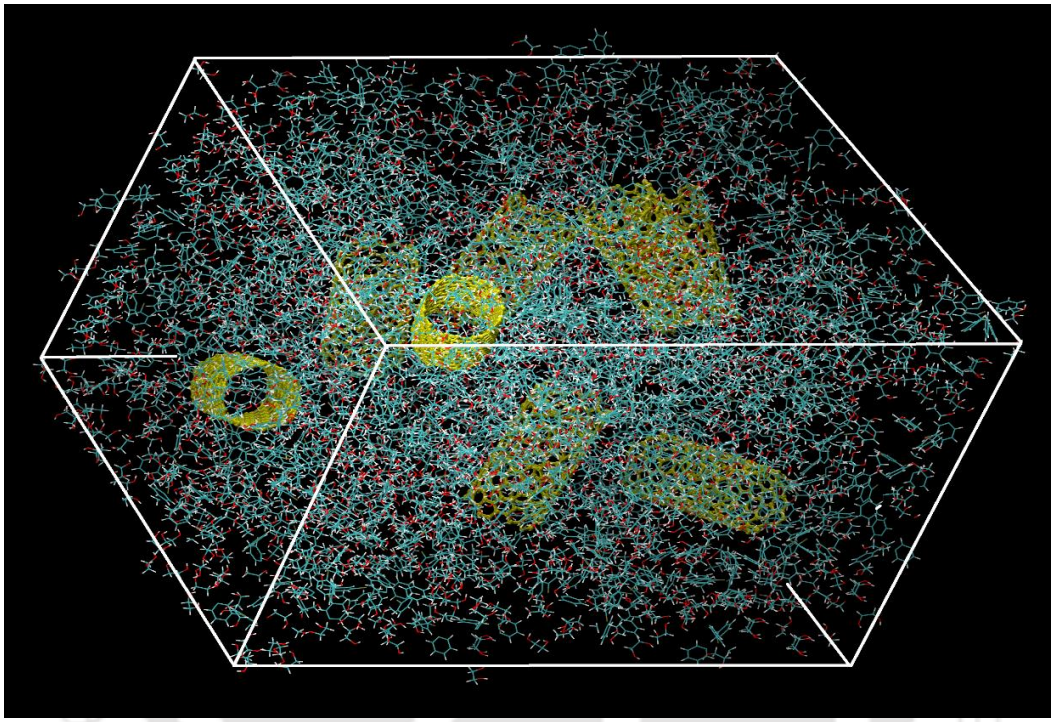

Figure 3.2. MD snapshot of the system

Generated structure from the Packmol software were then used for further simulations in GROMACS. Energy minimization was performed using the steepest descent method[68]. After energy minimization, the system is heated above 200 K when compared to the target temperature in the NVT ensemble. Thereafter the system was cooled to the respective temperature using the annealing method. In the annealing procedure, the temperature is decreased by 20 K for each nanosecond run for 10 steps. Surface effects were eliminated using the periodic boundary conditions. Integration of the equations of motion was carried out using Velocity-Verlet algorithm. Bonds that are linked to hydrogen atoms were constrained using the

LINCS algorithm. 10 ns equilibration was carried out using the NVT ensemble at the target temperature. 10 ns *NPT* run was performed using the V-rescale thermostat[69], using the Berendson barostat [70], with coupling constants of 0.1 and 2.0 ps, respectively. A 20 ns run in NPT run was performed using V-rescale thermostat[69] and Parrinello-Rahman[71] barostat. The V-rescale thermostat was used in the NVT ensemble for 20 ns. GRO2LAM software was used to convert the topology from GROMACS format to LAMMPS. 20 ns simulation was done to calculate the thermal conductivity. The reverse non equilibrium molecular dynamics (RNEMD) procedure was used to evaluate the thermal conductivity [72]. RNEMD is a widely used technique in previous literature [73-76]. Time step of 2 fs was used throughout the simulations. Cut off for non-bonded interactions was 1.2 nm.

3.4. Results and Discussions

3.4.1 ^{1}H NMR of DES

The composition of the DES was confirmed by ^{1}H NMR shown in Figure 3.3. The absence of extra peaks in the spectra implies that there is no chemical reaction, and the mixture is stable. The details of ^{1}H NMR analysis have been reported in our previous publication [77].

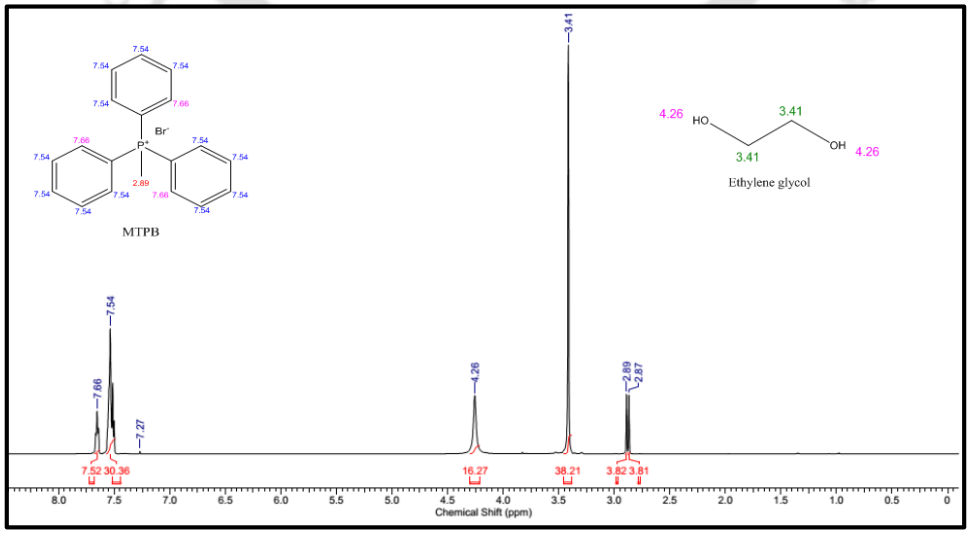

Figure 3.3. NMR spectra of pure DES 1H NMR

3.4.2 Characterization and Morphological Studies

Field Emission Transmission Electron Microscope (FETEM) was used to investigate the shape and morphology of the MWCNT nanoparticle. Figures 3.4(a) & (b) and 3.4(c) & (d) shows the FETEM and FESEM images of MWCNT with 200 nm and 100 nm scales, indicating that the diameter varies from 30nm to 50 nm. This diameter was confirmed by Scanning Electron Microscope (SEM) with 200 nm and 100 nm scale. Figure 3.5(a) shows the X-ray diffraction pattern of MWCNT. A sharp peak at (002) plane $2\theta=26.4°$ is visible. This implies the periodicity of the atom in MWCNT. However, low-intensity peak at (100), (004) and (110) planes at $2\theta =43.04°$,$2\theta =53.68°$, $2\theta =78.0°$ clearly indicates the crystalline structure of the MWCNT. No other peaks were observed, which implies the high purity and non-functionality of the nanotube. Fourier transform infrared spectroscopy (FT-IR) analysis of MWCNT, and DES-based nanofluid is shown in Figure 3.5(b). Characterization of FTIR spectroscopy was performed to analyze the presence of functional groups or impurity on the MWCNT. Different peaks were observed in the medium infrared region where wave number ranges between 500 to 4000 cm^{-1}. An absence of a peak in FTIR, MWCNT spectra negates the presence of functional groups, impurities, or C=C attachment. Further, there is no hydroxyl group (-OH) group as the analysis was performed in a moisture-free environment.

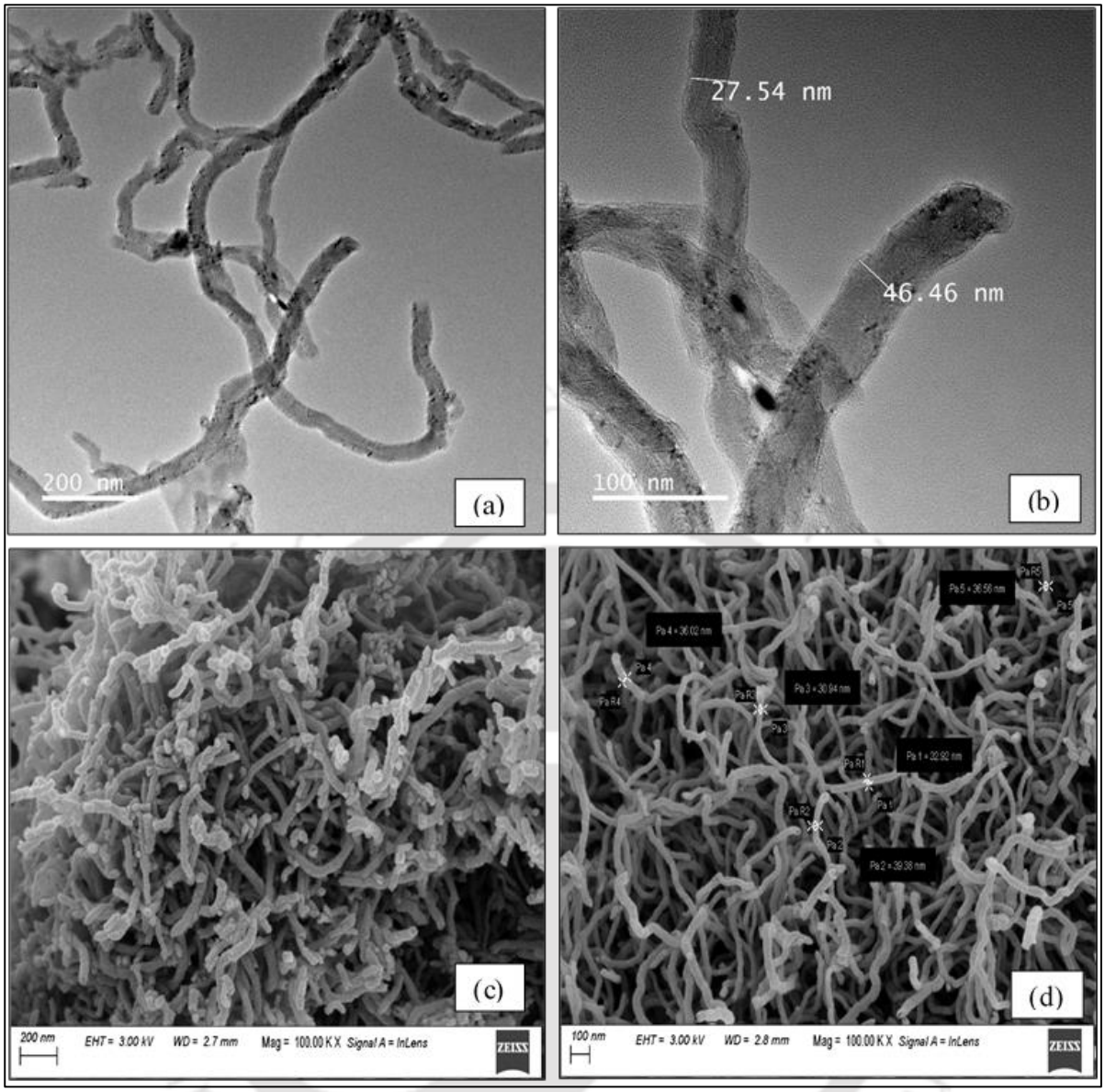

Figure 3.4. Field Emission Transmission Electron Microscope (FETEM) with scale (a) 200 nm; and (b) 100 nm and Field Emission Scanning Electron Microscope (FESEM) images of MWCNT with (c) 200 nm and (d) 100 nm

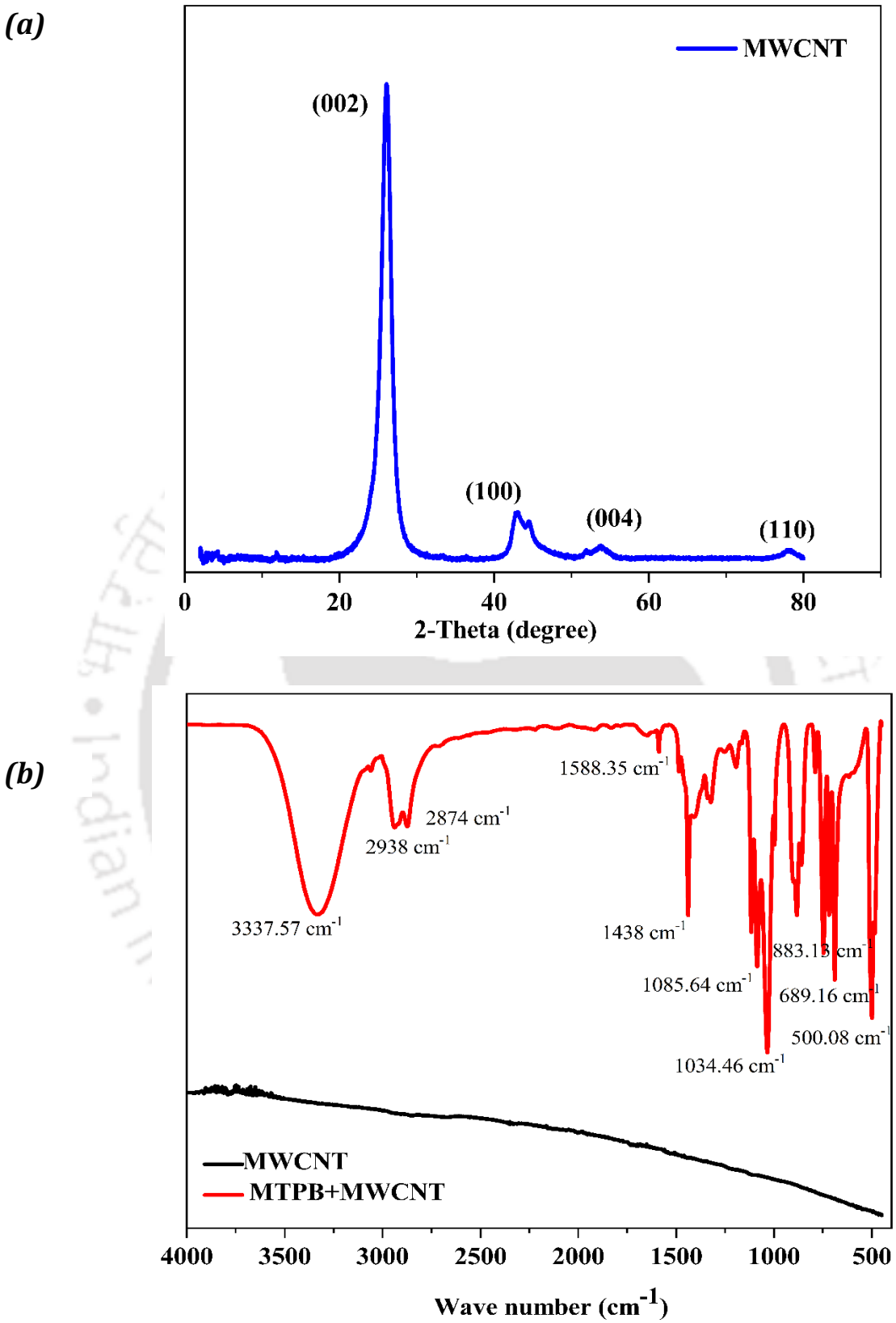

Figure 3.5. (a) XRD pattern of MWCNT (b) FTIR spectra of MWCNT and nanofluid

3.4.3 Stability Analysis

3.4.3.1 Visual Observation and Optical Microscopy

In the initial part, visual observation was used to analyze the stability of the nanofluid, NF4. Photographs of nanofluid NF4 were taken after sonication within a gap of 15, 20, and 29 days respectively, as shown in Figure 3.6(a). On visual inspection, there is no precipitation observed initially for the first two weeks. However, slight precipitation was observed on the 20th day, and some particles were observed to settle on the 29th day, displayed in the Figure 3.6(a). The visual observation method from the Figure 3.6 shows that 0.02 weight % MWCNT based nanofluid gave excellent stability till 15-20 days.

Figure 3.6(b) depicts optical microscopic pictures that reveal the homogeneous dispersion of nanoparticles in the working fluid. The photograph was captured in a high-resolution magnitude of 10X and 20X. From the images, it was noticed that nanoparticles are uniformly distributed in the DES base fluid. Images were captured by a normal light microscope, so it could not determine the accurate size and shape of the nanoparticle. However, it can provide a quality evaluation of the size of the nanoparticle in the base fluid.

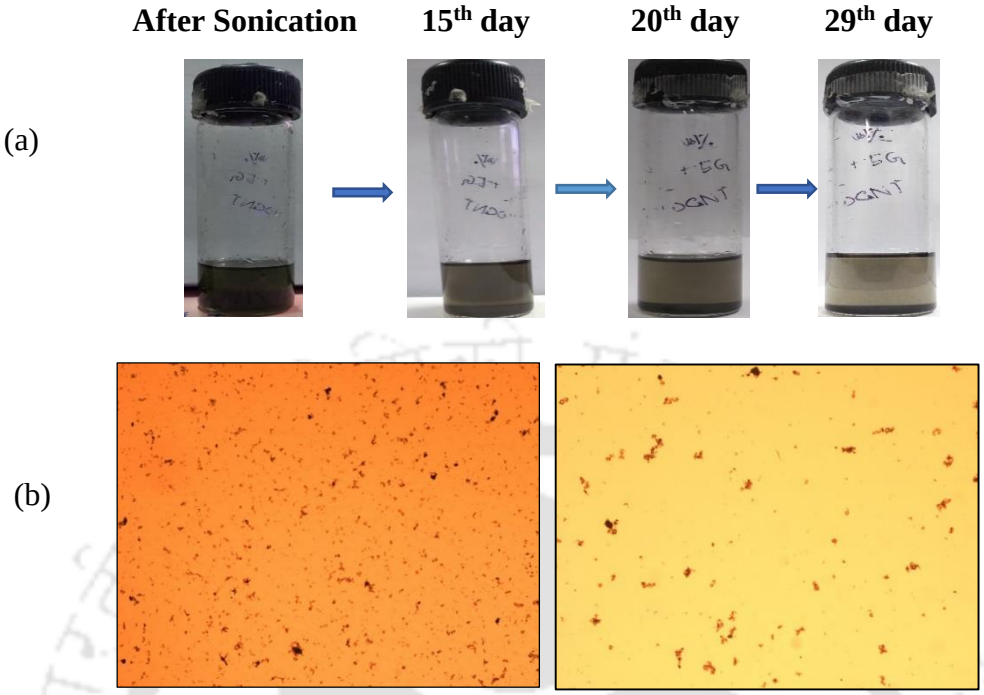

Figure 3.6. (a) Digital Photos and (b) Optical microscopic images of nanofluid NF4 with high resolutions, 10x and 20x

3.4.3.2 Zeta Potential and Thermo Gravimetric Analysis (TGA)

Thermo Gravimetric Analysis (TGA) was performed to determine the thermal stability of the nanofluid. TGA was performed at a heating rate of 10°C/min under nitrogen atmosphere. The degradation of MWCNT-DES nanofluid with respect to the temperature is shown in Figure 3.7. Two-stage mass losses were observed in the phosphonium-MWCNT based nanofluid. Degradation of the nanofluid was first observed at 96.88°C when the sample was heated from 25°C to 500°C. Thereafter degradation was observed from 110°C, which ends at ~180°C. The second weight loss was observed at 328.22°C. Complete decomposition was observed at 400ºC. Thereafter, a gradual loss was observed when heated up-to 500°C. In TGA, the two-stage degradation of the nanofluid indicated the high thermal stability of the nanofluid till 320°C.

The isothermal TGA has been done under nitrogen atmosphere at the heating rate of 20°C/min for 12 hours. DES based nanofluid shows rapid degradation after heating the samples at 80°C, 120°C and 160°C respectively (Figure 3.8). The thermal stability of the fluid is around the order of 50-60 minutes. It is visible from Figure 3.8 that the mass loss is very high at the beginning of the heating process primarily at higher temperatures of 120°C and 160°C and then almost constant after 100 min. Around 35% and 39% mass loss was observed at temperatures 160°C and 120°C respectively, whereas approximately 22% mass loss was observed at temperature 80°C. The steady outcome can be attributed to the low weight concentration of the nanoparticle in the deep eutectic solvent [78, 79].

Zeta potential measurement were performed to check the dispersion and stability of the nanofluid through the observation of electro-kinetic potential [80, 81]. From the definition, two separate layers arise around nanoparticles when they are distributed in the base fluid. The stern layer is the layer that is connected to the particle. The diffuse layer, the layer below the stern layer, is weakly bonded by the nanoparticle. The combination of both layers is electrically neutral and hence is known as the electric double layer (EDL). Zeta potential is generated in the interface of EDL and here is measured in millivolts (mV). A high zeta potential indicates stronger repulsive forces, which increases the probability of particle agglomeration. The nanoparticle's large surface area and small size combines to reduce their surface area, resulting in strong van der Waal forces. The strong van der Waal forces attract the other particles, resulting in the formation of an agglomeration. According to Vandsburger [52], nanofluids are nearly stable when particles having a zeta potential value is near about $\pm$ 30 mV. If the zeta potential value is close to 45 mV, the stability of nanofluids is ensured. Nanofluid gives excellent stability if its value lies above$\pm$ 60 mV. Figure 3.9 represents the value of the zeta potential curve, which came to be -90.12 mV indicating high stability.

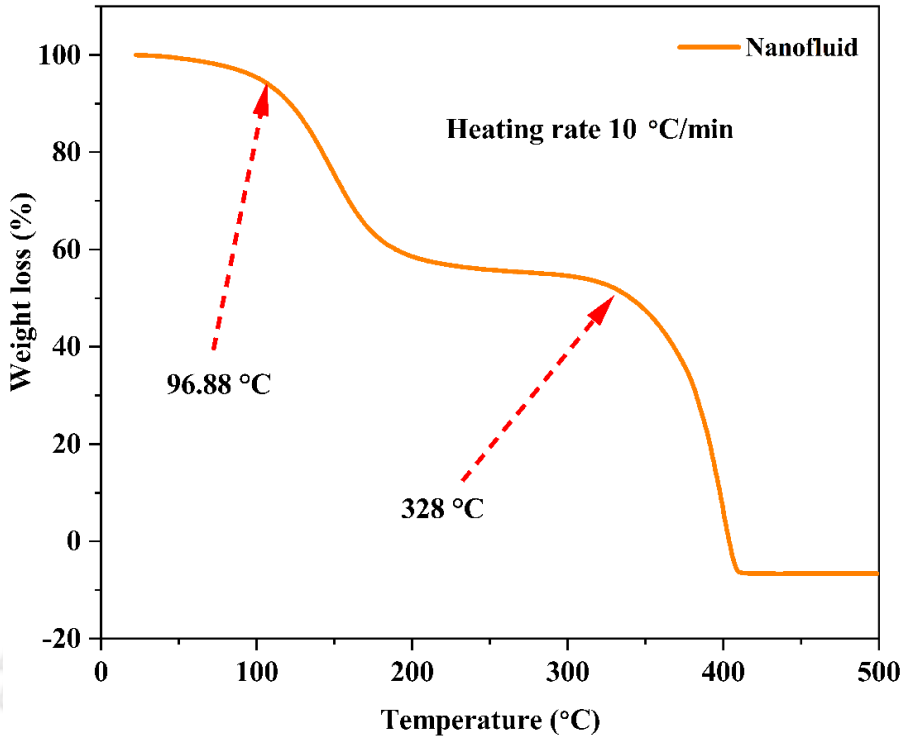

Figure 3.7. TGA Analysis of MTPB based nanofluid (Heating rate 10°C/min at nitrogen atmosphere

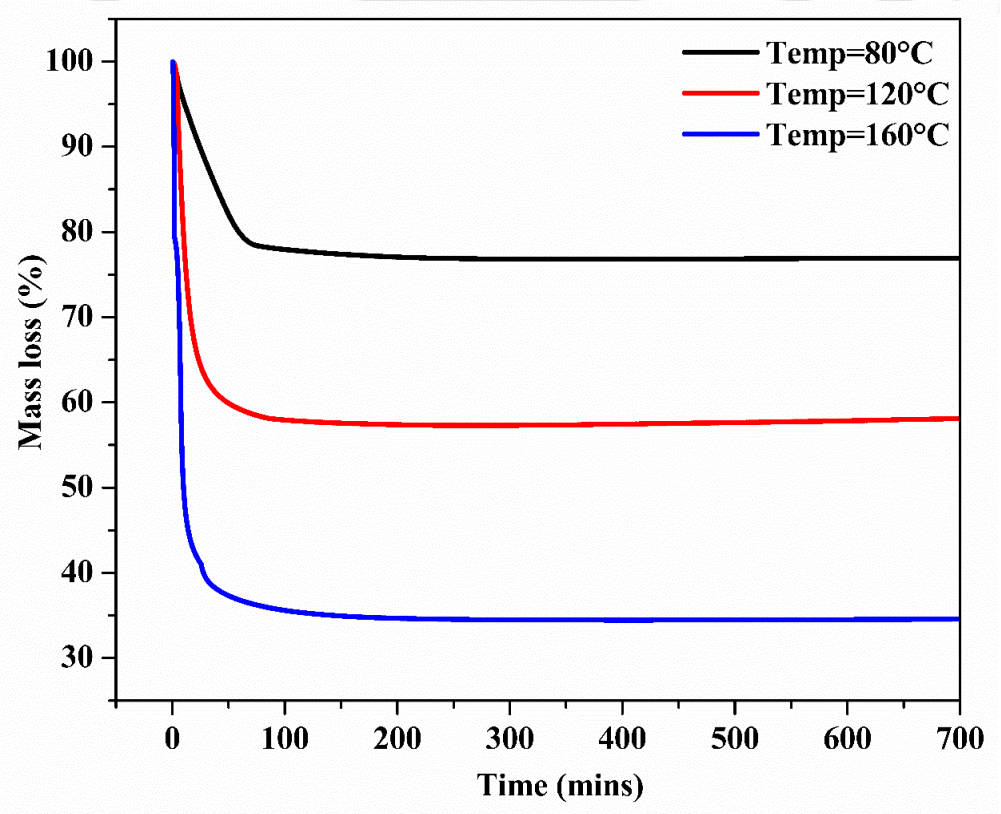

Figure 3.8. Isothermal TGA of DES+MWCNT nanofluid at different temperatures

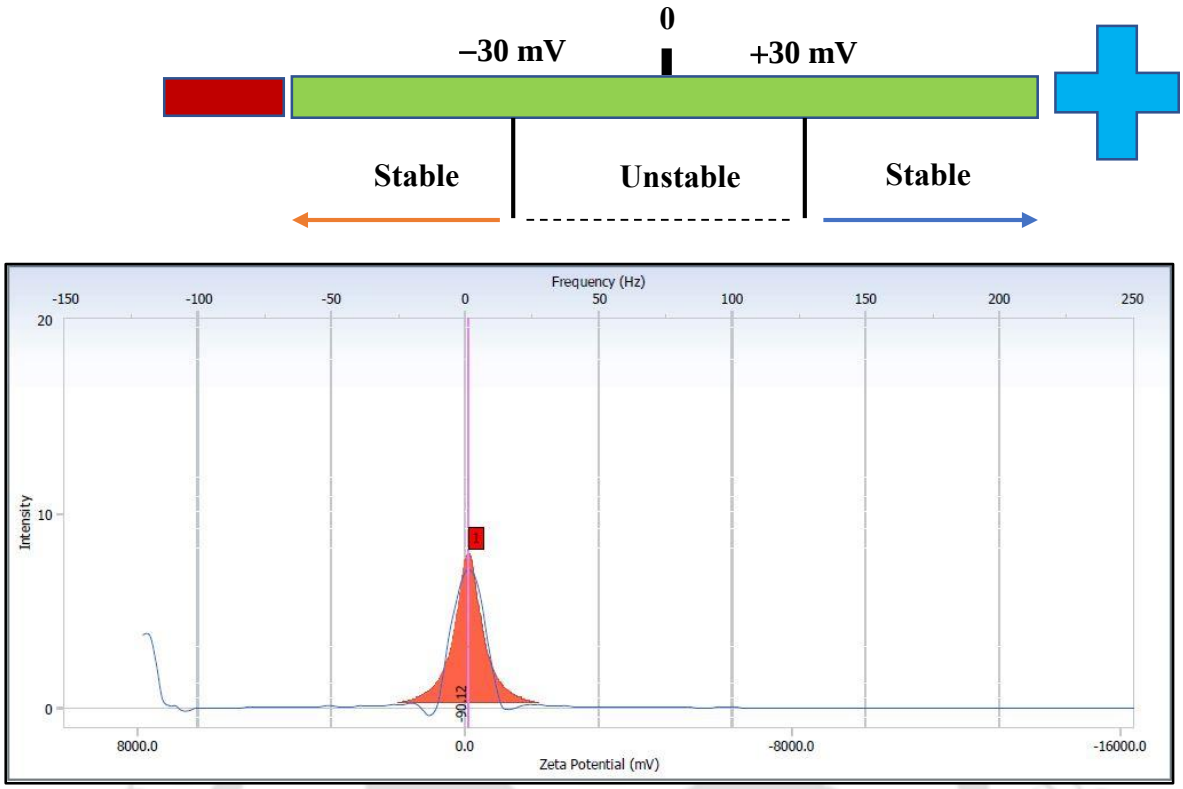

Figure 3.9. Zeta potential results of [MTBP][EG]+MWCNT

3.4.4 Density and Viscosity

Density is an essential factor for heat transfer fluid as it determines the flow behaviour of the fluid. Experimentally measurement of density is reported in Figure 3.10(a) and compared with commercially available heat transfer fluid Therminol VP-3 (Phenylcyclohexane + bicyclohexyl)[82].The experimental data indicated that the density of both DES and nanofluid decreases with temperature from 25-85°C. Also, it was noted from the Figure 3.10 that the density of both nanofluid and DES is more than that of commercial fluid Therminol VP-3. Experimentally, nanofluid containing 0.02 wt% of MWCNT has low density than that of the base fluid. However, measured density variation between the DES and nanofluid is insignificant. This is attributed to the size of the nanoparticle. Here, thermal expansion occurs due to the increase in temperature, which results in higher kinetic energy of the molecules. A

linear correlation was established between density and temperature as provided in equation 3.1 with regression value R^2=0.99952 and standard error value $\pm 4.542 \times 10^{-6}$

$$\rho = 1.2417\text{-}7.16 \times 10^{-4}T \pm 4.542 \times 10^{-6} \quad \textbf{(3.1)}$$

Where ρ (gm/cm^3)is the density and *T* (K) is the temperature of the DES or Nanofluid. Experimentally measured values are compared with the available conventional mode namely Pak and Cho model[83], given in equation 3.2. This model is based on the volumetric concentration and pure density of nanoparticle and base fluid. To compare the experimental results to this model, we have used equation 3.3 to convert the weight fraction into volume fraction.

$$\rho_{nf} = \varphi_v\rho_{np} + (1\text{-}\varphi_v)\rho_{bf} \quad \textbf{(3.2)}$$

Where, ρ_{nf}, ρ_{np}, ρ_{bf} and $\varphi_v$are the density of nanofluid, nanoparticle, basefluid,and volume fraction of nanoparticle, respectively.

$$\varphi = \left[\frac{\left(\frac{m}{\rho}\right)_{Nanoparticles}}{\left(\frac{m}{\rho}\right)_{Nanoparticles} + \left(\frac{m}{\rho}\right)_{base\ fluid}}\right] \times 100 \quad \textbf{(3.3)}$$

Where φ, *m*,and ρ denote volume fraction of the nanoparticles (%), solid mass (kg), and density (kg/m^3) of the nanoparticle, respectively. It was seen from the Figure 3.10(b) that the results of the Pak and Cho model were very close to the experimental data.

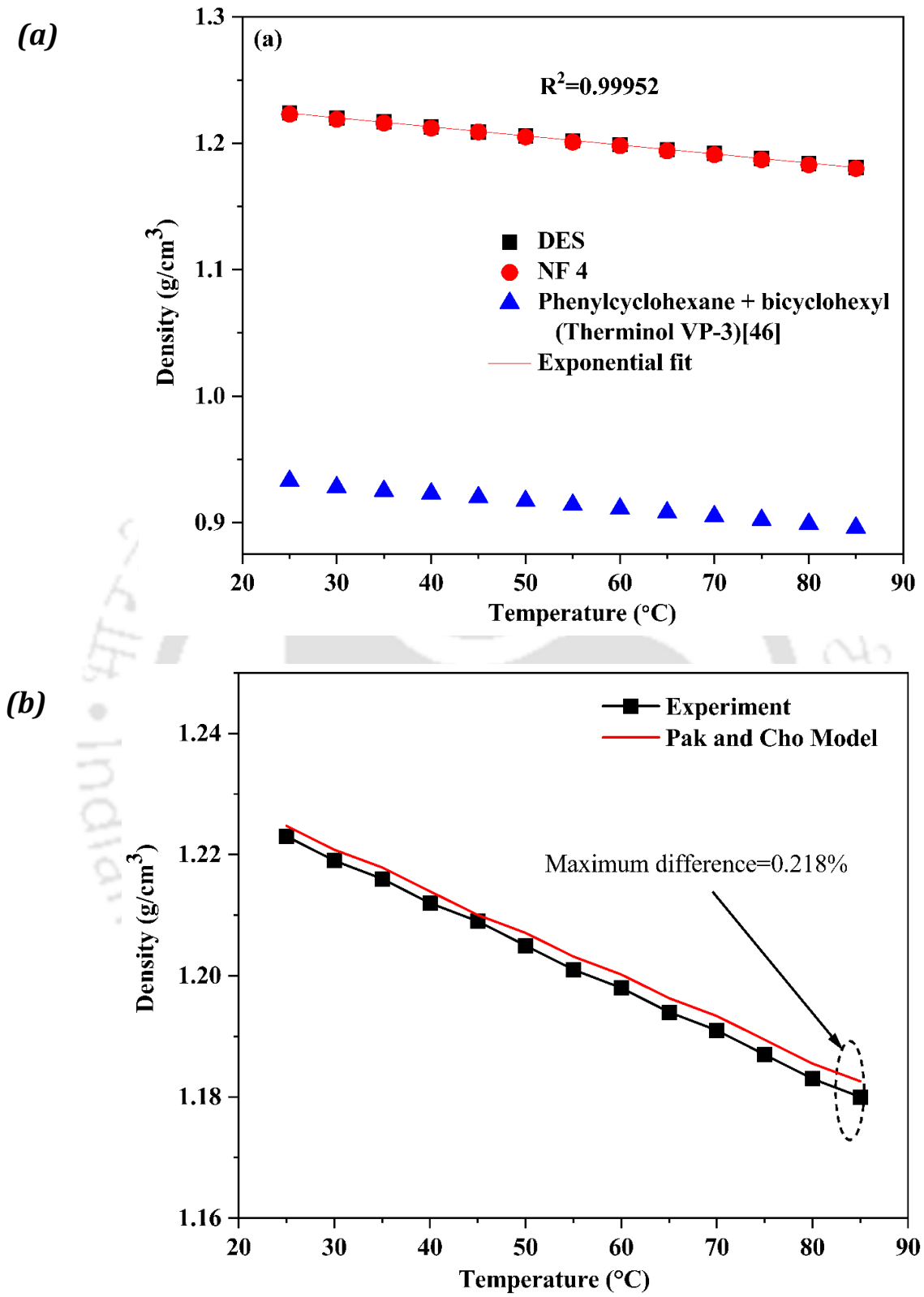

Figure 3.10. (a) Variation of density with different temperatures for DES and nanofluids (b) Comparison plot of density between experimental with Pak and Cho Model [83]

Experimental measurement of viscosity for both DES and nanofluid were performed at different temperatures for a constant shear rate ($d\gamma/dt$=50 sec^{-1}), shown in Figure 3.11(a). It is observed that the viscosity of DES decreases with an increase in temperature from 25-85°C. Similar results are observed when 0.02 wt% of MWCNT is added into the DES. Here the viscosity of the nanofluid decreases from 89.1 cP to 9.9 cP when temperature increases from 25-85°C. Both the nanofluid and DES show higher viscosity than commercial fluid Therminol VP-3. However, it was observed that the presence of DES makes the inherent viscosity lower than the base fluid. It was also observed that the viscosity decreases exponentially with temperature. An exponential correlation was established (equation 3.4) with a regression value of R^2=0.99 to predict the viscosity of the different volume concentrations of the nanofluid.

$$\mu = 0.00684 + 0.3523e^{-0.05947T} \quad \textbf{(3.4)}$$

Here μ is the viscosity in Pa.s and *T* is the temperature of the nanofluid in Celsius. It should be noted that a lower viscosity of the nanofluid results in lower pressure drop, which lessens the pumping costs. The measured experimental viscosity values were compared with the available theoretical model; Brinkman model[84] as given in equation 3.5.

$$\mu_{nf} = \frac{\mu_{bf}}{(1-\varphi)^{2.5}} \quad \textbf{(3.5)}$$

Where, μ_{nf} and μ_{bf} are the viscosity of nanofluid and base fluid, respectively. φ is the volume fraction.It should be noted that the Brinkman model (Figure 3.11(b))is suitable for bigger nanoparticle size, therefore the results for viscosity in smaller nanoparticle size is not accurate. Furthermore, the effect of temperature is not considered in this model. Newtonian fluid behaviour of the nanofluid was confirmed from shear stress and shear rate data. From Figure 3.12, a linear trend was observed at three different temperatures, namely 25°C, 30°C,

and 35°C. The data were obtained from different shearing times indicating the fluid's Newtonian behaviour. Figure 3.12 shows that as expected viscosity is strongly dependent on temperature.

We compared the obtained thermophysical properties with literature and observed the same results as Ilyas et al. [28, 85], who reported a minor difference in density between base fluid and nanofluids which is consistent with our findings. According to published data, the density difference between MWCNT-thermal oil nanofluid and base fluid was 0.76 kg/m^3 and 0.61 kg/m^3 at 30°C and 40°C, respectively. Our investigation found that the density changes between 30°C and 40°C were 0.001 and 0.002 kg/m^3, respectively. Similarly, the viscosity of the reported nanofluid and base fluid decreases with increased temperature, consistent with the literature [28]. Beheshti et al. [86] reported a 0.9% decrement of viscosity in nanofluid (MWCNT+ Transformer oil) with 0.01 wt% concentration. This work reported, 11.3% and 9.5% decrement at 30°C and 40°C in 0.02 wt% DES-based nanofluid. However, the literature showed the opposite result [28], where 11.8% and 11.3% increments were found in 0.1 wt% nanofluids at 30°C and 40°C respectively.

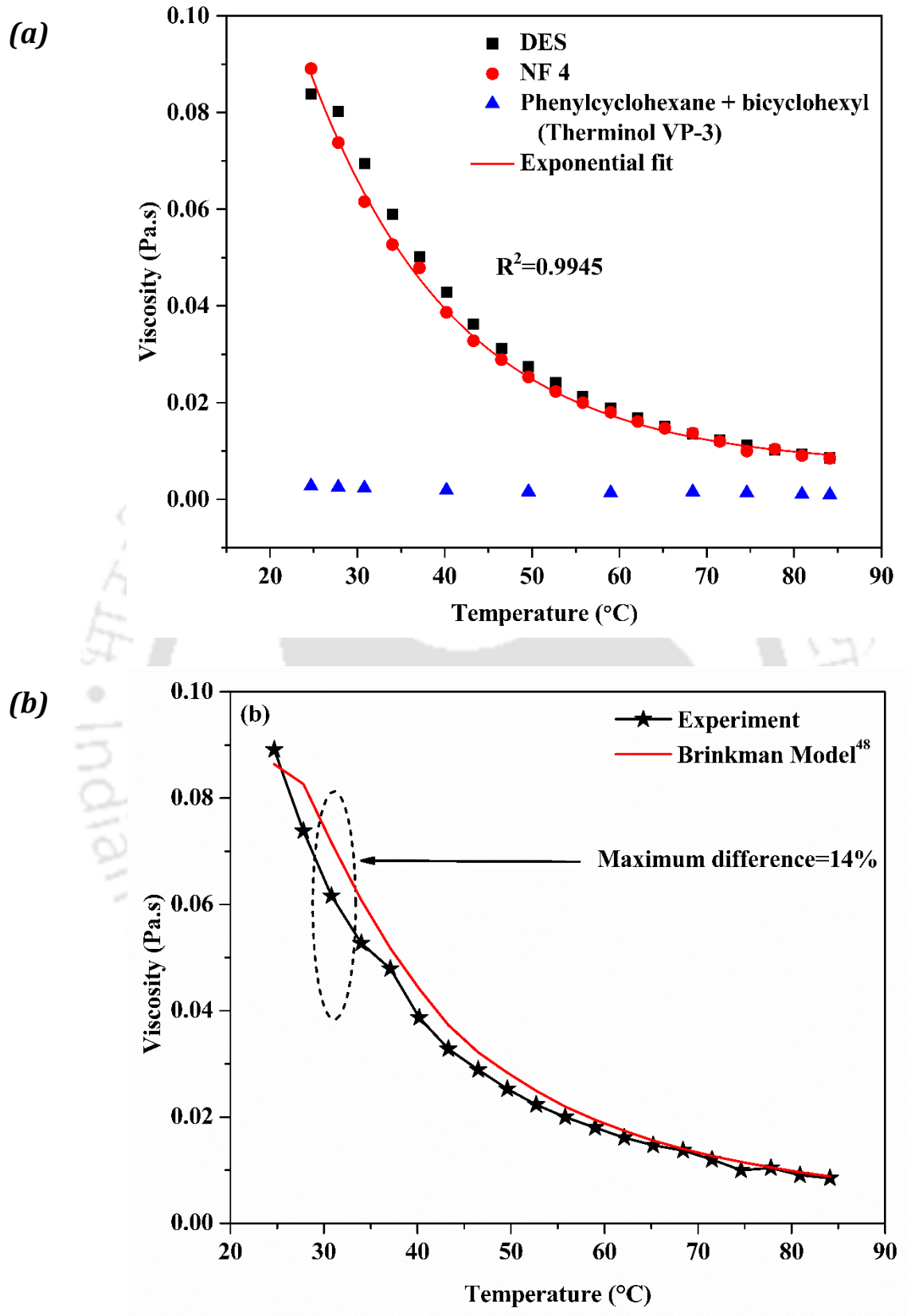

Figure 3.11. (a) Variations of viscosity at different temperatures for DES and nanofluids (b) Comparison plot of viscosity between experimental and Brinkman model [84]

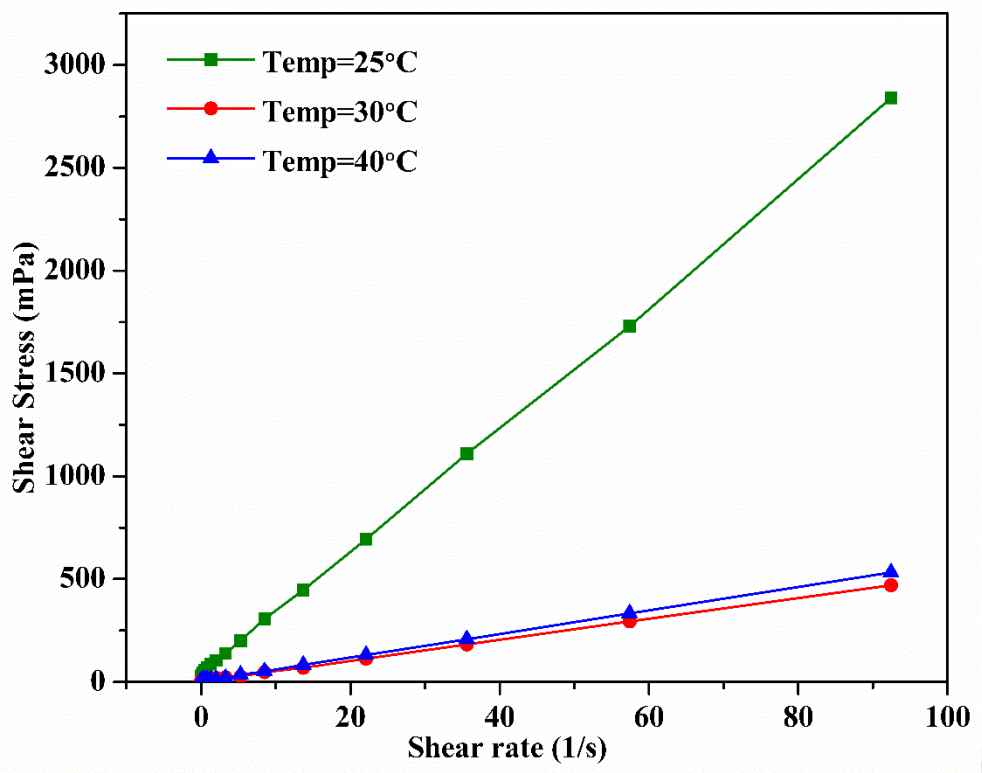

Figure 3.12. Shear stress versus shear rate of nanofluid at three different temperatures

3.4.5 Thermal Conductivity and Specific heat

Thermal conductivity of both base fluid and nanofluid (NF4) were measured against different temperatures and shown in Figure 3.13(a). The thermal conductivity of DES and nanofluid was first measured from 25-80°C. It was noted that the thermal conductivity of nanofluid gradually increases with temperature. However, the thermal conductivity of DES decreases with an increase in temperature from 25-80°C. From the experimental data, it was evident that the addition of MWCNT in the base fluid enhances the thermal conductivity as compared to the base fluid and commercial fluid .The enhancement of thermal conductivity was calculated from equation 3.6[28].

$$\mathrm{TCE} = \left(\frac{k_{nf}}{k_{bf}} - 1\right) \times 100\% \qquad \textbf{(3.6)}$$

The maximum enhancement of thermal conductivity was found at 361%. This is due to the interaction between the nanoparticles and the induced Brownian motion of the nanoparticle at high-temperature as nanoparticles can gain higher energy which increases their kinetic energy and leads in efficient transfer of heat. Nanoparticle's size and shape are another important factor which influence the thermal conductivity. Dong and Chen[87] reported the nanofluid thermal conductivity increases as the particle size decreased. In case of carbon nanotube nanoparticle, thermal conductivity increases with increase in the orders of large volume to surface ratio. Similar analogy was followed by Jhang and Choi [88] where it was observed that the thermal conductivity increases with the increase in size of the carbon nanotube. An exponential correlation of thermal conductivity as a function of temperature was developed for nanofluid with a regression value $R^2 = 0.91993$, as shown in Figure 3.13(a).

$$\kappa = 0.19607 + 4.3669 \times 10^{-5} e^{(0.09218T)} \quad \textbf{(3.7)}$$

Here, κ and T are the thermal conductivity in W/mK and Temperature in Kelvin respectively. Molecular diffusion takes place in DES at increased temperature and it becomes faster when temperature gradually increases. Because, DES molecules are closely packed, heat transfer occurs through conduction mode. Due to increase in temperature, it allows the liquid to expand. The free movement of the molecule ensures that the rate of collision of molecules decreases. As a result, the thermal conductivity of DES decreases with increasing temperature.

The experimental measured values are correlated with the theoretical model as provided by Maxwell[89] and given in equation 3.8 (Figure 3.13(b)). However this model does not give accurate thermal conductivity as it does not consider degree of aggregation, nanoparticle structure and Brownian motion [90]. A similar difference can be found in literature for other nanofluids [28, 91].

$$k_{nf} = k_{bf}\left[\frac{k_{np}+2k_{bf}+2\varphi(k_{np}-k_{bf})}{k_{np}+2k_{bf}-\varphi(k_{np}-k_{bf})}\right] \quad \textbf{(3.8)}$$

Where, k_{nf}, k_{bf}, k_{np} and φ are thermal conductivity of nanofluid, basefluid, nanoparticle and volume fraction of the nanofluid respectively.

(a)

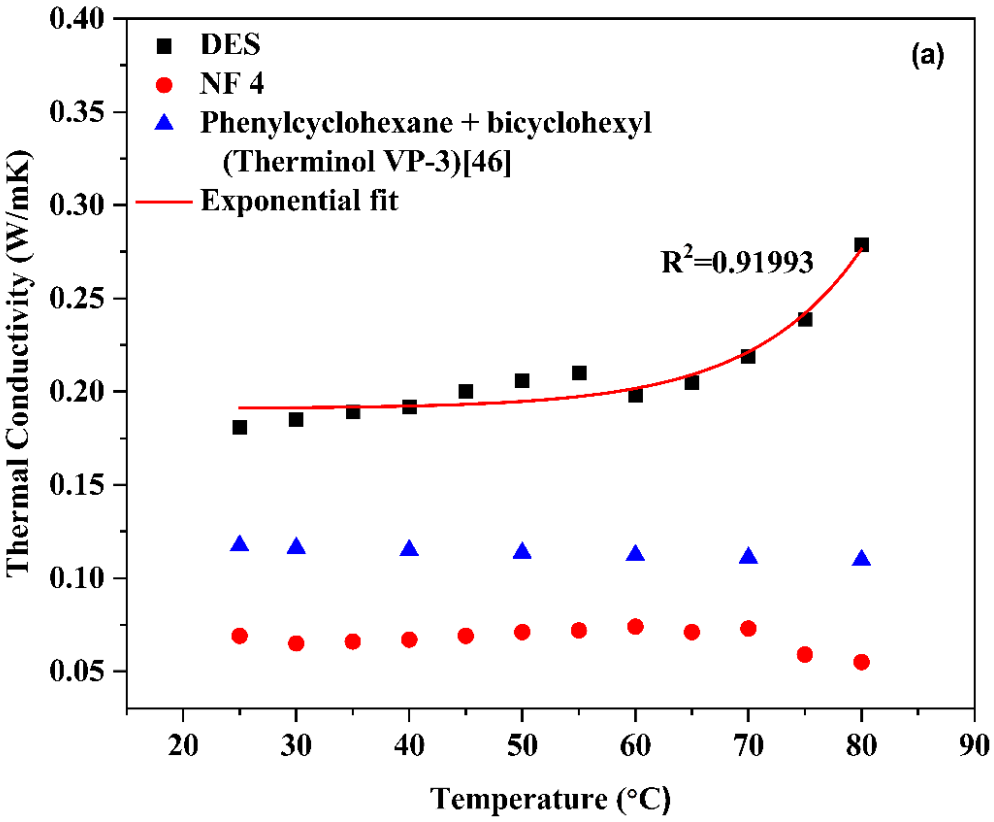

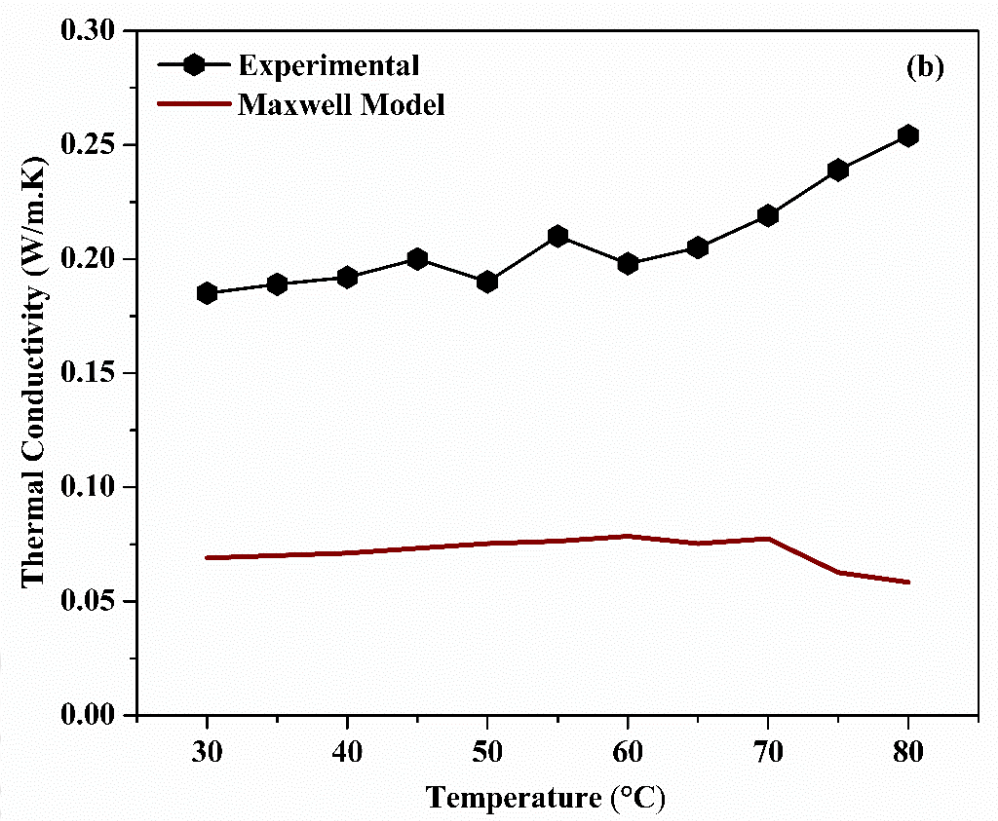

Figure 3.13. (a) Variation of thermal conductivity at different temperatures for DES and nanofluids (b) Comparison plot of thermal conductivity between experimental and Maxwell model [89]

Figure 3.14(a) shows the specific heat of DES and nanofluid NF4 at different temperatures from 45°C to 90°C with a heating rate 20°C/min. It is clear from the data that specific heat increases with an increase in temperatures. However, the addition of multi-walled carbon nanotube enhances the heat capacity of the nanofluid. Furthermore, the specific heat capacity of both nanofluid and base fluid is higher than Therminol VP-3. Further, it was reported that the specific heat of nanofluid decreases with increasing particle volume concentrations [92]. This can be attributed to the fact that to increase the temperature, the internal energy increases, which implies a rise in vibrational energy and rotational energy of the molecules. This in turn, allows the molecule to adsorb high molar heat capacity. Based on

the experimental data with the function of temperature, a mathematical correlation was developed as shown in Figure 3.14(a) and is given below:

$$Cp = 0.01223T + 1.45749 \quad \textbf{(3.9)}$$

Here Cp and is T are the specific heat capacity and temperature of the nanofluid .

There are two widely used theoretical models which correlate the experimental data are based on the straight average of specific heat capacities (equation (3.10)) and thermal equilibrium between particle-liquid (equation (3.11))[28].

Model 1: $$Cp_{nf} = \varphi_v Cp_{np} + (1-\varphi_v)Cp_{bf} \quad \textbf{(3.10)}$$

Model 2: $$Cp_{nf} = \frac{\varphi_v Cp_{np}\rho_{np} + (1-\varphi_v)Cp_{bf}\rho_{bf}}{\varphi_v \rho_{np} + (1-\varphi_v)\rho_{bf}} \quad \textbf{(3.11)}$$

Here Cp_{nf}, Cp_{np}, Cp_{bf} are the specific heat of the nanofluid, nanoparticle, and basefluid, respectively. ρ_{np}, ρ_{np}, ρ_{bf} are the density of nanofluid, nanoparticle, and basefluid, respectively. φ_v is the volume fraction. A comparison between theoretical models and experimental measured values is shown in Figure 3.14(b). Significance difference was observed from the experimental values to the theoretical models. Possible reasons that are reported in the literature and are not considered in these models are nanoparticle size, shape, and degree of aggregation [93].

We have found comparable results of thermal conductivity value with Ilyas et al.[28]. The values of thermal conductivity were directly proportional to the temperature. In our work, 184.61% and 65.10% enhancement was observed at temperatures 30°C and 40°C, whereas a maximum enhancement 28.7% was observed by Ilyas et al.[28]. Additionally, we compared our results to published literature [93-96] and found that, in both circumstances, the specific heat value rises as the temperature rises.

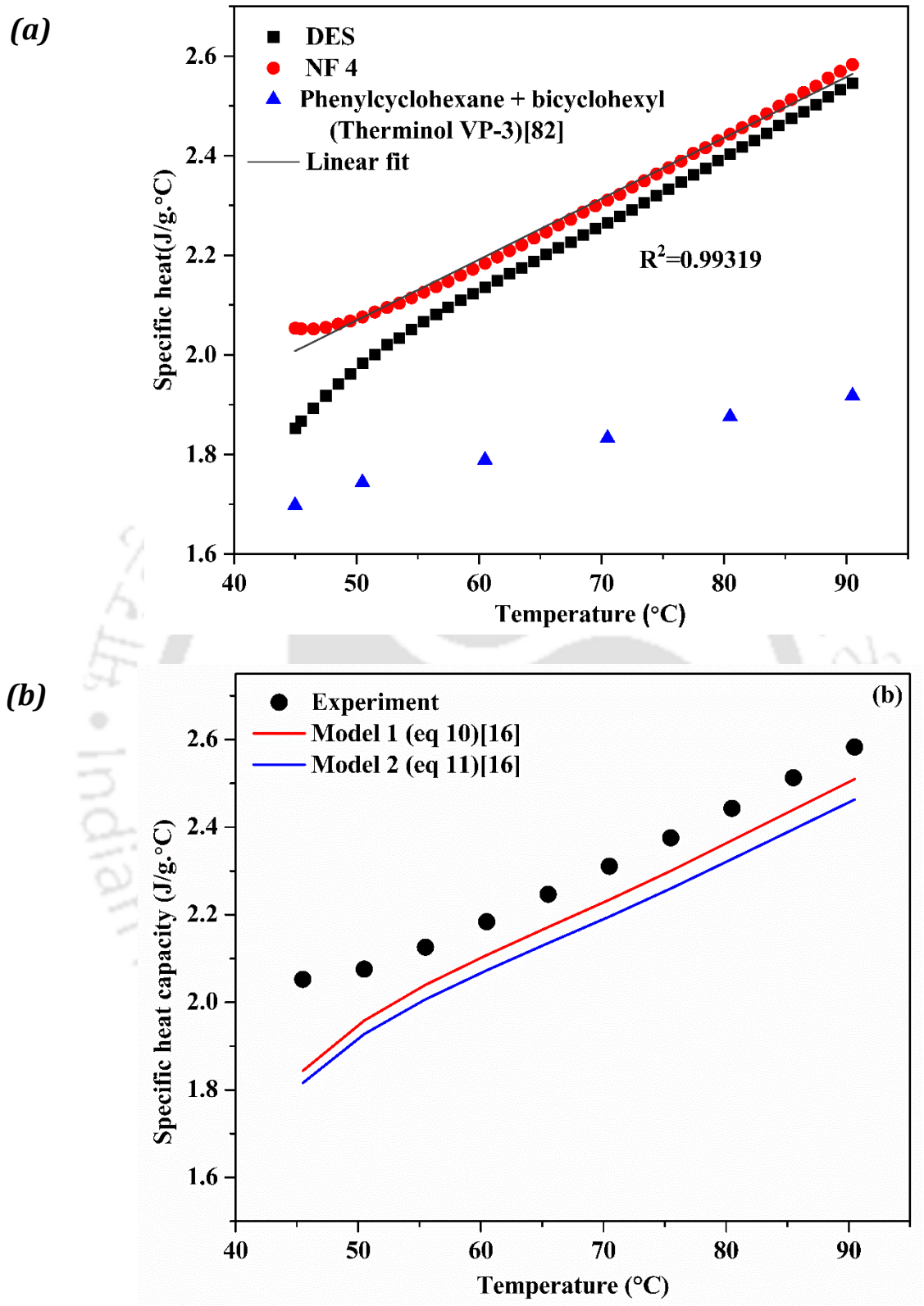

Figure 3.14. (a) Variation of specific heat at different temperatures for DES and nanofluids(b) Comparison plot of specific heat between experimental data and theoretical models [28]

3.4.6 MD simulations

The thermal conductivity is usually computed using Fourier's law heat conduction as mentioned in section 2.4.6.

The experimental values obtained at different temperatures are also shown in Figure 3.15. The values of thermal conductivity at 40°C is found to be a good match with the experiment. However, the simulations failed to reproduce the experimental trend from 30 to 40°C. A major deviation was observed when compared with experimental values from 60°C. The particle–fluid interface may have attributed this deviation, whereas this interaction is not considered in the simulation. The results from the mentioned manuscript showed that even though the experimental values change with temperature, the simulated values show minimal change.

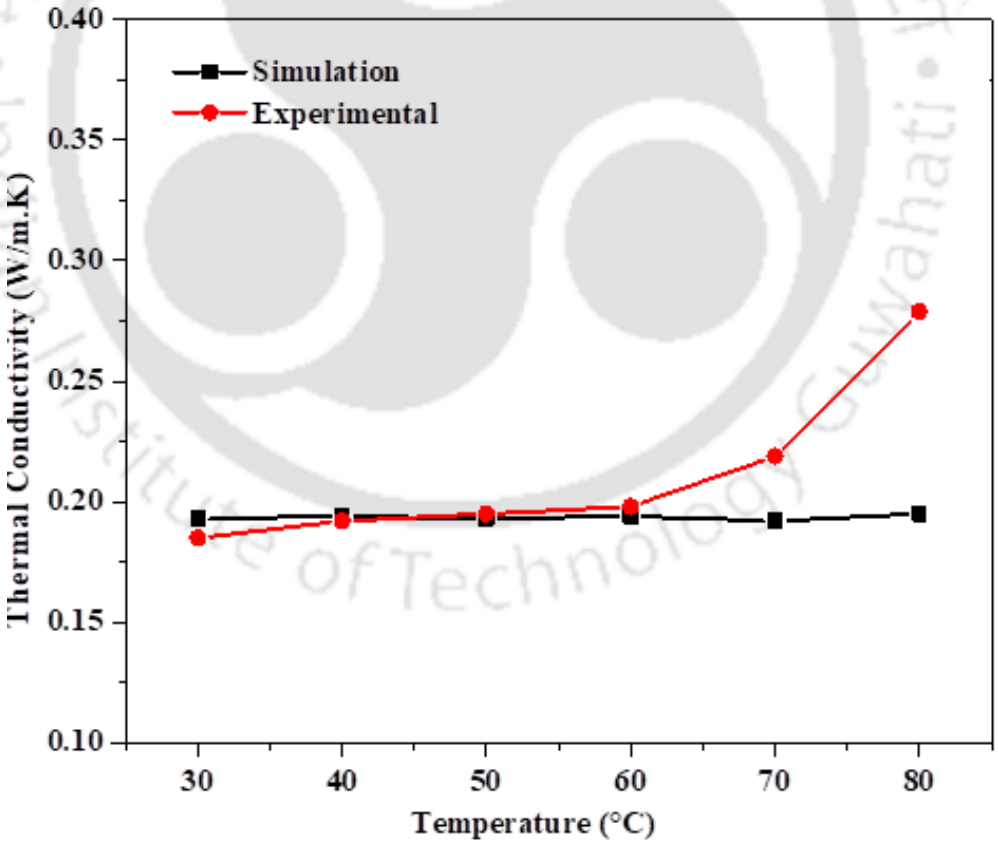

Figure 3.15. Comparison of experimental and MD predicted thermal conductivity values

3.5 Conclusion

This chapter aims to characterize the MWCNT nanoparticle and synthesized MWCNT based nanofluid by a two-step method of preparation. The nanofluid was prepared by mixing DES (MTPB salt and ethylene glycol in the molar ratio of 1:4) and 0.02 weight% of MWCNT. Thereafter thethermophysical properties, including thermal conductivity, viscosity, density, and specific heat of the nanofluid, were measured. MWCNT was characterized by FETEM and FESEM to visualize the morphology of the nanoparticles. Further from FT-IR and powder XRD experiment, conjugation of DES attached with MWCNT and crystallinity of the MWCNT was confirmed. Stability of the nanofluid was investigated through visual observation, optical microscope as well as zeta potential. The density and viscosity was found to decrease with an increase in the nanofluid temperature when 0.02wt% MWCNT is added. The DES exhibits Newtonian behaviour, as evidenced by the fact that its shear viscosity decreases with increasing temperature. At higher temperatures, there is a significant increase in thermal conductivity and specific heat. The thermophysical properties of nanofluid qualities revealed that it outperforms the traditional commercial HTFs and that it has tremendous promise for use as an advanced Heat Transfer Fluid in Concentrated Solar Power(CSP) and Multi-Stage Flash(MSF) column plants.

In the next chapter, we discuss the stability and potential application of DES based nanofluid.

Reference

[1] N. Menges, The role of green solvents and catalysts at the future of drug design and of synthesis, Green Chem 23 (2017) 254-257.

[2] E. Durand, J. Lecomte, B. Baréa, G. Piombo, E. Dubreucq, and P. Villeneuve, Evaluation of deep eutectic solvents as new media for Candida antarctica B lipase catalyzed reactions, Process biochemistry 47(12) (2012) 2081-2089.

[3] A.E. Ünlü, A. Arıkaya, and S. Takaç, Use of deep eutectic solvents as catalyst: A mini-review, Green Processing and Synthesis 8(1) (2019) 355-372.

[4] E.L. Smith, A.P. Abbott, and K.S. Ryder, Deep eutectic solvents (DESs) and their applications, Chemical reviews 114(21) (2014) 11060-11082.

[5] Y. Liu, J.B. Friesen, J.B. McAlpine, D.C. Lankin, S.-N. Chen, and G.F. Pauli, Natural deep eutectic solvents: properties, applications, and perspectives, Journal of natural products 81(3) (2018) 679-690.

[6] R.D. Rogers, K.R. Seddon, and S. Volkov, Green industrial applications of ionic liquids. Vol. 92. 2012: Springer Science & Business Media.

[7] N.R. Varma, A. Ramalingam, and T. Banerjee, Experiments, correlations and COSMO-RS predictions for the extraction of benzothiophene from n-hexane using imidazolium-based ionic liquids, Chemical engineering journal 166(1) (2011) 30-39.

[8] L. Kumar, T. Banerjee, and K. Mohanty, Prediction of selective extraction of cresols from aqueous solutions by ionic liquids using theoretical approach, Separation Science and Technology 46(13) (2011) 2075-2087.

[9] A.A.P. Kumar and T. Banerjee, Thiophene separation with ionic liquids for desulphurization: A quantum chemical approach, Fluid Phase Equilibria 278(1-2) (2009) 1-8.

[10] S.R. Pilli, T. Banerjee, and K. Mohanty, Ionic liquids as green solvents for the extraction of endosulfan from aqueous solution: a quantum chemical approach, Chemical Product and Process Modeling 8(1) (2013) 1-14.

[11] D. Rabari and T. Banerjee, Experimental and theoretical studies on the effectiveness of phosphonium-based ionic liquids for butanol removal at T= 298.15 K and p= 1 atm, Industrial & Engineering Chemistry Research 53(49) (2014) 18935-18942.

[12] A. Nann, C. Held, and G. Sadowski, Liquid–liquid equilibria of 1-butanol/water/IL systems, Industrial & Engineering Chemistry Research 52(51) (2013) 18472-18481.

[13] D. Rabari and T. Banerjee, Biobutanol and n-propanol recovery using a low density phosphonium based ionic liquid at T= 298.15 K and p= 1 atm, Fluid Phase Equilibria 355 (2013) 26-33.

[14] B. Wu, R.G. Reddy, and R.D. Rogers. Novel ionic liquid thermal storage for solar thermal electric power systems, in International Solar Energy Conference, 2001: American Society of Mechanical Engineers.

[15] K. Jafari, M.H. Fatemi, and P. Estellé, Deep eutectic solvents (DESs): A short overview of the thermophysical properties and current use as base fluid for heat transfer nanofluids, Journal of Molecular Liquids 321 (2021) 114752.

[16] C. Liu, H. Fang, X. Liu, B. Xu, and Z. Rao, Novel silica filled deep eutectic solvent based nanofluids for energy transportation, ACS Sustainable Chemistry & Engineering 7(24) (2019) 20159-20169.

[17] Y. Chen and T. Mu, Application of deep eutectic solvents in biomass pretreatment and conversion, Green Energy & Environment 4(2) (2019) 95-115.

[18] A. Shishov, A. Bulatov, M. Locatelli, S. Carradori, and V. Andruch, Application of deep eutectic solvents in analytical chemistry. A review, Microchemical Journal 135 (2017) 33-38.

[19] S.U. Choi and J.A. Eastman, Enhancing thermal conductivity of fluids with nanoparticles. 1995, Argonne National Lab.(ANL), Argonne, IL (United States).

[20] A. Karimipour, S.A. Bagherzadeh, M. Goodarzi, A.A. Alnaqi, M. Bahiraei, M.R. Safaei, and M.S. Shadloo, Synthesized CuFe2O4/SiO2 nanocomposites added to water/EG: evaluation of the thermophysical properties beside sensitivity analysis & EANN, International Journal of Heat and Mass Transfer 127 (2018) 1169-1179.

[21] A. Ghasemi, M. Hassani, M. Goodarzi, M. Afrand, and S. Manafi, Appraising influence of COOH-MWCNTs on thermal conductivity of antifreeze using curve fitting and neural network, Physica A: Statistical Mechanics and its Applications 514 (2019) 36-45.

[22] S.A. Bagherzadeh, A. D'Orazio, A. Karimipour, M. Goodarzi, and Q.-V. Bach, A novel sensitivity analysis model of EANN for F-MWCNTs–Fe3O4/EG nanofluid thermal conductivity: Outputs predicted analytically instead of numerically to more accuracy and less costs, Physica A: Statistical Mechanics and Its Applications 521 (2019) 406-415.

[23] R.E. Smalley, Carbon nanotubes: synthesis, structure, properties, and applications, (2003).

[24] A. Asadi, I.M. Alarifi, V. Ali, and H.M. Nguyen, An experimental investigation on the effects of ultrasonication time on stability and thermal conductivity of MWCNT-water nanofluid: Finding the optimum ultrasonication time, Ultrason. Sonochem. 58 (2019) 104639.

[25] I. Mahbubul, R. Saidur, M. Amalina, and M. Niza, Influence of ultrasonication duration on rheological properties of nanofluid: an experimental study with alumina–water nanofluid, International Communications in Heat and Mass Transfer 76 (2016) 33-40.

[26] Y.-j. Hwang, J. Lee, C. Lee, Y. Jung, S. Cheong, C. Lee, B. Ku, and S. Jang, Stability and thermal conductivity characteristics of nanofluids, Thermochimica Acta 455(1-2) (2007) 70-74.

[27] A.O. Borode, N.A. Ahmed, and P.A. Olubambi, A review of heat transfer application of carbon-based nanofluid in heat exchangers, Nano-Structures & Nano-Objects 20 (2019) 100394.

[28] S.U. Ilyas, R. Pendyala, and M. Narahari, Stability and thermal analysis of MWCNT-thermal oil-based nanofluids, Colloids and Surfaces A: Physicochemical and Engineering Aspects 527 (2017) 11-22.

[29] M.A. Salam and R. Burk, Synthesis and characterization of multi-walled carbon nanotubes modified with octadecylamine and polyethylene glycol, Arabian Journal of Chemistry 10 (2017) S921-S927.

[30] W. Yu and H. Xie, A review on nanofluids: preparation, stability mechanisms, and applications, Journal of nanomaterials 2012 (2012).

[31] K.V. Wong and O. De Leon, Applications of nanofluids: current and future, in Nanotechnology and Energy. 2017, Jenny Stanford Publishing. p. 105-132.

[32] H. Ma, C. Wilson, B. Borgmeyer, K. Park, Q. Yu, S. Choi, and M. Tirumala, Effect of nanofluid on the heat transport capability in an oscillating heat pipe, Applied Physics Letters 88(14) (2006) 143116.

[33] H. Ma, C. Wilson, Q. Yu, K. Park, U. Choi, and M. Tirumala, An experimental investigation of heat transport capability in a nanofluid oscillating heat pipe, (2006).

[34] P.X. Tran and D. Lyons, Nanofluids for use as ultra-deep drilling fluids, Fact Sheet, National Energy Technology Laboratory, Office of Fossil Energy, US Department of Energy, Jan., http://www. netl. doe. gov/publications/factsheets/rd/R&D108. pdf (2007).

[35] S. Vafaei, T. Borca-Tasciuc, M. Podowski, A. Purkayastha, G. Ramanath, and P. Ajayan, Effect of nanoparticles on sessile droplet contact angle, Nanotechnology 17(10) (2006) 2523.

[36] W. Chen, C. Zou, X. Li, and H. Liang, Application of recoverable carbon nanotube nanofluids in solar desalination system: An experimental investigation, Desalination 451 (2019) 92-101.

[37] R.S. Shawgo, A.C.R. Grayson, Y. Li, and M.J. Cima, BioMEMS for drug delivery, Current Opinion in Solid State and Materials Science 6(4) (2002) 329-334.

[38] A. Ovsianikov, B. Chichkov, P. Mente, N. Monteiro-Riviere, A. Doraiswamy, and R. Narayan, Two photon polymerization of polymer–ceramic hybrid materials for transdermal drug delivery, International journal of applied ceramic technology 4(1) (2007) 22-29.

[39] J.-F. Yan and J. Liu, Nanocryosurgery and its mechanisms for enhancing freezing efficiency of tumor tissues, Nanomedicine: Nanotechnology, Biology and Medicine 4(1) (2008) 79-87.

[40] P.-C. Chiang, D.-S. Hung, J.-W. Wang, C.-S. Ho, and Y.-D. Yao, Engineering water-dispersible FePt nanoparticles for biomedical applications, IEEE transactions on magnetics 43(6) (2007) 2445-2447.

[41] B. Chitra and K.S. Kumar, Heat transfer enhancement using single base and double base nanofluids, Journal of Molecular Liquids 221 (2016) 1128-1132.

[42] J. Eastmen, S. Choi, S. Li, W. Yu, and W. Thompson, Anomalously increased effective thermal conductivities of ethylene glycol-based nanofluids containing copper nanoparticles, Appl. Phys. Lett 78 (2001) 718-720.

[43] S. Murshed, K. Leong, and C. Yang, Enhanced thermal conductivity of TiO2—water based nanofluids, Int. J. Therm. Sci. 44(4) (2005) 367-373.

[44] Y. Xuan and Q. Li, Heat transfer enhancement of nanofluids, International Journal of heat and fluid flow 21(1) (2000) 58-64.

[45] Y. Hwang, J.-K. Lee, J.-K. Lee, Y.-M. Jeong, S.-i. Cheong, Y.-C. Ahn, and S.H. Kim, Production and dispersion stability of nanoparticles in nanofluids, Powder Technology 186(2) (2008) 145-153.

[46] E.K. Goharshadi, S. Samiee, and P. Nancarrow, Fabrication of cerium oxide nanoparticles: Characterization and optical properties, Journal of colloid and interface science 356(2) (2011) 473-480.

[47] E.K. Goharshadi, S.H. Sajjadi, R. Mehrkhah, and P. Nancarrow, Sonochemical synthesis and measurement of optical properties of zinc sulfide quantum dots, Chemical engineering journal 209 (2012) 113-117.

[48] H.-t. Zhu, Y.-s. Lin, and Y.-s. Yin, A novel one-step chemical method for preparation of copper nanofluids, Journal of colloid and interface science 277(1) (2004) 100-103.

[49] M. Khairul, K. Shah, E. Doroodchi, R. Azizian, and B. Moghtaderi, Effects of surfactant on stability and thermo-physical properties of metal oxide nanofluids, International Journal of Heat and Mass Transfer 98 (2016) 778-787.

[50] L. Yang, K. Du, X.S. Zhang, and B. Cheng, Preparation and stability of Al2O3 nano-particle suspension of ammonia–water solution, Applied Thermal Engineering 31(17-18) (2011) 3643-3647.

[51] M. Mehrali, E. Sadeghinezhad, S.T. Latibari, S.N. Kazi, M. Mehrali, M.N.B.M. Zubir, and H.S.C. Metselaar, Investigation of thermal conductivity and rheological properties of nanofluids containing graphene nanoplatelets, Nanoscale research letters 9(1) (2014) 1-12.

[52] L. Vandsburger, Synthesis and covalent surface modification of carbon nanotubes for preparation of stabilized nanofluid suspensions, (2009).

[53] P. Dehury, J. Singh, and T. Banerjee, Thermophysical and Forced Convection Studies on (Alumina+ Menthol)-Based Deep Eutectic Solvents for Their Use as a Heat Transfer Fluid, ACS omega 3(12) (2018) 18016-18027.

[54] D. Van Der Spoel, E. Lindahl, B. Hess, G. Groenhof, A.E. Mark, and H.J. Berendsen, GROMACS: fast, flexible, and free, Journal of computational chemistry 26(16) (2005) 1701-1718.

[55] M.J. Abraham, T. Murtola, R. Schulz, S. Páll, J.C. Smith, B. Hess, and E. Lindahl, GROMACS: High performance molecular simulations through multi-level parallelism from laptops to supercomputers, SoftwareX 1 (2015) 19-25.

[56] S. Plimpton, Fast parallel algorithms for short-range molecular dynamics, Journal of computational physics 117(1) (1995) 1-19.

[57] W.L. Jorgensen, D.S. Maxwell, and J. Tirado-Rives, Development and testing of the OPLS all-atom force field on conformational energetics and properties of organic liquids, Journal of the American Chemical Society 118(45) (1996) 11225-11236.

[58] H. Liu and E. Maginn, A molecular dynamics investigation of the structural and dynamic properties of the ionic liquid 1-n-butyl-3-methylimidazolium bis (trifluoromethanesulfonyl) imide, The Journal of chemical physics 135(12) (2011) 124507.

[59] N. Sieffert and G. Wipff, The [BMI][Tf2N] ionic liquid/water binary system: A molecular dynamics study of phase separation and of the liquid− liquid interface, The Journal of Physical Chemistry B 110(26) (2006) 13076-13085.

[60] T.D.N. Reddy and B.S. Mallik, Protic ammonium carboxylate ionic liquids: insight into structure, dynamics and thermophysical properties by alkyl group functionalization, Physical Chemistry Chemical Physics 19(16) (2017) 10358-10370.

[61] W. Humphrey, A. Dalke, and K. Schulten, VMD: Visual molecular dynamics, Journal of Molecular Graphics 14(1) (1996) 33-38, https://doi.org/10.1016/0263-7855(96)00018-5.

[62] M. Frisch and F. Clemente, Gaussian 09, Revision A. 01, MJ Frisch, GW Trucks, HB Schlegel, GE Scuseria, MA Robb, JR Cheeseman, G, Scalmani, V. Barone, B. Mennucci, GA Petersson, H. Nakatsuji, M. Caricato, X. Li, HP Hratchian, AF Izmaylov, J. Bloino, G. Zhe (2009).

[63] A.D. Becke, Density-functional exchange-energy approximation with correct asymptotic behaviour, Physical review A 38(6) (1988) 3098.

[64] A. Becke, Density-functional thermochemistry. III. The role of exact exchange (1993) J, Chem. Phys 98 5648.

[65] C. Lee, W. Yang, and R.G. Parr, Development of the Colle-Salvetti correlation-energy formula into a functional of the electron density, Physical review B 37(2) (1988) 785.

[66] J. Wang, W. Wang, P.A. Kollman, and D.A. Case, Automatic atom type and bond type perception in molecular mechanical calculations, Journal of molecular graphics and modelling 25(2) (2006) 247-260.

[67] L. Martínez, R. Andrade, E.G. Birgin, and J.M. Martínez, PACKMOL: a package for building initial configurations for molecular dynamics simulations, Journal of computational chemistry 30(13) (2009) 2157-2164.

[68] M.C. Payne, M.P. Teter, D.C. Allan, T. Arias, and a.J. Joannopoulos, Iterative minimization techniques for ab initio total-energy calculations: molecular dynamics and conjugate gradients, Reviews of modern physics 64(4) (1992) 1045.

[69] G. Bussi, D. Donadio, and M. Parrinello, Canonical sampling through velocity rescaling, The Journal of chemical physics 126(1) (2007) 014101.

[70] H.J. Berendsen, J.v. Postma, W.F. van Gunsteren, A. DiNola, and J.R. Haak, Molecular dynamics with coupling to an external bath, The Journal of chemical physics 81(8) (1984) 3684-3690.

[71] M. Parrinello and A. Rahman, Polymorphic transitions in single crystals: A new molecular dynamics method, Journal of Applied physics 52(12) (1981) 7182-7190.

[72] F. Müller-Plathe, A simple nonequilibrium molecular dynamics method for calculating the thermal conductivity, The Journal of chemical physics 106(14) (1997) 6082-6085.

[73] M. Zhang, E. Lussetti, L.E. de Souza, and F. Müller-Plathe, Thermal conductivities of molecular liquids by reverse nonequilibrium molecular dynamics, The Journal of Physical Chemistry B 109(31) (2005) 15060-15067.

[74] M.S. Kelkar and E.J. Maginn, Calculating the enthalpy of vaporization for ionic liquid clusters, The Journal of Physical Chemistry B 111(32) (2007) 9424-9427.

[75] C.M. Tenney and E.J. Maginn, Limitations and recommendations for the calculation of shear viscosity using reverse nonequilibrium molecular dynamics, The Journal of chemical physics 132(1) (2010) 014103.

[76] H. Liu, E. Maginn, A.E. Visser, N.J. Bridges, and E.B. Fox, Thermal and transport properties of six ionic liquids: an experimental and molecular dynamics study, Industrial & Engineering Chemistry Research 51(21) (2012) 7242-7254.

[77] P.K. Naik, S. Paul, and T. Banerjee, Physiochemical properties and molecular dynamics simulations of phosphonium and ammonium based deep eutectic solvents, Journal of Solution Chemistry 48(7) (2019) 1046-1065.

[78] S.U. Ilyas, R. Pendyala, M. Narahari, and L. Susin, Stability, rheology and thermal analysis of functionalized alumina-thermal oil-based nanofluids for advanced cooling systems, Energy conversion and management 142 (2017) 215-229.

[79] W.U. Rehman, Z.M.A. Merican, A.H. Bhat, B.G. Hoe, A.A. Sulaimon, O. Akbarzadeh, M.S. Khan, A. Mukhtar, S. Saqib, and A. Hameed, Synthesis, characterization, stability and thermal conductivity of multi-walled carbon nanotubes (MWCNTs) and eco-friendly jatropha seed oil based nanofluid: An experimental investigation and modeling approach, Journal of Molecular Liquids 293 (2019) 111534.

[80] P. Vadasz, Heat conduction in nanofluid suspensions, (2006).

[81] D. Lee, J.-W. Kim, and B.G. Kim, A new parameter to control heat transport in nanofluids: surface charge state of the particle in suspension, J. Phys. Chem. B 110(9) (2006) 4323-4328.

[82] Therminol_VP3 heat transfer fluid; Available from: https://www.therminol.com/sites/therminol/files/documents/TF22A_Therminol_VP3.pdf.

[83] B.C. Pak and Y.I. Cho, Hydrodynamic and heat transfer study of dispersed fluids with submicron metallic oxide particles, Exp. Heat Transf. 11(2) (1998) 151-170.

[84] O. Mahian, A. Kianifar, C. Kleinstreuer, A.-N. Moh'd A, I. Pop, A.Z. Sahin, and S. Wongwises, A review of entropy generation in nanofluid flow, International Journal of Heat and Mass Transfer 65 (2013) 514-532.

[85] S.U. Ilyas, R. Pendyala, and N. Marneni, Preparation, sedimentation, and agglomeration of nanofluids, Chemical Engineering & Technology 37(12) (2014) 2011-2021.

[86] A. Beheshti, M. Shanbedi, and S.Z. Heris, Heat transfer and rheological properties of transformer oil-oxidized MWCNT nanofluid, Journal of Thermal Analysis and Calorimetry 118(3) (2014) 1451-1460.

[87] S. Dong and X. Chen, An improved model for thermal conductivity of nanofluids with effects of particle size and Brownian motion, Journal of Thermal Analysis and Calorimetry 129(2) (2017) 1255-1263.

[88] S. Pil Jang and S.U. Choi, Effects of various parameters on nanofluid thermal conductivity, (2007).

[89] M.G. JC, Colours in metal glasses and in metallic films, Philos. Trans. Roy. Soc. London 203 (1904) 385-420.

[90] P. Keblinski, S. Phillpot, S. Choi, and J. Eastman, Mechanisms of heat flow in suspensions of nano-sized particles (nanofluids), International journal of heat and mass transfer 45(4) (2002) 855-863.

[91] X. Li, C. Zou, L. Zhou, and A. Qi, Experimental study on the thermo-physical properties of diathermic oil based SiC nanofluids for high temperature applications, International Journal of Heat and Mass Transfer 97 (2016) 631-637.

[92] S. Akilu, A. Baheta, K. Sharma, and M. Said. Experimental determination of nanofluid specific heat with SiO2 nanoparticles in different base fluids, in AIP Conference Proceedings, 2017: AIP Publishing LLC.

[93] B.-X. Wang, L.-P. Zhou, and X.-F. Peng, Surface and size effects on the specific heat capacity of nanoparticles, International journal of thermophysics 27(1) (2006) 139-151.

[94] M. Saeedian, M. Mahjour-Shafiei, E. Shojaee, and M. Mohammadizadeh, Specific heat capacity of TiO2 nanoparticles, Journal of Computational and Theoretical Nanoscience 9(4) (2012) 616-620.

[95] P. Andreu-Cabedo, R. Mondragon, L. Hernandez, R. Martinez-Cuenca, L. Cabedo, and J.E. Julia, Increment of specific heat capacity of solar salt with SiO 2 nanoparticles, Nanoscale research letters 9(1) (2014) 1-11.

[96] S.M.M. Rizvi and D. Shin, Specific heat capacity, viscosity, and thermal stability of carbonate-based molten salt nanofluids, Journal of Energy Storage 43 (2021) 103192.

Chapter- 4

Evaluation of Thermophysical Properties and Thermal Performance of Amine Functionalized Graphene Oxide (GO-NH_2)/Deep Eutectic Solvent Nanofluids as Heat Transfer Media for Desalination Systems

Evaluation of Thermophysical Properties and Thermal Performance of Amine Functionalized Graphene Oxide (GO-NH_2)/Deep Eutectic Solvent Nanofluids as Heat Transfer Media for Desalination Systems

The chapter mainly focuses on the synthesis and characterization of amine functionalized graphene oxide (GO-NH_2) nanoparticles. It also reports the thermal properties and stability analysis of Deep Eutectic Solvent (DES) and GO-NH_2 based nanofluid. DES is composed of Diphenyl ether as hydrogen bond acceptor and DL-Menthol as a hydrogen bond donor in the molar ratio 1:1. Nanofluid was prepared by a two-step method where two different concentrations of functionalized graphene nanofluids, namely 0.0033 volume fraction and 0.0101 volume fraction were reported. XRD and FTIR analyses were used to validate the nanoparticle's identity. Additionally, the morphology and composition of GO-NH_2 nanoparticles were investigated using FESEM, FETEM, and EDS analysis. After that, the stability of nanofluids was assessed using zeta potential measurements. The zeta potential measurements revealed increased stability, indicating that no agglomeration occurs in the DES-based nanofluid. Excellent thermal conductivity enhancement was observed at a higher temperature for the GO-NH_2 nanofluid. The density and viscosity of the base fluid and nanofluid decreased with an increase in temperature from 25-85°C. Further, the specific heat capacity of nanofluids also increased with the increase in temperature and volume fractions of nanofluid. Thermogravimetric analysis (TGA) was also performed to evaluate the thermal degradation of the nanofluid under nitrogen atmosphere. The nanolfuid was used in a brine recirculation multistage flash desalination where the Gained output ratio (GOR) of less than 10 was obtained through ASPEN simulation.

4.1 Introduction

Global energy consumption is expected to double by 2050 and more than quadruple by the end of the century. In order to meet this demand in a sustainable manner, incremental upgrades to current energy networks will be insufficient. Finding enough sustainable energy for the future is one of society's most difficult issues. The vast discrepancy between our current usage of solar energy and that energy's immense untapped potential constitutes a major energy research issue. There is no better way to meet our future energy needs than with abundant, clean solar power. The fact that it's easily available, free of international conflict, and does not pollute the environment or change the climate is a huge advantage[1]. Thermal or electrical energy storage of solar radiation is an essential and crucial component for solar energy applications. Solar energy systems (SESs) are widely regarded as one of the most important alternatives to conventional fossil fuels. They can transform solar energy directly into heat and electricity without causing adverse environmental effects such as greenhouse gas emissions. Solar photovoltaic (PV) and concentrated solar power (CSP) are the two main industrial systems for gathering solar energy. Depending on the temperature, solar energy may be used for a variety of different purposes[2]. Modern solar power systems necessitate high operating temperatures as well as thermal storage systems. Instead of using standard commercial heat transfer fluids, nanofluids can be utilized as a heat transfer medium since they have a propensity to increase heat transfer and thermal storage characteristics [3]. Thus this could reduce the cost of the concentrated solar power system. Hence, the study of nanofluids is important from energy point of view.

Graphene is a single graphite atomic plane, which is important to be considered independently isolated from its environment. Despite its short history, this purely two-dimensional material has outstanding crystal and electronic consistency [4]. High thermal conductivity and inert chemical behaviour of graphene oxide-based nanofluids encourage

researchers to employ it as a heat transfer fluid in solar energy desalination systems in order to enhance the heat transfer characteristics and thermophysical properties. Choi [5] invented the term "nanofluid" to describe various nanoparticles employed in various base fluids such as water, ethylene glycol, and oils to examine their thermal properties. In comparison to other nanoparticles, carbon based nanomaterials and carbon nanotubes (multi-walled and single-walled carbon nanotube) base nanofluids have superior physical and thermal properties [6-8]. Among all the thermophysical parameters of nanofluids, thermal conductivity is a critical parameter that affects the behaviour of nanofluids. Liu et al.[9] examined thermal conductivity of both nanofluids using two volume percentages of multiwall carbon nanotubes in ethylene glycol (0.2, 0.4, 0.5, and 1 vol%) and engine oil (1 vol% and 2 vol%. Similar investigation has conducted by H. Jiang et al.[10] in which they employed CNT/water nanofluid in their experiment. Like CNT, graphene is also an excellent material for thermal management and shows good thermal conductivity and other physical properties [11-13].

Solar desalination technique is the existing technique that has huge potential to purify saline water with low energy and operating cost. Only 13% of solar energy can be harvested directly by sea water from the solar energy. Kabeel et al [14] used Al_2O_3 nanoparticles contained brine water in solar still and 116% improvement of yield of condenser modified was bserved. Productivity of corrugated wick solar still was further improved by 285.10% and 254.88% using Cu_2O and Al_2O_3 nanoparticles[15]. Nowadays, nanofluids have gained prominence in solar energy applications. Many researchers have investigated the thermal performance of direct adsorption solar collector using different nanofluids. Otanicar et al.[16] used different nanofluids (graphite, carbon and silver) and calculated the thermal performance of DAPTC both experimentally and numerically. Results showed that thermal efficiency was enhanced with an increase in the volume fractions of nanofluid. Bortola et al. [17] calculated the thermal efficiency of SWCNT-water nanofluid in DAPTC experimentally. They have got

87% increment in thermal efficiency but found lack of stability in nanofluid. Multi Stage Flash (MSF) desalination system is the first choice of many researchers and industries over RO and MED plants as MSF plants can be used to produce both electricity and water and the plant is not affected by high feed temperature and salinity, produced high quality of feed water.

The dispersion behaviour of nanofluid is an important issue that limits its use in heat transfer systems [18]. An alternate strategy for enhancing the dispersion stability of graphene oxide-based nanofluid is surface fictionalization, which modifies the surface charge of graphene oxide nanoparticles. Chemical and physical functionalization methods are primarily divided into two categories: covalent (chemical) and noncovalent (physical). There are several methods for the chemical functionalization of graphene oxide, but the most common is a combination of acids and alkalis. Acidic functionalization has great promise for graphene oxide nanoparticles since it enhances the nanofluid's dispersion stability and thermal conductivity [19]. V. Irani et al. [20] reported amine functionalized graphene oxide and methyldiethylamine nanofluid for improving the CO_2 and H_2S adsorption efficiency of amine solution. They reported high adsorption capacity of 16.2 % and 17.7% of CO_2 and H_2S respectively. Compared with the non-functionalized GO solution at the same concentration, it showed greater improvement in the adsorption efficiency for functionalized GO solution. Abbasi et al. [21] used a solvo thermal method with different carboxylic group concentrations to prepare a nano-hybrid type of nanofluid of MWCNT with gamma alumina (γ-Al_2O_3) particles. However, heat transfer properties and dispersion behaviour of the nanoparticle was also investigated. Therefore, nanoparticle shows good dispersion behaviour when it is functionalized with carboxylic groups [22]. At present, very few literatures reported DES as a thermal fluid in solar collector desalination system.

The present chapter examined the use of deep eutectic solvent as a thermal fluid for solar desalination applications and measure thermal performance parameter of brine

recirculation multistage flash desalination system in terms of gained output ratio (GOR). Pyarimohan et al.[2] previously documented the synthesis and characteristics of all the elements in DES as a heat transfer fluid. The DES was a combination of Diphenyl ether (HBA)and DL-Menthol (HBD) in the molar ratio 1:1. The optimized structure of both HBA and HBD was shown in Figure 4.1. Thermal performance and thermophysical properties of Al_2O_3 nanoparticle and *h*-BN nanoparticles with DESs had been studied and reported by Pyarimohan et al.[2]. Both nanoparticles-DES based nanofluids exhibit excellent thermal conductivity and heat transfer coefficients. In this present work, we have functionalized GO nanoparticles with amine group (NH_2) and functionalized nanoparticles are dispersed into already synthesized DES (Diphenyl ether and DL-Menthol), to prepare nanoparticle dispersed deep eutectic solvent(NDDES). The characterization of GO-NH_2 nanoparticles and thermophysical properties of the DES/GO-NH_2 nanofluid were evaluated and analyzed for solar thermal energy applications.

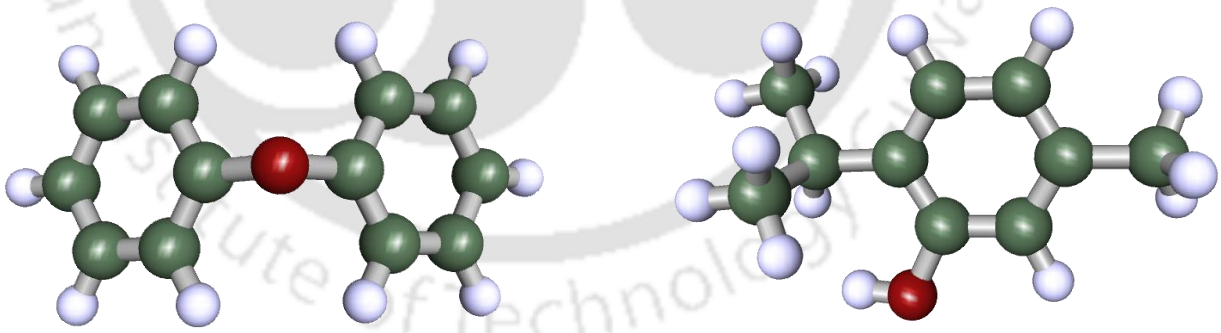

Diphenyl ether **DL-menthol**

Figure 4.1. Optimized structure of HBA and HBD

4.2. Experimental Details

4.2.1 Materials

Diphenyl ether has a purity of 99 % purchased fromSigma-Aldrich. DL-menthol having purity of 99.8 % was purchased from Sigma Aldrich. Graphene Oxide was purchased from Adnano Technologies Pvt Ltd with ~99% purity and thickness ~0.8-2 nm. All other chemicals purchase details are tabulated in table 4.1.

Table 4.1. List of chemicals used in this chapter

Chemical name	Molecular Formula	CAS number	Source	Purity (%)	MP (°C)	BP (°C)
Diphenyl ether	$C_{12}H_{10}O$	101-84-8	Sigma-Aldrich	99	230-233	258
DL-Menthol	$C_{10}H_{20}O$	89-78-1	Sigma-Aldrich	>95	-13	195-198
4,4′-Diaminodiphenylmethane	$C_{13}H_{14}N_2$	101-77-9	TCI Chemicals	98	25-27	259
N-(3-Dimethylaminopropyl)-N′-ethylcarbodiimide hydrochloride	$C_8H_{17}N_2.HCl$	25952-53-8	Spectrochem	99	34-36	216
N-Hydroxysuccinimide	$C_4H_5NO_3$	6066-82-6	Spectrochem	98	95	305

4.2.2 Functionalization of Graphene Oxide (GO) with NH_2

The presence of strong π-π interaction in the graphene oxide makes it hydrophobic in nature, leading to rapid accumulation and settlement in the base fluid, resulting in poor dispersion behaviour of graphene oxide in the base fluid [23]. Functionalization of graphene improves the dispersion behaviour in the base fluid by attaching other functional groups through covalent or non-covalent interaction by acid treatment methods. In covalent functionalization, convert carbon sp^2 hybridization into sp^3 orbitals while in non-covalent interactions, other functional groups are attached on the graphene sheet through π-πstacking, H-bonding and hydrophobic interactions [24]. In our work, we functionalized NH_2 group on graphene oxide through covalent bonds. Figure 4.2 depicts a schematic representation of the GO-NH_2 synthesis steps. There is no heating involved in the modification process. One gram of GO was dispersed in 400mL of DI water and sonicated for 30 minutes. Addition of 500mg. EDC (Ethylcarbodiimide hydrochloride) into it with continuous stirring for 30 minutes, followed by the addition of 500 mg. NHS (N-Hydroxysuccinimide) into the GO-DI water dispersion and stirring continues for one hour. (Both are to be added during the magnetic stirring). Again, the addition of 1.5 g. amine source (4. 4'-diaminodiphenylmethane) into the dispersion and continue the starring it for 36h. Finally, filter the dispersion using vacuum filtration, followed by washing with DI water continuously for 2h and washing with ethanol twice. A schematic illustration of the synthesis of amine functionalized GO from GO is shown in the Figure 4.3

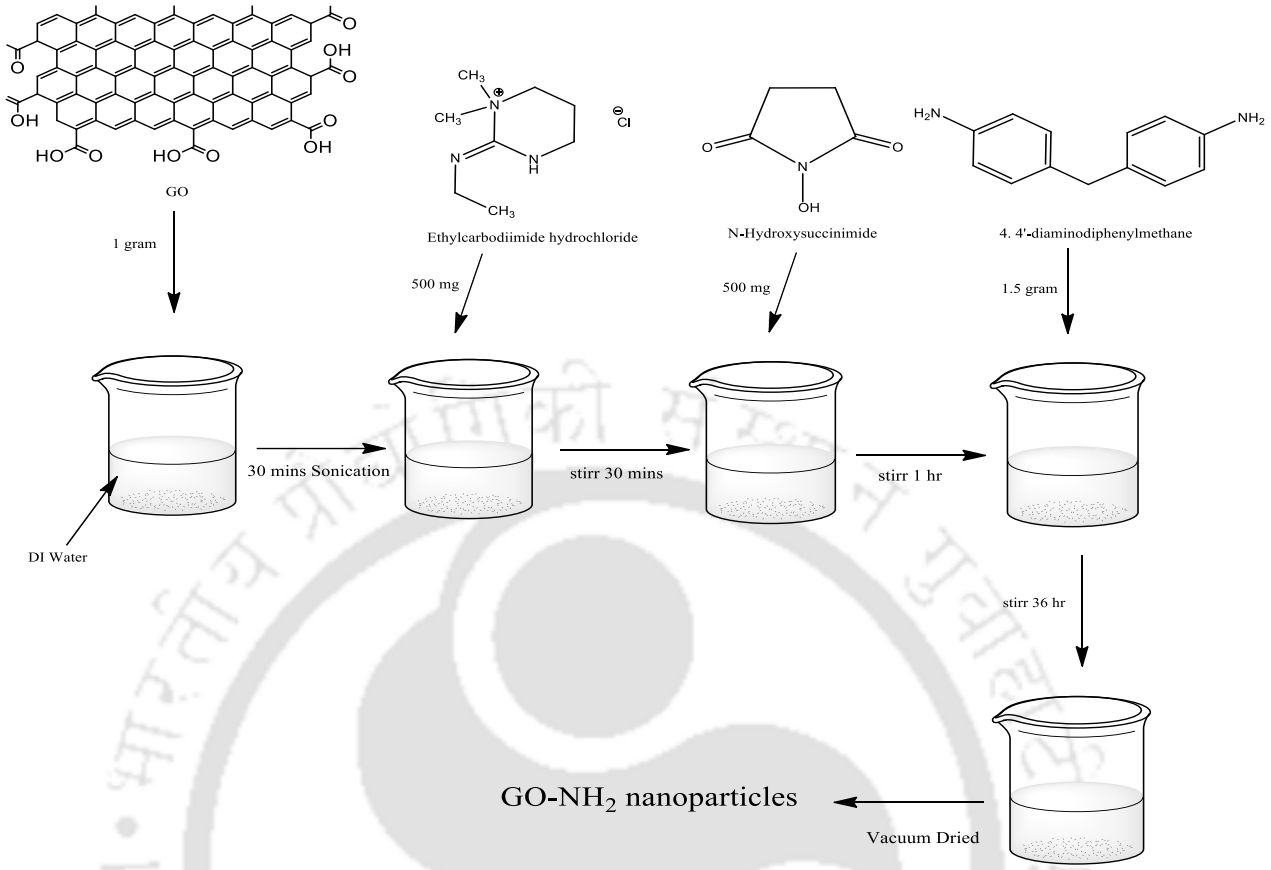

Figure 4.2. Preparation steps of ammonia functionalization with graphene oxide nanoparticles

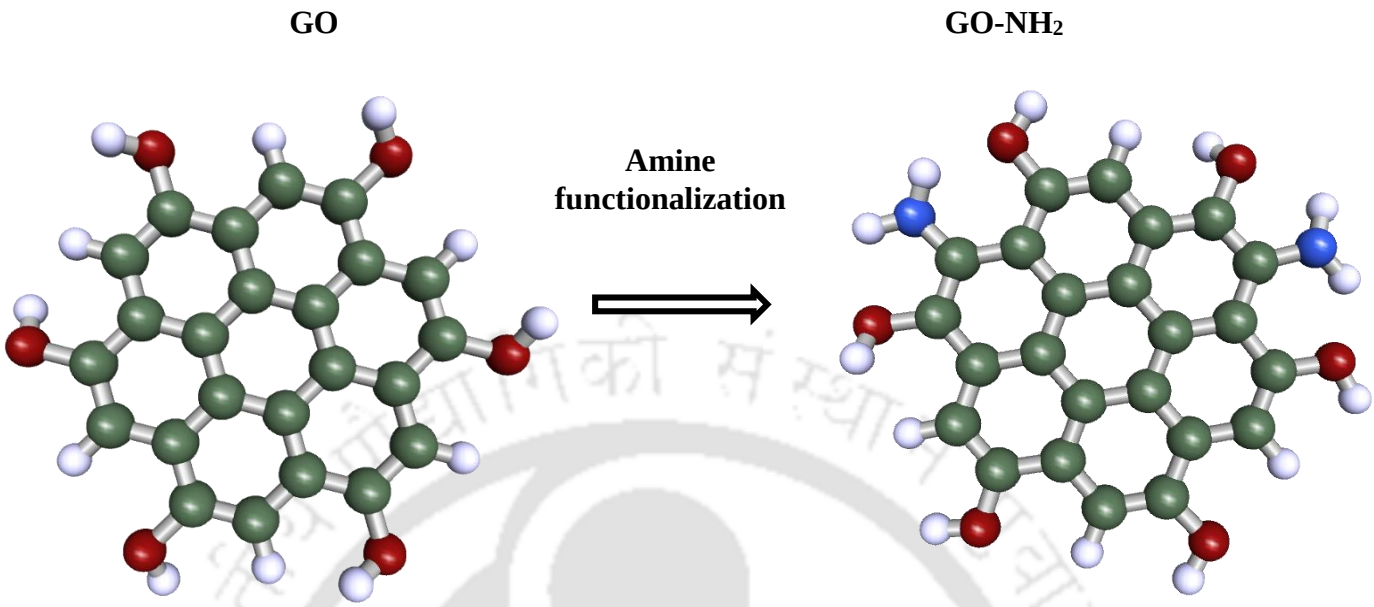

Figure 4.3. Schematic illustration of the synthesis of amine functionalized GO

4.2.3 Characterization of GO-NH_2 Nanoparticles

The synthesized GO-NH_2 was characterized by different techniques to confirm the morphology and functionalities group present on GO. The crystalline structure of GO and GO-NH_2 nanoparticles were investigated by the powder X-ray diffraction (XRD, Bruke D8, advanced X-ray diffraction measurement system) method at room temperature. Peaks were recorded between the 2θ angles from 10° to 80°. To further confirm the chemical structure and crystallinity of MWCNT, Raman spectroscopic analyses (Horiba JobinVyon, Model LabRam HR) was performed. Confirmation of functional groups and presence of others chemical compounds were determined by Fourier Transform Infrared (FTIR, Perkin–Elmer, Norwalk, USA) spectroscopy and Energy Disperse X-ray Spectroscopy (EDS, Zeiss). FT-IR spectra were obtained at wavenumbers ranging from 500 to 4000 cm^{-1}. Morphology and shape of the GO and GO-NH_2 nanoparticles were examined by performing Field Emission Scanning Electron

microscope (FESEM, Sigma 300, Zeiss) and Field Emission Transmission Electron Microscope (FETEM, JEOL-JEM2010). The nanoparticles' stability and particle size distribution in the base fluids were analyzed by performing zeta potential measurement with the help of Delsa Nano instrument (Delsa Nano C, BECKMAN COULTER). Thermogravimetric analysis (TGA, TG209 F1, Libra, NETZSCH, Germany) was performed to check the thermal stability of DES and nanofluid at a temperature close to 300°C at a heating rate of 10°C/min under nitrogen environment.

4.2.4 DES Synthesis and Nanofluid Preparation

Deep eutectic solvents are prepared by mixing HBD (Hydrogen Bond Donor) and HBA (Hydrogen Bond Acceptor) in the molar ratio 1:1 in a flat bottom flask at temperature 60°C and stirring continuously for 24 hours at room temperature until a clear liquid is obtained. Table 4.2 shows the optimized structure of HBD and HBA and their physical properties. For confirming the composition of DES, ^{1}H NMR (Nuclear Magnetic Resonance) was performed and compared with Pyarimohan et al. [2].

The two step method [25] has been adopted to prepare the nanofluid. In two-step method initially Graphene oxide was procured as a dry powder and then it was functionalized with NH_2 group by different chemical steps. Thereafter it was dispersed into DL Menthol and Diphenyl ether based DES. Then the prepared nano size particles was dispersed into the working fluid followed by ultra-sonication method for 60 to 90 minutes in order to obtaine a homogeneous solution. A schematic diagram of the nanofluid preparation method is shown in Figure 4.4. The primary disadvantage of two-step method is the possibility for nanoparticle aggregation driven by strong van der Waals attractive forces. The GO-NH_2 particles used in two different volume fractions: 0.0033 and 0.0101, labelled as NF5 and NF6, as schematically shown in Figure 4.4.This was calculated using the following equation 4.1 [26].

$$\varphi = \left[\frac{\left(\frac{m}{\rho}\right)_{Nanoparticles}}{\left(\frac{m}{\rho}\right)_{Nanoparticles} + \left(\frac{m}{\rho}\right)_{base\ fluid}}\right] \times 100 \qquad \textbf{(4.1)}$$

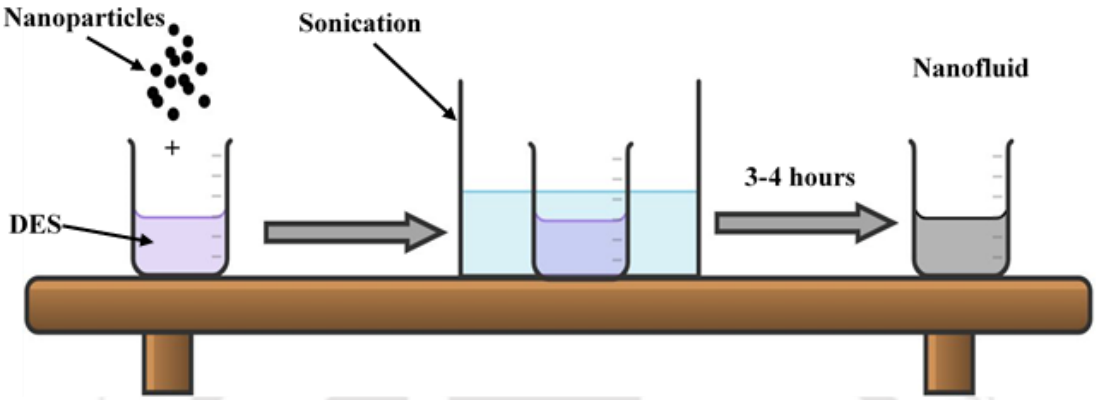

Figure 4.4. Schematic diagram of the two step method of nanofluid preparation

Here, φ, *m* and ρ denotes mass fraction of the nanoparticles (%), solid mass (kg) of the nanoparticles and density (kg/m^3) respectively. To ensure the stability of the nanofluid, prepared nanofluids were kept for 3 days at room temperature and observed for any settlement. Further stability of the nanofluid was investigated through Zeta potential measurement.

The measurement of zeta potential aided in the stability and dispersion characteristics of nanofluids. The observation of electrokinetic potential was used to verify the dispersion and stability of the nanofluid [27, 28]. When nanoparticles are close to each other, van der Waal force becomes strong and dominates the other forces, which results in agglomeration among the nanoparticles. Due to the agglomeration of the particles, thermal conductivity of the nanofluid decreases. Stability is ensured by high repulsive interaction potential. Lower the magnitude of the nanofluid, van der Waal force becomes stronger which results in the instability of the nanofluid. Repulsive forces must prevail in the solution for nanofluids to be stable. According to Vandsburger[29], nanofluids are nearly stable when particles with a zeta

potential value near about ± 30 mV.If the zeta potential value is close to 45 mV, the stability of nanofluids is ensured. Nanofluid gives excellent stability if its value lies above± 60 mV.

Table 4.2. Properties of HBD and HBA [Pyarimohan et al.[2]]

Solvent name	Density (kg/m3)	Molecular formula	Molar mass (g/mol)	Water content (ppm)	T_m(K)	T_b(K)
Diphenyl ether	1066.1	$C_{12}H_{10}O$	170.2	9	299.95	531.15
DL-Menthol	891.34	$C_{10}H_{20}O$	156.27	18	307.15	489.15

4.2.5 Thermophysical Properties Measurement

All thermophysical properties were measured at the in-house apparatus at temperature ranges from 30°C to 85°C. The viscosity measurements of base fluids and their respective nanofluids were done by an Interfacial Rheometer (MCR 301, Anton Paar, Austria) with a accuracy of 0.001 mPa.s. The density measurements were performed by using the Anton Paar DMA 4500 Densitometer. The uncertainty was found to be ±0.0001 g/cm^3. Thermal conductivity values of base fluid and nanofluids were obtained by using KD2 Pro thermometer device (Decagon device, USA) with an uncertainty of ± 0.0096 W/m K. Measurement was done with the principle based on transient hot-wire method. Hot plate with silicon oil bath used to maintain the constant temperature. The sensor's operating temperature was kept between 223.15 K and 423.15 K with an accuracy of ±5%. The resistance fluctuation of the hot wire is measured using a Wheatstone bridge, and the voltage across the bridge and the temperature of the hot wire were

subsequently determined. Thermal conductivity can be calculated using the following equation 4.2.

$$k = \frac{q}{4\pi(T_2\text{-}T_1)} \ln\left(\frac{t_2}{t_1}\right) \quad \textbf{(4.2)}$$

Where k is the thermal conductivity in W/m.K, q is the heat rate, T_2 and T_1 are the temperatures at time t_2 and t_1 respectively. Convection current should be avoided while measuring thermal conductivity since the thermal analyser only considers the conduction mode of heat transfer. Specific heat measurements were performed by Temperature Modulated Differential Scanning Calorimeter (TMDSC) (NETZSCH STA 449F3) with sapphire as the comparison standard materials under nitrogen environment. The measurements were taken with an uncertainty of $\pm$ 5.97 J/Kg.K. Thermo Gravimetric Analysis (TGA) (TG209 F1, Libra, NETZSCH, Germany) was performed for both base fluid and nanofluids to ascertain thermal stability under nitrogen conditions at a heating rate of 10°C/min.

4.2.6 Process Simulation

A process flowsheet of a multistage flash using nanofluid is conceptualised and simulated in ASPEN Plus software (V11) as illustrated in Figure 4.6. The process is divided into three sections, namely the heat absorption section, the distillation section, and the waste heat recovery section. In the heat absorption section, heat is absorbed by the solar collector and transferred to the nanofluid, which is used to heat up the salt water so as to partially vaporise it and send it to Flash 1. The distillation section consists of three adiabatic flash separators where vapour is separated out from the two-phase mixture and pressure is gradually decreased in each stage in order to maintain continuous stage wise flow. The waste heat recovery section consists of three condensers where feed is preheated using hot distillate as produced from the

top section of each flash drum. A part of the concentrated brine solution is rejected from the bottom product of the last flash drum, while the rest of the solution is mixed with fresh feed for cyclic utilization. Fresh distillate is collected from the top product of each flash separator. Overall, the feed contains 4.82 wt.% salt and the rejected brine contains 68.71 wt.% salt. The collector is assumed to be a heater with a constant heat flux of 15.27 kW. The seawater was simulated with 50,000 ppm NaCl. Detailed feed compositions, operating parameters of major equipment, and key parameters of important streams are shown in Table 4.3.

Table 4.3. Operating parameters and feed composition parameters of important streams

	Flash 1	**Flash 2**	**Flash 3**		
Pressure (bar)	0.68	0.5	0.25		
Temperature(°C)	105	105	105		
	H 1	**H 2**	**H 3**	**H 4**	**H 5**
Heat duty (cal/sec)	27	75	277	3471	3471
ΔT cold (°C)	1.45	1.50	5.50	66	64
ΔT hot (°C)	41	23.7	13	63.5	

	Flash 1	**Flash 2**	**Flash 3**
Vapor flow rate (kg/hr)	170.57	1.009	1.487
Liquid flow rate (kg/hr)	21.74	20.73	19.25
Salt concentration in bottom product (%)	61	64	69

	Feed	**Rejected Brine**	**Accumulated Water**
Flowrate (kg/hr)	186.54	13.47	173.07
Salt Concentration (%)	4.9	69	0

In the process simulation, the COSMO-SAC model [2, 30]has been chosen to describe the thermophysical properties and phase behaviour of the system. The concept of pseudo component was first introduced in the ASPEN simulation [31] for absorption and extraction process where unknown or new components such as DES can be introduced. Our previous work has introduced such solvent in extraction flowsheet within ASPEN [32, 33]. This requires an input concerning the screening charge density, COSMO volume, boiling point, density, viscosity and average molecular weight. For screening charge density and COSMO volume calculation, the initial structure of HBD and HBA were drawn and optimized through B3LYP [34] level of theory with the basis set of 6-31G* in Gauss View 5 [35] and Gausssian 09 [36] platform respectively. Similar steps were followed for GO-NH_2nanopartcles with 6-311G+ (d, p) as basis set. Thereafter, the COSMO files were generated through the BVP86/TZVP/DFT level of theory[37]. The sigma profile or the distribution of screening charge densities as obtained from their respective COSMO files are displayed in Figure 4.5. Temperature dependent physical properties such as viscosity, density, heat conductivity and heat capacity are correlated from the experimental data. These are now shown in table 4.5 and are used in ASPEN to define thermophysical properties of nanofluid.

The boiling point and average molecular weight of DES was calculated using the equations 4.3 and 4.4 respectively. The group contribution approach as used to determine the boiling point is referred to as the Joback method [38]. These are given below:

$$\overline{M_w} = \frac{\sum_i N_i M_i^2}{\sum_i N_i M_i} \qquad \textbf{(4.3)}$$

Where, N_i is the number of molecules of component *i* and M_i is the corresponding molecular weight.

$$T_b = 198.2 + \sum n_i \Delta T_{bM_i} \qquad \textbf{(4.4)}$$

Where n_i is the frequency of the appearance of the i^{th} group of atoms in the molecules and ΔT_{bM_i} is their contribution to the normal boiling temperature.

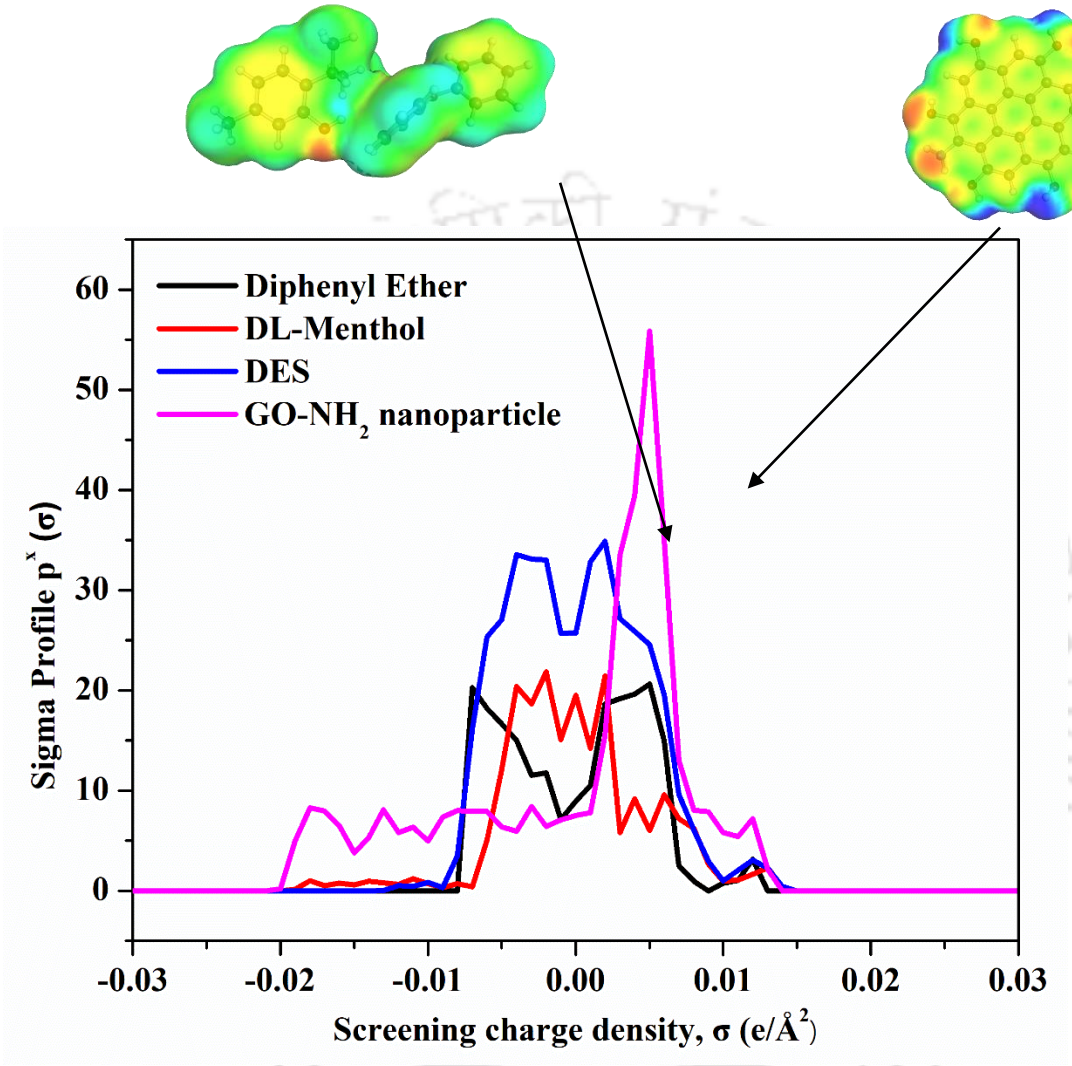

Figure 4.5. Sigma Profiles of HBD(black), HBA(red), DES(blue) and nanoparticles(pink)

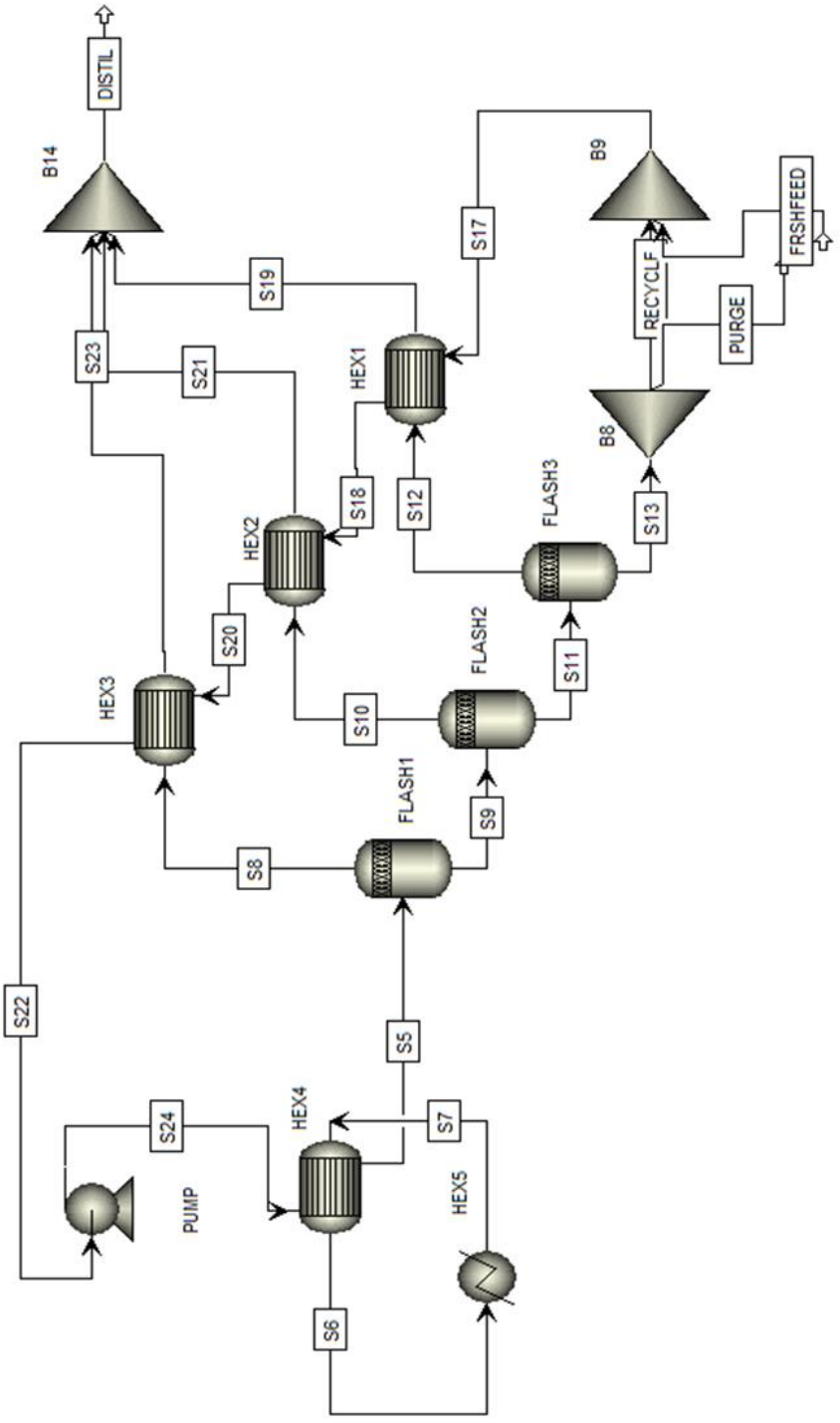

Figure 4.6. A process flowsheet of a multistage flash using nanofluid is conceptualised and simulated in ASPEN Plus software (V11)

4.3. Results and Discussion

4.3.1 Characterization of Functionalized Nanoparticles

The morphology structure of GO-NH_2 was analysed through Field Emission Scanning Electron Microscope (FESEM) as shown in Figures 4.7(a) and (b). Images were taken at 100nm and 200 nm scale. Figures 4.7(c) and (d) depict the FETEM images of GO-NH_2 nanoparticles. A relatively large surface can be seen which shows that graphite was properly exfoliated during the oxidation process. Generally, graphene oxide is physically bonded to each other by π-π interaction and are stacked regularly. It can be seen from the SEM images (Figure 4.7(a) & (b)) that the distance between graphene oxides increases which is due to the presence of oxygen containing functional groups on the surface of the graphite sheets, which is generated during the oxidation process. The wrinkled structure on the graphene sheet indicates the presence of functional groups in the graphene oxide. Further, the presence of NH_2 group in the nanoparticle was confirmed by the Energy Disperse Spectroscopy (EDS) as shown in Figure 4.7(e) and (f). From EDS analysis, Carbon, oxygen and nitrogen content in GO-NH_2 nanoparticles was 72%, 22.8% and 5.2% respectively, in spectrum 1. Table 4.4 shows the compositions of C, N and O in other spectrums 2 and 3 respectively.

Table 4.4. EDS data of GO-NH_2 as reported from Figure 6(e)

Elements	Spectrum 1	Spectrum 2	Spectrum 3
C	72 %	69.7 %	73.5 %
N	5.2%	6%	2.4%
O	22.8%	24.3%	24.2%

Figure 4.8 (a) shows the FT-IR spectra of GO-NH_2 nanoparticles. Different adsorption peaks were observed in the wavenumber ranges from 500 to 4000 cm^{-1}. The absorption peaks at around 3182 cm^{-1} imply OH vibrational groups [39]. Prominent peaks were obtained at absorptions bands around 1585 cm^{-1}. These are assigned to −NH bending of amine [40], which implies successfully functionalization of the amine groups in the GO sheets. The amine peaks remain even after multiple washing of functionalized GO thereby confirming the amine fictionalization of GO. Figure 4.8(b) represents the XRD pattern of GO and GO-NH_2functionalized graphene oxide nanoparticles. It shows the crystalline and stacked structure of the GO. The XRD peak of GO was observed at 10.8°, whereas there were three peaks observed at three different planes (2θ=9.43°, 2θ=18.51°and 2θ=43.69°) for the GO-NH_2nanoparticle. Also, there is a reduction the stacking between GO-NH_2 layers resulting in other peaks. A sharp peak was seen to shift from 10.8° to 9.43° indicating an increase in interlayer d- spacing of GO. The peak at 9.43° attributed to the reaction of amine group with GO. Further, Raman Spectroscopy has been used to analyses the carbon allotropic forms. In Figure 4.9, Raman spectra of GO and GO-NH_2 exhibit D band (double resonance mode) and G band (tangential stretching mode) at around 1319 cm^{-1} and 1568 cm^{-1} respectively. The D and G band refers to the structural disorder of the nanoparticles (sp3), eg. presence of amorphous material and bond stretching vibration of the C-C bond (sp2) within the graphene structure. The disorder density of GO-NH_2 can be confirmed by the ratio of D and G band (I_D/I_G), where smaller value of I_D/I_G indicate the less defects within the graphene sheet. It is worth noticing that the intensity peak of D resonant mode appeared high after the functionalized NH_2 group on the surface of graphene oxide. Through FTIR, XRD and Raman spectroscopy analysis it was established that amine group has been successfully functionalized on graphene oxide via chemical reduction.

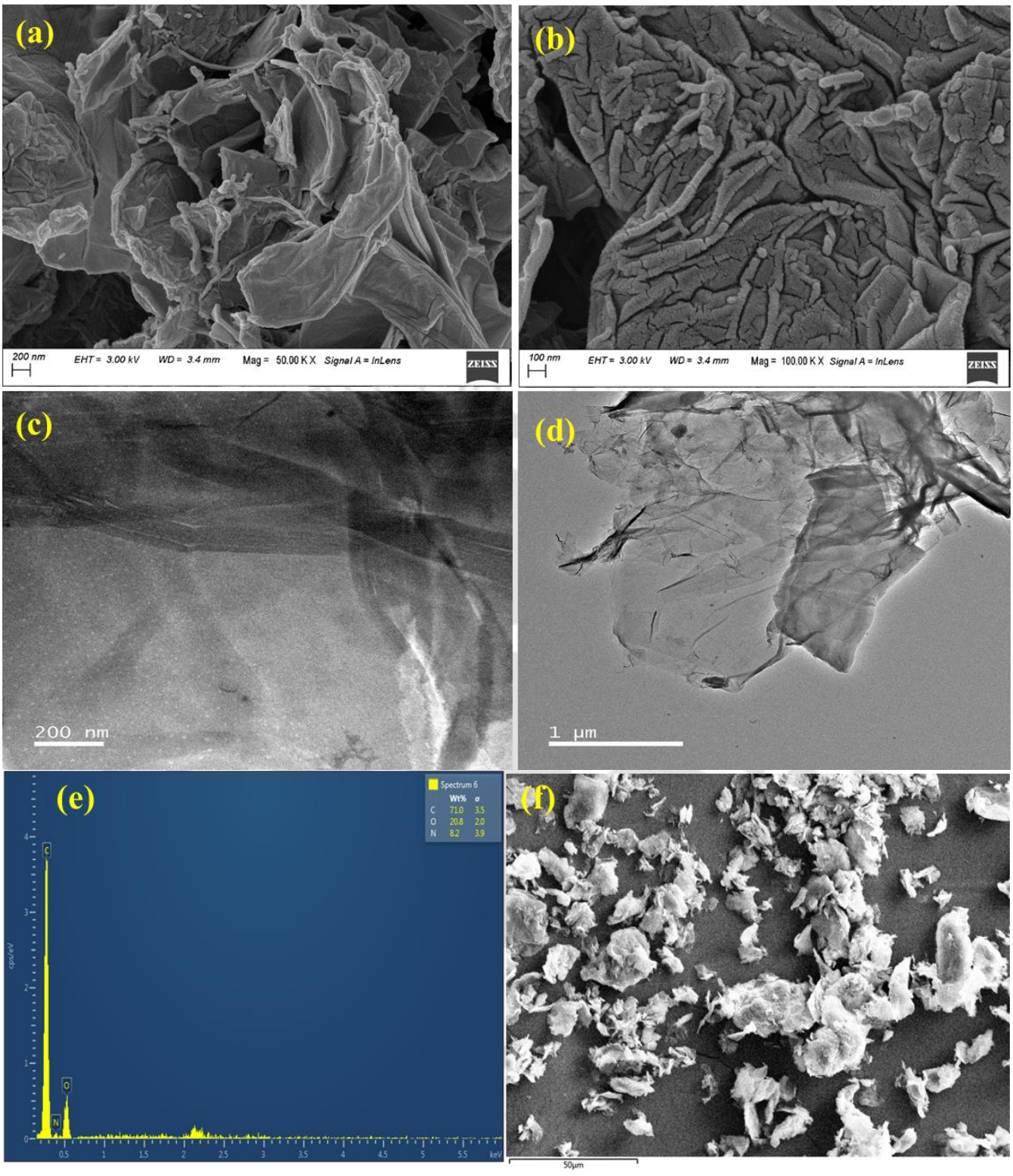

Figure 4.7. (a), (b) are FESEM images; (c), (d) FETEM images of GO-NH_2 nanoparticle, (e) and (f) EDS analysis of GO-NH_2

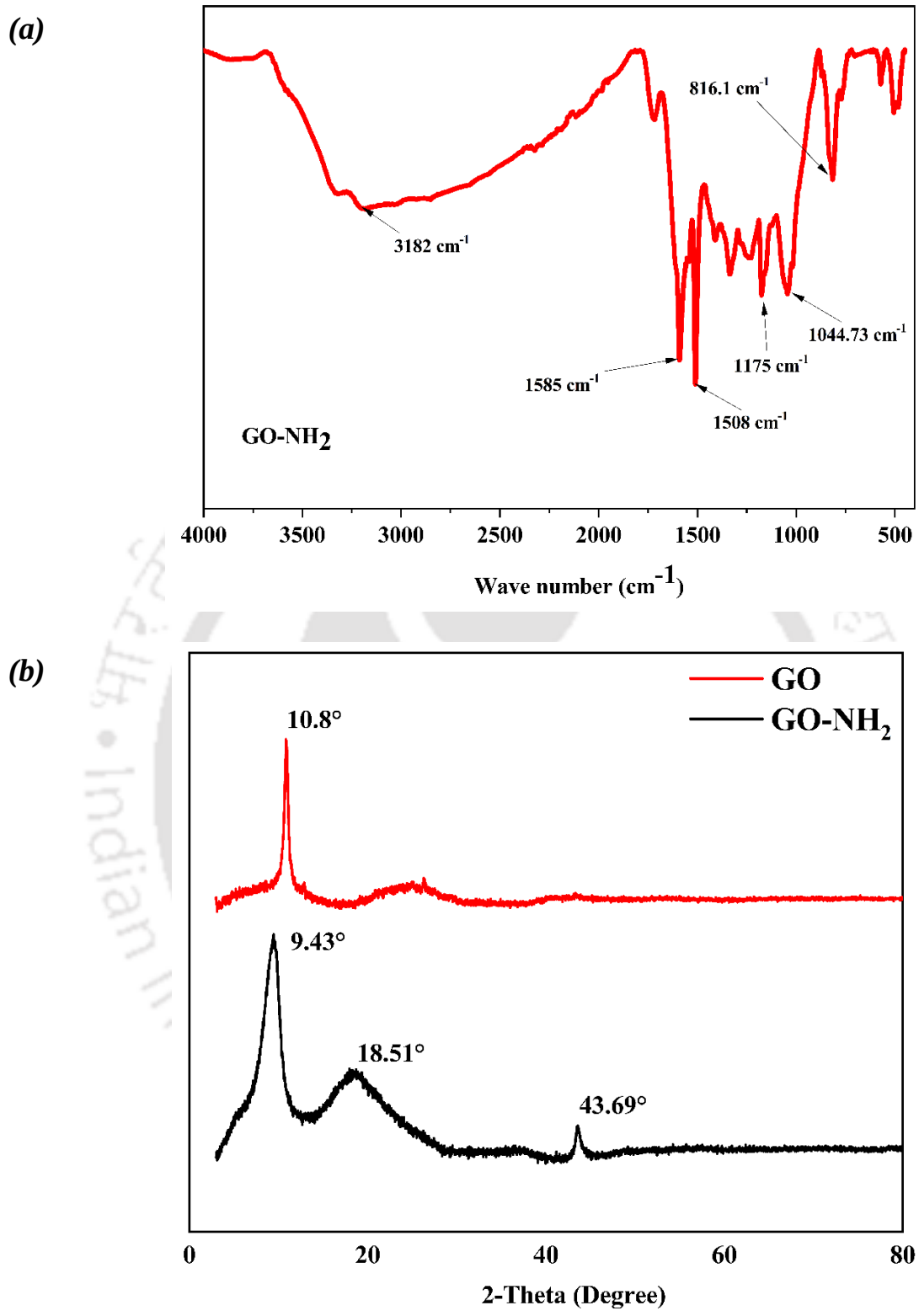

Figure 4.8. (a) FT-IR and (b) XRD of GO-NH_2 nanoparticle

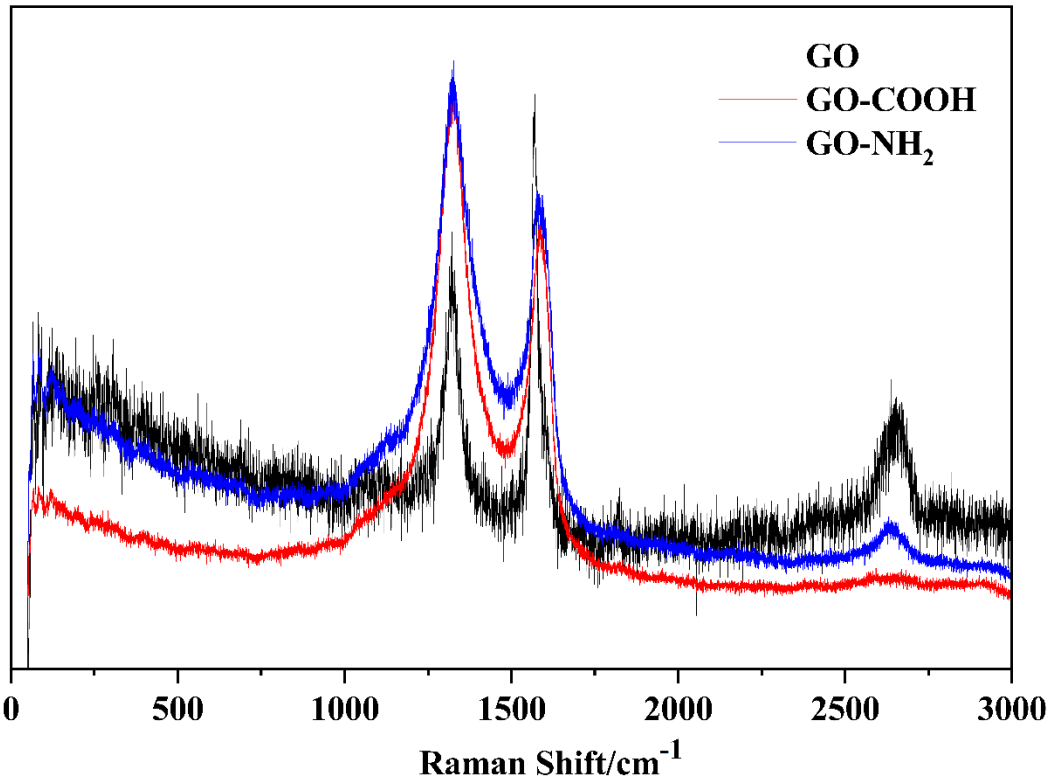

Figure 4.9. Raman spectra of GO-NH_2 nanoparticle

4.3.2 Stability of the Nanofluids

Study on stability of the nanofluid is the crucial factor towards the validation for the use of nanofluids. Different techniques for determining the nanofluids' stability include the visual observation method, sedimentation technique, optical microscopy, Dynamic Light Scattering technique (DLS) and zeta potential [41]. Figure 4.10(a) and (b) reports the zeta potential value of GO-NH_2 nanofluids of NF5 and NF6 obtained from the Delsa nano experiment. Results show good stability of both nanofluids, NF5 and NF6. From the results, it can be concluded that nanoparticles are homogeneously dispersed in the base fluid. The results imply that the nanoparticles in the base fluid are at sufficient distance. The van der Waal force of repulsion is sufficiently high such that no particles form agglomerate. If attraction force is more than that van der Waal forces, particles tend to form clusters and settles due to buoyancy force.

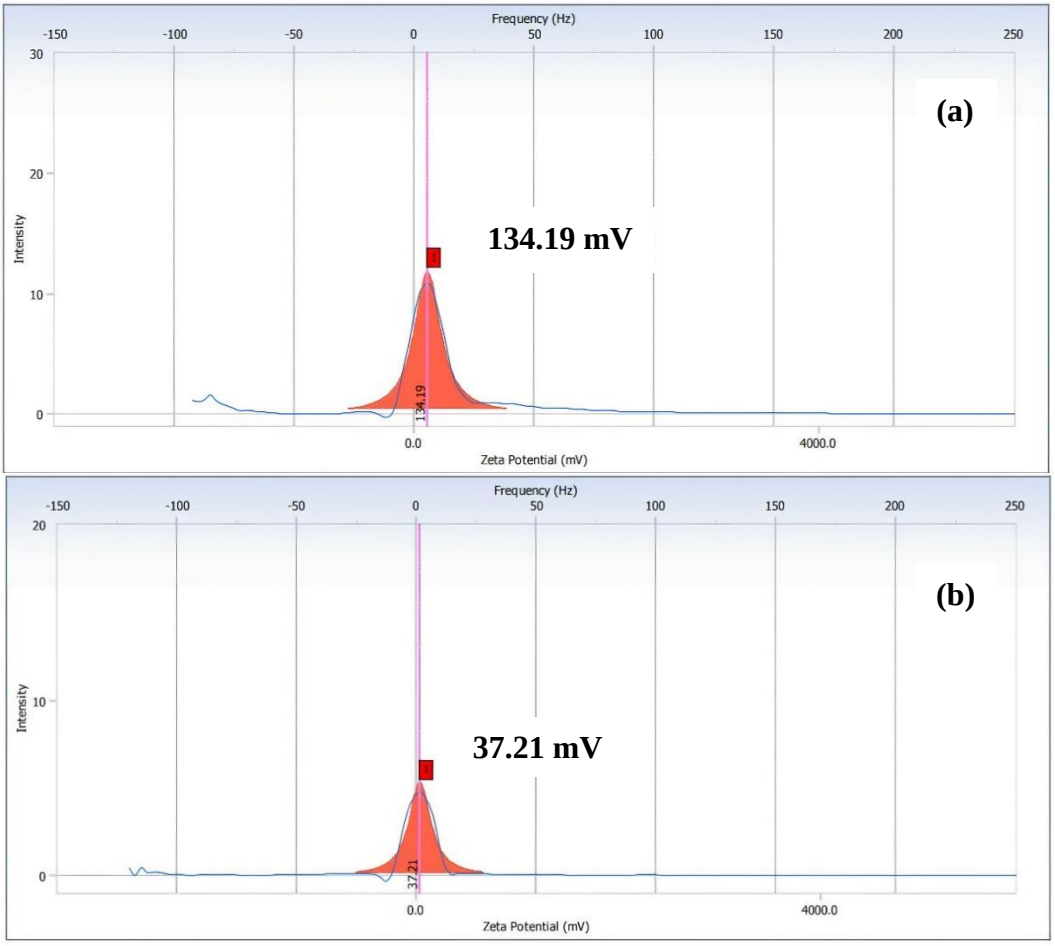

Figure 4.10. Zeta potential value (a) NF5 (0.0033 volume fraction) (b) NF6 (0.0101 volume fraction) of nanofluids

4.3.3 Thermo Gravimetric Analysis (TGA)

The study of thermal degradation is essential since it is commonly used to determine the maximum operating temperature. Thermo Gravimetric Analysis (TGA) was performed to measure the change in weight of the sample with increasing temperature. TGA was performed at a heating rate of 10°C/min under nitrogen atmosphere within the temperature range 25-300°C. Thermal degradation of DES and nanofluids with respect to the temperature is shown in Figure 4.11. In this figure, TG% refers to the mass change in percent. A slight slope of NF6

was observed above 50°C due to the removal of the residual water content. For the base fluid, the DES, thermal degradation was observed after 90°C. However, in the case of GO-NH_2 containing nanofluid NF5, thermal degradation was observed after 102°C, which is attributed to the decomposition of the amino group. Increase in GO-NH_2 content resulted in a shift in weight loss temperature. The decomposition temperature of nanofluid NF6 is increased to 104°C. This is due to the fact that the nanoparticles and molecules have a strong covalent link because of the homogenous dispersion of GO-NH_2 and the strong covalent interaction. During the heating process, the amino group decomposes so that the weight loss of GO-NH_2 is regarded as the weight loss of the amino group [42].

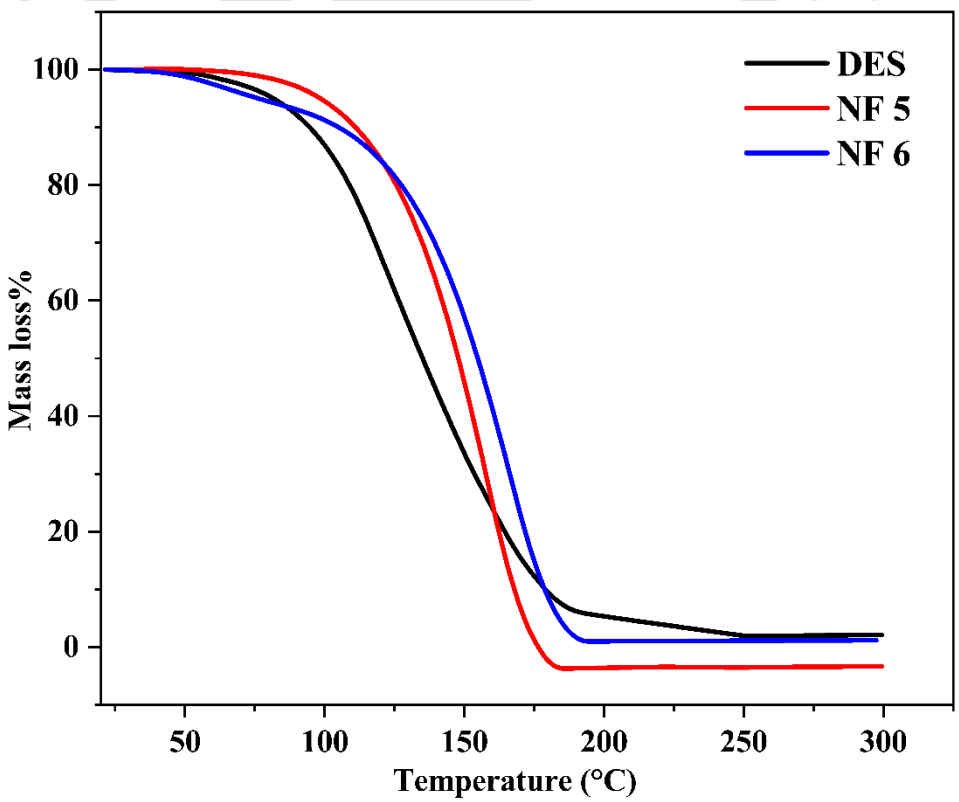

Figure 4.11. TGA plot of DES and nanofluids at heating rate 10°C/min under nitrogen atmosphere

4.3.4 Thermophysical Properties

Nanofluids are intended to be employed as a new class of heat transfer fluids, which possess superior viscosity and thermal conductivity. These are two most significant transport parameters of nanofluid that govern the overall thermal performance as heat transfer fluid. It is advantageous to use nanofluid as a heat transfer fluid in many industrial applications, mainly in the solar energy industry, for thermal energy storage due to its high thermal conductivity and effective viscosity, which would decrease pumping power and increase the heat transfer rate. Hence it is essential to study the conventional working fluid at high temperatures. Many factors influenced the viscosity and thermal conductivity of the nanofluid, such as particle size and shape, particle volume fraction, temperature, and the type of base fluid.

The viscosity of the GO-NH_2/ DES nanofluid at a constant shear rate 50 s^{-1} was reported in Figure 4.12(a) as a function of temperature. Here at GO-NH_2/DES nanofluid concentrations of 0.0033 and 0.0101 volume fraction is seen to decrease the base fluid's viscosity exponentially. As the temperature of both nanofluid and DES increases from 25-85 °C, the viscosity decreases exponentially. A similar result was reported by Pyarimohan et al.[2] where the viscosity of DES decreases exponentially due to the weakening of bonds. This may also be explained by the fact that thermal movement between molecules increases when the temperature rises, which enhances Brownian motion, resulting in weaker intermolecular interactions and decreased viscosity [43]. However, with the addition of a small amount of functionalized nanoparticles into the base fluid, viscosity is reduced, as shown in Figure 4.12(a). Most of the literature reported the viscosity of the nanofluid increases as the increase in volume fraction compared to the base fluid [44].

It is seen that on increasing the nanofluid concentration, the viscosity of the nanofluid increases as a result of the molecules' cohesive forces weakening at higher temperatures, resulting in more kinetic energy. As the kinetic energy of the molecules increases, the

molecules become more mobile, resulting in an increase in viscosity. Additionally, it can be concluded that the viscosity of nanofluid is affected by a variety of parameters, including volume concentration, shear rate, nanoparticle morphology, and temperature. The lower the viscosity of the nanofluid, the lower the pressure drop, and hence the lower the necessary pumping power.

The thermal conductivity of the nanofluids and base fluid at different temperatures was displayed in Figure 4.12 (b). The experimental values are compared with commercially available new heat transfer fluid Xceltherm [45]. As seen from the Figure 4.12(b), the thermal conductivity of DES decreases with increase in temperature from 25-90°C. Compared with the commercial heat transfer fluid, it shows almost similar results and both decrease with temperature. Further, the addition of functionalized GO-NH_2 into DES drastically increased the thermal conductivity as reflected in the Figure 4.12 (b). Figure 4.12(b), indicates that the thermal conductivity of both nanofluid concentrations (NF5 and NF6) is greater than that of the base fluid. 38.35% and 49.40% thermal conductivity enhancement (TCE) were observed at temperatures 35 and 65°C when 0.0033 volume fraction (NF5) nanoparticle was added to the base fluid DES. Further, the increase of nanoparticle concentration 0.0101 volume fraction (NF6) in the DES, 44.89% and 55.28% enhancement was observed at temperatures 35 and 65°C respectively. This is due to the small size of the particles where micro-convection of the fluid takes place, which results in faster dispersion of heat in the fluid. This follows a general trend i.e. with an increase in temperature; nanoparticles gain higher energy, resulting in a higher collision rate between the nanoparticles. Although the nanofluid temperature greatly affects the Brownian motion of the nanoparticle, which influences the thermal conductivity of the nanofluid. Due to Brownian motion, nanoparticle aggregation may occur, resulting in collision between the particles. Along with Brownian motion, clustering and interfacial stacking also aid in heat transfer enhancement. Different models, including Bhattacharya et al.[46] model, K-K

[47] model, Xuan model [48] predict the influence of the Brownian motion and aggregation of the nanoparticles on heat transfer rate.

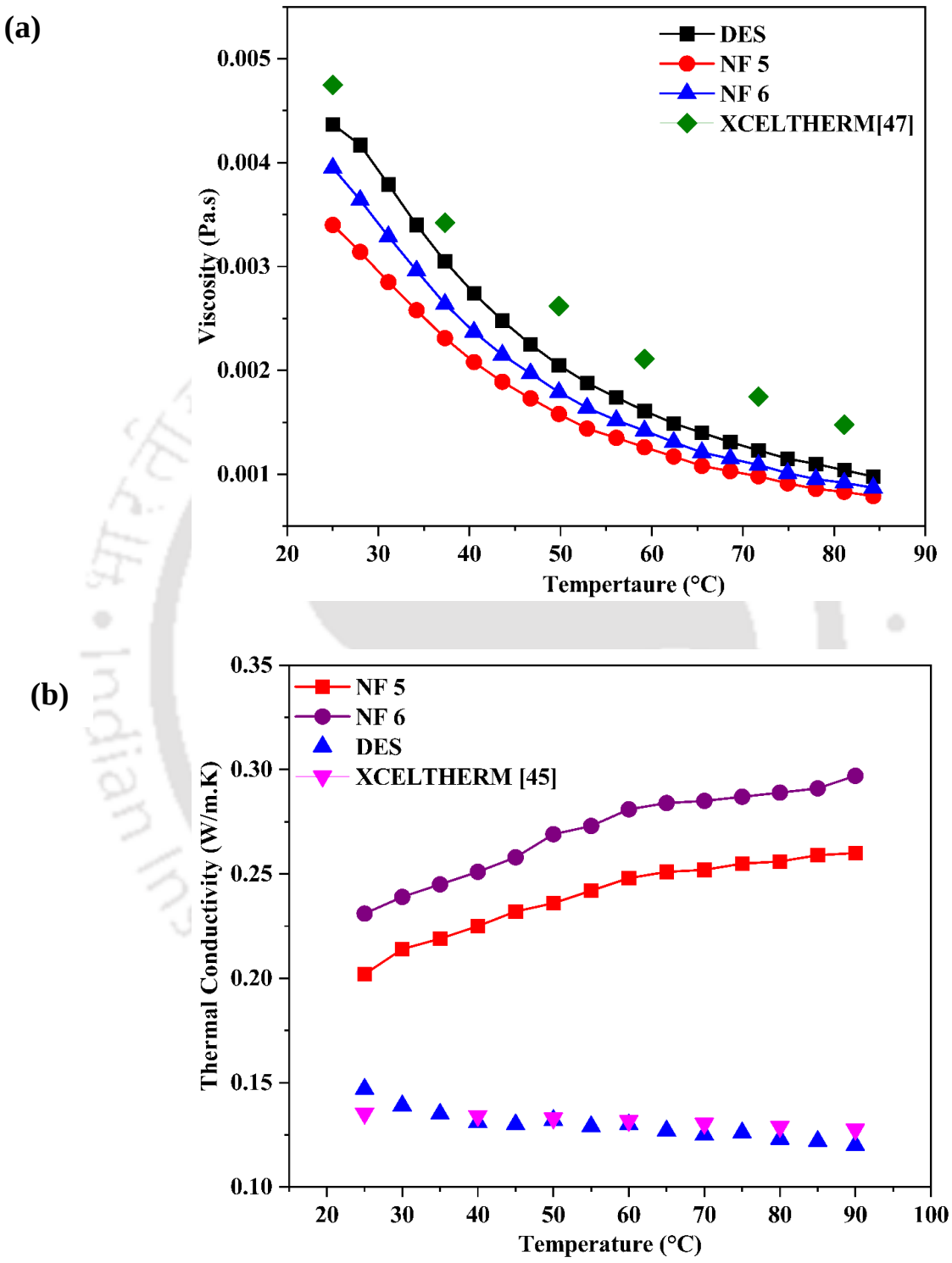

Figure 4.12. Variation of (a) viscosity and (b) thermal conductivity of nanofluids and DES at different temperatures.

Figure 4.13 depicts the density of the nanofluids and base fluid DES at different temperatures which is then compared to the experimental results with heat transfer fluid Xceltherm [45]. As expected density of both nanofluids and DES decreases with an increase in temperature. As compared with the heat transfer fluid Xceltherm, density of nanoflluids and DES is very low [45]. As the temperature increases movement of the molecules in the fluid increases thereby decreasing the intermolecular attraction. The volume of the fluid also increases which cause kinetic energy of the molecules to increase, which result in decrease in density. However, very less effect of nanoparticle on density of base fluid was observed. It should be noted that the size of the nanoparticle is responsible for thermal expansion with an increase in temperature, which results in higher kinetic energy of the molecules.

The specific heat capacity of nanofluids is another critical parameter for increasing the rate of heat transfer, which boosts the efficiency of the solar cell energy system. The specific heat capacities of DES and its related nanofluids, NF5 and NF6, are reported in Figure 4.14 and were compared to those of the commercial heat transfer fluid Xceltherm [45]. It was observed that the specific heat capacity of DES and nanofluids increases as the temperature is increased from 35 to 100°C. When a small quantity of nanoparticles was added to the base fluid, the studied thermal fluid exhibited a greater specific heat capacity than the commercial heat transfer fluid Xceltherm [45]. The interaction of solid particles and the base fluid significantly affects the specific heat of nanofluids. Higher temperatures cause molecules to vibrate, rotate, and translate, which increases internal energy. As a result, the molecules absorb more energy, which increases the specific heat of the fluid. As the specific heat capacity of GO-NH_2 nanoparticle is higher than the base fluid, is explains the fact that the specific heat capacity of nanofluid is higher than base fluid DES.

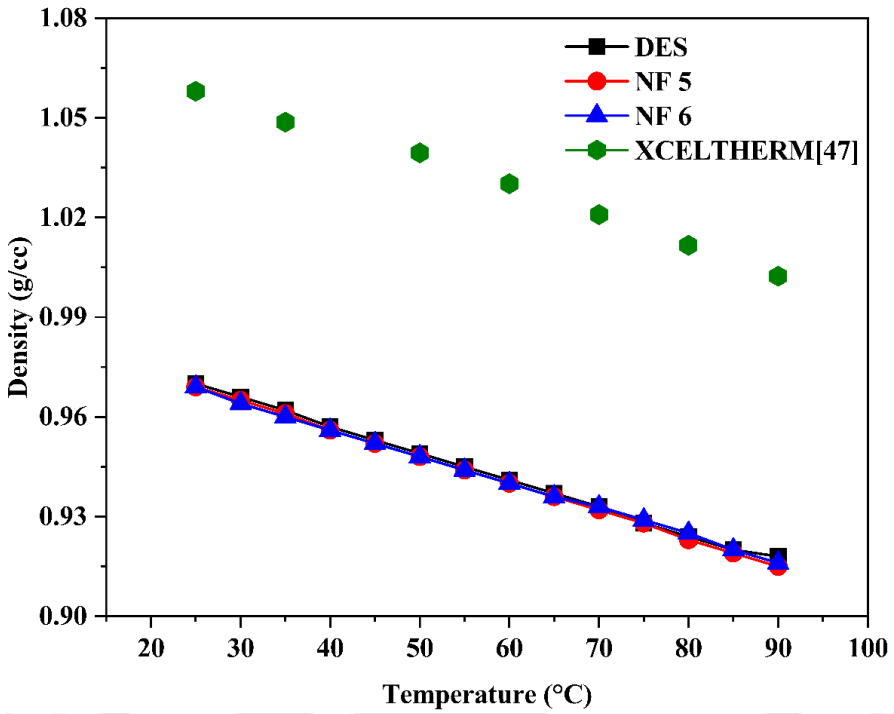

Figure 4.13. Variation of density of nanofluids and basefluid at different temperature.

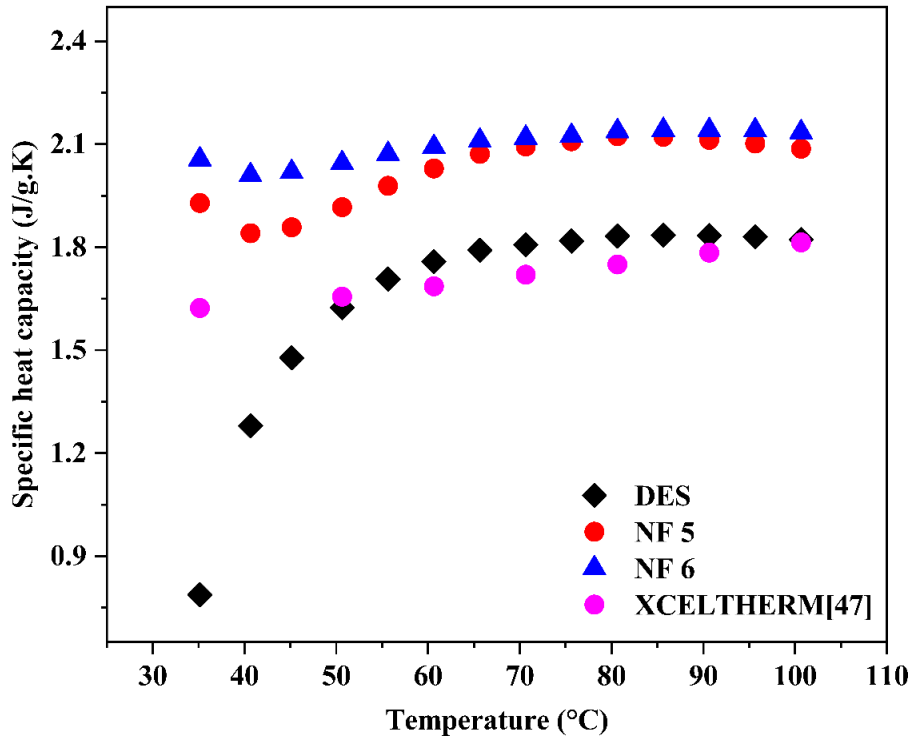

Figure 4.14. Variation of specific heat of nanofluids and base fluid at different temperatures

4.3.5. Process Simulation Results

Performance of the BR-MSF (Brine Multi Stage Flash) desalination system has been evaluated using the gained output ratio (GOR) which is the ratio of distillate formed to the amount of heat transfer in the heat exchanger. This is calculated by the following equation:

$$GOR=\frac{M_d h_{fgavg}}{Q_{transfer}} \quad \textbf{(4.5)}$$

Where the $Q_{transfer}$ is the energy transferred to the recycled brine solution, M_d is the distillate mass flow rate and h_{fgavg} is the average enthalpy of the distilled water. In physical terms, GOR is the ratio of latent heat energy of the distillate formed during flashing in each stage to the energy gained by the recycled brine in the heat exchanger. It is a non-dimensional parameter that reveals the amount of energy consumed for water production. Along with GOR, top brine temperature is the important parameter that influence the thermal performance of the desalination system. Initially, we explored the effects of GOR of nanofluids by taking top brine temperature and particle volume concentrations into consideration. It should be noted that in an actual MSF setup the solar collector geometry determines the incident flux which is the amount of heat trapped within the nanofluid. In our case in place of incident radiation, we have varied the volume fraction. A larger volume fraction implies an increase in the scattering of the incident radiation and higher heat absorption.

Comparing our results with the previous results [49], a similar trend was observed with respect to volume fraction i.e increase of GOR with volume fraction (Figure 4.15(b) and 4.15(c)). This is compared with the base fluid in Figure 4.15(a). It implies that the nanoparticle absorbs more energy when heated at higher temperatures, which in turn increases distillate flow rate as the heat is indirectly transferred to the flash section. A higher GOR is thus ensured by a higher distillate flowrate, which offers higher latent heat recovery. We also used a series of top brine temperatures to calculate GOR. Here an inverse relation was obtained. Again, at

constant heat flux, as the top brine temperature increases, the distillate flow rate rises, thereby increasing the GOR value for both the base fluid and the nanofluids (Figure 4.15).

We have also calculated the Gained Output Ratio (GOR) of base fluid and nanofluid at four different Top Brine Temperatures (TBT) namely 100°C, 105°C, 110°C and 115°C with a constant heat flux of 3690 cal/sec. It should be noted that the TBT temperature obtained is the result of the higher heat transfer from the nanofluid cycle which is a function of volume fraction. The GOR was found to increase with top brine temperature from 100-115 °C. Due to the high rate of heat absorption by the nanofluids, the use of nanoparticles increases the distillate flow rate due to higher latent heat recovery which leads to an increase of GOR of the system. Figure 4.16 displays the comparison of GOR values of base fluid with different volume fraction of nanofluids. At TBT of 110°C, 27.02% enhancement of GOR was observed for 0.0101 volume fraction of nanofluid, whereas 22.78% enhancement was found for 0.0033 volume fraction. As a result, a higher volume fraction increases the rate of heat transfer, which raises the GOR. However, in real scenario, the use of volume fraction is constrained due to issues with stability and agglomeration of the nanofluids; as a result, GOR rise is not appreciable at higher volume fraction. Further ASPEN does not take into account the hydrodynamic losses which is not in the scope of the current work as it involves CFD simulation.

(a)

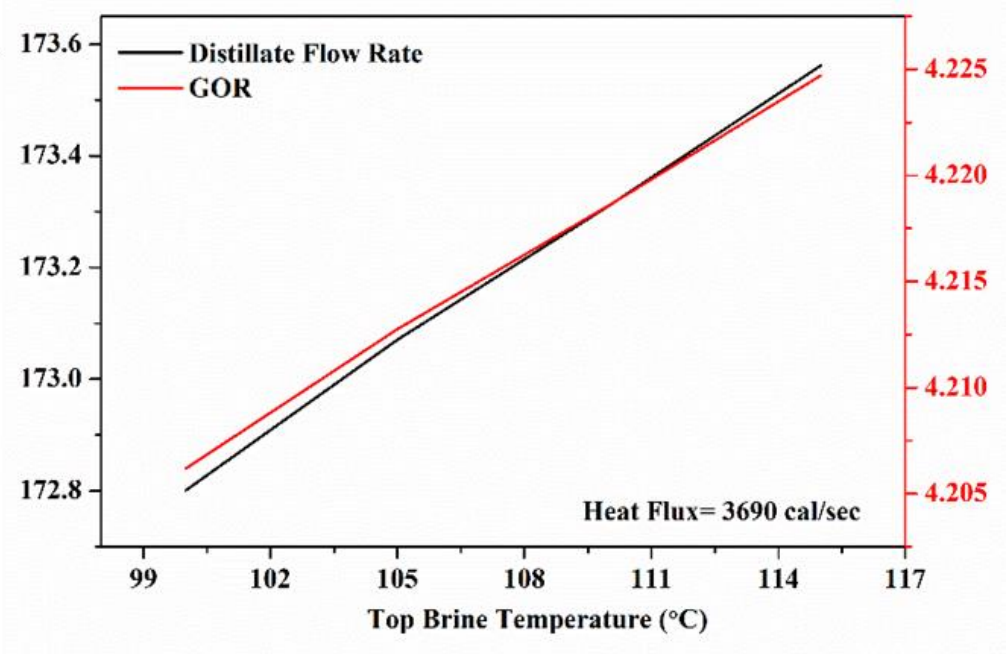

Base fluid

(b)

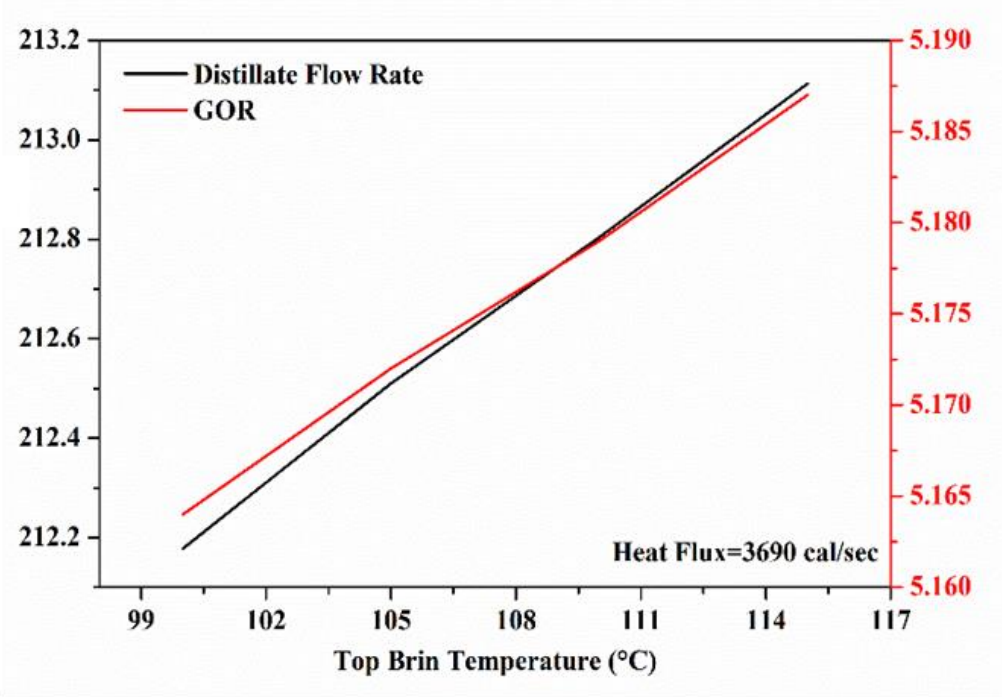

0.0033 volume fraction nanofluid

(c)

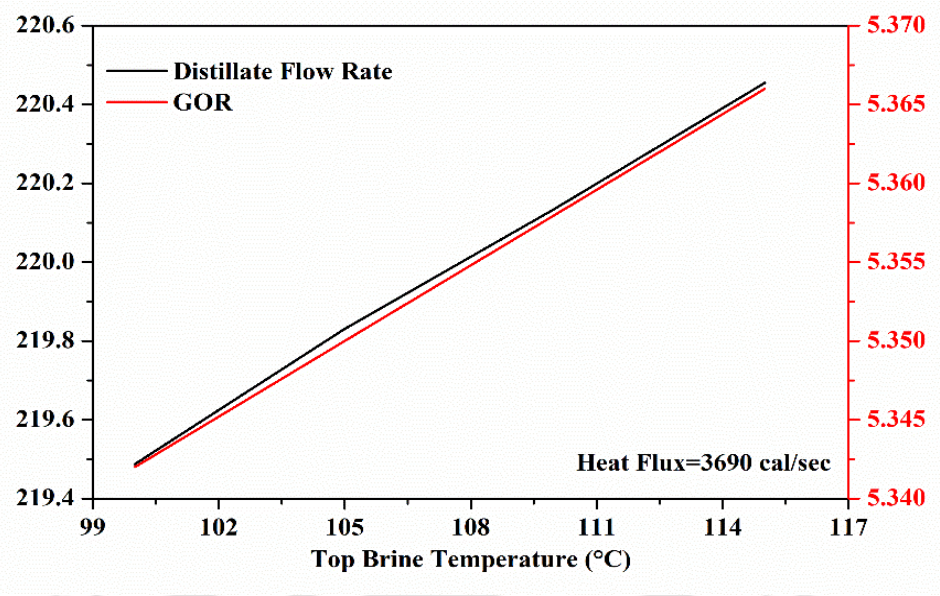

Figure 4.15. Variation of GOR and distillate flow rate (kg/hr) of basefluids and nanofluids at different top brine temperatures

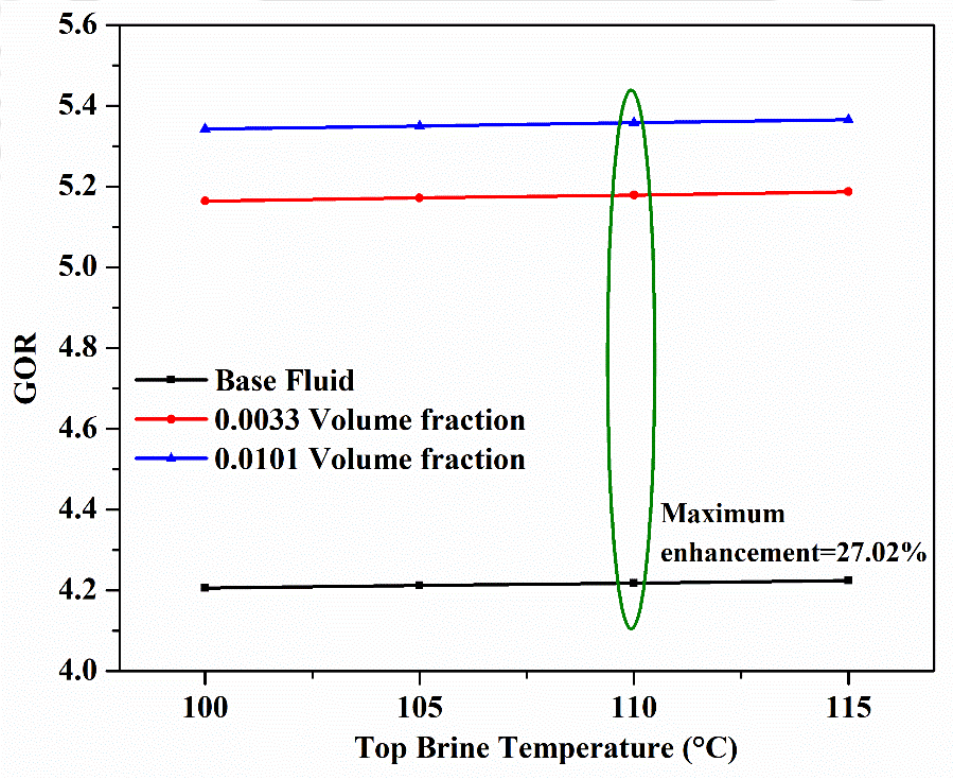

Figure 4.16. Variation of GOR with TBT of base fluids and nanofluids respectively

Table 4.5. Correlation equation of physical properties used in ASPEN simulation

Properties	Nanofluids	Correlated equation	Unit	Values of parameter
viscosity	Basefluid	$\mu = \mu_o\, e[-(E_\mu/RT)]$	mPa.s	μ_0=9.72 E_μ=0.026
	0.0033 vol%			μ_0=5.497 E_μ=0.025
	0.0101vol%			μ_0=8.25 E_μ=0.026
Density	Basefluid	$\rho = a\, t(°C) + b$	g cm^{-3}	*a* =-0.00008 b=0.9903
	0.0033 vol%			*a* =-0.00008 b=0.9897
	0.0101vol%			*a* =-0.00008 b=0.9881
Heat Capacity	basefluid	$C_p = a_1 + a_2T+a_3\, T^2 + a_3\, T^3$	J mol^{-1-} K^{-1}	a_1=-4.2 a_2= 0.23 a_3= -0.003 a_4= 1E-05
	0.0033 vol%			a_1=2.52 a_2= -0.04 a_3= 0.008 a_4= -4E-06
	0.0101vol%			a_1=2.35a_2= -0.0193 a_3= 0.0004 a_4= -2E-06
Thermal Conductivity	basefluid	$k = a_1 + a_2T+a_3\, T^2 + a_3\, T^3$		a_1=0.19 a_2=-0.0033 a_3=5E-05 a_4=-3E-07
	0.0033 vol%			a_1=0.15 a_2=0.0027 a_3=2E-05 a_4=5E-08
	0.0101vol%			a_1=0.18 a_2=0.0022 a_3=-8E-06 a_4=-3E-08

4.4 Conclusion

The synthesis of graphene oxide functionalized with amine was addressed in this chapter, as well as the characterization of nanoparticles using several techniques (FESEM, FETEM, EDS, FTIR, and XRD). It was confirmed that the nanoparticles were functionalized with amine via covalent contact using these characterization methods. Additionally, this chapter examines the synthesis of DES and the methods for preparing nanofluids. Further the stability of nanofluids was determined using zeta potential measurements. When nanoparticles were linked to a functional group, excellent dispersion and stability were reported in DES. Thus, at elevated temperatures, the functional group-containing nanoparticles-DES nanofluid exhibited favorable thermophysical properties. Thermal conductivity and specific heat, the required properties of nanofluid, demonstrated significant improvement at elevated temperatures compared to commercially available heat transfer fluid. The attractive thermophysical features of nanofluids indicated a high potential for use as a heat transfer fluid in solar energy systems.Through ASPEN simulation, a conceptualized multistage flash desalination with brine recirculation system coupled with nanofluid based counterflow heat exchanger was proposed to produce distilled water. Thermal performance of the desalination system was measured by the GOR, where GOR was evaluated with increasing incident flux of the system. GOR (<10) was found to be a desirable value, indicating that fresh water may be produced from the proposed BR-MSF system using DES-based nanofluid as the heat transfer fluid.

In summary, this chapter gives detailes about the application of DES based heat tranfer media in multistage flash desalination system. In the next chapter, possibility of natural deep eutectic solvent (NADES) as a potential heat transfer media will be addressed.

Reference

1. Lewis, N.S., et al., *Basic research needs for solar energy utilization. report of the basic energy sciences workshop on solar energy utilization, april 18-21, 2005*. 2005, DOESC (USDOE Office of Science (SC)).
2. Dehury, P., U. Mahanta, and T. Banerjee, *Comprehensive Assessment on the Use of Boron Nitride-Based Nanofluids Comprising Eutectic Mixtures of Diphenyl Ether and Menthol for Enhanced Thermal Media.* ACS Sustainable Chemistry & Engineering, 2020. **8**(38): p. 14595-14604.
3. Munyalo, J.M. and X. Zhang, *Particle size effect on thermophysical properties of nanofluid and nanofluid based phase change materials: A review*. Journal of Molecular Liquids, 2018. **265**: p. 77-87.
4. Geim, A.K., *Graphene: status and prospects.* science, 2009. **324**(5934): p. 1530-1534.
5. Choi, S.U. and J.A. Eastman, *Enhancing thermal conductivity of fluids with nanoparticles*. 1995, Argonne National Lab., IL (United States).
6. Xie, H., A. Cai, and X. Wang, *Thermal diffusivity and conductivity of multiwalled carbon nanotube arrays.* Physics Letters A, 2007. **369**(1-2): p. 120-123.
7. Che, J., T. Cagin, and W.A. Goddard III, *Thermal conductivity of carbon nanotubes.* Nanotechnology, 2000. **11**(2): p. 65.
8. Berber, S., Y.-K. Kwon, and D. Tománek, *Unusually high thermal conductivity of carbon nanotubes.* Physical review letters, 2000. **84**(20): p. 4613.
9. Liu, M.-S., et al., *Enhancement of thermal conductivity with carbon nanotube for nanofluids.* International communications in heat and mass transfer, 2005. **32**(9): p. 1202-1210.

10. Jiang, H., Q. Zhang, and L. Shi, *Effective thermal conductivity of carbon nanotube-based nanofluid.* Journal of the Taiwan Institute of Chemical Engineers, 2015. **55**: p. 76-81.

11. Le Ba, T., et al., *Review on the recent progress in the preparation and stability of graphene-based nanofluids.* Journal of Thermal Analysis and Calorimetry, 2020. **142**(3): p. 1145-1172.

12. Ravi, A., et al., *Graphene based nanocomposites: Synthesis, properties and application as electrochemical sensors*, in *Comprehensive Analytical Chemistry*. 2020, Elsevier. p. 1-849.

13. Arshad, A., et al., *A review on graphene based nanofluids: Preparation, characterization and applications.* Journal of Molecular Liquids, 2019. **279**: p. 444-484.

14. Kabeel, A., Z. Omara, and F. Essa, *Enhancement of modified solar still integrated with external condenser using nanofluids: An experimental approach.* Energy conversion and management, 2014. **78**: p. 493-498.

15. Omara, Z., A. Kabeel, and F. Essa, *Effect of using nanofluids and providing vacuum on the yield of corrugated wick solar still.* Energy conversion and management, 2015. **103**: p. 965-972.

16. Otanicar, T.P., et al., *Nanofluid-based direct absorption solar collector.* Journal of renewable and sustainable energy, 2010. **2**(3): p. 033102.

17. Bortolato, M., et al., *Investigation of a single wall carbon nanohorn-based nanofluid in a full-scale direct absorption parabolic trough solar collector.* Energy conversion and management, 2017. **150**: p. 693-703.

18. Goharshadi, E., et al., *Nanofluids for heat transfer enhancement-a review.* 2013.

19. Selvaraj, V., K. Senthilkumar, and H. Krishnan, *Covalent Functionalization of Graphene for the Enhancement of Thermophysical Properties in Nanofluids.* Chemical Engineering & Technology, 2021. **44**(5): p. 811-818.

20. Irani, V., A. Tavasoli, and M. Vahidi, *Preparation of amine functionalized reduced graphene oxide/methyl diethanolamine nanofluid and its application for improving the CO2 and H2S absorption.* Journal of colloid and interface science, 2018. **527**: p. 57-67.

21. Abbasi, S.M., et al., *The effect of functionalisation method on the stability and the thermal conductivity of nanofluid hybrids of carbon nanotubes/gamma alumina.* Ceramics International, 2013. **39**(4): p. 3885-3891.

22. Nasrollahi, N., et al., *The effect of amine functionalization of CuO and ZnO nanoparticles used as additives on the morphology and the permeation properties of polyethersulfone ultrafiltration nanocomposite membranes.* Composites Part B: Engineering, 2018. **154**: p. 388-409.

23. Hamze, S., D. Cabaleiro, and P. Estellé, *Graphene-based nanofluids: A comprehensive review about rheological behaviour and dynamic viscosity.* Journal of Molecular Liquids, 2020: p. 115207.

24. Punetha, V.D., et al., *Functionalization of carbon nanomaterials for advanced polymer nanocomposites: A comparison study between CNT and graphene.* Progress in Polymer Science, 2017. **67**: p. 1-47.

25. Yu, W. and H. Xie, *A review on nanofluids: preparation, stability mechanisms, and applications.* Journal of nanomaterials, 2012. **2012**.

26. Afrand, M., *Experimental study on thermal conductivity of ethylene glycol containing hybrid nano-additives and development of a new correlation.* Applied Thermal Engineering, 2017. **110**: p. 1111-1119.

27. Vadasz, P., *Heat conduction in nanofluid suspensions.* 2006.

28. Lee, D., J.-W. Kim, and B.G. Kim, *A new parameter to control heat transport in nanofluids: surface charge state of the particle in suspension.* The Journal of Physical Chemistry B, 2006. **110**(9): p. 4323-4328.

29. Vandsburger, L., *Synthesis and covalent surface modification of carbon nanotubes for preparation of stabilized nanofluid suspensions.* 2009.

30. Lin, S.-T. and S.I. Sandler, *A priori phase equilibrium prediction from a segment contribution solvation model.* Industrial & engineering chemistry research, 2002. **41**(5): p. 899-913.

31. de Riva, J., et al., *Ionic liquids for post-combustion CO2 capture by physical absorption: Thermodynamic, kinetic and process analysis.* International Journal of Greenhouse Gas Control, 2017. **61**: p. 61-70.

32. Verma, R., et al., *Liquid-liquid extraction, COSMO-SAC predictions and process flow sheeting of 1-butanol enhancement using mesitylene and oleyl alcohol.* Journal of Molecular Liquids, 2018. **265**: p. 824-839.

33. Verma, R., et al., *Separation of low molecular weight alcohols from water with deep eutectic solvents: liquid-liquid equilibria and process simulations.* Fluid Phase Equilibria, 2021. **533**: p. 112949.

34. Kohn, W., A.D. Becke, and R.G. Parr, *Density functional theory of electronic structure.* The Journal of Physical Chemistry, 1996. **100**(31): p. 12974-12980.

35. GaussView, V., *3.07, Dennington II, Roy; Keith, Todd; Millam, John; Eppinnett, Ken; Hovell, W. Lee; and Gilliland, Ray; Semichem.* Inc., Shawnee Mission, KS, 2003.

36. Frisch, M.J., et al., *Gaussian 09, Revision D. 01, Gaussian.* Inc.: Wallingford, CT, 2009.

37. Dehury, P., J. Singh, and T. Banerjee, *Thermophysical and forced convection studies on (alumina+ menthol)-based deep eutectic solvents for their use as a heat transfer fluid.* ACS omega, 2018. **3**(12): p. 18016-18027.

38. Joback, K.G. and R.C. Reid, *Estimation of pure-component properties from group-contributions.* Chem. Eng. Commun., 1987. **57**(1–6): p. 233.

39. Gharehkhani, S., et al., *Basic effects of pulp refining on fiber properties—A review.* Carbohydrate polymers, 2015. **115**: p. 785-803.

40. Ederer, J., et al., *Determination of amino groups on functionalized graphene oxide for polyurethane nanomaterials: XPS quantitation vs. functional speciation.* RSC advances, 2017. **7**(21): p. 12464-12473.

41. Said, Z., et al., *Recent advances on the fundamental physical phenomena behind stability, dynamic motion, thermophysical properties, heat transport, applications, and challenges of nanofluids.* Physics Reports, 2021.

42. Zhang, W., et al., *Preparation of amino-functionalized graphene oxide by Hoffman rearrangement and its performances on polyacrylate coating latex.* Progress in Organic Coatings, 2016. **94**: p. 9-17.

43. Esfahani, M.R., E.M. Languri, and M.R. Nunna, *Effect of particle size and viscosity on thermal conductivity enhancement of graphene oxide nanofluid.* International Communications in Heat and Mass Transfer, 2016. **76**: p. 308-315.

44. Esfe, M.H., et al., *Experimental determination of thermal conductivity and dynamic viscosity of Ag–MgO/water hybrid nanofluid.* International Communications in Heat and Mass Transfer, 2015. **66**: p. 189-195.

45. *XCELTHERM®LV1 – Liquid Phase Engineering Properties*. Available from: https://www.radcoind.com/media/e-lit-Xceltherm-LV1-Engineering-Properties-2020.pdf.

46. Bhattacharya, P., et al., *Brownian dynamics simulation to determine the effective thermal conductivity of nanofluids.* Journal of Applied Physics, 2004. **95**(11): p. 6492-6494.

47. Koo, J. and C. Kleinstreuer, *A new thermal conductivity model for nanofluids.* Journal of Nanoparticle research, 2004. **6**(6): p. 577-588.

48. Xuan, Y., Q. Li, and W. Hu, *Aggregation structure and thermal conductivity of nanofluids.* AIChE Journal, 2003. **49**(4): p. 1038-1043.

49. Garg, K., et al., *Performance evaluation of a brine-recirculation multistage flash desalination system coupled with nanofluid-based direct absorption solar collector.* Renewable Energy, 2018. **122**: p. 140-151.

Chapter-5

Thermophysical Properties of Menthol-Based NADES with Functionalized MWCNTs: Assessing Thermal Efficiency and DFT Investigations for Enhancing Thermal Energy Storage Potential

Thermophysical Properties of Menthol-Based NADES with Functionalized MWCNTs: Assessing Thermal Efficiency and DFT Investigations for Enhancing Thermal Energy Storage Potential

This chapter focuses on natural deep eutectic solvent (NADES), which replaced ionic liquid (IL), is considered a new class of bio-based heat transfer fluid. NADES are environmentally friendly solvents derived from natural, biodegradable substances such as sugars, amino acids, and organic acids. NADES serve as sustainable substitutes for conventional solvents, encouraging the use of ecologically conscious methods. In this work, NADES comprises of Lauric acid and DL menthol as hydrogen bond donor(HBD) and hydrogen bond acceptor (HBA) at specific molar ratio. Two nanoparticles, MWCNT and MWCNT-COOH, are dispersed to prepare different volume fractions of nanofluids. Different Characterization methods, including XRD, FT-IR, Raman, EDS, FESEM, and FETEM, have been adopted to characterize the MWCNT and MWCNT-COOH nanoparticles. The measurement of viscosity, density, and specific heat was performed in the temperature range of 30-90°C. Thermal conductivity, one of the key factors in thermal energy storage, is measured and compared with the Hamilton-Crossover model. The maximum enhancement of thermal conductivity was found to be 40.93% and 108.05% at 50 °C for MWCNT and MWCNT-COOH nanoparticles respectively. Dispersion behaviour and stability analysis have been evaluated through zeta potential analysis. Heat transfer coefficients and Nusselt number were determined at 0.125 vol% of MWCNT-COOH nanofluids under constant heat flux within the forced convection regimet. The experiment was carried out at three different Reynolds number in the laminar region. Higher heat transfer coefficient was observed for nanofluids compared to the NADES. The DFT calculation, including QTAIM and non-covalent interaction (NCI), pointed out to the interaction between nanoparticles and base fluid. The results showed that MWCNT-COOH

based nanofluids could be prepared successfully on a large scale, and their exceptional performance highlights their potential utility in thermal energy systems.

5.1 Introduction

Fresh water scarcity across the globe is the next challengeable quest for mankind. Solar energy can be used as a substitute for conventional energy sources to meet worldwide energy demand. This is the most frequent and easily accessible sustainable energy source without impacting the environment. Heat transfer fluid (HTF) plays an important role in the conservation of solar energy that can be used in potential challenging technologies, including power sources, solar thermal applications, automobile industries and petrochemical industries [1-3]. Some of the common HTFs, such as Therminol VP-1, Therminol 66, Therminol VP-3, Dowtherm 4000, and Paratherm CR are available commercially [4-7]. Therminol VP-1's decomposition produces hydrogen that must be collected, causing energy loss [4]. Nanofluids are gaining attention as they have shown potential to enhance the heat transfer properties of organic fluids. They have been studied in various applications, including refrigeration, lubrication, and energy production. Nanofluid, first coined by Choi[8], has been found to possess enhanced thermophysical properties. The addition of nano-size particles to the base fluid can lead to improved thermal conductivity, viscosity, and heat transfer rates, which can increase the efficiency of the thermal processes. Carbon-based nanoparticles are of great interest to the research community. Carbon-based nanomaterials always show good properties and exhibit a wide range of novel features in industrial applications, agricultural sectors, and medical fields. Carbon is one of the most fascinating components in the world has ability to form different structures with excellent properties[9]. Nanoparticles, including Multi-Walled Carbon nanotubes (MWCNT) and graphene oxide possess remarkable properties due to large surface area and smaller size which leads to improve heat transfer rates[10]. He et al.[11] used three different nanoparticle, graphene nano platelets, MWCNT and nano graphites, and investigated their thermal conductivity. At a concentration of 3 wt%, the results demonstrated that GNP greatly increased thermal conductivity when compared to MWCNT. Aqib et al.[12]

investigated the effect of MWCNT and Al_2O_3 nanoparticles on the phase change behaviour of paraffin wax PCM with a temperature of 58°C. Results indicated that MWCNT with a paraffin wax content of 6wt% performs better.

Dispersion of CNT in aqueous media can be difficult due to carbon nanotubes' high aspect ratio (L/D), extremely large specific surface areas, and strong van der Waal's interactions between carbon surfaces. Amrollahi et al. [13] synthesized MWCNT-water nanofluid and analyzed thermophysical properties and heat transfer coefficient. They have reported 30-40% improvement on heat transfer coefficient under both laminar and turbulent flows at 0.25 wt% concentration. It has also been reported that mixture of carbon tube nanoparticles with other base fluids, including water, ethylene glycol, and motor oil, results in nanofluids that act as heat storage media in solar thermal collectors. [14, 15]. Thus, the choice of base solvent is critical since it influences nanofluid properties, including thermal conductivity, stability, and dispersion behaviour [16].

Functionalization of carbon nanomaterials shows better stability and dispersion behaviour in heat transfer fluids for solar applications [17], they are also beneficial for energy conversation [18], electrochemical energy storage [19], and biomedical applications [20]. The process of nanoparticle functionalization involves attaching functional groups onto the nanoparticle surface. This technique is commonly employed to decrease the abundant van der Waals forces present on the particle surface, which arise due to their small size and expansive surface area. Agglomeration of nanoparticles, leading to sedimentation, is primarily caused by these attractive forces [21]. Strong oxidants like sulphuric acid and nitric acid are frequently used to create functional groups on nanotubes. These groups attached to the defect of the nanotube surface and makes the CNT hydrophilic in nature [22, 23]. Aggressive chemical functionalization, however, can harm the sidewalls of CNTs and even shorten it. Bolodo et al. [24] compared the optical transmittance and thermal conductivity of MWCNT and MWCNT-

COOH/Ethylene glycol nanofluid. Results showed that MWCNT-COOH has higher thermal conductivity and better dispersion stability compared to the non-functionalized MWCNT nanofluid. A stability experiment on MWCNT nanofluid that had been covalently functionalized was conducted by Farbod et al. [25]. They have reported that after 80 days, MWCNT nanofluid showed no signs of sedimentation. Investigation for nanofluids has been done on a number of basic fluids, including water, alcohols, glycols, oils, and their combinations, categorized as water base and oil base nanofluids. However, stable dispersion of thermal nanofluid is essential studies to realize industrial applications. After adding nanoparticles, strong aggregation occurs due to the poor compatibility with base fluid. The aggregation causes the nanoparticles' deposition and loss of enhanced heat transfer. Further aggregation leads to the cause of clogging problems in microelectronic systems [26]. Ionic liquids (ILs), suggested as possible substitute heat transfer fluid (HTF), have better chemical and thermal stability, are non-flammable, and have lower vapor pressure [27]. High thermal conductivity and heat capacity per unit volume permit its used as heat transfer fluid. Franca et al. [27] determined the thermal conductivity of ILs trihexyltetradecylphosphonium dicyanamide ($[P_{66614}][N\text{-}(CN)_2]$), trihexyltetradecylphosphonium bromide ($[P_{66614}]$-[Br]), 1-ethyl-3-methyl-imidazolium thiocyanate ($[C_2mim]$-[SCN]), 1-n-butyl-3-methyl-imidazolium thiocyanate($[C_4mim][SCN]$), 1-ethyl-3-methyl-imidazolium tricyanomethanide ($[C_2mim][C(CN)_3]$), and 1-n-butyl-3-methyl-imidazolium tricyanomethanide ($[C_4mim][C(CN)_3]$) at temperature range 293-243K with their respective MWCNT based nanoparticles. It was reported that ionic nanofluids have higher thermal conductivity than their corresponding base fluid.

In this chapter, we have studied the different concentrations of organic nanofluids comprising of MWCNT and MWCNT-COOH nanoparticles dispersed into NADES, and thereafter investigated the stability and thermal properties of prepared nanofluids. This work

employed DL-Menthol and Lauric acid as HBA and HBD respectively with a molar ratio of 2:1 to synthesize NADES. All thermophysical properties, including density, isobaric heat capacity and viscosity, were measured at temperature range 25-85°C. The thermal performance has been investigated through a forced convection experiments. The forced convective experiment has been carried out for both NADES and nanofluid at constant heat flux under laminar regime at three different Reynolds numbers. In order to correlate the dispersion of the nanoparticles in the base fluid, additional interactions between the NADES and SWCNT are examined utilizing quantum chemical-based studies, namely, the reduced density gradient (RDG), and QTAIM studies which has been discussed in the previous chapter.

5.2. Experimental Methods

5.2.1 Materials and Methods

DL-menthol having purity of 99.8 % was purchased from Sigma Aldrich. Lauric acid, having purity of > 98%, was purchased from Sigma Aldrich. Multi-walled carbon nanotube and carboxylic functionalized multiwall carbon nanotubes were purchased from TCI chemicals with 20-40 nm diameter, 5-15 micro meter length, and Ossila chemicals with inner diameter 5-10 nanometer, 10-20 micrometer length respectively. Table 5.1 provides the physical properties of the MWCNT-COOH nanoparticle.

Table 5.1. Properties of MWCNT-COOH nanoparticle

Parameter	Value
Purity	>99.9%
True density (kg/m3)	2100
Outer diameter (nm)	25
Inner diameter (nm)	5-10
Length (μm)	10-20
Thermal conductivity (W/m.K)	1500

5.2.2 Formulation of NADES

NADES are prepared by mixing by two components, Hydrogen Bond Donor (HBD) and Hydrogen Bond Acceptor (HBA). The preparation method of hydrophobic deep eutectic solvent has been reported in our previous chapter 4 and our earlier published work [28]. Figure 5.1 shows the optimized structures of HBD, HBA, NADES and pair of SWCNTs/NADES. The molar ratio has been chosen so as to form a eutectic mixture. Temperature Modulated Differential Scanning Calorimetry (TMDSC) has been used to determine the melting point of the NADES. As shown in the Figure 5.2, the melting point of NADES is found to be 15°C which is less than the corresponding components.

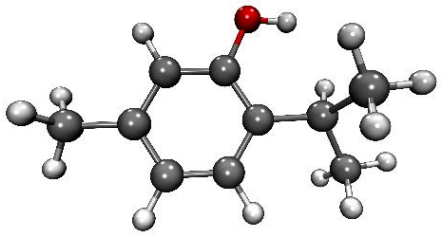

(a) Dl-menthol

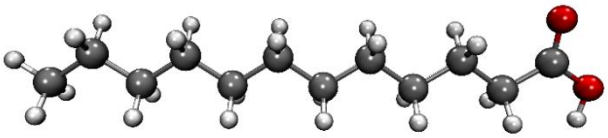

(b) Lauric acid

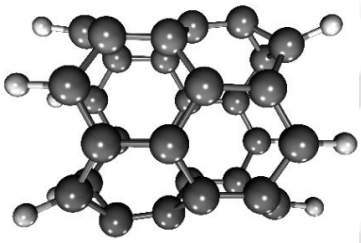

(c) SWCNT

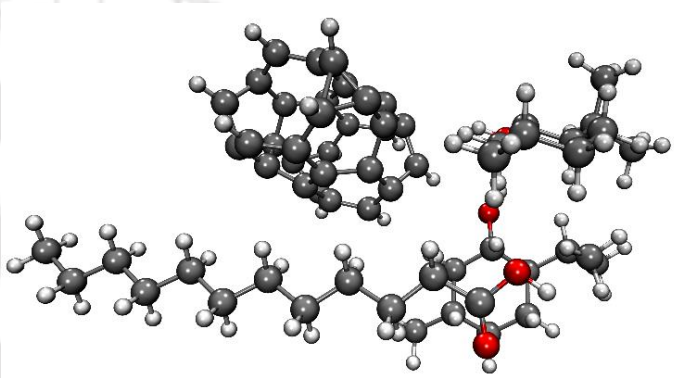

(d) NADES+ SWCNT

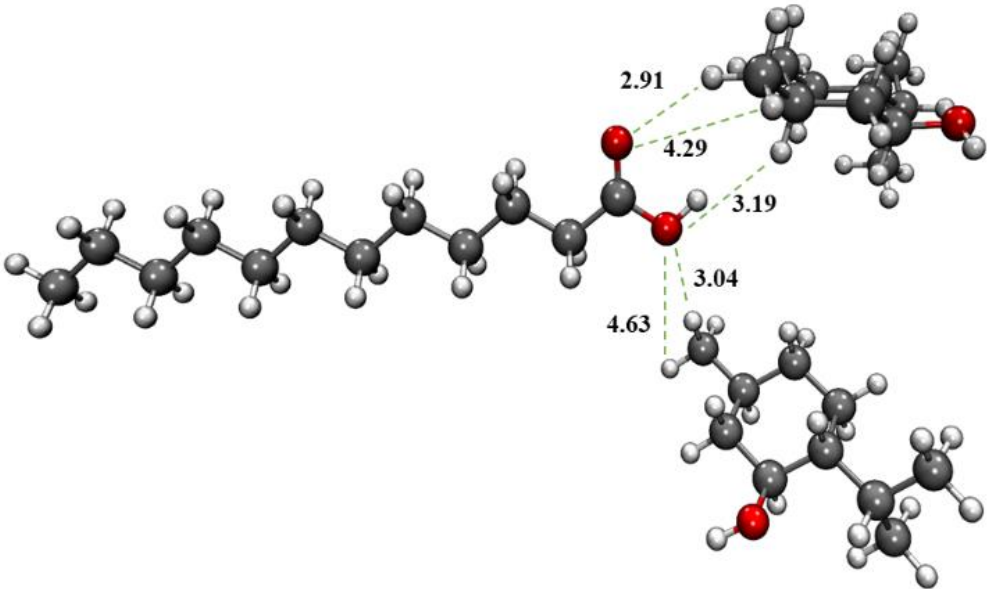

(e) NADES

Figure 5.1. Optimized structures of (a) Dl-menthol, (b) Lauric acid, (c) SWCNT, (d) NADES+SWCNT, and (e) NADES obtained using ωB97XD/6-311++G (d, p) level of theory. (All bond distances are in Å)

The nanofluid preparation process employed the two-step method [29] as discussed in the previous chapter. Initially, the purchased MWCNT and MWCNT-COOH nanoparticles, were dispersed into a NADES comprising of DL-Menthol and Lauric acid. Thereafter, the resulting mixture was undergoing ultra-sonication for a certain period of time ranging from 90 to 120 minutes to get uniform and homogeneous solution (Figure 5.3). A schematic diagram of the nanofluid preparation method was described in the previous chapter 4. However, it is important to note that the two-step method has a primary drawback, which is the potential for nanoparticle aggregation due to the strong van der Waals interactions. The MWCNT and MWCNT-COOH nanoparticles were utilized in three different volume percentages, namely 0.125, 0.3 and 0.5 vol%, as shown in Figure 5.3. The abbreviation of the nanofluids were shown in table 5.2. The following formula [30] has been used to calculate the volume percent of the nanofluid concentration.

$$\varphi = \left[\frac{\left(\frac{m}{\rho}\right)_{Nanoparticles}}{\left(\frac{m}{\rho}\right)_{Nanoparticles} + \left(\frac{m}{\rho}\right)_{base\ fluid}} \right] \times 100 \qquad \textbf{(5.1)}$$

Where, φ, m and ρ denotes mass fraction of the nanoparticles (%), solid mass (kg) of the nanoparticles and density (kg/m^3) respectively. To ensure the stability of the nanofluid, prepared nanofluids were kept for three days at room temperature and observed for any settlement. Further stability of the nanofluid was investigated through visual observation up to 2 months along with their zeta potential measurement.

Table 5.2 Abbreviation of nanofluids

Volume%	MWCNT	MWCNT-COOH
0.125	NF 7	f-NF 7
0.3	NF 8	f-NF 8
0.5	NF 9	f-NF 9

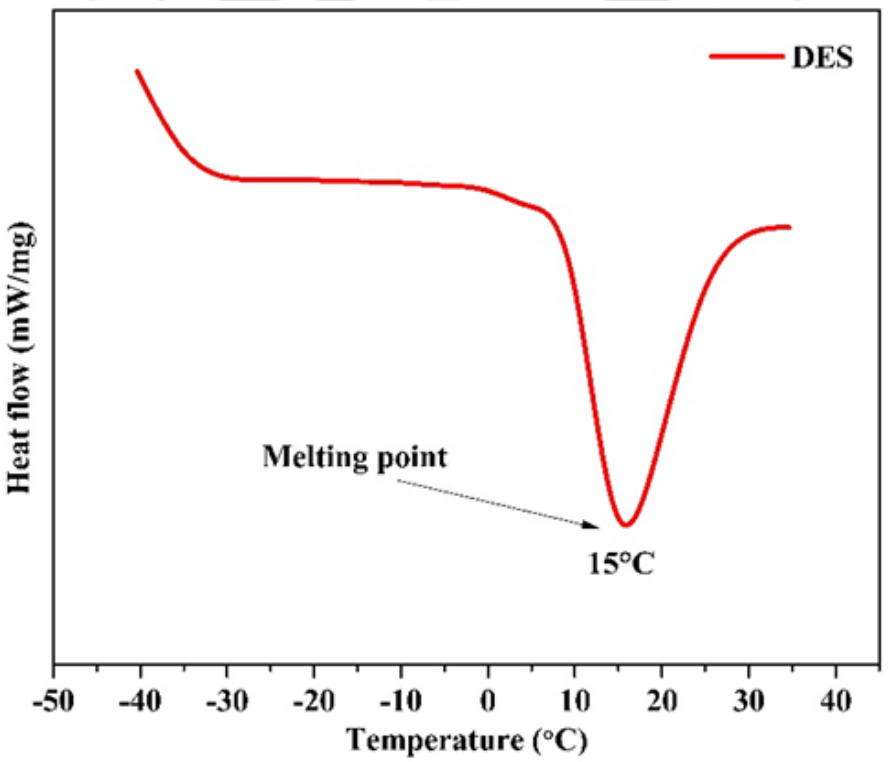

Figure 5.2. TM-DSC curve of NADES

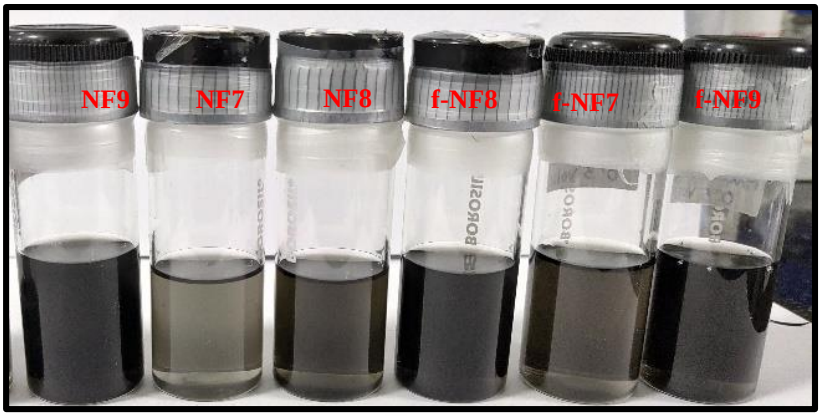

Figure 5.3. MWCNT and MWCNT-COOH based NADES nanofluids at volume percentage of 0.125 vol%, 0.3 vol% and 0.5 vol%

5.2.3 Thermophysical Properties of Nanofluid

The thermophysical characteristics of nanofluids increases with a rise in the volume percentage of nanoparticles and decrease with temperature rises. The Anton Paar DMA 4500 Densitometer was used to measure the density of the nanofluids. The measurements are estimate to be accurate to within 0.0001 g/cm^3. The viscosity of the nanofluid was measured by an Interfacial Rheometer (MCR 301, Anton Paar, Austria) with an accuracy of 0.001 mPa.s. Temperature Module Differential Scanning Calorimeter (TMDSC) (NETZSCH STA 449F3) was utilized to conduct specific heat measurements in nitrogen environment using sapphire as the reference material. The recorded measurements had an uncertainty of ± 5.97 J/Kg.K. Additionally thermal conductivity values for both base fluid and nanofluids were acquired using the KD2 Pro thermometer device (Decagon device, USA) with an uncertainty of ± 0.0096 W/m K. The measurement employed the transient hot-wire method, where a hot wire was placed between a hot plate and a silicon oil bath to maintain constant temperature. The operating temperature of the sensor ranged from 223.15 K to 423.15 K with an accuracy of ±5%. The resistance fluctuation of the hot wire was measured using a Wheatstone bridge, and the voltage across the

bridge and the temperature of the hot wire were obtained. The thermal conductivity was calculated using equation 5.2 as below.

$$k = \frac{q}{4\pi(T_2 - T_1)} ln\left(\frac{t_2}{t_1}\right) \quad \textbf{(5.2)}$$

In the given equation, the thermal conductivity (k) is expressed in W/m.K. The variables q, T_2, and T_1 represent the heat rate, temperatures at times t_2 and t_1 respectively. It is important to avoid convection currents during thermal conductivity measurements as the thermal analyser solely considers the conduction mode of heat transfer. The uncertainty of the thermal conductivity can be calculated employing following formula

$$U = \sqrt{\frac{\sum_{i=1}^{n}(X_i - \bar{X})^2}{n(n-1)}} \quad \textbf{(5.3)}$$

Where, U is the standard uncertainty, n is the sample content, X is the sample thermal conductivity, and $\bar{X}$ is the average of sample thermal. The maximum uncertainty was calculated after series of experiment was 0.0056 W/m.K.

5.2.4 Forced Convection Experiment of Nanofluids and Base Fluid

The details of the forced convection experimental setup were discussed in previous chapter 3. The experimental setup comprises several components, including a chemical pump, flow control valve, rotameter, stainless steel testing section, cooling unit, heat transfer fluid tank, thermocouples, and a pressure transducer. The pump was connected to a control valve, followed by the rotameter to regulate the flow rate. The testing section tube, made of stainless steel, had dimensions of 9 mm inner diameter, 12 mm outer diameter, and a length of 1000 mm. To ensure uniform heating across the testing section, a flexible heating tape (Brisk Heat SDCJCA-BIH101060L) was utilized. The heating tape was powered by a DC power supply

(GATTS MX1174A). The details of the experimental procedure have already been reported in our previous chapter [31].

To minimize heat loss and maintain a constant heat flux condition, the test section was insulated with fibre glass insulation. Five J-type thermocouples were carefully attached to the surface of the test section, while two additional thermocouples were welded at the inlet and outlet for measuring the liquid temperatures. The inlet and outlet of the test section were connected to appropriate pressure transducers. These pressure transducers, with an accuracy of ±0.2 mV, and thermocouples, with an accuracy of ±2 °C, were connected to a National Instrument (NI) data acquisition system called cDAQ-9178. The data acquisition system was set up using a temperature card (NI 9211) and a pressure card (NI 9203). Finally, the LabVIEW software was employed for data processing purposes.

From the forced convection experimental data, the local heat transfer coefficients of the base fluid and the corresponding nanofluids can be evaluated from the following equation 5.4

$$h(x) = \frac{q}{T_W^{/}(x) - T_f^{/}(x)} \qquad \textbf{(5.4)}$$

Where, $T_W^{/}(x)$ and $T_f^{/}(x)$ stand for the inner surface and liquid respective local temperatures. The detail calculations of the local heat transfer coefficient and Nusselt number are provided in the Appendix A.

5.2.5. Computational Methods

The molecular structures of Dl-menthol, Lauric acid, and single-walled carbon nanotubes (SWCNT) were initially constructed using Gauss View 6.0 software[32]. Subsequently, the optimization of these structures was conducted utilizing the ωB97XD/6-311++G(d,p) level of theory [33]. The decision to employ Density Functional Theory (DFT) computations using a

particular basis set was driven by their capacity to replicate energy values, in contrast to the computationally intensive M06 and MP2 approaches[34].

`The ωB97XD functional, which is an expansion of Becke's 97 functional involving a dispersion correction term was utilized. The functional under Hartree-Fock exchange term, contributes 22% in the short-range regime and 100% in the long-range regime. In order to accurately define the intermediate zone, a standard error function was utilized, incorporating a range separation parameter of ω = 0.2. In contrast to standard density functional theory (DFT) methods such as B3LYP, this particular methodology demonstrates a high level of suitability in precisely computing non-covalent interactions. Consequently, it emerges as an appealing option for investigating the properties of single-walled carbon nanotubes (SWCNTs) and their interactions with solvents.

Following this, geometric structures of (5,5) SWCNT were generated utilizing the nanotube modeller [35]. The optimization of solvent-nanotube architectures was conducted using the ω B97XD technique, which is based on density functional theory. The 6-311++G(d, p) basis set with proper implementation of the diffuse and polarization functions was employed for this purpose to treat all the atoms equally on a higher level of theory[36-38]. The optimization of geometric parameters for several molecules and solvent-SWCNT systems was conducted without imposing any symmetry requirements. The selection of the optimal structure for each complex system was determined by considering the lowest ground state energy. The electronic structures were computed using the Gaussian 16.0 software package [39].

In addition, the study included non-covalent interaction (NCI) and reduced density gradient (RDG) evaluations to assess both attractive and repulsive interactions. NCI analysis [40] offers extensive information regarding the spatial configurations of electron density in systems characterized by low electron density and gradient values [41]. The aforementioned methodology is frequently employed for the investigation of van der Waals (vdW) interactions,

steric hindrance, and hydrogen bonds (HBs) [42]. The present study employed an Atom in Molecules (AIM) analysis proposed by Bader et al. to investigate the pairwise interactions between atoms, considering their respective van der Waals radii. The studies were conducted utilizing the Multiwfn 3.8 software package[43]. The systems explored in this study were processed using the Visual Molecular Dynamics (VMD) tool [44].

5.3. Results and Discussion

5.3.1 Characterization of Nanoparticles

The microstructure of MWCNT and MWCNT-COOH were investigated through FETEM and FESEM images as shown in Figure 5.4 (a, c) and (b, d). The FESEM images were captured at 100 nm scale, where a randomly oriented fibre-like CNT (order of micrometres) is readily visible. As seen in Figure 5.4 (b), white spot on the surface of the CNT indicated the presence of functional group. Several multi walled or layer structure of CNT was clearly seen in FETEM images (Figure 5.4 (c) and 5.4(d)). It reveals the diameter of the MWCNT which was in the range of ca. 20-40 nm. The XRD pattern of MWCNT and MWCNT-COOH were displayed in Figure 5.5 (a), which indicates the crystalline structure of CNT. A sharp peak was observed at $2\theta=25.50°$ for MWCNT-COOH and $2\theta=26.02°$ for MWCNT indicated the crystalline structure of the carbon nanotubes. As evident, a peak shift from 26.02° to 25.50° indicates an expansion in the interlayer d-spacing of the CNT. The peak present at 25.50° is attributed to the presence of the COOH group attached to the surface of the CNT.

However, the (100), (004), and (110) atomic planes exhibit a low-intensity peak with 2θ values of 43.04°, 53.68°, 78.0° respectively showing that CNTs have crystalline structure. There were no additional peaks detected, indicating the nanotube's exceptional purity. Further, the structures of both MWCNT and MWCNT-COOH have been analyzed by Raman spectroscopy where it can identify the carbon allotropic forms, presence of functional groups

and structure disorder degree. The Raman spectra of MWCNT and MWCNT-COOH nanoparticles are shown in Figure 5.5 (b), where the patterns appear comparable. From the Figure 5.5 (b) the bands detected at 1360 and 1587 cm^{-1}, refers to the D and G mode for MWCNT at 1352 cm^{-1} and 1581 cm^{-1}respectively for D and G mode. Generally, CNTs can exhibit two distinct characteristic Raman band, D mode (disorder band 380–1200 cm^{-1}) and G mode (graphite band 1550–1590 cm^{-1}) [45] band. A double resonance or the D band Raman mode is a measure of the structural disorder caused by amorphous carbon structure defects [46] whereas G band is the high frequency first order mode [47]. The introduction of functional groups is quantified by the ratio of G band to D band intensities. A lower I_D/I_G ratio and a higher sp3 group concentration suggested the existence of functional groups[48]. The I_D/I_G ratio for MWCNT is 1.162 and for MWCNT-COOH is 0.5360. The value indicated the existence of functional groups in MWCNT nanoparticle. The amount of functional groups present can be investigated through EDS analysis. From Figure 5.5 (c), the amount of carbon and oxygen are 77.8wt% and 22.2 wt% respectively. During the preparation of sample for EDX analysis, some impurities have appeared which can be seen in Figure 5.5 (c). Further behaviour of functional groups present on the surface of MWCNT can be summarized through FT-IR spectra as shown in Figure 5.5 (d). The O-H stretch appears as a very broad peak at 2943 cm^{-1} [49]. On the MWCNT-COOH surface, the C-O bands typical of carboxyl functional groups can be seen at 1767 cm^{-1} and 1534 cm^{-1}. The carboxylate anion stretch mode here is associated with the peak 1534 cm^{-1} [50].

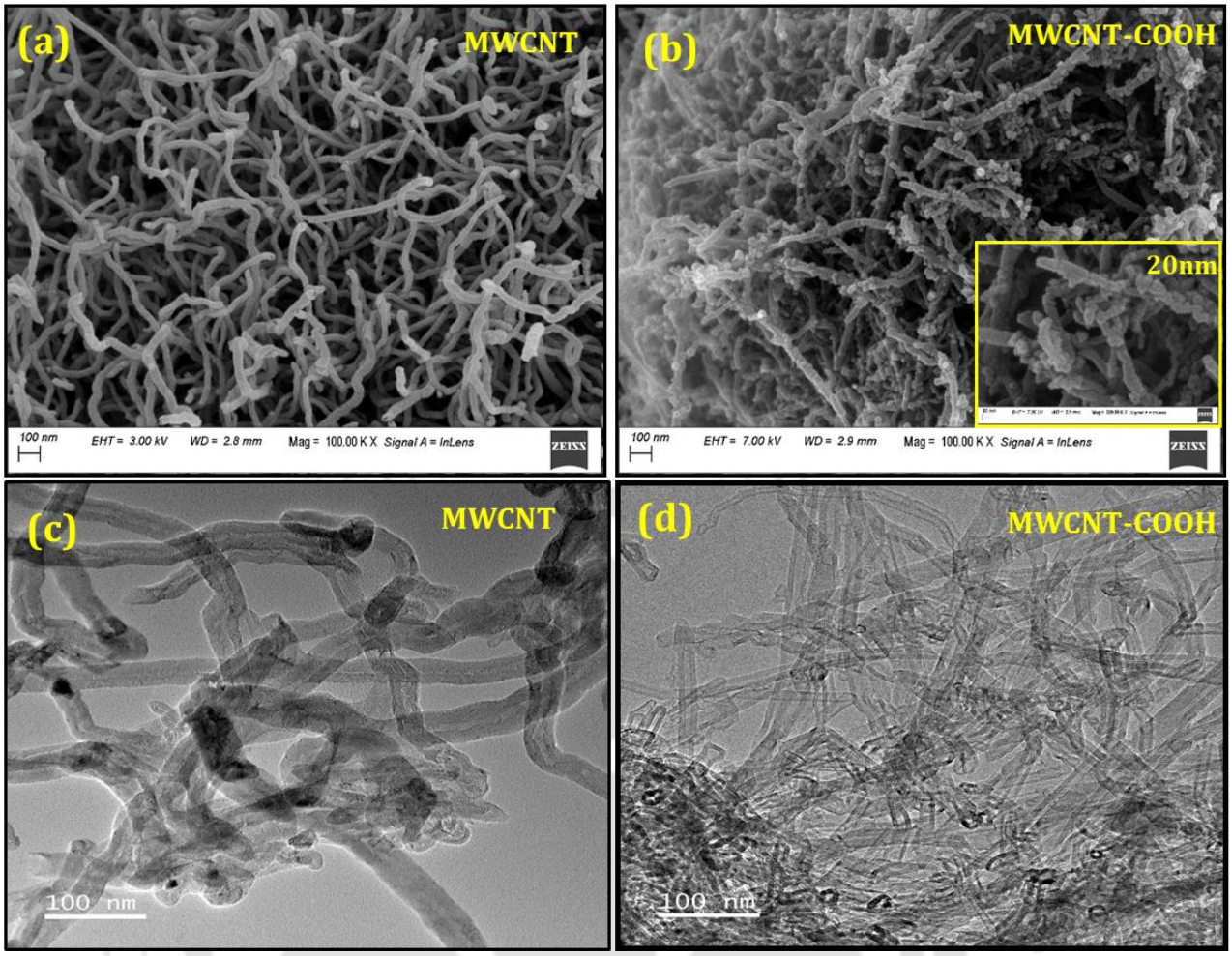

Figure 5.4. (a,b) FESEM and (b, d) FETEM images of MWCNT and MWCNT-COOH

(a)

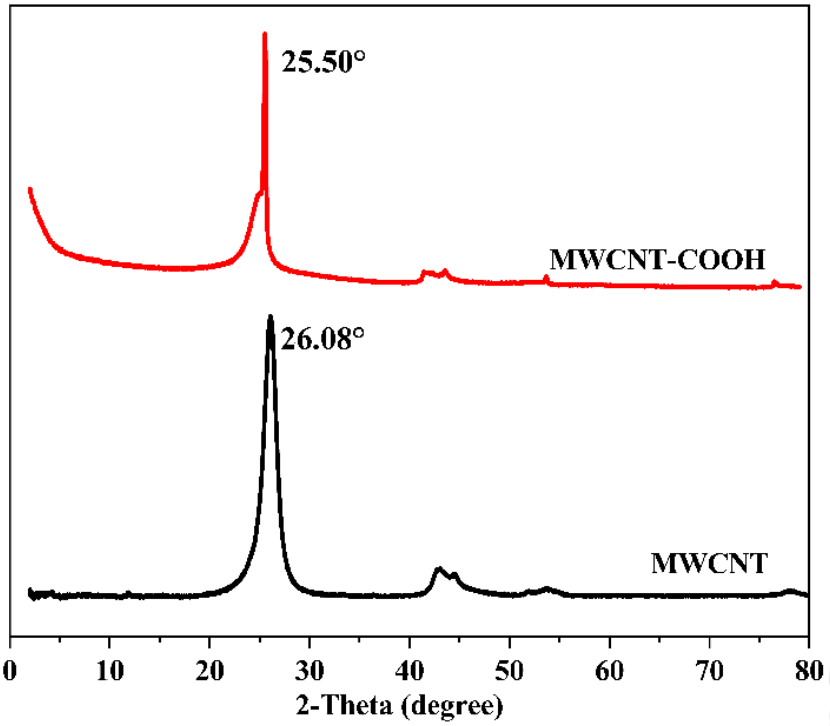

(b)

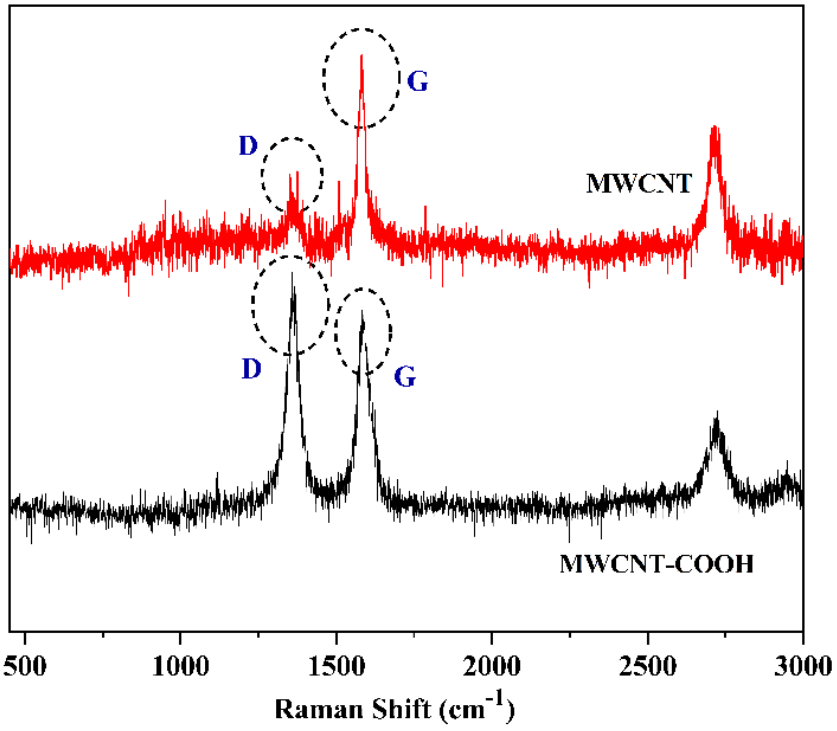

(c)

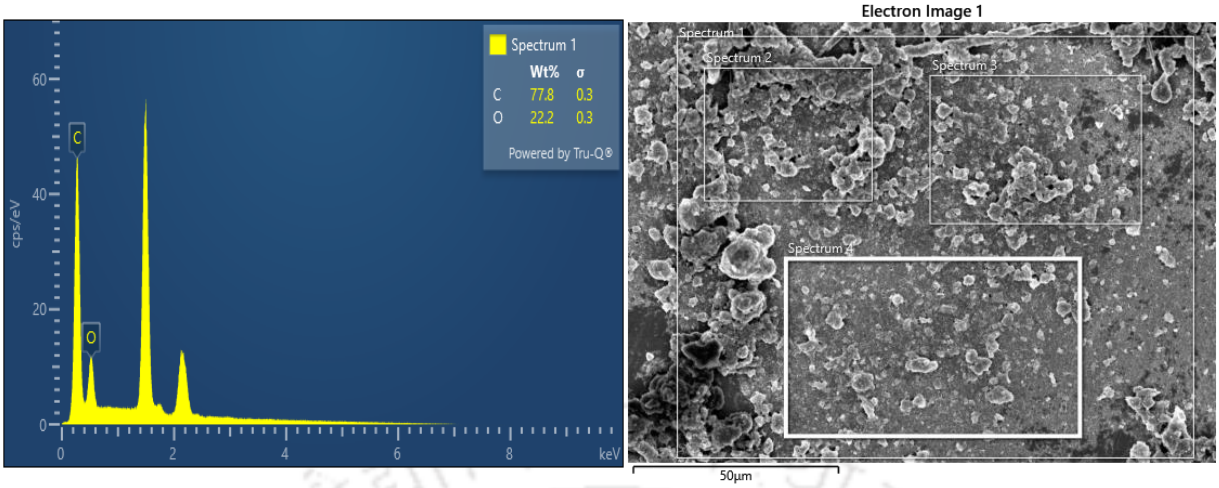

(d)

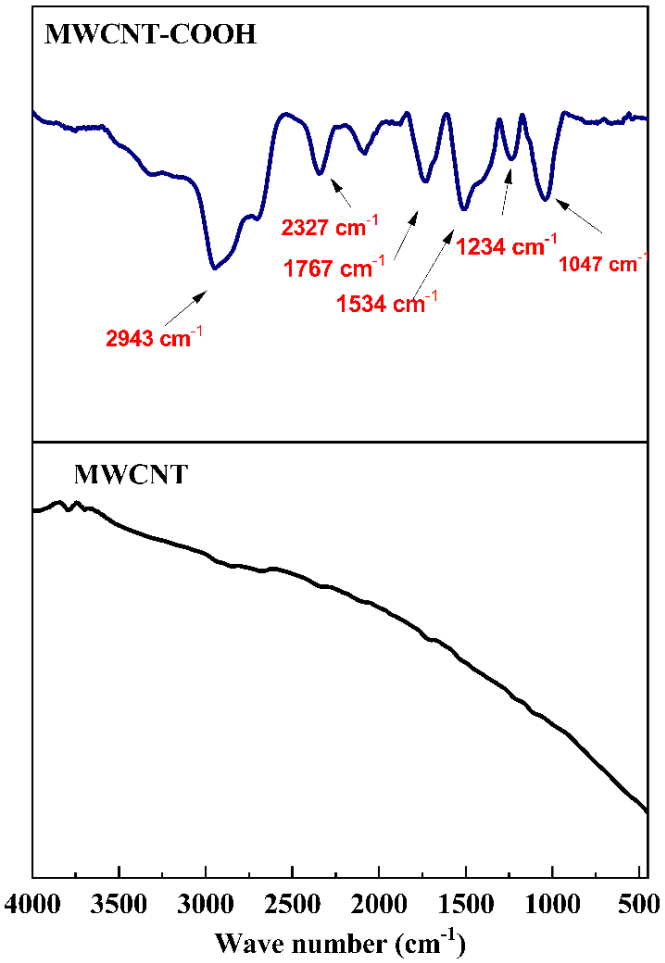

Figure 5.5. Characterization methods of MWCNT and f-MWCNT nanoparticles (a) XRD, (b) Raman, (c) EDX and (d) FT-IR

5.3.2 Thermophysical Properties of Nanofluid

5.3.2.1 Density, Viscosity and Specific Heat of Nanofluids and NADES

Density of the prepared nanofluids (NFs and f-NFs) and NADES values are displayed in Figure 5.6 (a) and 5.6 (b). Values were measured at temperatures up to 85 °C. Figure 5.6 implies that as the temperature increases the density of the samples decreases. There is little variation in the density values with increase in the nanofluid concentrations. It is clearly seen that there is no density variation after addition of nanoparticle concentration for both MWCNT and f-MWCNT. Similar density trend was observed in our previous work [28] and the literature Tao et al.[51]. Here the molecules within the fluid experience faster movement, leading to reduced intermolecular attraction. Consequently, the volume of the fluid expands, resulting in an increase in the kinetic energy of the molecules. As a result, the density of the fluid decreases. The density can be calculated as described by polynomial function of temperatures, given by equation 5.5.

$$\rho = \sum_{i=0}^{2} a_i T^i(K) \qquad \textbf{(5.5)}$$

Where, ρ is in kg/m^3

The viscosity of nanofluids and NADES has been reported in the Figure 5.6 (c) and 5.6 (d). Viscosity of all nanofluids and NADES has done at a constant shear rate 50 s^{-1}. It can be noted that the viscosity of nanofluids ranges from higher to lower values over a wide range of temperature. However, increasing the concentrations of the nanofluids leads to a decrease in viscosity as compared to NADES, which is reflected in Figures 5.6 (c) and 5.6 (d). The values are good agreement with the reported work of Santis et al. [52]. The increase in temperature leads to heigher thermal movement among molecules, which in turn enhances Brownian motion and weakens the intermolecular bonds, causing a decrease in viscosity [53]. Nevertheless, the introduction of a small quantity of functionalized nanoparticles into the base

fluid effectively reduces its viscosity. The temperature dependant viscosity of nanofluids are well fitted with Vogel–Fulcher–Tammann (VFT) equation[54, 55], given by

$$\eta = \eta_O exp\left(\frac{k}{T-T_V}\right) \quad \textbf{(5.6)}$$

Here, η is the viscosity at temperature T, T_V is the characteristic temperature and η_O is the reference viscosity and k is represent structural strength of the system, a constant value. The VFT curve and the parameters in the equation are reported in the Figure 5.6 (c) and 5.6 (d) and table 5.3. The viscosity graph was seen to follow the VFT model.

The molar isobaric heat capacity of NFs and f-NFs has been measured in the temperature range of 35 °C to 200 °C, as displayed in Figures 5.6 (e) and 5.6 (f). It reveals the higher specific heat of nanoparticles containing NADES compared to the base fluid. The specific heat of NF 9 showed higher values, followed by NF 8 and NF 7. A similar trend was observed for f-NFs as well. However, the addition of functionalized nanoparticles, MWCNT-COOH, enhanced the specific heat at higher temperatures, as can be seen in Figure 5.6 (f). This is due to the fact that at higher temperatures, the system gains more kinetic energy, and as a result, molecules are free to move, vibrate, rotate, and translate, which increases internal energy. Additionally, greater the specific surface area of the nanoparticles, greater is the surface energy of the system capacity. This increases the thermal resistance between nanoparticles and surrounding liquid molecules. Many researchers claim that the specific heat of nanofluid decreases with an increase in volume concentration [56, 57]. According to Zhou and Ni [58] , the specific heat of an Al_2O_3/Water nanofluid reduced by 21% and 45%, respectively, with an increase in nanoparticle volume percentage from 0 to 25%.

(a)

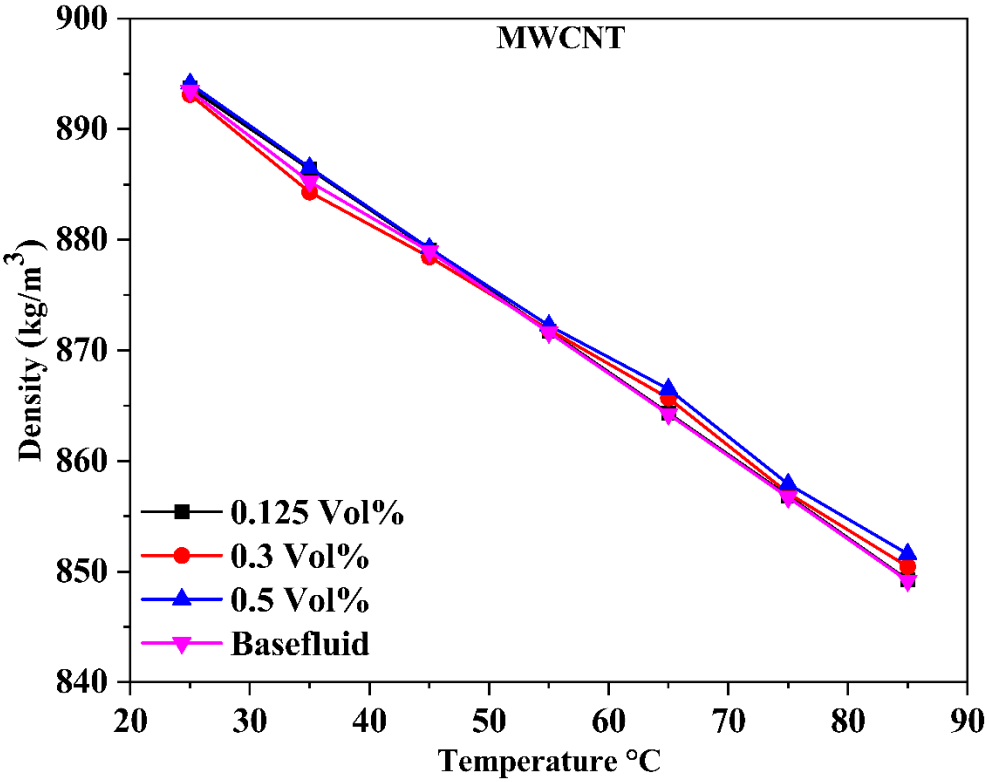

(b)

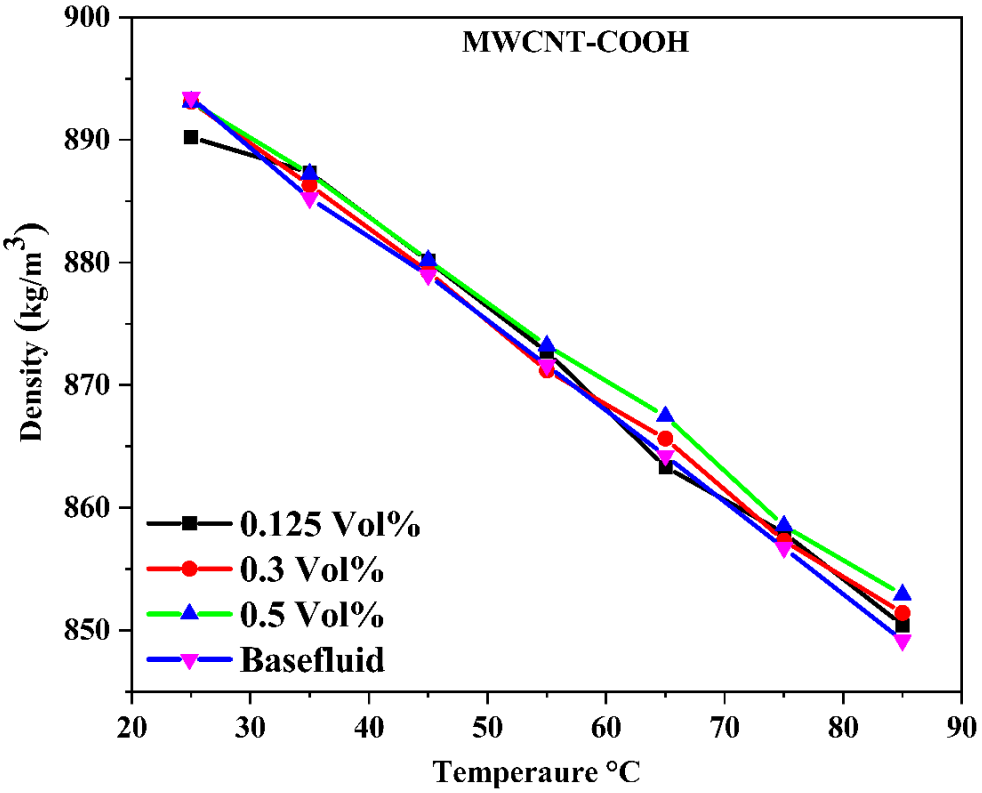

(c)

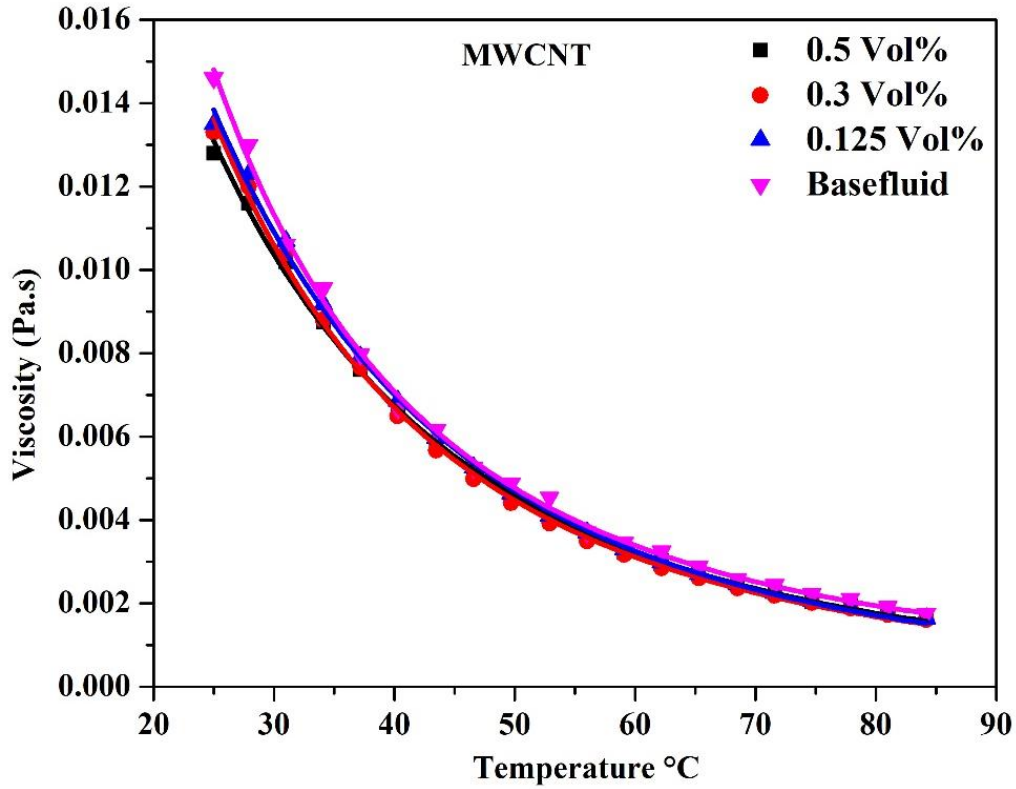

(d)

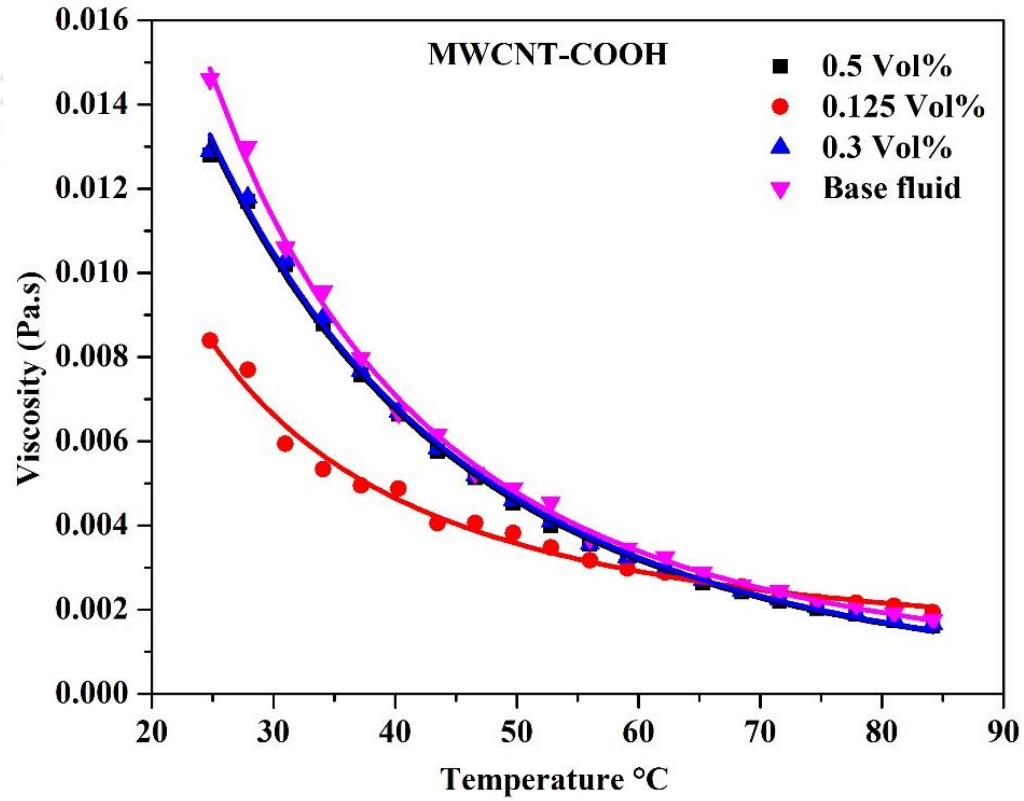

(e)

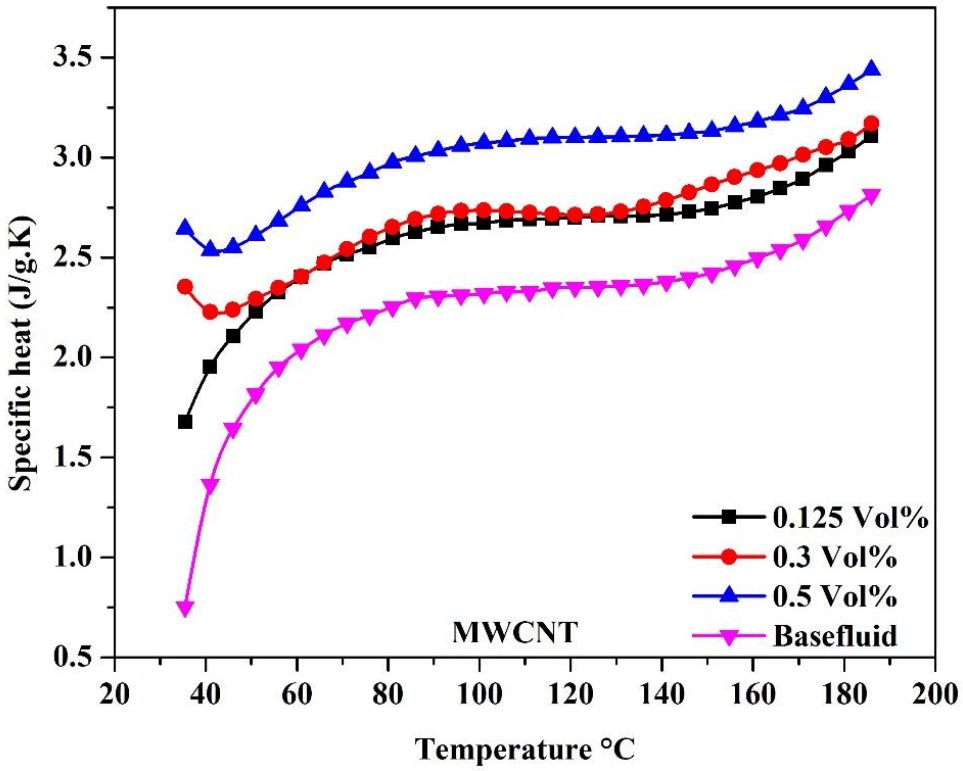

(f)

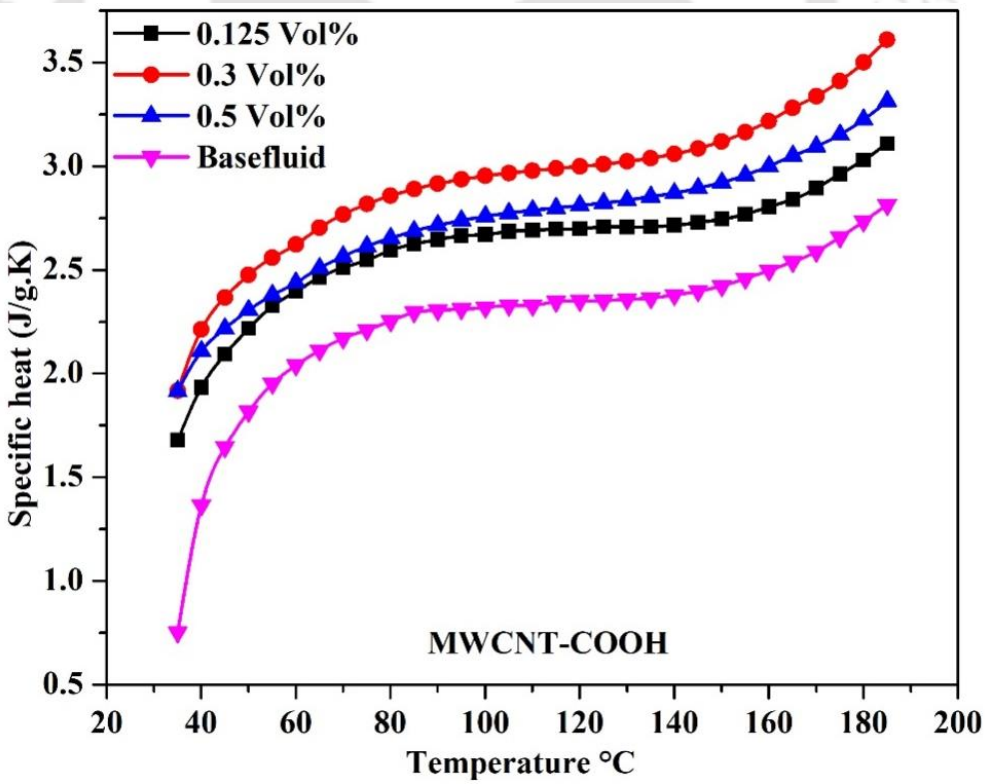

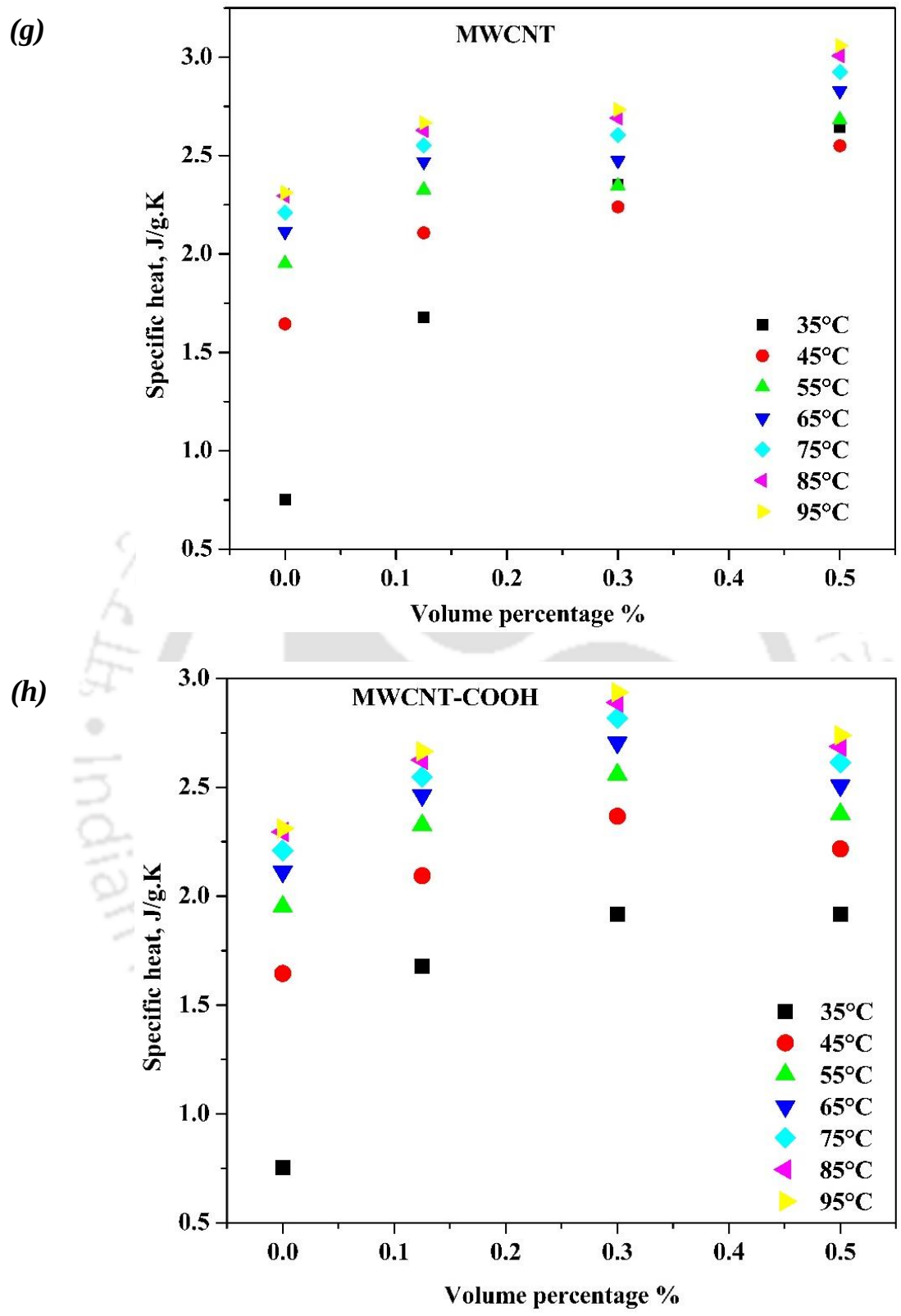

Figure 5.6. (a,b) Density, (c,d) Viscosity with VFT fitting and (e,f) specific heat with variation of temperatures and volume fractions (g,h) of nanofluids and NADES

Table 5.3. Parameters of the VFT fit of temperature dependence viscosity (Pa.s)

Systems	η_o	k	T_V	R
NADES	5.88×10^{-7}	2134.52	-188.301	0.99794
NF7	1.19	1790.19	-166.37	0.99784
NF8	5.84	1154.65	-123.90	0.99824
NF9	3.28×10^{-6}	1431.51	-147.656	0.99843
f-NF7	5.86×10^{-7}	2156.99	-190.290	0.99779
f-NF8	3.08×10^{-7}	692.03	-87.255	0.99756
f-NF9	5.87×10^{-7}	141.29	-28.288	0.98685

5.3.2.2 Thermal Conductivity of Nanofluid and NADES

The thermal conductivity data were obtained at a higher temperature range of 50 °C for all volume fractions of nanofluids. Figure 5.7 (a) and 5.7 (b) depicts the fact that the thermal conductivity of nanofluids increases as the temperature rises up to 50 °C. Maximum enhancement 40.93% and 108.05% were observed when MWCNT and MWCNT-COOH nanoparticles were dispersed into NADES. It can be noted that MWCNT-COOH/NADES nanofluids (f-NF7, f-NF8 and f-NF9) has higher thermal conductivity as compared to MWCNT/NADES nanofluid (NF7, NF8 and NF9). This is due to the stable non-covalent interactions established between MWCNT-COOH particles and the base fluid NADES. Further, the nanoparticle volume concentration attributed to the enhancement of thermal conductivity which can be seen in Figures 5.7 (c) and 5.7 (d). As the volume fraction increases, the number of nanotubes in the fluid increases, thus increasing the surface-to-volume ratio, and particles collide. Thus thermal conductivity of the nanofluid increases. On the other hand, our result has good agreement with the literature of Soltanimehr [59]. It can be seen that thermal conductivity of f-NFs (MWCNT-COOH/NADES) has shown better thermal conductivity as

compared to the NFs (MWCNT/NADES). As the temperature rises, molecules gain more thermal energy. As a result, free movement of molecules increases the distance between two molecules, which causes a higher heat transfer rate. Brownian motion makes it possible for nanoparticles to collide due to their ability to come into contact with one another. The mechanisms of clustering and interfacial stacking, in addition to Brownian motion, aid in the improvement of heat transfer. Different models, including Bhattacharya et al. [60] model, K-K model [61], Xuan model [62] predict the influence of the Brownian motion and aggregation of the nanoparticles on heat transfer rate.

The experimental results has been compared to the existing theoretical model Hamilton-Crossover (HC) model [63], given by equation (9). The results indicated that the measured thermal conductivities exceed those predicted by the Hamilton Crosser model, shown in Figure 5.7 (e) and 5.7 (f). When the nanoparticles are uniformly dispersed into the solvent, this form a solid like layer at interface which transports heat from solid wall to nearest liquid layer [64]. But HC model does not consider this interaction for predicting the thermal conductivity of nanofluid. Another problem with the HC model is that the shape factor does not take into account the orders-of-magnitude rise in the surface area to volume ratio that comes with decreasing particle size into the mono-crystalline zone [65, 66]. This shows that the current models are not good enough to explain how heat moves through the nanofluid system because they only look at the size and shape of the particles in suspension and the differences in how well particles and fluids conduct heat.

Thermal conductivity ratio and thermal conductivity enhancement has been defined as

$$k_r = \frac{k_{nf}}{k_{bf}} \quad \textbf{(5.7)}$$

$$TCE = \frac{k_{nf} - k_{bf}}{k_{bf}} \times 100 \quad \textbf{(5.8)}$$

The Hamilton Crosser model is defined as

$$k_r = \frac{k_{nf}}{k_{bf}} = \frac{k_p+(n-1)k_{bf}-(n-1)\phi(k_{bf}-k_p)}{k_p+(n-1)k_{bf}+\phi(k_{bf}-k_p)} \quad \textbf{(5.9)}$$

$$n = \frac{3}{\psi} \quad \textbf{(5.10)}$$

Here, the thermal conductivities of the base fluid, nanofluid and nanoparticles are denoted by k_{bf}, k_{nf} and k_p respectively. ϕ is the volume fraction of the nanofluid, and n is the empirical shape factor (6 for cylinder and 3 for sphere).

(a)

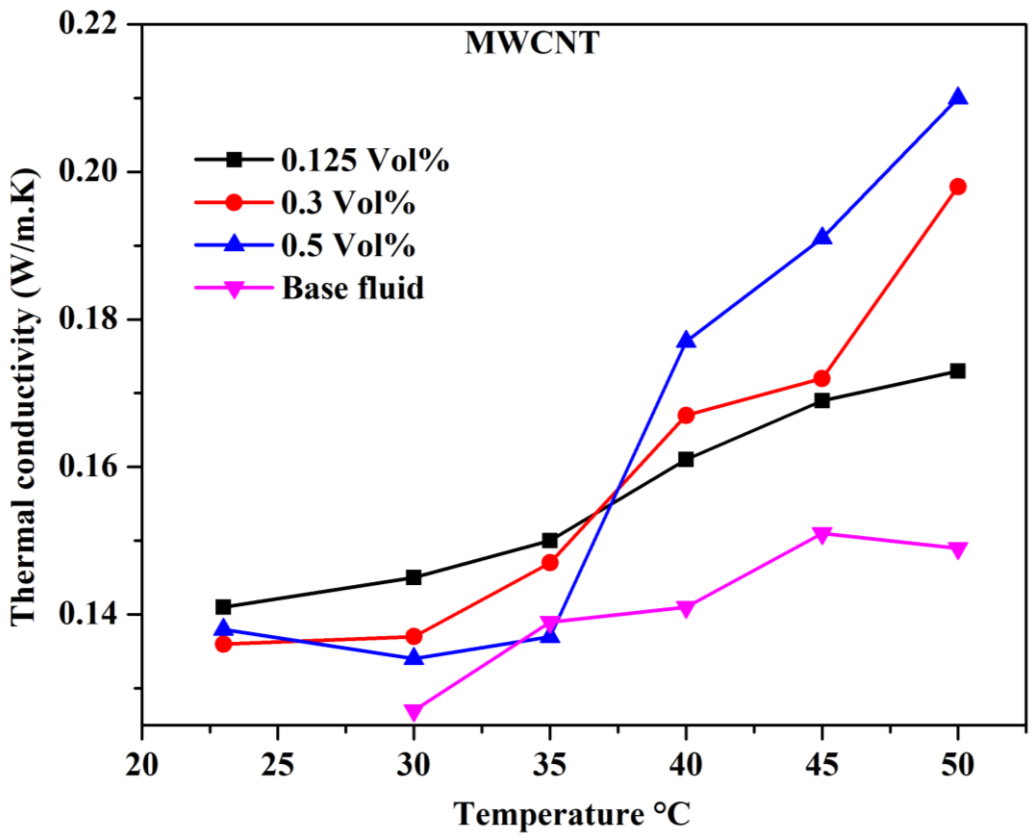

(b)

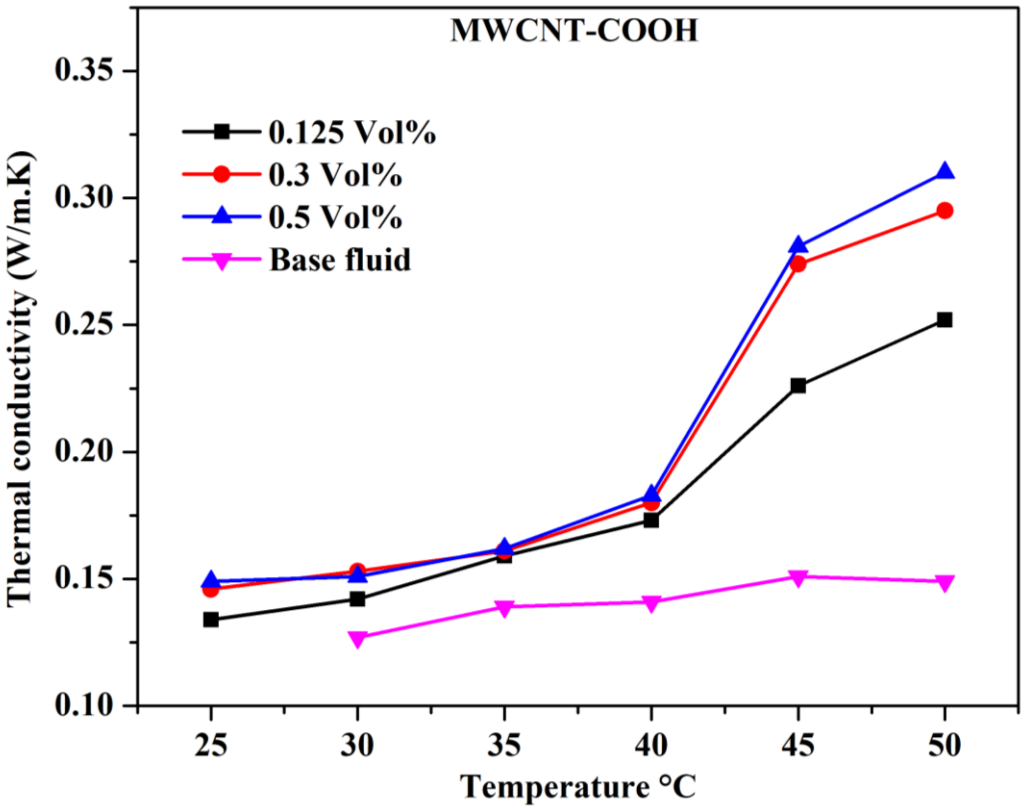

(c)

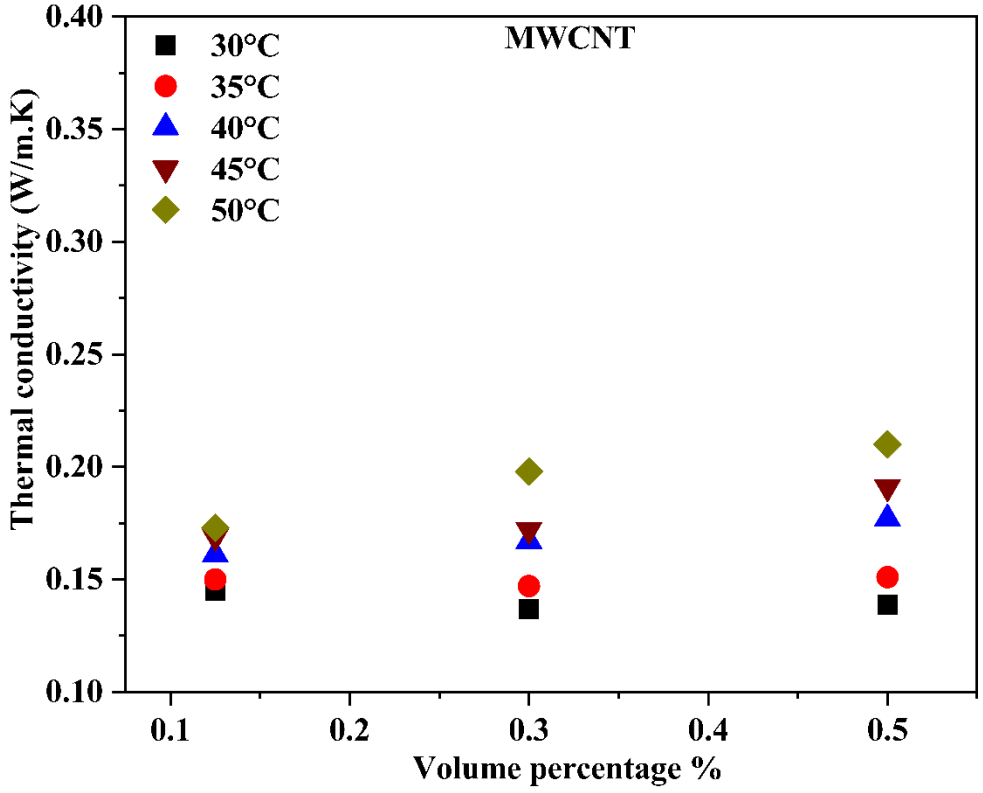

(d)

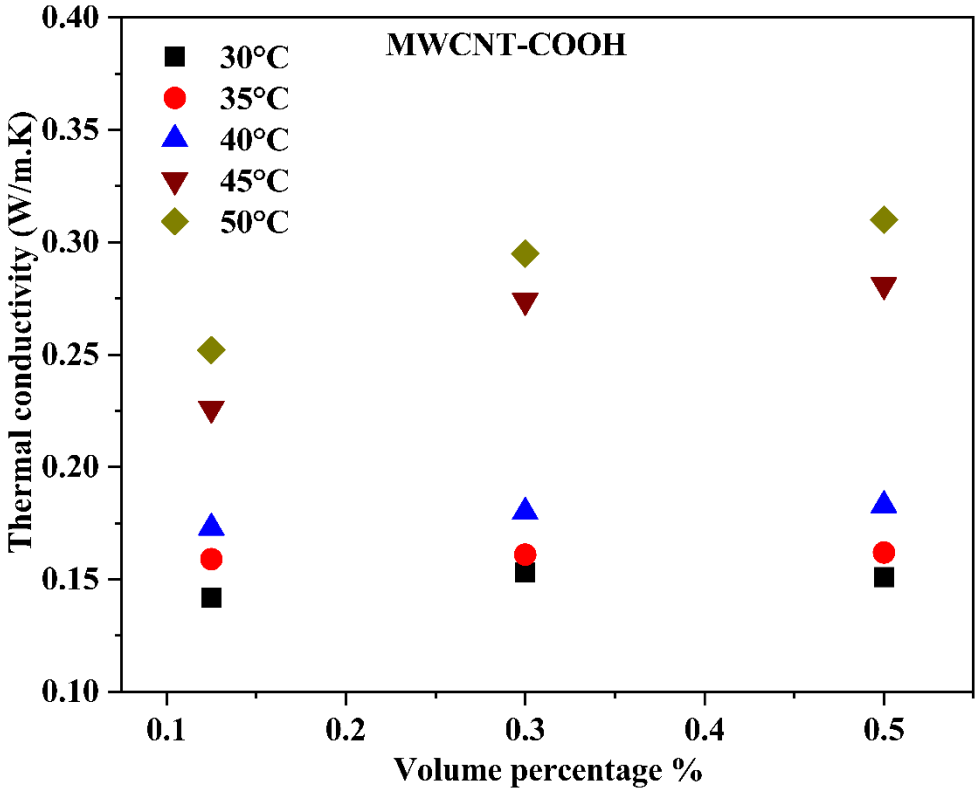

(e)

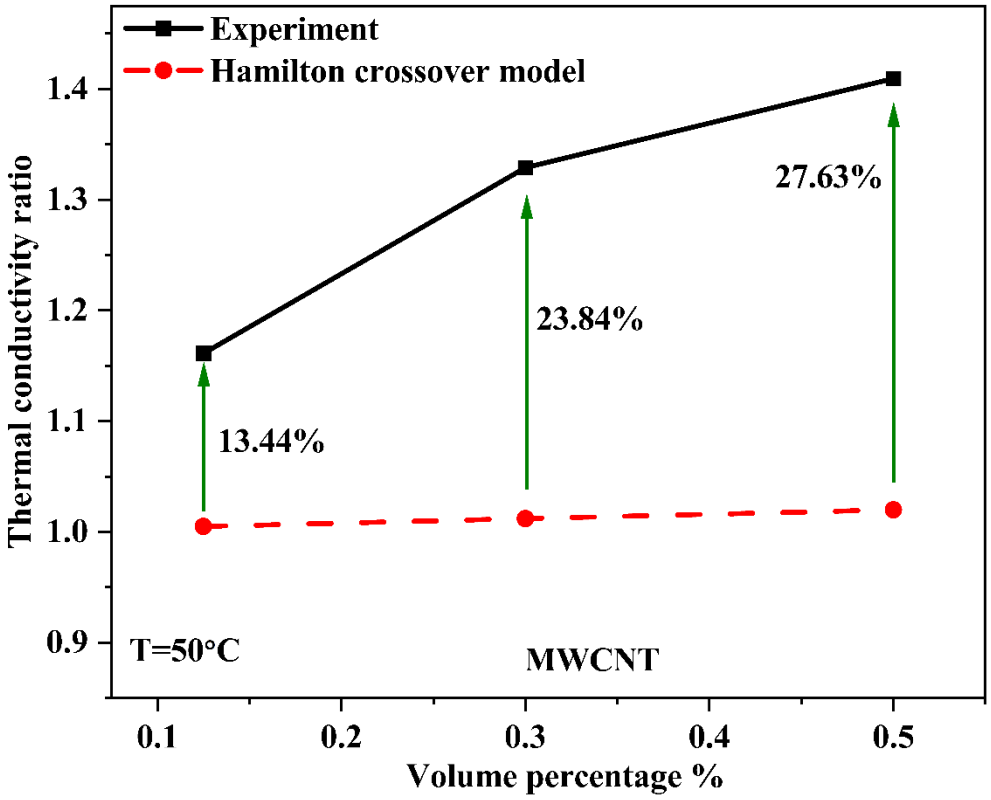

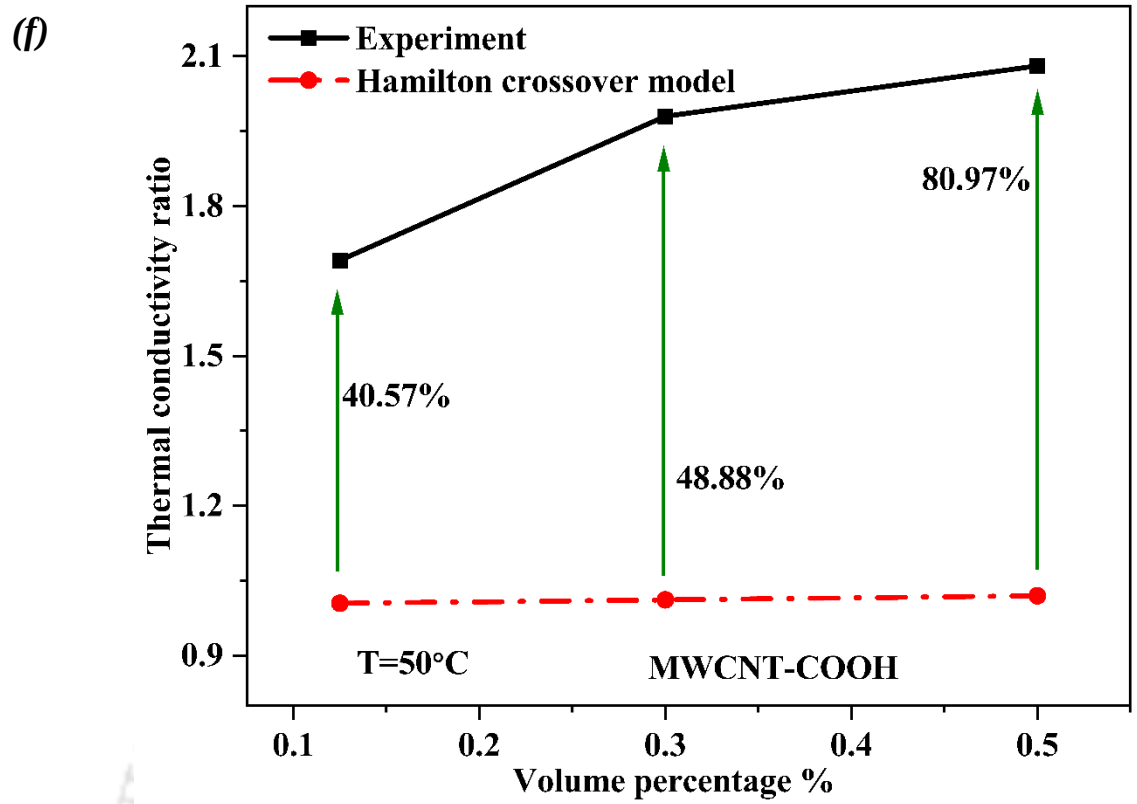

Figure 5.7 Thermal conductivity of NADES and nanofluids (a) MWCNT/NADES (b) MWCNT-COOH/NADES, volume fractions (c) MWCNT/NADES, (d) MWCNT-COOH/NADES and Thermal conductivity ratio (e) MWCNT/NADES and (f) MWCNT-COOH/NADES

5.3.3 Thermal Stability Analysis

5.3.3.1 Visual Observation and Zeta Potential Method

The large surface-to-volume ratio of carbon nanotubes in the fluid leads to strong van der Waal interactions between the nanoparticles, which move towards agglomeration. Various steps have been taken to investigate the stability of the nanofluid. At the very first step, mechanical stirring and thereafter ultra-sonication have been adopted for the preparation of nanofluid for long-term stability. The prepared nanofluid was then kept for 2 months to observe any settlement. Figure 5.8 (a) shows a visual observation of nanofluids just after sonication and after 2 months. It was seen that settlement occurs in MWCNT/NADES nanofluids whereas lesser effect is observed in MWCNT-COOH/NADES nanofluid.

The assessment of zeta potential delved deeper into the examination of nanofluid stability and dispersion behaviour. Figure 5.8 (b) shows the zeta potential values of MWCNT (NF7, NF8, NF9) and MWCNT-COOH (f-NF7, f-NF8, f-NF9) nanoparticle-based nanofluids. Results showed that f-NF7, f-NF8, and f-NF9 have good zeta potential values as compared to the non-functionalized MWCNT nanoparticles. Among all these, f-NF7 and f-NF8 has shown better stability (-270 mV & -91 mV). The electro-kinetic potential observation served as confirmation for both the dispersion quality and stability of the nanofluid [67, 68]. When nanoparticles approach one another, the dominance of the van der Waals force overpowers other forces, leading to the aggregation of nanoparticles. This aggregation causes a reduction in the thermal conductivity of the nanofluid. The presence of a high repulsive interaction potential is vital for maintaining stability. In cases where the nanofluid possesses a relatively lower magnitude, the van der Waals force gains strength, thereby contributing to the instability of the nanofluid. In order for nanofluids to remain stable, it is imperative for repulsive forces to prevail within the solution. According to Vandsburger [69], nanofluids reach a state of near-stability when their particles have a zeta potential value of about 30 mV. Optimal stability for nanofluids is achieved when the zeta potential value is in proximity to 45 mV. The exceptional stability of a nanofluid is realised when its zeta potential value exceeds ± 60 mV. From the zeta potential analysis, it was seen that COOH-functionalized MWCNT has good dispersion behaviour and good stability in the base fluid NADES. This is due to the fact that COOH-modified MWCNT nanofluids can have favourable non-covalent interactions with the base fluid NADES.

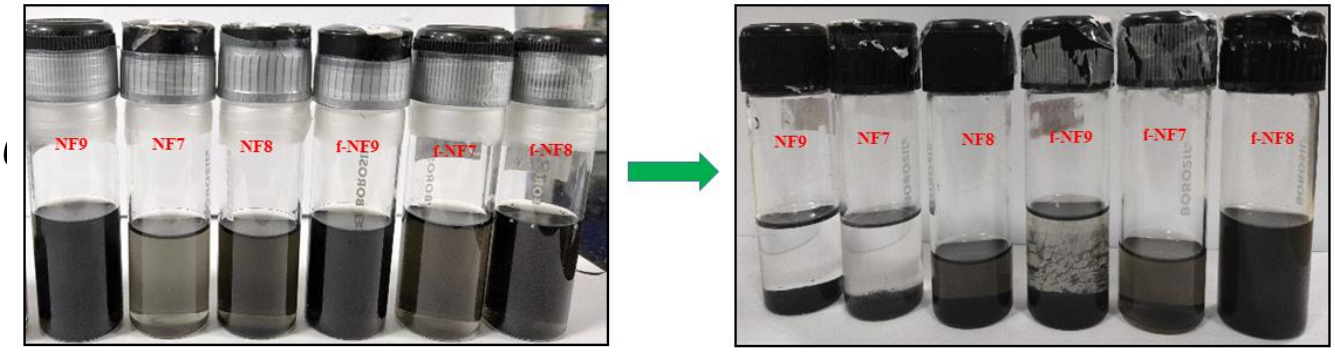

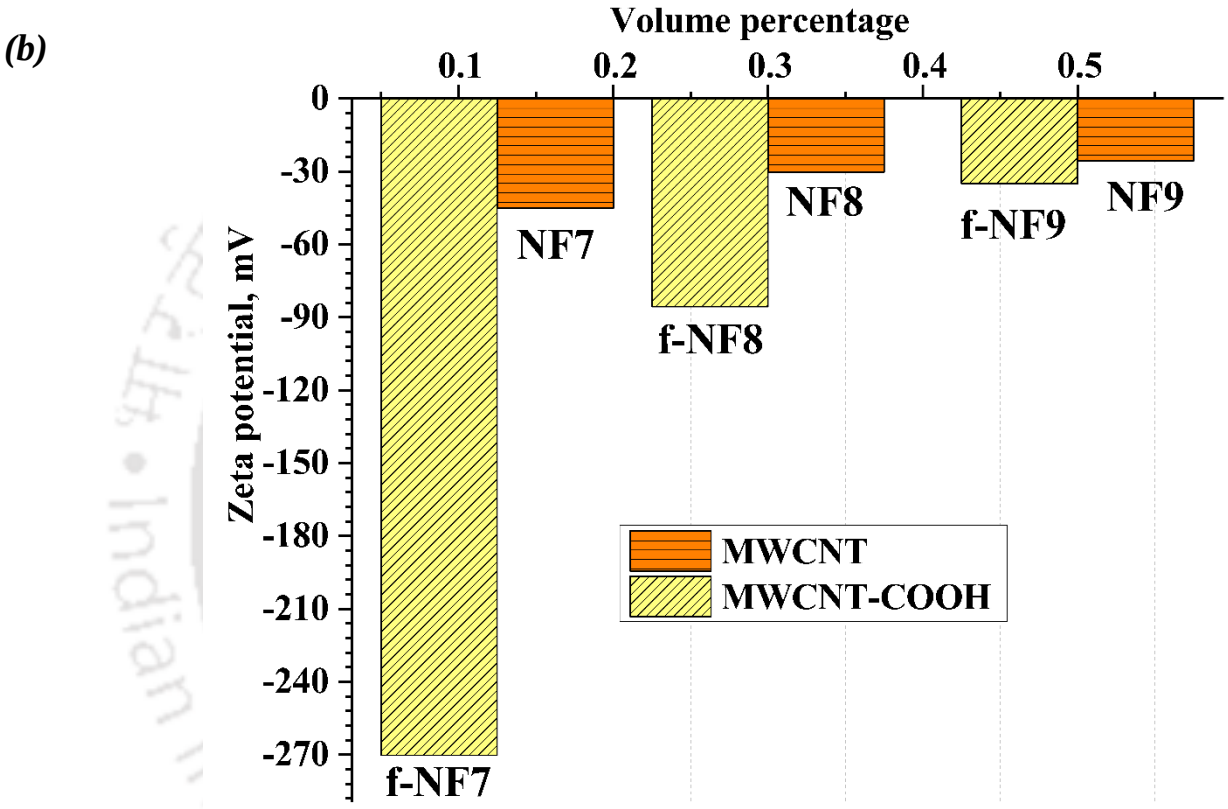

Figure 5.8. Images of nanofluids after sonication and Zeta potential values of MWCNT/NADES and MWCNT-COOH/NADES nanofluids

5.3.4 Forced Convection Experiment

With a constant heat flow of 12484.076 W/m^2, three different Reynolds numbers were used in the forced convection tests. Following the experimental setup, heat transfer coefficients were calculated for the laminar condition within each tube test segment. In Figure 5.9 (a), the axial

evolution of the heat transfer coefficient is depicted for the base fluid at three distinct Reynolds numbers. It was observed that the convective heat transfer coefficient rises as the Reynolds number grows. The maximum heat transfer coefficient is observed at N_{re} = 1745, followed by a non-linear decrease along the axial distance. A similar trend has been observed in our previous work when conventional fluid was used [31]. This trend can be rationalised by considering that an elevated Reynolds number results in a thinner boundary layer, subsequently enhancing the heat transfer rate. The local Nusselt number was calculted and is presented in Figure 5.9 (b).

(a)

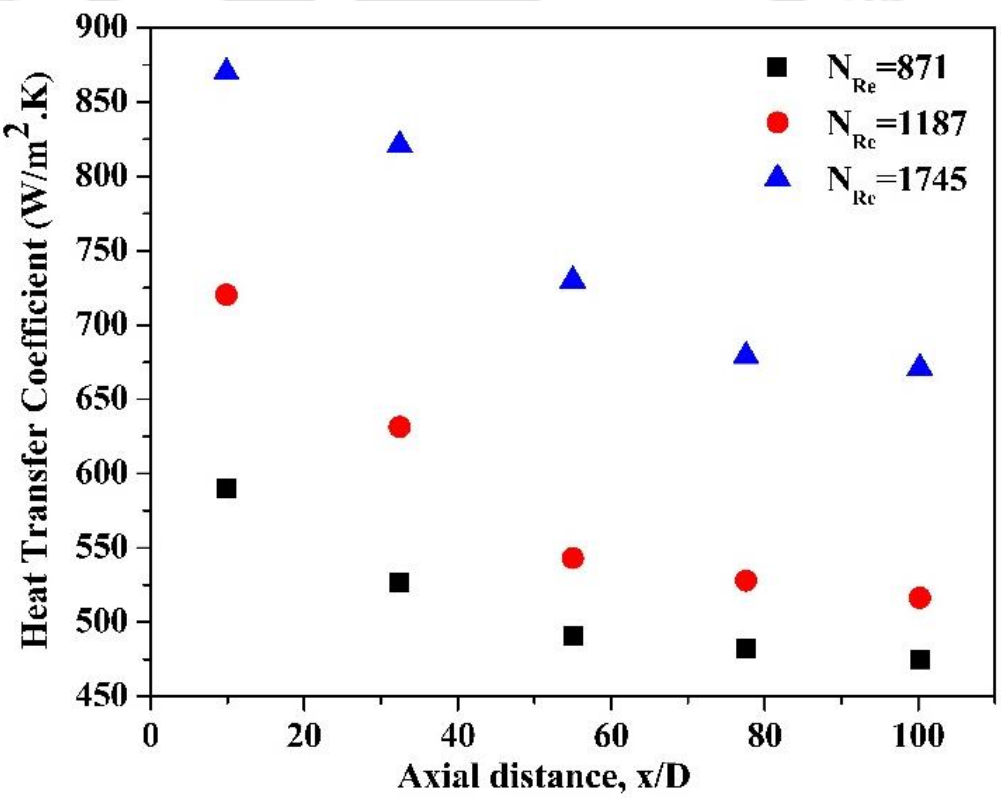

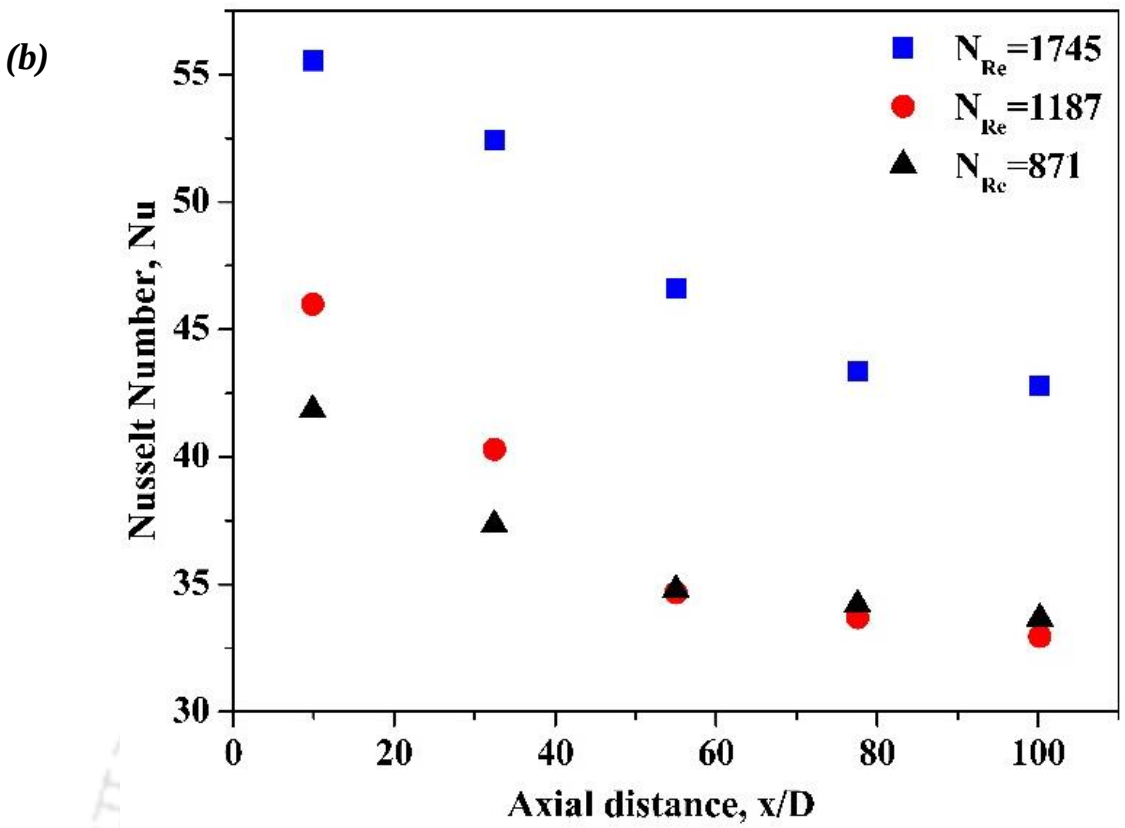

Figure 5.9 Heat transfer coefficient and Nusselt number of NADES along with the axial distance of the tube

In contrast to heat transfer that occurs through conduction, a higher Reynolds number increases the amount of heat transfer that results from fluid motion. In Figure 5.10 (a), the influence of carbon nanotube concentrations on the heat transfer coefficient along the axial length of the tube is illustrated for Reynolds numbers N_{re}=1745, N_{re}=1181, and N_{re}=871, respectively. The forced convection experiment was carried out with 0.125 vol% of MWCNT-COOH nanoparticles dispersed in the base fluid NADES, as it has shown excellent stability in zeta potential experiments. Maximum enhancement was observed at the entrance of the tube compared to the base solvent, NADES. A maximum 27.70% enhancement has been observed in the heat transfer coefficient at the entrance of the tube at Reynolds number 1864, followed by 43.48% and 47.75% enhancement for Reynolds numbers 1217 and 810, respectively. Potential justifications for this improvement include factors like the size of

nanoparticles and the effects of Brownian motion on particles. These factors contribute to the reduction of the particle's boundary layer thickness and enhance the mixing effect, as indicated in references [70, 71]. Local Nusselt number was calculated for the nanofluids, and the results are depicted in Figure 5.10 (b) alongside data for the base fluid. Owing to the notably elevated thermal conductivity and specific heat of the nanofluids in comparison to the base fluid, the Nusselt number exhibited a more rapid increase. In both the case of the base fluid and the nanofluids, during the process of heat transfer from the pipe's surface to the fluid via conduction, the boundary layer thickness diminishes significantly. This phenomenon is linked to the heightened heat transfer coefficient within the inlet section [72]. The observed increase in boundary layer thickness during fluid motion causes a decline in the heat transfer coefficient along the pipe's length. Additionally, the entrance area has the highest concentration of nanoparticles, which causes viscosity and heat conductivity to be distributed unevenly. Due to the uneven distribution, the thermal barrier layer's thickness is reduced, which increases the heat transfer coefficient in the entrance area. According to research done in the past [73, 74], A higher heat transfer coefficient is also affected by the mixing of particles close to the wall, leading to an increase in thermal conductivity and decrease in the thickness of the boundary layer. It also involoves a delay in the formation of the boundary layer.

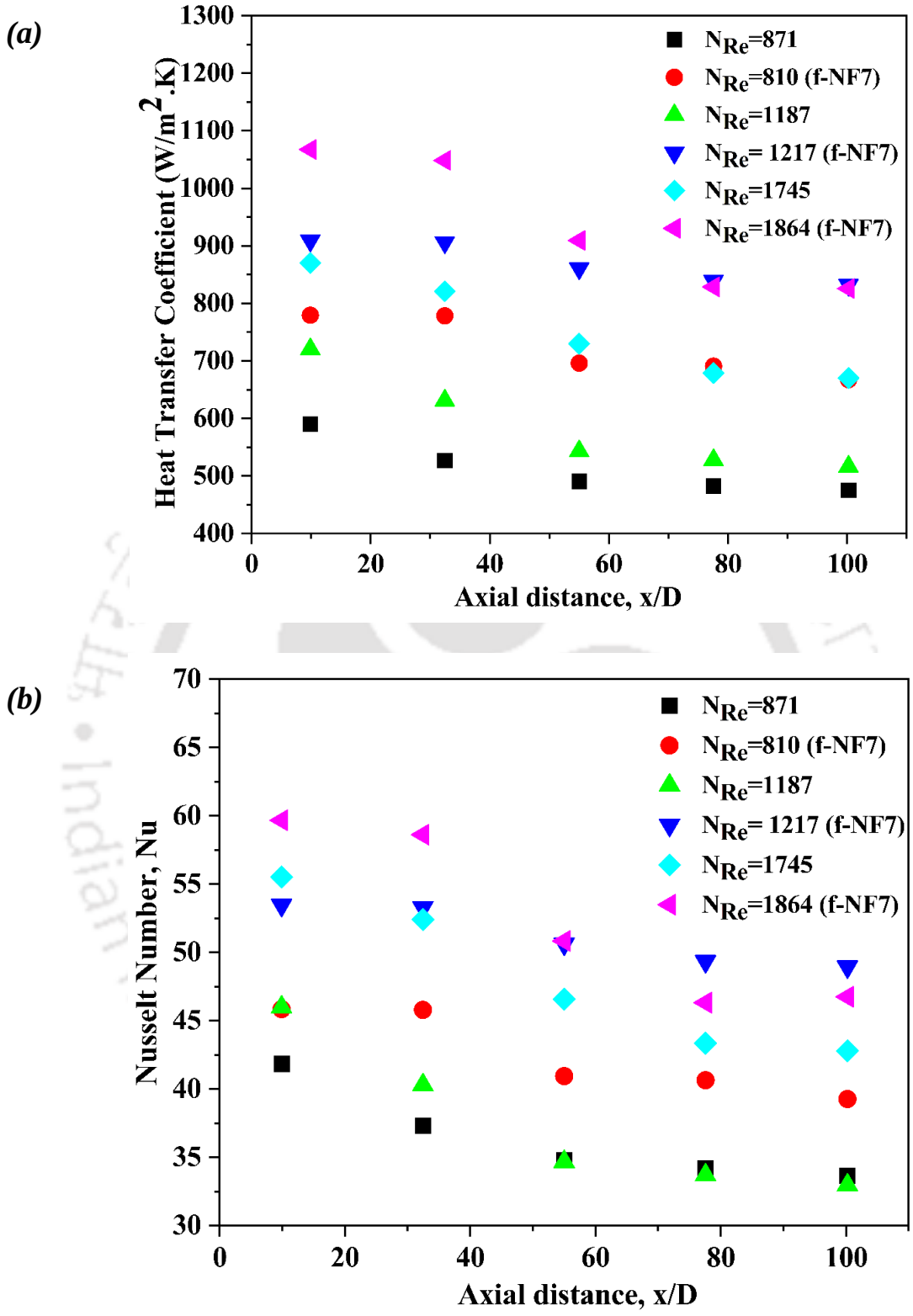

Figure 5.10. Comparison of heat transfer coefficient and Nusselt number of base fluid (NADES) and nanofluid (NF) at different Reynolds numbers

Figure 5.11 (a) and 5.11 (b) illustrate the profiles of wall temperature and fluid temperature for both the base fluid and the corresponding nanofluids. It was found that both the base fluid and the nanofluids have higher inner wall temperatures at lower Reynolds numbers. The wall temperatures of the nanofluids are lower than those of the base fluid, and this lower temperature is increasingly prominent as the Reynolds number increases. The basic reason is the interaction of nanoparticles with the tube wall when the nanofluid travels through the tube, which makes it easier for thermal energy to be transferred from the wall to the nanofluid. As a result, the fluid's wall temperature drops. Fotukia [75] reported a similar result, observing a drop in tube wall temperature following the addition of nanoparticles to the base fluid. When a fluid first enters a pipe, it does not develop fully. This holds true even as the fluid passes over a pipe system curve, where the curve changes the fluid's velocity profile. The fluid must therefore travel a certain distance in a straight conduit in order for its full development. The Nusselt number values for the nanofluids that were determined through experiments were also compared with those found in the literature Pyarimohan et al. [76] showing a consistent pattern. In general, enhancements in convective heat transfer coefficient and Nusselt number were observed in the laminar region. The increased heat transfer coefficient was attributed to the improved thermal conductivity, as well as the thickness of the hydrodynamic boundary layer and the nanoparticle shape.

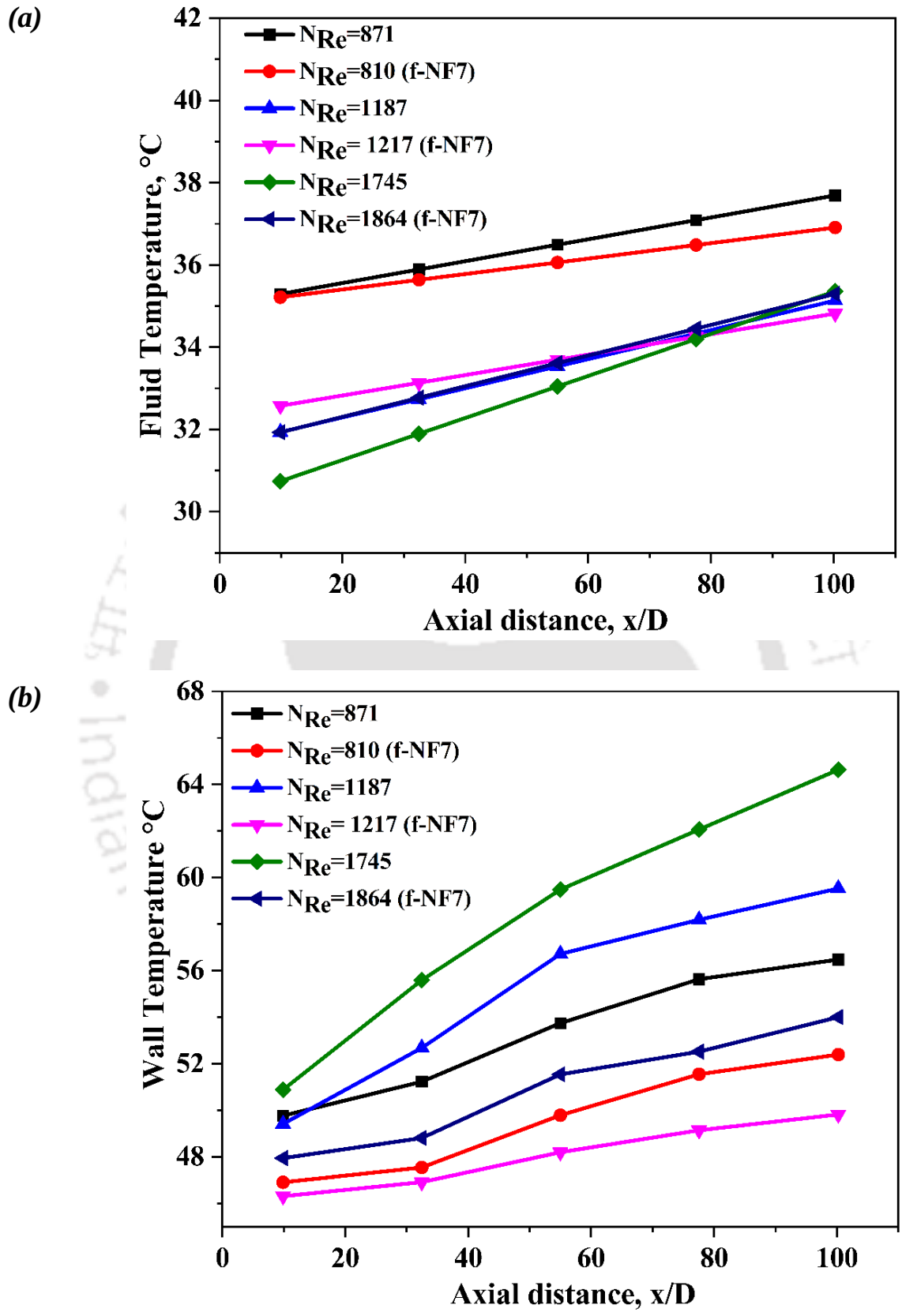

Figure 5.11. (a) Fluid temperature and (b) wall temperature of respective base fluid and nanofluid

5.3.5 Quantum Chemical Calculations

5.3.5.1 Geometry Optimization

In this investigation, the computations commenced with the geometry optimization of a simple (5,5) single-walled carbon nanotube, with its terminations saturated using ten hydrogen atoms. This model had previously been employed in our earlier research to comprehend the interactions of SWCNTs with a bio-based fluid named Cyrene (as detailed in chapter 2). The initially optimized structures of individual molecules were utilized to generate the paired configuration of the NADES/SWCNT system (as depicted in Figure 5.1).

From the optimized geometry, it is evident that the –OH groups associated with the Dl-menthol molecule experience inducement towards distinct positions on the carbon nanotube (as shown in Figure 5.1 (d)). The NADES/SWCNT pair system reveals slightly increased bond distances between NADES/SWCNT atoms. Upon introducing the studied NADES system, specifically a combination of Dl-menthol with Lauric acid (in a molar ratio of 2:1) with SWCNT, there is a slight augmentation in bond distances within the NADES. However, these increments in bond distances are of minor magnitude, indicating that the dominant interactions consist of weak van der Waals forces. The presence of a –OH and –COOH groups within the NADES is the reason for the enhancement of the extent of charge transfer within the NADES/SWCNT system. The slight change in the bond distances within the NADES system can be attributed to the weak interactions present within the hydrophobic NADES system. [77]

The optimized geometry outcomes for structure suggest a weaken interaction between NADES molecules and SWCNT. This implies that the interplay between NADES and SWCNT constitutes a physical phenomenon primarily governed by van der Waals interactions. Nevertheless, the notable interactions within the complex NADES and SWCNT system align with experimental observations, particularly concerning the zeta potential, which serves as an

indicator of dispersive nature and ensuing stability (as referenced in the experimental stability section). The primary aim of the DFT analysis within this study was to fathom the significance of functional groups that could be incorporated into CNTs or solvent molecules to enhance interactions and achieve superior dispersion. The robustness of the van der Waals (vdW) interactions within the solvent and SWCNT complex system leads to the aggregation of CNT nanoparticles, subsequently contributing to the short-term stability of nanofluids [31].

5.3.5.2 Non-Covalent Interactions present Within NADES-SWCNT System

Reduced Density Gradient (RDG) analysis was performed to determine the significance of non-covalent interactions in the base fluid-SWCNT surface interaction. RDG establishes a relationship between the real-space function and the second intrinsic value of the hessian matrix representing electron density. This analysis indicates the categories of weak interactions that exist within the system. Intermolecular interactions can be illustrated based on their strength, and nature using RDG analysis. Examining NCIs using the electron density ($\rho(r)$) and its associated scalar and vector fields can be executed. This method shares a fundamental concept with the Density Functional Theory (DFT): the electron density can be directly correlated with energy, allowing the exploration of interactions based solely on the electron density. Except for zero-order electrostatics, all contributions to the interaction energy can be associated with a deformation in ($\rho(r)$). These methodologies offer obvious advantages in terms of interpretation. They are invariant with respect to unitary transformations of molecular orbitals, generally robust, and visually observable due to their intrinsic three-dimensionality. The detailed theory of NCI and RDG [78] analysis was discussed in the appendix A.

Non-covalent interaction (NCI) plot analysis (Figure 5.12) was used to visualize non-covalent interactions and classify them as repulsive or attractive by plotting 2D scatter graphs, the magnitude of the electron density signed by the second Eigen value of the Hessian matrix

(sign(λ_2)) versus regions of very low-reduced density gradient (RDG), and 3D colour graphs of RDG. These iso-surfaces illustrate both favourable and adverse interactions between unbound atoms, as indicated by the sign of the second Hessian Eigen value of the electron density (λ_2). The colorimetric scale provides a quantitative representation of the interaction intensities (Figure 5.12). van der Waals (vdW) interactions, whose values are close to zero regardless of the direction of the horizontal axis in the 2D scatter plot, are depicted in green. Strong attractions, such as hydrogen bonds, electrostatic interactions, and covalent bonds, are indicated in blue, which corresponds to the small negative values on the horizontal ordinate of the 2D scatter plot. Strong repulsive interactions, such as steric effects in ring and cage, are shown in red and correspond to large positive values on the ordinate axis [79].

As shown in Figure 5.12, when the NADES system was exposed on the surface of SWCNT, several spikes appeared in the low charge density region of the NADES/SWCNT complexes, indicating that weak vdW interactions dominate the investigated complex. van der Waals interaction between the SWCNT surface and NADES is mediated by X...π, where X represents the C, H, and O atoms of NADES. In a previous investigation, where van der Waals interactions dominated intermolecular forces in the reactive Cyrene/SWCNT complex, a similar pattern of results was observed. The red region indicates the presence of a steric hindrance within the interior core of the SWCNT structure, which is consistent with the findings of earlier investigations on carbon-based nanomaterials. In addition, as seen in Figure 5.12 (b), the blue colour in the 2D scatter plots represents the interactions between the hydroxyl and carboxyl groups present with the NADES. The structure with the lowest energy consists of parallel stacks of SWCNT, with the oxygen of the carboxylic acid positioned directly over the menthol molecule's attack site. The presence of weak vdW interaction within the NADES/SWCNT system increases with a decrease in electrostatic interactions within the NADES complex, which is broadly visible and consistent with geometry optimization. van der

Waals forces govern the interactions between surfaces and NADESs. This result is in excellent agreement with the outcomes of experimental investigations. In general, the NCI interaction plots indicate that attractive and repulsive interactions are roughly balanced, with a significant preference for short range (vdW) attractive interactions [42].

According to NCI analysis, the distinct character of interactions between NADES/SWCNT complex systems increases the interaction strength of NADES molecules on SWCNT surfaces, resulting in a stable complex system. However, the study points to the functionalization of both the solvent and the SWCNT surface, which will increase the nanofluid's stability and make it a viable candidate for various thermal energy systems. The functionalization of CNTs with carboxylic acids, which is capable of enhancing the nanofluid system's stability, has been incorporated into the scheme of the experiment.

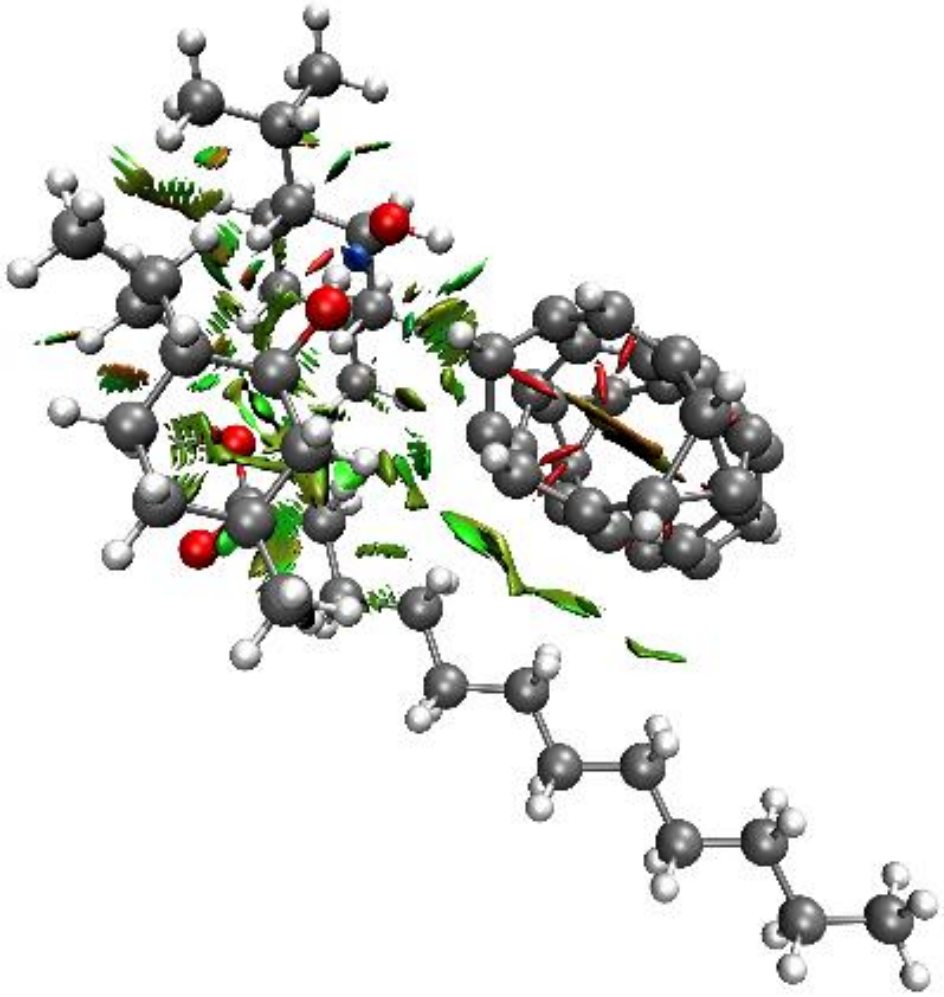

(a)

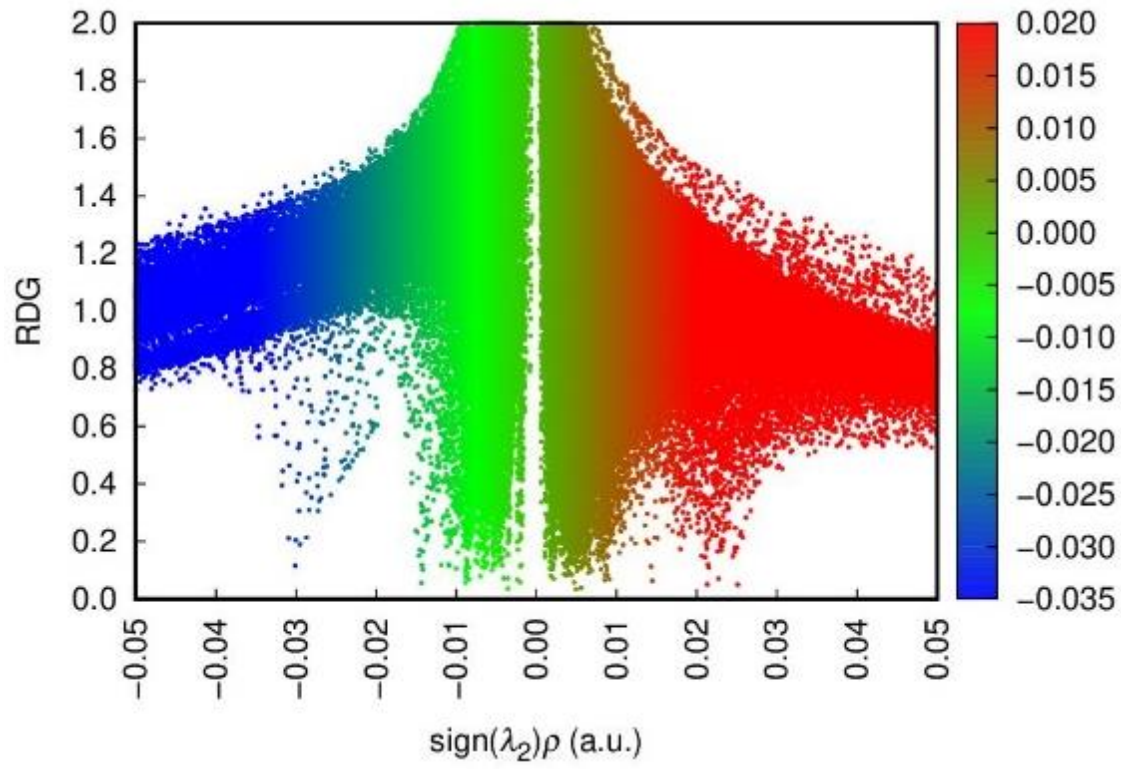

(b)

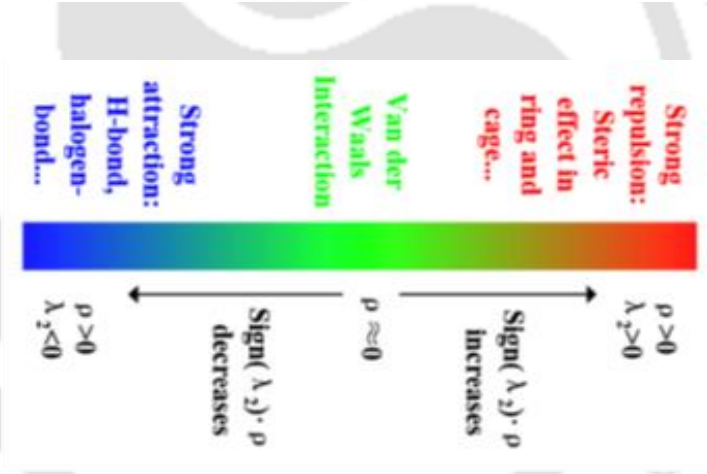

Figure 5.12 RDG isosurface and scatter graph of RDG for SWCNT-NADES complex system

In the subsequent section, the Quantum Theory of Atoms in Molecules (QTAIM) analysis was employed to gain further insights into the nature of interactions within the studied SWCNT/NADES systems [80]. QTAIM offers an effective method for investigating intermolecular interactions. The electron density at bond critical points (BCPs), denoted as

ρ_{BCP}, serves as a valuable parameter for characterizing the strength of intermolecular interactions. Additionally, the Laplacian of the electron density at BCP ($\nabla^2\rho$) indicates areas of charge concentration (negative sign) and charge depletion (positive sign) in a chemical bond. The QTAIM approach was utilized to comprehend the type and potency of interactions in the SWCNT/NADES complexes (Figure 5.13). The BCP properties for the mentioned complexes are detailed in table 5.4. Notably, the signs of the Laplacian of electron density at BCP ($\nabla^2\rho_{BCP}$) are consistently positive, suggesting that the interactions within SWCNT/NADES complexes are predominantly closed-shell interactions, such as hydrogen bonds (HBs) or van der Waals (vdW) forces. A criterion for X−H (X=C, N, O) type hydrogen bonds was proposed that if the ρ_{BCP} value lies between 0.002 and 0.04 (au), and the $\nabla^2\rho_{BCP}$ value is between 0.02 and 0.15 au, it can be identified as a hydrogen bond [81]. With this criterion, barring BCP numbers 285 and 287, all pairs meet the established conditions (as seen in Table 5.4). This implies that all the remaining BCPs are indicative of hydrogen bonds, affirming the preliminary identification of the interaction type based on the van der Waals radius. Based on the correlation between electron density and energy, Bader introduced a key parameter: the total electron energy density (H) at BCPs. It was suggested that $\nabla^2\rho_{BCP} > 0$ and $H_{BCP} > 0$ signify a weak hydrogen bond, $\nabla^2\rho_{BCP} > 0$ and $H_{BCP} < 0$ indicate a medium-strength hydrogen bond, and $\nabla^2\rho_{BCP} < 0$ and $H_{BCP} < 0$ represent a strong hydrogen bond [80, 82]. According to this classification, all identified BCPs almost fall within the category of weak hydrogen bonds.

The outcomes of the QTAIM analysis align with the previously conducted NCI analysis. In combination, these analyses establish that the interactions between NADES and SWCNTs primarily consist of weak hydrogen bonds and van der Waals dispersion forces. This suggests that for thermal nanofluids in energy storage systems, enhancing interactions between solvents and nano-systems (like NADES and CNTs) through the integration of tunable functional groups could lead to improved interaction with solute-solvent systems. This could

have positive implications for energy efficiency in processes such as thermal storage systems and desalination.

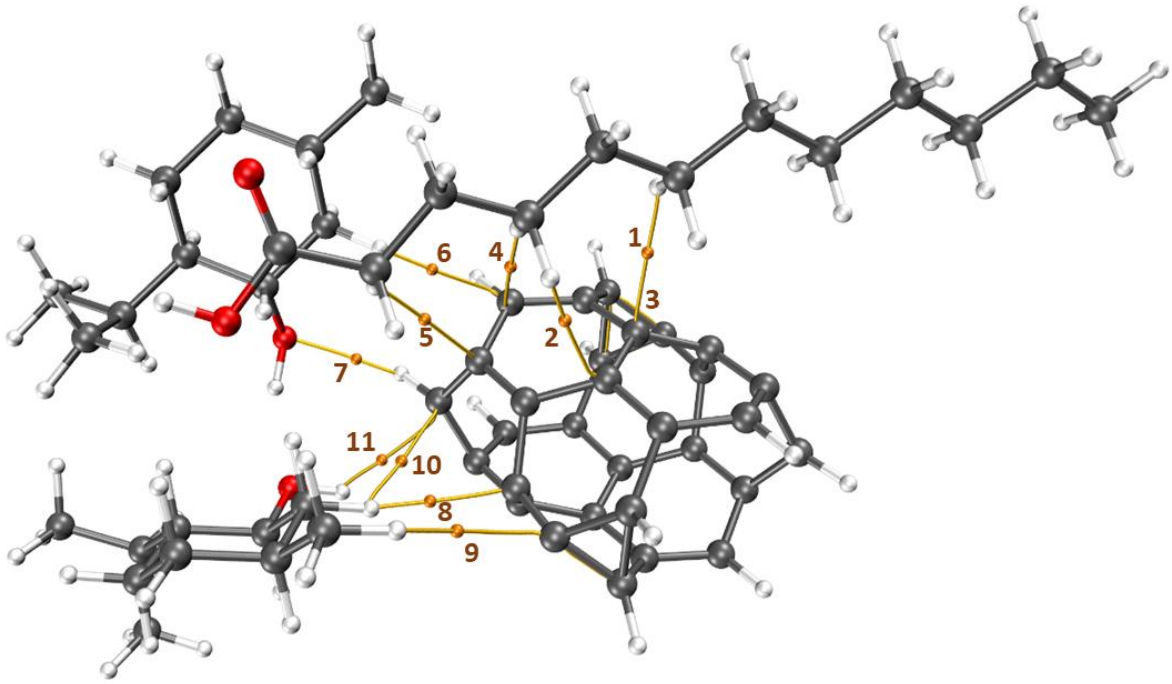

Figure 5.13 Atoms in Molecules (AIM) molecular graphs of SWCNT/NADES system calculated at the ωB97XD/6-311++G(d,p) level of theory

Table 5.4 Bond Critical Point (BCP) values between SWCNT and NADES

SL No.	BCP No.	Interaction	ρ_{BCP} (au)	$\nabla^2\rho_{BCP}$ (au)	H_{BCP} (au)
1	**BCP 285**	124C···77H	0.00239	0.00730	0.00043
2	**BCP 311**	121C···84H	0.00738	0.02410	0.00125
3	**BCP 283**	128C···89H	0.00654	0.02154	0.00116
4	**BCP 313**	126C···90H	0.00706	0.02237	0.00108
5	**BCP 287**	125C···96H	0.00461	0.01368	0.00075
6	**BCP 317**	126C···43H	0.00888	0.03275	0.00170
7	**BCP 276**	137C···61O	0.01501	0.04459	0.00010
8	**BCP 190**	12H···104C	0.01077	0.03071	0.00106
9	**BCP 173**	106C···18H	0.00356	0.00990	0.00055
10	**BCP 206**	12H···102C	0.00471	0.01469	0.00073
11	**BCP 202**	31H···102C	0.01123	0.03675	0.00138

5.4. Conclusion

This study investigated the combination of NADES formulaion of nanofluids, MWCNT/NADES and MWCNT-COOH/NADES, prepared by two-step methods. It gave excellent thermal conductivity along with other physical properties including density, viscosity, and specific heat at higher temperatures when compared to the base fluid. Different characterization methods, including XRD, FESEM, FETEM, Raman, FT-IR, and EDX, have been performed to analyse the morphology, crystallinity, and presence of functional groups. The stability of these nanofluids was assessed through zeta potential measurements. Remarkable dispersion and stability within NADES were observed when nanoparticles were bonded to functional groups. This led to notable enhancements in the crucial nanofluid properties of thermal conductivity and specific heat under elevated temperature conditions. Thus, nanofluids have a significant potential for usage as a heat transfer fluid in solar energy systems due to their alluring thermophysical properties and excellent stability. A better heat transfer coefficient and Nusselt number of nanofluid have been shown at different Reynolds numbers as compared to the base fluid NADES, noticeably higher thermal conductivity and heat transfer coefficient of nanofluids. The NCI and RDG studies reveal that the distinctive nature of interactions between NADES/SWCNT complex systems strengthens NADES molecules connections with SWCNT surfaces, producing a stable complex system. The nanofluids developed in this work have a significant amount of potential for future thermal management and energy harvesting applications due to their wide liquid range at higher temperatures, high static thermal conductivity, and convective heat transfer performance.

References

1. Bhanushali, S., et al., *Enhanced thermal conductivity of copper nanofluids: the effect of filler geometry.* ACS applied materials & interfaces, 2017. **9**(22): p. 18925-18935.
2. Dehury, P., et al., *Evaluation of thermophysical properties of menthol-based deep eutectic solvent as a thermal fluid: Forced convection and numerical studies.* Industrial & Engineering Chemistry Research, 2019. **58**(43): p. 20125-20133.
3. Paul, T.C., et al., *Experimental investigation of natural convection heat transfer of Al2O3 Nanoparticle Enhanced Ionic Liquids (NEILs).* International Journal of Heat and Mass Transfer, 2015. **83**: p. 753-761.
4. Liang, K.-H., et al., *Feasibility of 1-Ethyl-4-butyl-1, 2, 4-triazolium Acetyl Amino Acid Ionic Liquids as Sustainable Heat-Transfer Fluids.* ACS Sustainable Chemistry & Engineering, 2022. **10**(11): p. 3417-3429.
5. Zorebski, E., et al., *Isobaric and isochoric heat capacities of imidazolium-based and pyrrolidinium-based ionic liquids as a function of temperature: modeling of isobaric heat capacity.* Industrial & Engineering Chemistry Research, 2017. **56**(9): p. 2592-2606.
6. Musiał, M., et al., *Pyrrolidinium-based ionic liquids as sustainable media in heat-transfer processes.* ACS Sustainable Chemistry & Engineering, 2017. **5**(11): p. 11024-11033.
7. Paredes, X., et al., *Thermal conductivity of ionic liquids and ionanofluids. Can molecular theory help?* Fluids, 2021. **6**(3): p. 116.
8. Choi, S.U. and J.A. Eastman, *Enhancing thermal conductivity of fluids with nanoparticles*. 1995, Argonne National Lab.(ANL), Argonne, IL (United States).
9. Roston, E., *The carbon age: how life's core element has become civilization's greatest threat*. 2010: Bloomsbury Publishing USA.

10. Saidur, R., K. Leong, and H.A. Mohammed, *A review on applications and challenges of nanofluids.* Renewable and sustainable energy reviews, 2011. **15**(3): p. 1646-1668.

11. He, M., et al., *Preparation, thermal characterization and examination of phase change materials (PCMs) enhanced by carbon-based nanoparticles for solar thermal energy storage.* Journal of Energy Storage, 2019. **25**: p. 100874.

12. Aqib, M., et al., *Experimental case studies of the effect of Al2O3 and MWCNTs nanoparticles on heating and cooling of PCM.* Case Studies in Thermal Engineering, 2020. **22**: p. 100753.

13. Amrollahi, A., et al., *Convection heat transfer of functionalized MWNT in aqueous fluids in laminar and turbulent flow at the entrance region.* International Communications in Heat and Mass Transfer, 2010. **37**(6): p. 717-723.

14. Jo, B. and D. Banerjee. *Study of high temperature nanofluids using carbon nanotubes (CNT) for solar thermal storage applications*. in *Energy Sustainability*. 2010.

15. Marcos, M.A., et al., *Influence of molecular mass of PEG on rheological behaviour of MWCNT-based nanofluids for thermal energy storage.* Journal of Molecular Liquids, 2020. **318**: p. 113965.

16. Kanti, P.K., et al., *Experimental and computational determination of heat transfer, entropy generation and pressure drop under turbulent flow in a tube with fly ash-Cu hybrid nanofluid.* International Journal of Thermal Sciences, 2021. **167**: p. 107016.

17. Khullar, V., et al., *Solar energy harvesting using nanofluids-based concentrating solar collector.* Journal of Nanotechnology in Engineering and Medicine, 2012. **3**(3).

18. Jóźwiak, B., et al., *Remarkable thermal conductivity enhancement in carbon-based ionanofluids: effect of nanoparticle morphology.* ACS applied materials & interfaces, 2020. **12**(34): p. 38113-38123.

19. Timofeeva, E.V., et al. *Rechargeable nanofluid electrodes for high energy density flow battery*. in *NSTI-Nanotech*. 2013.

20. Taylor, R., et al., *Small particles, big impacts: A review of the diverse applications of nanofluids.* Journal of applied physics, 2013. **113**(1): p. 1.

21. Ilyas, S.U., R. Pendyala, and N. Marneni, *Preparation, sedimentation, and agglomeration of nanofluids.* Chemical Engineering & Technology, 2014. **37**(12): p. 2011-2021.

22. Nasiri, A., et al., *Effect of dispersion method on thermal conductivity and stability of nanofluid.* Experimental thermal and fluid science, 2011. **35**(4): p. 717-723.

23. Jia, B. and L. Gao, *Fabrication of "tadpole"-like magnetite/multiwalled carbon nanotube heterojunctions and their self-assembly under external magnetic field.* The Journal of Physical Chemistry B, 2007. **111**(19): p. 5337-5343.

24. Boldoo, T., J. Ham, and H. Cho, *Comparison study on photo-thermal energy conversion performance of functionalized and non-functionalized MWCNT nanofluid.* Energies, 2019. **12**(19): p. 3763.

25. Farbod, M., A. Ahangarpour, and S.G. Etemad, *Stability and thermal conductivity of water-based carbon nanotube nanofluids.* Particuology, 2015. **22**: p. 59-65.

26. Yu, F., et al., *Dispersion stability of thermal nanofluids.* Progress in natural science: Materials International, 2017. **27**(5): p. 531-542.

27. França, J.o.M., et al., *Thermal conductivity of ionic liquids and ionanofluids and their feasibility as heat transfer fluids.* Industrial & Engineering Chemistry Research, 2018. **57**(18): p. 6516-6529.

28. Das, N.K., et al., *Evaluation of thermophysical properties and thermal performance of amine-functionalized graphene oxide/deep eutectic solvent nanofluids as heat-transfer*

media for desalination systems. ACS Sustainable Chemistry & Engineering, 2023. **11**(14): p. 5376-5389.

29. Yu, W. and H. Xie, *A review on nanofluids: preparation, stability mechanisms, and applications.* Journal of nanomaterials, 2012. **2012**.
30. Afrand, M., *Experimental study on thermal conductivity of ethylene glycol containing hybrid nano-additives and development of a new correlation.* Applied Thermal Engineering, 2017. **110**: p. 1111-1119.
31. Das, N.K., et al., *Dihydrolevoglycosenone as a novel bio-based nanofluid for thermal energy storage: Physiochemical and quantum chemical insights.* Journal of Energy Storage, 2023. **59**: p. 106365.
32. GaussView, V., *3.07, Dennington II, Roy; Keith, Todd; Millam, John; Eppinnett, Ken; Hovell, W. Lee; and Gilliland, Ray; Semichem.* Inc., Shawnee Mission, KS, 2003.
33. Frisch, M., *gaussian.* http://www. gaussian. com/, 2009.
34. Grimme, S., *Accurate calculation of the heats of formation for large main group compounds with spin-component scaled MP2 methods.* The Journal of Physical Chemistry A, 2005. **109**(13): p. 3067-3077.
35. *Nanotube Modeler, © JCrystalSoft, 2005-2018*. 2018; Available from: http://www.jcrystal.com/.
36. Schäfer, A., H. Horn, and R. Ahlrichs, *Fully optimized contracted Gaussian basis sets for atoms Li to Kr.* The Journal of Chemical Physics, 1992. **97**(4): p. 2571-2577.
37. Fu, Y. and D.J. Singh, *Applicability of the strongly constrained and appropriately normed density functional to transition-metal magnetism.* Physical Review Letters, 2018. **121**(20): p. 207201.
38. Becke, A.D., *Density-functional exchange-energy approximation with correct asymptotic behaviour*. Physical review A, 1988. **38**(6): p. 3098.

39. Frisch, M.J., et al., *Gaussian 16 Rev. C.01*. 2016: Wallingford, CT.

40. Johnson, E.R., et al., *Revealing Noncovalent Interactions.* Journal of the American Chemical Society, 2010. **132**(18): p. 6498-6506.

41. Boto, R.A., et al., *Interpretation of the reduced density gradient.* Molecular Physics, 2016. **114**(7-8): p. 1406-1414.

42. Mishra, D.K., et al., *Molecular and spectroscopic insights into a metal salt-based deep eutectic solvent: a combined quantum theory of atoms in molecules, noncovalent interaction, and density functional theory study.* The Journal of Physical Chemistry A, 2021. **125**(44): p. 9680-9690.

43. Lu, T., *Multiwfn.* Software manual. Version, 2014. **3**(6).

44. Humphrey, W., A. Dalke, and K. Schulten, *VMD: visual molecular dynamics.* Journal of molecular graphics, 1996. **14**(1): p. 33-38.

45. Dresselhaus, M.S. and P.T. Araujo, *Perspectives on the 2010 nobel prize in physics for graphene*. 2010, ACS Publications.

46. Osswald, S., M. Havel, and Y. Gogotsi, *Monitoring oxidation of multiwalled carbon nanotubes by Raman spectroscopy.* Journal of Raman Spectroscopy: An International Journal for Original Work in all Aspects of Raman Spectroscopy, Including Higher Order Processes, and also Brillouin and Rayleigh Scattering, 2007. **38**(6): p. 728-736.

47. Antunes, E., et al., *Comparative study of first-and second-order Raman spectra of MWCNT at visible and infrared laser excitation.* Carbon, 2006. **44**(11): p. 2202-2211.

48. do Amaral Montanheiro, T.L., et al., *Effect of MWCNT functionalization on thermal and electrical properties of PHBV/MWCNT nanocomposites.* Journal of Materials Research, 2015. **30**(1): p. 55-65.

49. Arrechea, S., et al., *Effect of additions of multiwall carbon nanotubes (MWCNT, MWCNT-COOH and MWCNT-Thiazol) in mechanical compression properties of a cement-based material.* Materialia, 2020. **11**: p. 100739.

50. Atieh, M.A., et al., *Effect of carboxylic functional group functionalized on carbon nanotubes surface on the removal of lead from water.* Bioinorganic chemistry and applications, 2010. **2010**.

51. Tao, D.-J., et al., *Synthesis and thermophysical properties of biocompatible cholinium-based amino acid ionic liquids.* Journal of Chemical & Engineering Data, 2013. **58**(6): p. 1542-1548.

52. De Santis, S., et al., *Cholinium-amino acid based ionic liquids: a new method of synthesis and physico-chemical characterization.* Physical Chemistry Chemical Physics, 2015. **17**(32): p. 20687-20698.

53. Esfahani, M.R., E.M. Languri, and M.R. Nunna, *Effect of particle size and viscosity on thermal conductivity enhancement of graphene oxide nanofluid.* International Communications in Heat and Mass Transfer, 2016. **76**: p. 308-315.

54. Vogel, H., *Flűssigkeiten das temperaturabhängigkeitsgesetz der viskosität von.* Phys. Zeitschr, 1921. **22**: p. 645-646.

55. Fulcher, G.S., *Analysis of recent measurements of the viscosity of glasses.* Journal of the American Ceramic Society, 1925. **8**(6): p. 339-355.

56. Pak, B.C. and Y.I. Cho, *Hydrodynamic and heat transfer study of dispersed fluids with submicron metallic oxide particles.* Experimental Heat Transfer an International Journal, 1998. **11**(2): p. 151-170.

57. Pakdaman, M.F., M. Akhavan-Behabadi, and P. Razi, *An experimental investigation on thermo-physical properties and overall performance of MWCNT/heat transfer oil*

nanofluid flow inside vertical helically coiled tubes. Experimental thermal and fluid science, 2012. **40**: p. 103-111.

58. Zhou, S.-Q. and R. Ni, *Measurement of the specific heat capacity of water-based Al2O3 nanofluid.* Applied Physics Letters, 2008. **92**(9).

59. Soltanimehr, M. and M. Afrand, *Thermal conductivity enhancement of COOH-functionalized MWCNTs/ethylene glycol–water nanofluid for application in heating and cooling systems.* Applied Thermal Engineering, 2016. **105**: p. 716-723.

60. Bhattacharya, P., et al., *Brownian dynamics simulation to determine the effective thermal conductivity of nanofluids.* Journal of Applied Physics, 2004. **95**(11): p. 6492-6494.

61. Koo, J. and C. Kleinstreuer, *A new thermal conductivity model for nanofluids.* Journal of Nanoparticle research, 2004. **6**(6): p. 577-588.

62. Xuan, Y., Q. Li, and W. Hu, *Aggregation structure and thermal conductivity of nanofluids.* AIChE Journal, 2003. **49**(4): p. 1038-1043.

63. Hamilton, R.L. and O. Crosser, *Thermal conductivity of heterogeneous two-component systems.* Industrial & Engineering chemistry fundamentals, 1962. **1**(3): p. 187-191.

64. Hwang, Y., et al., *Investigation on characteristics of thermal conductivity enhancement of nanofluids.* Current Applied Physics, 2006. **6**(6): p. 1068-1071.

65. Lee, S., et al., *Measuring thermal conductivity of fluids containing oxide nanoparticles.* 1999.

66. Choi, S., et al., *Anomalous thermal conductivity enhancement in nanotube suspensions.* Applied physics letters, 2001. **79**(14): p. 2252-2254.

67. Vadasz, P., *Heat conduction in nanofluid suspensions.* 2006.

68. Lee, D., J.-W. Kim, and B.G. Kim, *A new parameter to control heat transport in nanofluids: surface charge state of the particle in suspension.* The Journal of Physical Chemistry B, 2006. **110**(9): p. 4323-4328.

69. Vandsburger, L., *Synthesis and covalent surface modification of carbon nanotubes for preparation of stabilized nanofluid suspensions.* 2009.

70. Chen, H., et al., *Heat transfer and flow behaviour of aqueous suspensions of titanate nanotubes (nanofluids).* Powder technology, 2008. **183**(1): p. 63-72.

71. Rashidi, F. and N.M. Nezamabad. *Experimental investigation of convective heat transfer coefficient of CNTs nanofluid under constant heat flux*. in *Proceedings of the world congress on engineering*. 2011. WCE London, UK.

72. Kanti, P., et al., *Thermal performance of fly ash nanofluids at various inlet fluid temperatures: An experimental study.* International Communications in Heat and Mass Transfer, 2020. **119**: p. 104926.

73. Ding, Y., et al., *Heat transfer of aqueous suspensions of carbon nanotubes (CNT nanofluids).* International Journal of Heat and Mass Transfer, 2006. **49**(1-2): p. 240-250.

74. Wen, D. and Y. Ding, *Experimental investigation into convective heat transfer of nanofluids at the entrance region under laminar flow conditions.* International journal of heat and mass transfer, 2004. **47**(24): p. 5181-5188.

75. Fotukian, S. and M.N. Esfahany, *Experimental study of turbulent convective heat transfer and pressure drop of dilute CuO/water nanofluid inside a circular tube.* International communications in heat and mass transfer, 2010. **37**(2): p. 214-219.

76. Dehury, P., U. Mahanta, and T. Banerjee, *Comprehensive Assessment on the Use of Boron Nitride-Based Nanofluids Comprising Eutectic Mixtures of Diphenyl Ether and*

Menthol for Enhanced Thermal Media. ACS Sustainable Chemistry & Engineering, 2020. **8**(38): p. 14595-14604.

77. Malik, A., H.S. Dhattarwal, and H.K. Kashyap, *An overview of structure and dynamics associated with hydrophobic deep eutectic solvents and their applications in extraction processes.* ChemPhysChem, 2022. **23**(18): p. e202200239.

78. Laplaza, R., et al., *NCIPLOT and the analysis of noncovalent interactions using the reduced density gradient.* Wiley Interdisciplinary Reviews: Computational Molecular Science, 2021. **11**(2): p. e1497.

79. Contreras-García, J., et al., *NCIPLOT: a program for plotting noncovalent interaction regions.* Journal of chemical theory and computation, 2011. **7**(3): p. 625-632.

80. Bader, R.F., *Atoms in molecules.* Accounts of chemical research, 1985. **18**(1): p. 9-15.

81. Lipkowski, P., et al., *Properties of the C− H⊙⊙⊙ H dihydrogen bond: an ab initio and topological analysis.* The Journal of Physical Chemistry A, 2004. **108**(49): p. 10865-10872.

82. Bader, R.F., *A quantum theory of molecular structure and its applications.* Chemical Reviews, 1991. **91**(5): p. 893-928.

Chapter- 6

Research Conclusions and Future Scope

6.1 Research Conclusion

The primary conclusion of this thesis are discussed below

In the initial part of the thesis, i.e chapter 2, biomass-derived Cyrene was used as a base fluid. Different volume fraction of carbon nanotube based nanofluids were prepared and seen to significantly enhance the thermophysical properties (density, viscosity, thermal conductivity, and specific heat capacity) as compared to base media namely Cyrene. The morphology and structure of MWCNT were investigated using FESEM, FETEM, XRD, and Raman spectroscopy. The flow behaviour and thermal performance of Cyrene, Cyrene/MWCNT, and Cyrene/MWCNT-COOH nanofluids were studied in the laminar region. Further, geometry optimization and frontier molecular orbital analysis were carried out to show the stability in the nanofluid systems. RDG analysis confirmed weak vdW interactions leading to nanoparticle agglomeration. DFT calculations revealed that Cyrene and CNT interactions are primarily governed by vdW forces. Reverse NEMD simulations validated experimental thermal conductivity measurements.

In chapter 3, multiwalled carbon nanotube has been used to prepared nanofluid where DES (Methyltriphenylphosphonium bromide and ethylene glycol) was used as base fluid. MWCNT nanoparticle was characterized by different characterization methods and thereafter MWCNT based nanofluid was synthesized at particular volume fractions *via* two-step method. The nanofluid was prepared by mixing DES (MTPB salt and ethylene glycol, 1:4 ratio) with 0.02 wt% MWCNT. Its thermophysical properties—thermal conductivity, viscosity, density, and specific heat—were measured, with MWCNT's morphology confirmed by FETEM and FESEM analysis. FT-IR and XRD experiments verified the conjugation of DES to MWCNT and its crystallinity. Stability was assessed visually, *via* optical microscopy and zeta potential.

Chapter 4, study focused on synthesizing amine-functionalized graphene oxide in DES (Diphenyl ether and DL menthol) as a basefluid and characterizing the nanoparticles using

techniques like FESEM, FETEM, EDS, FTIR, and XRD. The functionalization was confirmed via covalent bonding, and the nanofluids showed excellent stability and dispersion in DES, especially with zeta potential measurements. At higher temperatures, these nanofluids demonstrated improved thermal conductivity and specific heat, making them suitable for solar energy systems. Furthermore, ASPEN Plus software was used to design a conceptual multistage flash desalination system, were a nanofluid-based heat exchanger was proposed, showing promising thermal performance and efficient fresh water production.

In the final chapter of the thesis, we investigated the green heat transfer media comprised of natural deep eutectic solvent (NADES) and functionalised multi-walled carbon nanotube. The study explored the synthesis of NADES combined with the development of organic nanofluids, specifically MWCNT/NADES and MWCNT-COOH/NADES. Characterization techniques were adopted to assess the morphology, crystallinity, and functional groups. Zeta potential measurements confirmed the stability of the nanofluids, with exceptional dispersion and stability observed when nanoparticles were functionalized. The functionalized nanoparticle-NADES nanofluids exhibited improved thermophysical properties, including significantly higher thermal conductivity and specific heat at higher temperatures, making them promising heat transfer fluids for solar energy systems. Moreover, the nanofluids displayed better heat transfer coefficients and Nusselt numbers across different Reynolds numbers compared to NADES alone. NCI and RDG studies revealed strong interactions between NADES and SWCNT, forming stable complex systems. Given their wide range of thermal conductivity, and enhanced convective heat transfer, these nanofluids offer great potential for future thermal management and energy harvesting applications.

6.2 Future Scope

The present research was conducted to investigate the organic nanofluid which was the combination of different DES, NADES and Cyrene bio-solvent with different nanoparticles. The research highlighted NADES based nanofluid having high thermophysical properties and better heat transfer efficiency compared to DES and Cyrene bio-solvent which make them potential heat transfer media for industrial applications. The lingering concerns with DES and NADES based nanofluid provide us with some prospective areas that can be addressed in future work. The following are some future works

a) Improvement of thermal conductivity and stability at higher temperature to make DES-based nanofluid good candidate for renewable energy storage.
b) Investigation can be done on novel functionalized green nanoparticles in DES that shows potential for improving heat transfer efficiency as well as stability of the nanofluid. Focus on green nanoparticles can offer a biodegradable and non-toxic route for nanofluid which eventually shall reduce the ecological footprint in industries as it is evidenced that CNTs are toxic.
c) DES in combination with other innovative materials like ionic liquids or phase changing materials that can make hybrid nanofluid with superior thermophysical properties.
d) Detailed mechanism between fluid and nanoparticles can be studied through quantum chemical approach. Further, MD simulations can be performed to study the optimization of DES-based nanofluid that can accelerate the design and development of new thermal management system.

Appendix

Appendix A (Chapter 2)

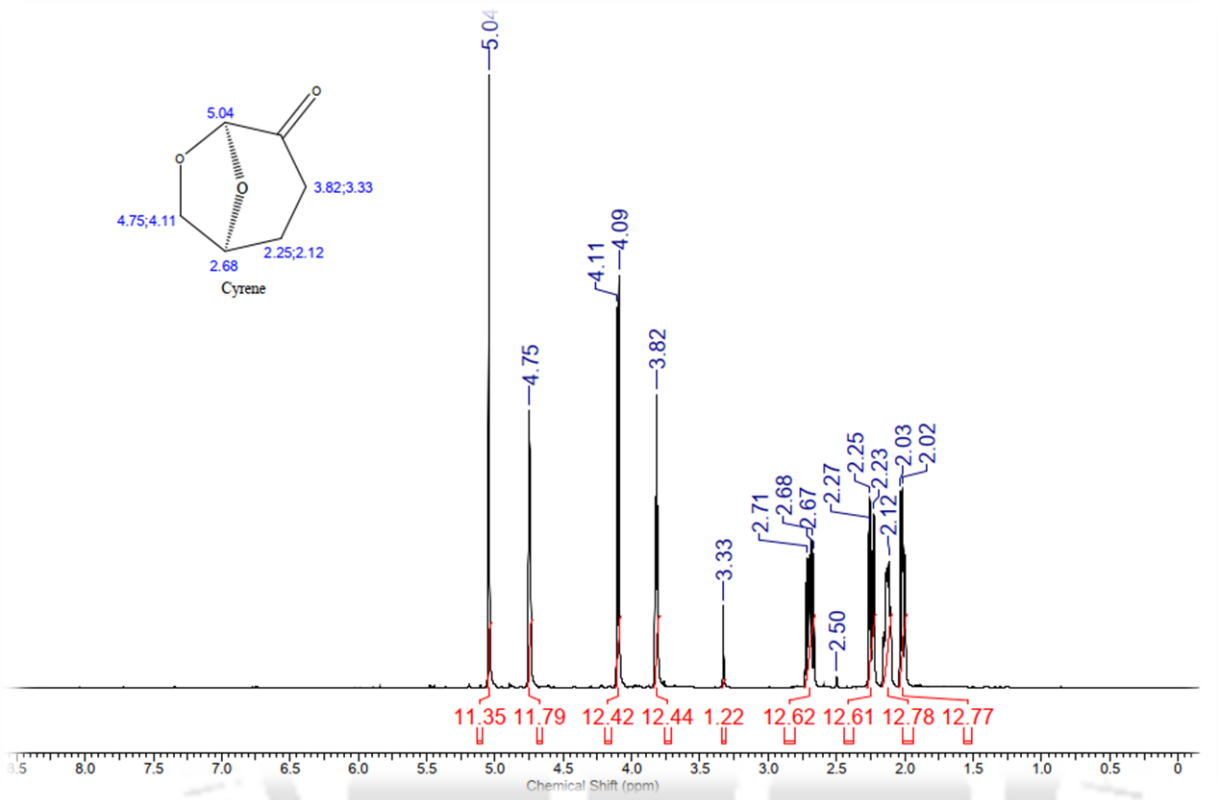

Figure A1. NMR analysis of Cyrene

A1. Experimental Setup and Forced Convection Studies

The setup consisted of a circular pipe of 1-meter length, 9 mm inner diameter and 12 mm outer diameter in which nanofluid was made to flow through the tube. The respective thermocouples and transducer measured the inlet/outlet temperatures and pressures of the fluid respectively. The nanofluid was stored in a 4-liter storage tank and pumped into the tube at different inlet temperatures. Thereafter the fluid was allowed to flow through the tube, where temperatures at five different sections (Corresponding to different x/D) in the tube were recorded. The temperatures of the fluid were measured at different testing sections by using the five

thermocouples. A heating tape heated the fluid through DC power. Power to the heater was provided by a controlled DC power (GATTS MX1174A) supply. The experiment was run at a laminar condition at three different flow rates 1.5, 3 and 5 litres per minute (LPM). Insulation of the pipe was done to maintain uniform heating throughout the test section. In this study, a flexible heating tape (Brisk Heat SDCJCA-BIH101060L) was used. The thermocouple and transducer were connected to a National Instrument control (NI cDAQ-9178) system. LAB VIEW software was used to measure and record the temperatures of the test section. The schematic of the setup is given below in figure 4(b).

Heat transfer was achieved through the power delivered to the experimental setup. The heat flux (q) was calculated from the heater input power (Q) and heating surface area (A) as per equation 2:

$$q = \frac{Q}{A} = \frac{VI}{\pi d_0 l} \quad \textbf{(1)}$$

In this equation, d_0 represents the outer diameter of the tube, l represents the length of the measuring portion, and V and I are the input voltage and current, respectively. The following equation was used to calculate the local heat transfer coefficient h(x) throughout the test section:

$$h(x) = \frac{q}{T_w^{'}(x) - T_f^{'}(x)} \quad \textbf{(2)}$$

Where $T_w'(x)$ and $T_f'(x)$ are the inner surface temperature and liquid local temperature respectively. The inner surface temperature was determined using a constant heat flux boundary condition, i.e., the one-dimensional steady-state heat conduction equation. The final expression for the inner surface temperature takes the form:

$$T_w^{'}(x) = T_w(x) - \frac{Q \ln\left(r_o / r_i\right)}{2\pi L k_s} \quad \textbf{(3)}$$

Here $T_w(x)$ is the outer surface local temperature measured by the thermocouples. The outer and inner radii of the testing channel are denoted by r_o and r_i respectively. The thermal conductivity of stainless steel is denoted by k_s. The heating length duration of the testing portion is denoted by L. Similarly, the following energy equation was used to determine the liquid local temperature:

$$T_f(x) = T_{fi} + \frac{Q}{\rho C_p V'} \frac{x}{L} \quad \textbf{(4)}$$

Where T_{fi} is the liquid inlet temperature of the test section, ρ and C_p are the density and heat capacity of the liquid respectively, and V' is the volumetric flow rate (in m^3/s) and x is the axial distance. The accuracy of thermocouples, voltage, and current is in the range of ±0.57 C, ±2 V, and ±0.1 A respectively. The uncertainties of the Reynolds number and Nusselt number were estimated to be ±6.54 % and ±5.21 % respectively. The following equation was used to compute the local Nusselt number as below:

$$Nu_x = h(x)D_i/k \quad \textbf{(5)}$$

Here, $h(x)$ is the local heat transfer coefficient from equation 3, D_i is the inner diameter of the tube and k is the thermal conductivity of the fluid. From the above expression, average Nusselt number was calculated as:

$$Nu = \frac{1}{L}\int_0^L Nu_x dx \quad \textbf{(6)}$$

Here L is the length of the tube and Simpson's 1/3rd rule was used to perform the numerical integration.

Table A1: Uncertainty calculations and values of thermophysical properties

Properties	Formula	Uncertainty
Density	$U = \pm\sqrt{\left(\frac{\Delta\rho}{\rho}\right)^2 + \left(\frac{\Delta w}{w}\right)^2}$	$\pm$ 0.002 kg/m^3
Viscosity	$U = \pm\sqrt{\left(\frac{\Delta\mu}{\mu}\right)^2 + \left(\frac{\Delta T}{T}\right)^2}$	$\pm$ 0.0014 Pa.s
Thermal conductivity	$U = \pm\sqrt{\left(\frac{\Delta k}{k}\right)^2 + \left(\frac{\Delta T}{T}\right)^2}$	$\pm$ 0.0096 W/m^2·K
Specific heat	$U = \pm\sqrt{\left(\frac{\Delta Cp}{Cp}\right)^2 + \left(\frac{\Delta T}{T}\right)^2}$	$\pm$ 5.97 J/Kg.K

Table A2. Thermal conductivity (W/m.K) enhancement (TCE) of nanofluids

Temperature (ºC)	TCE % (NF1)	TCE % (NF2)
25	25.89	20.86
35	52.41	31.72
45	65.35	33.98
55	83.01	47.16
65	89.88	51.78
75	85.87	56.49
85	80.43	52.71

Table A3. Density (gm/cc) correlation

Temperature (°C)	**NF1**		**NF2**	
	Experiment	Model	Experiment	Model
25	1.245	1.2467392	1.243	1.2453696
30	1.241	1.242752	1.239	1.241376
35	1.237	1.2387648	1.235	1.2373824
40	1.232	1.2347776	1.231	1.2333888
45	1.228	1.2297936	1.227	1.2283968
50	1.224	1.2258064	1.223	1.2244032
55	1.22	1.2218192	1.219	1.2204096
60	1.216	1.217832	1.215	1.216416
65	1.212	1.212848	1.211	1.211424
70	1.208	1.2088608	1.207	1.2074304
75	1.204	1.2048736	1.203	1.2034368
80	1.2	1.2008864	1.199	1.1994432
85	1.196	1.1968992	1.195	1.1954496

Table A4. Viscosity (Pa.s) Correlation

Temperature (ºC)	**NF1**		**NF2**	
	Experiment	**Model**	**Experiment**	**Model**
25	0.011	0.00901152	0.0111	0.00897576
28	0.0103	0.00864864	0.0103	0.00861432
31.1	0.00936	0.00790272	0.00915	0.00787136
34.2	0.00843	0.00711648	0.00806	0.00708824
37.3	0.00755	0.00644112	0.00711	0.00641556
40.4	0.00683	0.00587664	0.00634	0.00585332
43.5	0.00621	0.0053424	0.00567	0.0053212
46.7	0.00568	0.0048384	0.00512	0.0048192

49.8	0.00518	0.00445536	0.00463	0.00443768
52.9	0.00477	0.00415296	0.00423	0.00413648
56.1	0.00442	0.0038304	0.00388	0.0038152
59.2	0.00411	0.00351792	0.00356	0.00350396
62.3	0.00382	0.00330624	0.00329	0.00329312
65.4	0.00357	0.00314496	0.00306	0.00313248
68.6	0.00334	0.00290304	0.00286	0.00289152
71.7	0.00314	0.0027216	0.00267	0.0027108
74.8	0.00295	0.00260064	0.0025	0.00259032
78	0.00279	0.00248976	0.00236	0.00247988
81.1	0.00264	0.0023184	0.00223	0.0023092
84.2	0.00249	0.00218736	0.00211	0.00217868

Figure A2. Photography of nanofluids (a) just after sonication (b) 24 hours (c) 36 hours (d) 48 hours, Optical microscopic images of nanofluid (e) 0.0016 volume fraction and (b) 0.0032 volume fraction at 50x scale

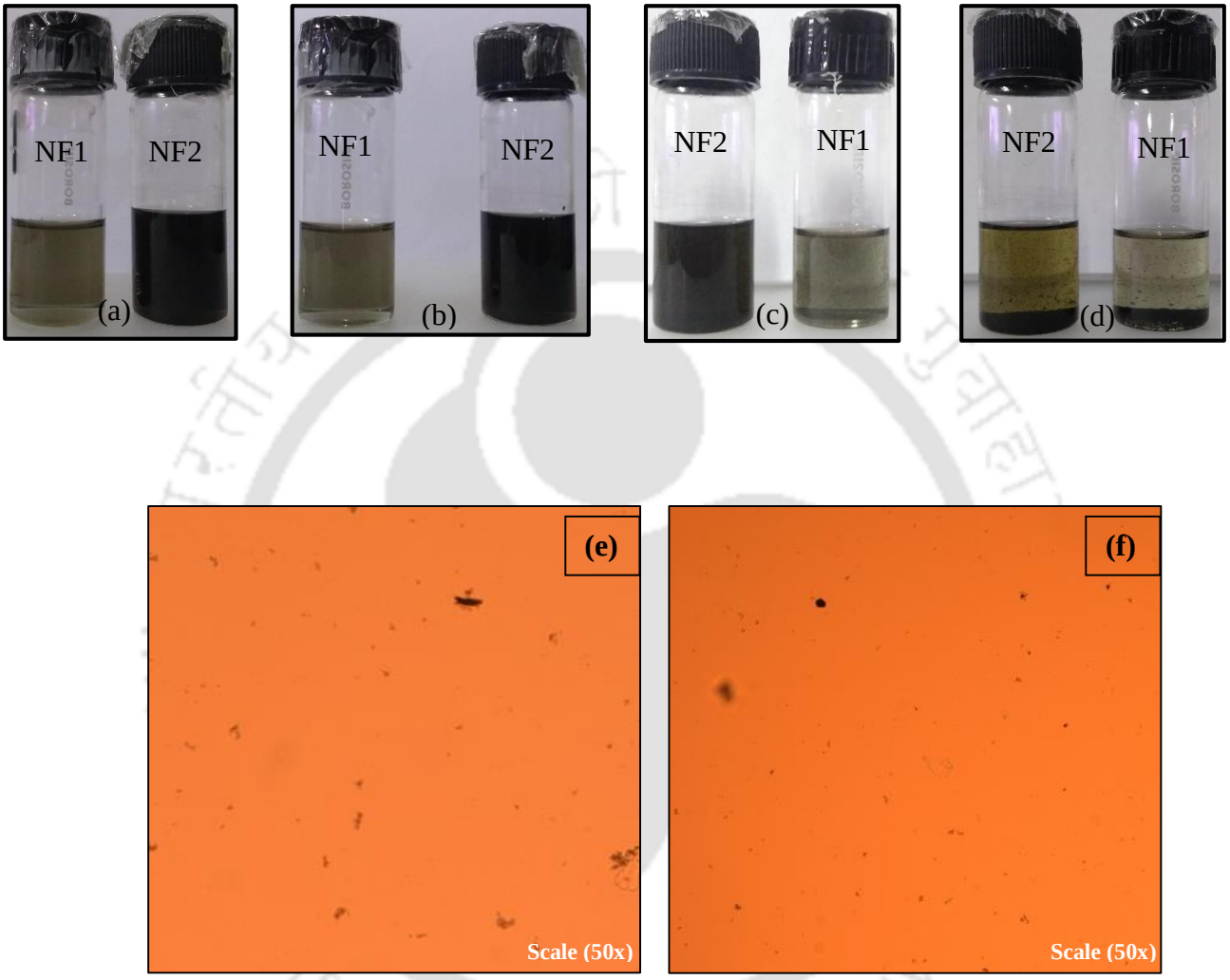

Table A5. Experimental data of thermal conductivity

	Thermal Conductivity (W/m.K)			
Temperature (°C)	**Cyrene**	**Cyrene+MWCNT**	**Paratherm GLT**	**Therminol 55**
30	0.139	0.157	0.1198	0.1273
40	0.179	0.21	0.119	0.1261
50	0.183	0.247	0.1182	0.1249
60	0.232	0.275	0.1173	0.1238
70	0.278	0.359	0.1169	0.1226
80	0.272	0.397	0.1157	0.1214
90	0.28	0.445		0.1203
95	0.308	0.398		

Table A6. Experimental data of thermal conductivity (comparison of experimental results to the Maxwell model, Maxwell-Eucken model and H-C model**)**

Temperature **(°C)**	Experimental	Maxwell model	Maxwell-Eucken model	H-C model
30	1.1295	0.50035	1.00083	0.9982
40	1.17318	0.50037	1.00081	0.9982
50	1.14973	0.50037	1.00081	0.9982
60	1.18534	0.50039	1.00078	0.9982
70	1.29137	0.5004	1.00076	0.9982
80	1.45956	0.5004	1.00076	0.9982
90	1.58929	0.5004	1.00076	0.9982
95	1.69221	0.50042	1.00075	0.9982

Research Output

Journal Publications from the Thesis

1) **N.K. Das**, P. Naik, D. N. Reddy, B. S. Mallik, S. S. Bose and T. Banerjee, "Experimental and Molecular Dynamic Insights on the Thermophysical properties for MWCNT based Phosphonium based Eutectic Thermal Media" (**Journal of Molecular liquid**). ***https://doi.org/10.1016/j.molliq.2022.118892***

2) **N.K. Das**, P. Naik, P. Dehury, S. S. Bose and T. Banerjee, "Thermophysical Characterization of Dihydrolevoglucosenone based Nanofluid and its Evaluation as a Novel Heat Transfer Media" (**Journal of energy storage**). ***https://doi.org/10.1016/j.est.2022.106365***

3) **N K Das**, P Naik, S Santra , M Vasa, R Raj, and S. S. Bose and T. Banerjee "Evaluation of Thermal Properties and Performance of Amine-Functionalized Graphene Oxide/Deep Eutectic Solvent Nanofluids as Heat Transfer Media in Desalination Systems" (**ACS sustainable chemistry and engineering**). ***https://doi.org/10.1021/acssuschemeng.2c06325***

4) **N K Das**, Raghibul Hussain, Anoop Kishore Vatti and T. Banerjee "Thermal Performance of Bio-Nanofluid Dihydrolevoglucosenone: Experimental and Atomistic Simulation Investigations" (**AIChE journal**). ***https:// doi.org/10.1002/aic.18718***

Journal Publications in Line

5) **N K Das**, D.K. Mishra and T. Banerjee, "Investigation of $GONH_2$/Deep Eutectic Solvent nanofluids as possibility heat transfer media for solar desalination system" **(Renewable Energy**, **Under Review**)

6) **N K Das**, D.K. Mishra and and T. Banerjee, "Exploration of Thermophysical Characteristics and Dispersion Behaviour in a Menthol-Based Deep Eutectic Solvent Incorporating Carboxylate-Functionalized MWCNT Nanofluid: Assessing Thermal Efficiency and DFT Investigations for Enhancing Thermal Energy Storage Potential **(Ready to submit**)

Other Publications

1) Nikhil Rahul Dhongde, **N K Das**, Tamal Banerjee, Prasanna Venkatesh Rajaraman. "Synthesis of carbon quantum dots from rice husk for anti-corrosive coating applications: Experimental and theoretical investigations". *Industrial Crops and Products* 212(2024):118329

2) Nikhil Rahul Dhongde, **N K Das**, Jenasree Hazarika, Jin-Goo Park, Tamal Banerjee, Prasanna Venkatesh Rajaraman. "Azoles as corrosion inhibitors in alkaline medium for Ruthenium chemical mechanical planarization applications: Electrochemical and Theoretical analysis". *Journal of molecular structure,* 1320 (2024):139651

3) Rifat Muradymov, Nabendu Paul, **N K Das**, Tamal Banerjee, Andrey Shishov, " Quasi-hydrophobic deep eutectic solvents for simultaneous automated determination of polar and non-polar dyes in food products". *Microchemical Journal,* 206(2024):111510

4) Mangal Mangal, Chebrolu Venkateswara Rao, **N K Das**, Suryasarathi Bose and Tamal Banerjee, "Impact of Cellulose Enrichment on Castor Oil Polyurethane Sheets: A Path to Greener Materials", *Journal of Applied Polymer Science, doi: 10.1002/app.56364*

5) Ulyana Markova; Valeriia Mulloyarova; Peter Tolstoy; Natalya Shkaeva; Dmitry Kosyakov; **N K Das**; Tamal Banerjee, "1-(o-Tolyl) thiourea-based deep eutectic solvent as a stationary phase in flow injection analysis system for mercury and copper determination in edible oils", *Talanta journal,* 282(2025):127079

6) Ulyana Markova; Valeriia Mulloyarova; Peter Tolstoy; Natalya Shkaeva; Dmitry Kosyakov; **N K Das**; Tamal Banerjee, "Deep eutectic solvent as stationary phase for flow analysis: automated trace metal determination in food products", *Analytica Chimica Acta* 1332(2024):343356

7) Andrey Shishov, Sergey Savinov, Nipu Kumar Das, Tamal Banerjee, Andrey Bulatov, "Automated simultaneous determination of mercury and copper in edible oils by reversed-phase column-based extraction with deep eutectic solvent", *Journal of Food Composition and Analysis*, 137(2025):106919

Conferences and Workshop

1) **Nipu Kumar Das**, Papu Kumar Naik, and Tamal Banerjee, "Evaluation of thermo-physical properties of amine functionalized graphene oxide/Deep Eutectic Solvent nanofluids as heat transfer media for solar desalination system" International Conference on Emerging Trends in Nanomaterials Science and Technology, 27-29 January 2022, NIT Nagaland, India
2) **Nipu Kumar Das**, Papu Kumar Naik, and Tamal Banerjee, "Thermophysical properties for MWCNT based Phosphonium Eutectic Nanofluid: An Emerging Heat Transfer Media for Solar Desalination System" 1st International Conference on Advances in Water Treatmentand Management (ICAWTM-22) March 25-26, 2022, Pandit Deendayal Energy University, Gandhinagar, Gujarat, India (Virtual)
3) **Nipu Kumar Das**, Papu Kumar Naik, and Tamal Banerjee, "Investigation on thermal performance of Carbon based Nanoparticle with Cyrene as Nanofluid: A Green Heat Transfer Media for Solar Desalination System" International conference on Desalination and Water Treatment: Recent Technological Advancement, Challenges and Opportunities (InDACON-

2022), March 26–27, 2022, MBM University in association with Indian Desalination Association (InDA) and DRDO, Jodhpur (Virtual)

4) **Nipu Kumar Das**, and Tamal Banerjee, "Evaluation of thermal performance of bio-based nanofluids comprising of dihydrolevoglycosenone and functionalised carbon nanotube" International conference on Biotechnology for Sustainable Bioresources and Bioeconomy (BSBB-2022), December 7–11, 2022, Indian Institute of Technology Guwahati, Assam
5) **Nipu Kumar Das**, and Tamal Banerjee, "Characteristics and computational studies of bio-based Nanofluids as Thermal Energy Storage Media for Heat Transfer Application" 16th Complex Fluids Symposium 2022 (CompFlu-2022), Indian Society of Rheology & Indian Institute of Technology Kharagpur, Kharagpur-721302
6) **Nipu Kumar Das**, and Tamal Banerjee, DAE-BRNS national workshop on "Atomistic Modeling of Molecules and Materials (AMMM-2023), Anushaktinagar, BARC, Mumbai, December 11-14, 2023
7) **Nipu Kumar Das** and Tamal Banerjee, "Thermophysical Properties and Dispersion behaviour of Menthol-Based Deep Eutectic Solvent with Carboxylate-Functionalized MWCNT Nanofluids: Evaluating Thermal Efficiency and DFT Insights to Enhance Thermal Energy Storage Capacity", International Conference on New Frontiers in Chemical, Energy and Environmental Engineering (INCEEE-2023) 24-25 Nov., 2023, NIT Warangal, India

ACS Sustainable Chemistry & Engineering

pubs.acs.org/journal/ascecg

Research Article

Evaluation of Thermophysical Properties and Thermal Performance of Amine-Functionalized Graphene Oxide/Deep Eutectic Solvent Nanofluids as Heat-Transfer Media for Desalination Systems

Nipu Kumar Das, Somtirtha Santra, Papu Kumar Naik, Maureen Shama Vasa, Rishi Raj, Suryasarathi Bose, and Tamal Banerjee*

Cite This: ACS Sustainable Chem. Eng. 2023, 11, 5376−5389

Read Online

ACCESS | Metrics & More | Article Recommendations

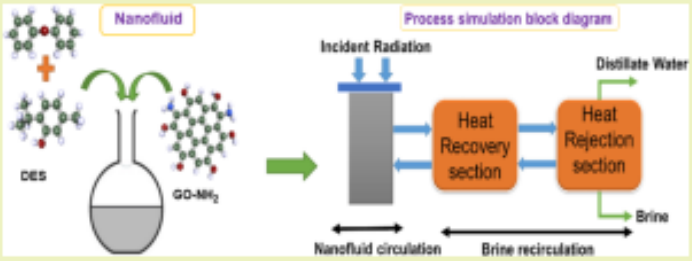

ABSTRACT: The study mainly focuses on the synthesis and characterization of amine-functionalized graphene oxide (GO-NH_2) nanoparticles. It also reports the thermal properties and stability analysis of deep eutectic solvent (DES)- and GO-NH_2-based nanofluids. DES is composed of diphenyl ether as the hydrogen bond acceptor and DL-menthol as the hydrogen bond donor in the molar ratio 1:1. The nanofluid was prepared by a two-step method where two different concentrations of functionalized graphene nanofluids, namely, 0.0033 volume fraction (NF1) and 0.0101 volume fraction (NF2), were reported. XRD and FTIR analyses were used to validate the nanoparticle's identity. Additionally, the morphology and composition of GO-NH_2 nanoparticles were investigated using FESEM, FETEM, EDS, and Raman analyses. After that, the stability of the nanofluids was assessed using ζ potential measurements. The ζ potential measurements revealed increased stability, indicating that no agglomeration occurred in the DES-based nanofluid. Excellent thermal conductivity enhancement was observed at a higher temperature for the GO-NH_2 nanofluid. The density and viscosity of the base fluid and nanofluid decreased with an increase in temperature from 25 to 85 °C. Further, the specific heat capacity of the nanofluids also increased with the increase in temperature and volume fractions of the nanofluid. Thermogravimetric analysis was also performed to evaluate the thermal degradation of the nanofluid under a nitrogen atmosphere. The nanofluid was used in brine recirculation multistage flash desalination where the gained output ratio of less than 10 was obtained through ASPEN simulation.

KEYWORDS: *deep eutectic solvents, nanofluids, GOR, nanoparticle*

INTRODUCTION

Global energy consumption is expected to double by 2050 and more than quadruple by the end of the century. In order to meet this demand in a sustainable manner, incremental upgrades to current energy networks will be insufficient. Finding enough sustainable energy for the future is one of society's most difficult issues. The vast discrepancy between our current usage of solar energy and its immense untapped potential constitutes a major energy research issue. There is no better way to meet our future energy needs than with abundant, clean solar power. The fact that it is easily available, free of international conflict, and does not pollute the environment or change the climate is a huge advantage.[1] Thermal or electrical energy storage of solar radiation is an essential and crucial component for solar energy applications. Solar energy systems (SESs) are widely regarded as one of the

Received: October 28, 2022
Revised: March 14, 2023
Published: March 27, 2023

Journal of Molecular Liquids 354 (2022) 118892

Contents lists available at ScienceDirect

Journal of Molecular Liquids

journal homepage: www.elsevier.com/locate/molliq

Experimental and molecular dynamic insights on the thermophysical properties for MWCNT-Phosphonium based eutectic thermal media

Nipu Kumar Das [a], Papu Kumar Naik [a], Dhileep N. Reddy [b], Bhabani S. Mallik [b], Suryasarathi Bose [c], Tamal Banerjee [a,*]

[a] Department of Chemical Engineering, Indian Institute of Technology Guwahati, Guwahati 781039, Assam, India
[b] Department of Chemistry, Indian Institute of Technology Hyderabad, Hyderabad 502284, Telangana, India
[c] Department of Materials Science and Engineering, Indian Institute of Science Bangalore, Bangalore 560012, Karnataka, India

ARTICLE INFO

Article history:
Received 19 November 2021
Revised 3 March 2022
Accepted 4 March 2022
Available online 7 March 2022

Keywords:
Nanofluid
Stability
Deep Eutectic Solvent
MWCNT
MD

ABSTRACT

In this study, a thermal media is synthesized by mixing hydrogen bond acceptor (HBA) [Methyltriphenylphosphonium bromide (MTPB)] salt with hydrogen bond donor (HBD) [ethylene glycol] at a molar ratio of 1:4. Thereafter the corresponding nanofluid was prepared by dispersing 0.02 wt% Multi-Walled Carbon Nanotube (MWCNT) having a diameter 10–30 nm in the base fluid. Prior to dispersion, the shape and morphology of the MWCNT were ascertained using both Field Emission Scanning Electron Microscope (FESEM) and Field Emission Transmission Electron Microscope (FETEM). The crystallinity and functional groups were investigated by X-ray Powder Diffraction meter (XRD) and Fourier Transform Infrared Spectroscopy (FTIR). The stability of the prepared nanofluid was initially performed using visual observation followed by zeta potential measurements. Thermogravimetric analysis (TGA) was performed to check the stability of nanofluid at a temperature close to 500 °C at a heating rate of 10 °C/min under nitrogen environment. Thermophysical properties such as density, viscosity, thermal conductivity, and specific heat of nanofluid were measured in the temperature range 25–85 °C. It is evident from the experimental data that viscosity and density decrease with an increase in temperature. On the contrary, the specific heat and thermal conductivity of the nanofluid were found to increase with temperature. This is due to the induced Brownian motion of the nanoparticle, which results in higher kinetic energy at high temperature. In the penultimate section, Molecular Dynamic (MD) simulations were performed to compare and validate the results of thermal conductivity of nanofluid.

1. Introduction

Environmental concerns have initiated researchers to create alternative, inexpensive, efficient, and sustainable energy sources due to the global warming induced by fossil fuel use. In terms of environmental concerns, the green solvent is one of the alternate methods for reducing the impact of pollution in applications such as extraction and thermal media. The use of green solvent or technology reduces wastewater pollutants, toxic chemical substances and also improves technology. Here 'green' refers to the preparation of chemicals such as solvents and fluids through non-fossil fuel sources. Pharmaceutical companies are now using greener synthesis routes for drug development so as to reduce pollution and manufacturing costs [1].

Deep Eutectic Solvents (DES) are a new class of organic solvents. It is gaining attraction due to its various beneficial physical and chemical properties [2–5]. They are analogous to Ionic Liquids (IL's), which are known for recent industrial applications[6]. Applications concerning IL's for extractions are also well documented [7–10]. The physicochemical properties of ILs are similar to DES and include low volatility, low flammability, higher thermal and chemical stability. For their interesting properties, IL's are alternative to conventional organic solvents [11–13]. But due to its high manufacturing and toxicity issues, primarily from their petroleum-based precursors, alternative solvents are still gaining importance. Further, most of the IL's are highly viscous and difficult to synthesize. With respect to thermal media, Wu et al. [14] synthesized IL's namely [C_4min] [PF_6], [C_8min] [PF_6], and [C_4 min] [Tf_2N] (Tf_2N: bis trifluoromethane sulfonimide) and used them as heat transfer fluid for solar thermal power plant.

Ionic liquids (ILs) can also be referred to as green solvents due to their excellent thermal and chemical stability and low volatility.

* Corresponding author.
E-mail address: tamalb@iitg.ac.in (T. Banerjee).

https://doi.org/10.1016/j.molliq.2022.118892
0167-7322/

Journal of Energy Storage 59 (2023) 106365

Contents lists available at ScienceDirect

Journal of Energy Storage

journal homepage: www.elsevier.com/locate/est

Research Papers

Dihydrolevoglycosenone as a novel bio-based nanofluid for thermal energy storage: Physiochemical and quantum chemical insights

Nipu Kumar Das [a,1], Dhirendra Kumar Mishra [a,1], Papu Kumar Naik [c], Pyarimohan Dehury [a], Suryasarathi Bose [b], Tamal Banerjee [a,*]

[a] Department of Chemical Engineering, Indian Institute of Technology Guwahati, Assam 781039, India
[b] Department of Materials Engineering, Indian Institute of Science, Bangalore 560012, India
[c] Department of Environmental Science, Parul Institute of Applied Science, Parul University, Vadodara, Gujarat 391760, India

ARTICLE INFO

Keywords:
Cyrene
Heat transfer fluid
Forced convection, thermal conductivity
Brownian motion
DFT
RDG analysis

ABSTRACT

Dihydrolevoglycosenone, commercially known as Cyrene, is a biodegradable solvent with a multitude of potential applications such as chemical reactions and heat transfer media. The current work reports a nanofluid comprising cyrene as a potential bio-organic thermal base media dispersed with Multi-walled carbon nanotube (MWCNT) nanoparticles. Two volume fractions (0.0016 and 0.0032) of nanoparticles were added to enhance the heat transfer capacity of the resulting nanofluid. Thereafter, thermophysical properties were reported in the temperature range of 30–85 °C for both base fluid and nanofluid. The measured values were then compared with a commercial heat transfer fluid, *Paramtherm GLT*, within the temperature range of 30–85 °C. Further, the stability of the nanofluid was investigated by a combination of visual observation, microscopic analysis, and zeta potential measurements. Thereafter, forced convection experiments were performed in a circular tube section under laminar conditions to measure the local heat transfer coefficient alongside temperature profiles. Results showed that the nanofluid possessing 0.0032 volume fraction of MWCNT-Cyrene nanofluid at $N_{Gz} = 1881$ gave the highest heat transfer coefficient. Density Functional Theory was also used to investigate the microstructure formed by Cyrene on the surface of Single-walled carbon nanotube (SWCNT). The orbital energy and influence of interaction energy on the van der Waals (vdW) interactions of Cyrene and ethylene glycol with SWCNT were examined and correlated with the dispersive forces within the fluid. The orbital energy revealed the fact that the HOMO-LUMO energy gap of the Cyrene/SWCNT was reduced due to the approach of Cyrene towards SWCNT surface, making it a stable nanofluid system. Reduced density gradient (RDG) analysis further demonstrated that weak vdW interactions were the primary driving force between solvent-SWCNT systems, primarily through $X^{-}\pi$ interactions.

1. Introduction

With the recent demand for renewable energies, it is important to give attention to cost-effective techniques dealing with solar energy. Solar energy is one of the major renewable sources for thermal applications, including desalination systems, due to the ease of availability and predictability [1]. But the efficiency of the thermal performance of solar energy-based desalination systems is the primary concern among the researchers. Modification of efficiency can be categorized based on improving solar radiation absorption, improving the efficiency of the applied media, and improving the heat transfer media [2]. One of the major applications of nanofluid is used in solar desalination systems, where nanofluid is employed as heat transfer media. A lot of research have been carried out on the selection of nanofluids for heat transfer applications using nanoparticles [3–5].

Attractive physical properties such as high thermal stability at higher temperatures makes nanofluid a potential heat transfer fluid. Overall, they possess higher specific heat capacity and heat transfer coefficient. Researchers working on nanofluids have concluded that the base fluid thermal conductivity and heat transfer coefficient significantly increase with concentration [3,4]. Colangelo et al. [5] used 3.0 % volume concentration in a flat-type solar thermal collector and compared the thermophysical properties with water based nanofluid. They concluded

* Corresponding author.
E-mail address: tamalb@iitg.ac.in (T. Banerjee).
[1] Indicates equal contribution.

https://doi.org/10.1016/j.est.2022.106365
Received 29 August 2022; Received in revised form 23 November 2022; Accepted 8 December 2022
Available online 23 December 2022
2352-152X/